Quality of real-time functional magnetic resonance imaging

Quality of real-time functional magnetic resonance imaging: novel software, sequences, and signals.

Quality of real-time functional magnetic resonance imaging: novel software, sequences, and signals.

PROEFSCHRIFT

ter verkrijging van de graad van doctor aan de Technische Universiteit Eindhoven, op gezag van de rector magnificus prof.dr.ir. F.P.T. Baaijens, voor een commissie aangewezen door het College voor Promoties, in het openbaar te verdedigen op vrijdag 25 juni 2021 om 13:30 uur

door

Jacobus Stephanus Heunis

geboren te Kaapstad, Zuid-Afrika

Dit proefschrift is goedgekeurd door de promotor en de samenstelling van de promotiecommissie is als volgt:

voorzitter:	prof.dr. K.A. Williams
1e promotor:	dr. S. Zinger
2e promotor:	prof.dr.ir. M. Breeuwer
copromotor:	dr.ir. R.M.J.N. Lamerichs
promotiecommissieleden:	prof.dr. A.P. Aldenkamp
	prof.dr.ir. M. Mischi
	prof.dr. D.E.J. Linden (Universiteit Maastricht)
	prof.dr. F. Scharnowski (University of Vienna)
	prof.dr. R. Van Ee (Radboud Universiteit)

Het onderzoek of ontwerp dat in dit proefschrift wordt beschreven is uitgevoerd in overeenstemming met de TU/e Gedragscode Wetenschapsbeoefening.

Quality of real-time functional magnetic resonance imaging: novel software, sequences, and signals.

Cover background: Sam Karanja via Pixabay, adapted by Stephan Heunis
Cover design: Stephan Heunis.
Printed by: Gildeprint drukkers.

A catalogue record is available from the Eindhoven University of Technology Library
ISBN: 978-90-386-5310-5
NUR-code: 959

Summary

Quality of real-time functional magnetic resonance imaging: novel software, sequences, and signals.

Breaking down the complexities of the human mind in order to understand and develop treatments for mental health conditions is an ongoing challenge in neuroscience research and global healthcare. If we are to make a practical difference in our understanding of these complexities, and ideally in the lives of those who are impacted daily, we have to rigorously and critically question the validity of our own research. It is therefore imperative that we ensure the quality of our own scientific measures, methods, and inferences.

Real-time functional magnetic resonance imaging (fMRI) is an advanced method that shows promise in allowing us to probe and explore the human mind in a virtual, real-time and non-invasive manner. Functional MRI involves the time-dependent imaging of the oxygen concentration in cerebral blood vessels, which approximates the amount of energy consumed by the neurons in our brain to support its function, hence *functional* MRI. With real-time fMRI, these images of our brain activity are acquired, processed, and visualised while a person is inside the MRI scanner, essentially providing a window into the human mind as we think, feel, process information, and make decisions. But how well do we understand this technology and its practical implications, especially for healthcare?

As a research field, real-time fMRI is undergoing rapid development to support applications like brain computer interfaces, neuroimaging-based interventions for neuropsychological or -psychiatric patients, adaptive experimental paradigms, and neurofeedback training, the latter two being of increased interest in neuroscientific and healthcare research. Adaptive experimental paradigms allow the study of mental health conditions under more naturalistic circumstances by allowing experimental stimuli to adapt to a patient's measured brain activity in real-time, while neurofeedback allows brain activity to be fed back to the patient in the MRI scanner such that they can train themselves to exert control over it. Both have great potential to improve our understanding and treatment of the human mind, but they also require state-of-the-art methodology to mitigate the detrimental effects of known fMRI artefacts - such as magnetic interference, head movement, or physiological noise signals - on the data quality and derivative measures. The importance of quality control is emphasised even more due to the real-time nature of the technology, which does not allow time for the data to be processed offline.

It is therefore pertinent to ask: can we trust the measures derived from real-time fMRI and the inferences we draw from them? And if this technology is to play an increasingly important role in mental healthcare, what can and should we do to improve the quality of real-time fMRI?

While the vast majority of real-time fMRI literature focuses on applications (often clinical), there is a stark lack of studies exploring and quantifying the quality of the real-time data, the effects of real-time processing methods, the validity of the employed methods and practices, and potential improvements to the aforementioned. That is the overarching goal of this thesis.

We approach the research topic in three parts: (I) *Understanding real-time fMRI data quality*, in which we present the complexities of the neuronal signal, noise sources, artefacts, and confounding factors, and develop a comprehensive understanding of real-time fMRI data quality; (II) *Hardware and software for real-time fMRI analysis and quality control*, where we develop, describe and share innovative hardware and software solutions for improving the quality and reproducibility of the real-time fMRI signal; and (III) *Real-time multi-echo fMRI*, where we explore novel data acquisition and signal processing methods that lead to sensitivity improvements for real-time fMRI.

In Chapter 2, a comprehensive understanding of the real-time fMRI signal, noise sources, artefacts, confounding factors, and ultimately data quality form the necessary backdrop against which we investigate ways to improve it. We identify real-time multi-echo fMRI acquisition and analysis as a promising research direction and the core focus of the third theme of this thesis.

Chapter 3 follows by presenting a methods review of real-time fMRI signal quality in 128 recent fMRI neurofeedback studies. The literature review addressed questions regarding the employed denoising methods, quality control mechanisms, and reporting practices that promote or hinder computational reproducibility in this representative sample of studies. This work found that: (1) methods reporting in fMRI neurofeedback can and should improve in order to allow methods reproducibility, and to help delineating the sources of variance in and effects of the real-time fMRI signal; (2) there is a need for tools and best practices for calculating, reporting and interpreting real-time fMRI quality measures; (3) the influence of real-time processing steps on the quality of the fMRI data and neurofeedback signal are not well studied/understood; (4) there is much room for developing new and improved real-time fMRI sequences, denoising methods and pipelines. Based on these findings, we generated and published a best practices checklist for implementation and reporting of signal processing steps employed in real-time fMRI neurofeedback studies.

The focus then shifts to improving infrastructure, tools and methods to support real-time quality control of fMRI data. To be able to acquire, transfer and process fMRI data in real-time, we developed and demonstrated the validity of a technical setup using a 3T Philips scanner and MATLAB/SPM12 software (Chapter 4). With the knowledge and experience gained during this process, we developed an open source software toolbox for real-time quality control of fMRI data, covered in

Chapter 5. Apart from improving the quality of fMRI data as they are acquired, this tool can help with time and money savings (by flagging and stopping problematic scans in real-time) and can improve reporting practices on the validity of research data. Additionally, it was created with the intention of being a shared, community-based effort for contributing to best practices in real-time fMRI quality.

As part of the third theme of this thesis, and to address the remaining shortcomings highlighted in the methods review, we developed novel acquisition and processing methods to improve the sensitivity of the blood oxygen level-dependent (BOLD) fMRI signal in real-time. Multi-echo fMRI acquires multiple images along the magnetic decay curve (as opposed to the more ubiquitous single-echo sequences), allows quantification of magnetic decay parameters, and has been shown to improve signal-to-noise ratio and denoising efforts in conventional fMRI studies. However, comprehensive details of its implementation and effects in real-time fMRI have previously not been demonstrated. In Chapter 7, we started by collecting, curating and openly publishing a resting state and task-based multi-echo fMRI dataset to support novel methods development in the field of real-time fMRI. Further, in Chapter 8, we developed new real-time multi-echo combination and decay parameter mapping methods, and demonstrated its use in this and other fMRI datasets. We found that real-time combination of multi-echo data using a newly developed, per-volume, T2*FIT-weighting scheme could increase the temporal signal-to-noise ratio beyond the capability of existing combination methods, and that per-volume estimates of T2*FIT could lead to increased effect sizes of activity in task-based data.

To promote the reproducibility of this work and to assist further improvements of the developed real-time processing methods, we have made all of the developed methods and pipelines publicly available as part of a general MATLAB/Octave-based toolbox for real-time and offline fMRI preprocessing and quality control (Chapter 6).

Samenvatting

Kwaliteit van real-time functionele magnetische resonantiebeeldvorming: nieuwe software, sequenties en signalen.

Het ontrafelen van de complexiteit van de menselijke geest om behandelingen voor geestelijke gezondheidsproblemen te begrijpen en te ontwikkelen, is een voortdurende uitdaging in neurowetenschappelijk onderzoek en de wereldwijde gezondheidszorg. Als we een praktisch verschil willen maken in ons begrip van deze complexiteiten, en idealiter in het leven van degenen die er dagelijks mee te maken hebben, moeten we de validiteit van ons eigen onderzoek rigoureus en kritisch in twijfel trekken. Het is daarom absoluut noodzakelijk dat we de kwaliteit van onze eigen wetenschappelijke metingen, methoden en conclusies waarborgen.

Real-time functionele magnetische resonantiebeeldvorming (fMRI) is een geavanceerde methode die veelbelovend is omdat het ons in staat stelt om de menselijke geest op een virtuele, real-time en niet-invasieve manier te onderzoeken en te verkennen. Functionele MRI is de tijdsafhankelijke beeldvorming van de zuurstofconcentratie in cerebrale bloedvaten, wat bij benadering overeenkomt met de hoeveelheid energie die door de neuronen in onze hersenen wordt verbruikt om hun functie te ondersteunen, vandaar de term functionele MRI. Met real-time fMRI worden deze beelden van onze hersenactiviteit verkregen, verwerkt en gevisualiseerd terwijl een persoon in de MRI-scanner ligt, wat ons als het ware een soort kijk geeft op de menselijke geest terwijl we denken, voelen, informatie verwerken en beslissingen nemen. Maar hoe goed begrijpen we deze technologie en de praktische implicaties ervan, vooral voor de gezondheidszorg?

Als onderzoeksgebied maakt real-time fMRI een snelle ontwikkeling door ter ondersteuning van toepassingen zoals brein-computer interfaces, op neuroimaging gebaseerde interventies voor neuropsychologische of -psychiatrische patiënten, adaptieve experimentele paradigma's, en neurofeedback training, waarbij de laatste twee van toenemend belang zijn in neurowetenschappelijk onderzoek en onderzoek in de gezondheidszorg. Adaptieve experimentele paradigma's maken het mogelijk psychische aandoeningen onder meer naturalistische omstandigheden te bestuderen doordat experimentele stimuli zich in real time kunnen aanpassen aan de gemeten hersenactiviteit van een patiënt, terwijl neurofeedback het mogelijk maakt hersenactiviteit terug te koppelen naar de patiënt in de MRI-scanner, zodat deze zichzelf kan trainen om er controle over uit te oefenen. Beide hebben een groot potentieel om ons begrip en onze behandeling van de menselijke

geest te verbeteren, maar ze vereisen ook een geavanceerde methodologie om de nadelige effecten van bekende fMRI-artefacten - zoals magnetische interferentie, hoofdbeweging of fysiologische ruissignalen - op de kwaliteit van de gegevens en de afgeleide maten te beperken. Het belang van kwaliteitscontrole wordt nog meer benadrukt door het real-time karakter van de technologie, waardoor er geen tijd is om de gegevens offline te verwerken. Het is daarom van belang om de volgende kwesties aan te kaarten: kunnen we de metingen die worden afgeleid uit real-time fMRI en de conclusies die we daaruit trekken, vertrouwen? En als deze technologie een steeds belangrijkere rol gaat spelen in de geestelijke gezondheidszorg, wat kunnen en moeten we dan doen om de kwaliteit van real-time fMRI te verbeteren?

Terwijl de overgrote meerderheid van de real-time fMRI literatuur zich richt op toepassingen (vaak klinisch), is er een schrijnend gebrek aan studies die de kwaliteit van de real-time data, de effecten van real-time verwerkingsmethoden, de validiteit van de gebruikte methoden en praktijken, en potentiële verbeteringen van het hiervoor genoemde onderzoeken en kwantificeren. Dat is het overkoepelende doel van dit proefschrift.

We benaderen het onderzoeksonderwerp in drie delen: (I) Inzicht in real-time fMRI data kwaliteit, waarin we de complexiteit van het neuronale signaal, ruisbronnen, artefacten en verstorende factoren behandelen, en een uitgebreid begrip van real-time fMRI data kwaliteit creëeren; (II) Hardware en software voor real-time fMRI analyse en kwaliteitscontrole, waarin we innovatieve hardware- en softwareoplossingen voor het verbeteren van de kwaliteit en reproduceerbaarheid van het real-time fMRI signaal ontwikkelen, beschrijven en delen; en (III) Real-time multi-echo fMRI, waarin we nieuwe data-acquisitie en signaalverwerkingsmethoden verkennen die leiden tot gevoeligheidsverbeteringen voor real-time fMRI.

In Hoofdstuk 2 vormen een uitgebreid begrip van het real-time fMRI-signaal, ruisbronnen, artefacten, verstorende factoren, en uiteindelijk de kwaliteit van de gegevens de noodzakelijke achtergrond waartegen we manieren onderzoeken die deze zullen verbeteren. We identificeren real-time multi-echo fMRI acquisitie en analyse als een veelbelovende onderzoeksrichting en de focus van het derde thema van dit proefschrift.

In Hoofdstuk 3 wordt een overzicht gegeven van de methoden die zijn gebruikt om de kwaliteit van real-time fMRI-signalen in 128 recente fMRI neurofeedback studies te beoordelen. Het literatuuronderzoek richtte zich op vragen met betrekking tot de gebruikte ruisverminderingsmethoden, manieren voor kwaliteitscontrole en de wijze van rapporteren die de computationele reproduceerbaarheid bevorderen of belemmeren in deze representatieve steekproef van studies. Uit dit onderzoek bleek dat: (1) de rapportage van methoden over fMRI-neurofeedback verbeterd kan en moet worden om reproduceerbaarheid van methoden mogelijk te maken en om de bronnen van variantie in en de effecten van het real-time fMRI-signaal helpen af te bakenen; (2) er behoefte is aan hulpmiddelen en beste praktijken voor het berekenen, rapporteren en interpreteren van real-time fMRI-

kwaliteitsmetingen; (3) de invloed van verschillende real-time verwerkingsstappen op de kwaliteit van de fMRI data en het neurofeedback signaal niet goed zijn onderzocht/begrepen; (4) er veel ruimte is voor het ontwikkelen van nieuwe en verbeterde real-time fMRI sequenties, ruisverminderingsmethoden en pipelines. Op basis van deze bevindingen hebben we een beste praktijken checklist voor de implementatie en rapportage van signaalverwerkingsstappen in real-time fMRI neurofeedback studies opgesteld en gepubliceerd.

De focus verschuift vervolgens naar het verbeteren van infrastructuur, hulpmiddelen en methoden om real-time kwaliteitscontrole van fMRI-gegevens te ondersteunen. Om fMRI data in real-time te kunnen verzamelen, overdragen en verwerken, hebben we een technische opstelling ontwikkeld en gedemonstreerd met behulp van een 3T Philips scanner en MATLAB/SPM12 software (Hoofdstuk 4). Met de kennis en ervaring die zijn opgedaan tijdens dit proces, ontwikkelden we een open source software toolbox voor real-time kwaliteitscontrole van fMRI data, zoals wordt behandeld in Hoofdstuk 5. Naast het verbeteren van de kwaliteit van fMRI data die tegelijkertijd worden verkregen, kan deze tool helpen bij het besparen van tijd en geld (door problematische scans in real-time te markeren en te stoppen) en kan het de rapportage over de validiteit van onderzoeksgegevens verbeteren. Bovendien werd het ontwikkeld met de intentie om een gedeelde, gemeenschapsgerichte inzet te zijn die bijdraagt aan beste praktijken in real-time fMRI-kwaliteit.

Als onderdeel van het derde thema van dit proefschrift, en om de overige tekortkomingen aan te pakken die in de methodologie review naar voren kwamen, hebben we nieuwe acquisitie- en verwerkingsmethoden ontwikkeld om de gevoeligheid van het bloedzuurstofniveau-afhankelijke (BOLD) fMRI-signaal in real-time te verbeteren. Multi-echo fMRI acquireert meerdere beelden langs de magnetische verval curve (in tegenstelling tot de meer overal aanwezige single-echo sequenties), maakt kwantificering van magnetische verval parameters mogelijk, en heeft aangetoond dat het in staat is om de signaal-ruisverhouding en ruisverbeteringsdoeleindes in conventionele fMRI-studies te verbeteren. Echter, uitgebreide details van de implementatie en de effecten in real-time fMRI zijn nog niet eerder aangetoond. In hoofdstuk 7 zijn we begonnen met het verzamelen, samenstellen en openlijk publiceren van een rusttoestand en taak-gebaseerde multi-echo fMRI dataset ter ondersteuning van de ontwikkeling van nieuwe methoden op het gebied van real-time fMRI. Verder hebben we in Hoofdstuk 8 nieuwe real-time multi-echo combinatie en vervalparameter mapping methoden ontwikkeld, en het gebruik ervan gedemonstreerd in deze en andere fMRI datasets. We ontdekten dat real-time combinatie van multi-echo data met behulp van een nieuw ontwikkeld, per volume, T2*FIT-gewogen schema de temporele signaal-ruisverhouding kon verhogen, nog meer dan de mogelijkheden van bestaande combinatiemethoden, en dat per-volume schattingen van T2*FIT konden leiden tot verhoogde effectgroottes van activiteit in taak-gebaseerde data.

Om de reproduceerbaarheid van dit werk te bevorderen en om verdere verbeteringen van de ontwikkelde real-time verwerkingsmethoden te ondersteunen,

hebben we alle bovengenoemde methoden en pipelines openbaar beschikbaar gesteld als onderdeel van een algemene MATLAB/Octave-gebaseerde toolbox voor real-time en offline fMRI beeldvoorbewerking en kwaliteitscontrole (Hoofdstuk 6).

Contents

Chapter 1 Introduction

1.1 Background

Humans want to read minds - that is no secret. We have been obsessed with the possibility of mind reading, and of understanding consciousness, since times untold. It is written in our legends, in our cultural history, we sing about it, philosophers muse about it, scientists study it, we write dystopian novels about it, we even attempt it (inadvertently or purposefully?) in our daily lives. *I wonder why he is frowning at me, he must think I did something wrong… She must be so frustrated after what happened, I wish I could understand what she's going through… They did what?? What were they thinking?* Or to move from the mundane to the purpose-driven: if we could completely understand the human mind, its building blocks, and the intricacies of how they fit together to yield a functioning, awe-inspiring mechanism, imagine what we could achieve with that knowledge. Would we be able to measure consciousness or its levels of function empirically? Would we be able to quantify how a functioning mind differs from one with so-called dysfunction? Could we unpack that systematically, to see which levers we can pull to set a course of corrective action, if so desired? Could we make inroads into addressing some of the most challenging mental conditions of our time, such as depression, Alzheimer's disease, developmental disorders, schizophrenia and many more that are affecting the lives and livelihoods of too many?

As it stands, we do not have to do too much imagining. For just as long as we have been obsessed with mind reading and consciousness, we have also developed theories, conducted experiments, and created technologies to generate and test viable answers. From ancient spiritualism to Descarte, from behaviourism to neurons, from dissecting the nervous system of a frog to the magnetic resonance imaging of a human brain, we have steadily and very concretely added to the body of knowledge of the mind. During the past century this has culminated in the exponential growth of technology-assisted discoveries and inventions that are now synonymous with neuroscience. What was thought of as dystopian a century ago, is common practice today, and will be seen as outdated and even naive a few decades from now. Such is the nature of what we call scientific progress. And the technologies, methods and practices that we develop are paving the way.

But what of the unintended consequences? Are the technologies we build and the methods we develop particularly appropriate to answer such fundamental,

sometimes ill-posed, questions? How sure are we that we aren't fooling ourselves, that the elusive object of our study is not in fact playing tricks on, well, itself? And in our rush to improve our models, to build better measurement systems, to make more accurate inferences, and to answer deeper questions, what are we prioritising? Could we be choosing competition over democratisation of ideas, novelty over robustness, quantity over quality, and rationalised conclusions over embracing the complexity of the unknown? As scientists we walk this tightrope every day, balancing our dreams to uncover the unknown with the possibility and responsibility of improving the lives of those whose minds prevent it. So what suffices as our balancing pole?

Transparency in science has this potential. By opening up our data, our methods, and our practices, we allow diverse ideas to enter the pool of knowledge generation. And by sharing these ideas openly, we allow others to error-check our work, to reuse it, and to extend it. Scientists should be no strangers to this iterative process, yet we cannot be complacent in driving it forward to its full potential. If we sincerely want to answer some of life's most profound questions with the high quality, rigourous, robust, and reproducible effort that it requires, we cannot shy away from holding up the magnifying glass to our own work, to our own practices, and to the technologies whose praises we sing.

This thesis documents a single thread along this global tapestry of scientific inquiry: of dreams, to ideation, to technology, to structured and constructive doubt, and ultimately to building shared knowledge on which to iterate. It starts with the question of reading the mind, particularly: how can we explore the human brain in order to understand and treat it? One advanced technology that has allowed us a glimpse into the mind is real-time functional magnetic resonance imaging, where we exploit the magnetic properties of the atoms we consist of by putting them into a large magnet, and watching the scene unfold. Modern day scanners have the ability to image the anatomical properties of our brains at submillimeter accuracy, as well as record brain activity over time as we conduct mental tasks or lie still in the scanner. While anatomical images are ideal for identifying tumours, blood clots and other visible anomalies, functional brain images tell us all about how we process information, how brain regions specialise for certain tasks, and how our brain forms a dynamic functional network. The real-time aspect allows us to do all of this while a person is lying in the scanner, essentially providing a direct window into the mind as we think, feel, process and decide. It has inspired scientists to design novel methods for studying and treating the human brain. Adaptive experiments, for example, are designed to dynamically update the stimuli or tasks presented to the person in the scanner based on their changing brain activity, allowing the study environment to adapt to our mental processes. Another is neurofeedback, where people can learn to self-regulate their brain function by receiving visual feedback of their brain activity at that very moment. The act of self-regulation may lead to changes in mental or physical behaviours, and has been studied as a treatment option in neurological and psychiatric conditions.

So what, one might wonder, are the drawbacks of real-time functional magnetic resonance imaging (or for short, real-time fMRI)? Since it allows us to peer into the human mind, can we say that we have the tools to understand it? Can we now break it down into its building blocks and start rebuilding the minds that require care? As with many advanced technologies, the inner workings of real-time fMRI rest on many levels of intricate details, each with its own complexities. From the physical properties of atoms, to the micro- and macroscopic movement of oxygen and blood through the brain, to the magnetic properties of the scanner, and the eventual context within which the technology is applied: the devil could be in any of these details. A useful example is the underlying assumptions of fMRI, which measures brain activity through the proxy of oxygen concentration in blood vessels in the brain. It is known that physiological factors like respiration, heart rate and blood flow, and not only neuronal activity, influence the concentration of blood oxygen in the brain. This can bias both our measurement and our interpretation of said measurement. Are we perhaps adapting the experimental stimuli, or providing neurofeedback, purely based on a higher breathing rate of the person in the scanner, and not based on their changing brain activity? Or could the person's head be moving slightly each time they receive an updated instruction, which is known to lead to synchronised fluctuations in brain image intensity, that we then misinterpret as brain activity? Importantly, are we acquiring enough data and using state-of-the-art methods to ascertain that these confounding factors are indeed accounted for? Or, by not accounting for these drawbacks, are we drawing incorrect conclusions from our experiments that could ultimately lead to the technology being considered beneficial to patients when in fact it is not? Or the reverse?

Thus, what of the quality of our technology, our measurements, our methods, and of our inferences? What should we be investigating as possible confounding factors when measuring and interpreting brain activity? Can we quantify these, ideally in real-time, in order to capture and discard bad quality data as they are acquired? Can we develop new MRI sequences that already provide an improved quality fMRI signal upon acquisition, with higher sensitivity to brain activity changes? And could we improve our existing real-time signal processing methods, and develop novel ones, so as to extract an increasingly truer version of brain activity? By posing these questions, and developing robust methods and experiments to answer them, we approach our work through a necessary critical lense, systematically breaking down the ultimate challenge of understanding the human mind into smaller, manageable pieces.

What follows - having identified the dream, the technology, and the structured approach to self-critical inquiry and improvement - is to prioritise transparency. If we develop new signal processing methods for improving the quality of measured brain activity in real-time, can we describe them in such a way that others can understand, reuse and improve on them? And can we openly share the software implementation of said methods, providing an inclusive platform for all to learn from and contribute to? If we collect a novel dataset using a newly developed

sequence, can we make this dataset available to the fMRI community for future research while simultaneously prioritising the personal data privacy of study participants?

By making each quantifiable step of our research as transparent and accessible as is practically and ethically possible, we take part in the global process of iterative progress. If our ultimate goal is to understand the human mind and to use our understanding for the betterment of humankind, all of humankind should be able to weigh in, and all of humankind should be able to contribute to and benefit from the outcomes.

1.2 Problem statement, research questions and contributions

With the previous thread as backdrop, we now focus on the core problem statement, the research questions and the contributions of this thesis to the quality of real-time fMRI.

1.2.1 Problem statement

Data quality has received little attention in the field of real-time fMRI, while the drawbacks of fMRI and the effects of not accounting for them, on the other hand, are well known. This discrepancy is substantiated by a notable absence of methods for improving real-time fMRI data quality and of practices for methods reporting in the literature. This absence prevents a thorough, community-wide, understanding of real-time fMRI data quality and aspects that might influence, or better yet, improve it. Consequently, adoption of improved methods lags behind in practice, since a lack of understanding and validation hinders implementation at the level of hardware and software tools. Multi-echo fMRI is a core example: its benefits for conventional fMRI are documented, but it is hardly used in real-time applications. In order to validate its possible benefits for improving the quality of real-time fMRI, it requires a thorough understanding, new methods development for real-time use cases, toolset implementations, novel datasets, and validation experiments.

1.2.2 Research questions

The research questions identified in response to this problem statement are summarised according to three main parts:

Part I: Understanding real-time fMRI data quality

A comprehensive understanding of the blood oxygen level-dependent (BOLD) signal, real-time fMRI, noise sources, artefacts, confounding factors, and ultimately data quality should form the necessary backdrop against which we investigate ways to improve it.

RQI.1: Can we provide a comprehensive review of existing methods for improving the quality of real-time fMRI?

RQI.2: What does an improved understanding reveal about the state of real-time quality control methodology and reporting? Do proven signal processing methods exist for removing noise sources that are not of interest? Are there standardised quality control measures and ways to report them?

RQI.3: If our understanding, denoising methodology and reporting practices are lacking, which measures can be introduced to improve the research community's understanding and implementation of improved data quality?

Part II: Hardware and software for real-time fMRI analysis and quality control

Real-time fMRI data quality can benefit greatly from standardised quality control measures, agreed practices for reporting them, improved acquisition and processing methods for increasing BOLD sensitivity, and community-driven tool and practice development to underlie all of the aforementioned. Additionally, these implementations are all necessary in order to test and validate novel methods such as real-time multi-echo fMRI.

RQII.1: Can we implement the infrastructure on the scanner level to allow the transfer and processing of (multi-echo) fMRI in real-time?

RQII.2: Can we implement real-time quality control methods on a software level to provide the research community with a tool for methods standardisation and quality control and improvement?

RQII.3: Can we develop and implement novel algorithms for processing multi-echo fMRI data in real-time, allowing validation experiments to be conducted?

Part III: Real-time multi-echo fMRI

Assuming a thorough understanding of the possible benefits of multi-echo fMRI for conventional and real-time data quality, and assuming successful implementation of the required real-time scanning infrastructure and software tools to support it, the development and validation of real-time multi-echo fMRI methods remain to be tested.

RQIII.1: As a starting point, can we design and collect a novel, real-time multi-echo dataset that will allow the exploration and development of improved signal processing methods? Can we annotate and structure such datasets so as to ensure interoperability with standard tools and pipelines? And can we share this data publicly while still prioritising research ethics and the personal data privacy of data participants?

RQIII.2: Given that no comparable literature exists, can we explore and report possible BOLD sensitivity improvements with real-time multi-echo fMRI? How

do newly developed methods perform against current state of the art or conventional offline multi-echo fMRI methods?

RQIII.3: Can we consequently derive preferred multi-echo methods for improving real-time fMRI data quality and develop these into publicly available pipelines for community use and contribution?

1.2.3 Contributions

This work contributes to the improvement of real-time fMRI data quality along the three presented themes.

Part I: Understanding real-time fMRI data quality

Acknowledging the noisy nature of functional magnetic resonance imaging and its drawbacks, Part I of this thesis presents existing and recently developed methods that improve our ability to gain useful insights from noisy real-time data. This contribution takes the form of a thorough description of the core concepts relating to real-time multi-echo fMRI and data quality, as well as a comprehensive review of denoising methods and tools in real-time fMRI literature. In particular, it highlights the relatively underexplored nature of denoising methodology in the field of real-time compared to offline fMRI analysis, presents a comprehensive checklist for inclusion and reporting of real-time denoising steps, and identifies real-time multi-echo fMRI as a promising tool to improve sensitivity of the blood oxygen level-dependent (BOLD) signal.

Part II: Hardware and software for real-time fMRI analysis and quality control

With the background knowledge in place, Part II then covers the chronologically stacked development of tools for improving the quality of real-time fMRI. The first contribution details the practical setup of real-time fMRI acquisition, transfer, processing and display, including a newly developed graphical user interface to facilitate these aspects. Additionally, this thesis facilitates community standardisation via the development of an open software tool for calculating, displaying and reporting real-time data quality measures. The final software contribution provides novel functionality to process multi-echo fMRI data in real-time, in the form of open and automated software pipelines, thus laying the practical foundation for carrying out multi-echo experiments and validation tests in real-time.

Part III: Real-time multi-echo fMRI

The thesis then covers comprehensive efforts to consolidate advancements in real-time multi-echo acquisition and analysis into practically useful contributions. Part III contributes both a novel real-time multi-echo dataset that is annotated and made available publicly, and the first comprehensive exploration of the effects of multi-echo fMRI combination and rapid T2*-mapping on offline and real-time BOLD sensitivity. Findings show clear benefits of multi-echo for real-time use cases, especially in terms of increased functional contrast in task-related regions

of interest, and brain-wide increased signal-to-noise ratio.

1.3 Thesis outline

To form the basis of our understanding, **Chapter 2** provides technical backgrounds of each of the core concepts covered in this thesis: functional MRI, real-time fMRI, BOLD sensitivity and confounds, acquisition and denoising methods for BOLD improvements, and finally multi-echo fMRI and its application in real-time use cases.

Next, understanding the current state of the art with regards to methods and quality control in real-time fMRI is an essential step. **Chapter 3** covers a comprehensive review of recent studies in the field of real-time fMRI neurofeedback, investigating their use of real-time denoising methods (or lack thereof), and their implementation of quality control standards. This work finds that: (1) methods reporting in fMRI neurofeedback can and should improve in order to allow methods reproducibility, and to help delineating the sources of variance in and effects of the real-time fMRI signal; (2) there is a need for tools and best practices for calculating, reporting and interpreting real-time fMRI quality measures; (3) the influence of real-time processing steps on the quality of the fMRI data and neurofeedback signal are not well studied/understood; (4) there is much room for developing new and improved real-time fMRI sequences, denoising methods and pipelines.

Chapter 4 then focuses on infrastructure, tools and methods to support real-time fMRI quality control, without which further experimentation and methodological validation would not be possible. This chapter covers the development and validation of a technical setup using a 3T Philips scanner and MATLAB/SPM12, allowing fMRI to be acquired, transferred and processed in real-time.

Shifting from infrastructure to software, **Chapter 5** and **Chapter 6** describe two open source software toolboxes developed over the course of this project. One tool (**Chapter 5**) assists researchers in calculating and visualising multiple real-time image quality metrics that improve the quality of fMRI data as they are acquired, can help with time and money savings (by flagging and stopping problematic scans in real-time) and can improve reporting practices on the validity of research data. A second tool (**Chapter 6**) provides functionality to process multi-echo fMRI data in real-time, functionality which is lacking in the wider ecosystem of open neuroimage analysis tools. Both of these software tools lay the practical and algorithmic groundwork for what follows.

Then we turn our focus to sequences and signals. Building on top of the advancements of real-time processing and benefits of multi-echo fMRI, **Chapter 7** and **Chapter 8** present extensive work to collect multi-echo fMRI data, develop novel real-time multi-echo fMRI methods, and validate these new approaches. **Chapter 7** presents a collected, curated and openly published resting state and task-based multi-echo fMRI dataset to support novel methods development in the field of real-time fMRI. **Chapter 8** presents novel real-time multi-echo combi-

nation and T2*-mapping methods, highlighting their effects on real-time BOLD sensitivity and the benefits for real-time data quality.

Throughout the course of these chapters, we provide complementary information on how all methods and results have been made accessible to the research community and transparent to the general public. All developments and findings are then placed into context and discussed in **Chapter 9**. We summarise the contributions that this project has made to the field of real-time fMRI, and provide insight into how future developments could benefit from these contributions.

Part I: Understanding real-time fMRI data quality

Chapter 2 Core concepts

Abstract

Real-time functional magnetic resonance imaging (fMRI) is a tool that assists researchers in understanding the intricacies of the human mind as we think, feel and process information. To improve our inferences based on real-time fMRI data, the quality and sensitivity of this approximate measure of brain activity is paramount. However, there is a notable absence of methods for improving real-time fMRI data quality and of practices for methods reporting in the literature. This absence prevents a thorough, community-wide, understanding of real-time fMRI data quality and aspects that might influence, or better yet, improve it. A comprehensive understanding of the blood oxygen level-dependent (BOLD) signal, of real-time fMRI, of its noise sources, artefacts, and confounding factors, and ultimately of data quality should form the necessary backdrop against which we investigate ways to improve it. This chapter reviews the core concepts we need to yield this understanding: the mechanisms of real-time functional MRI, BOLD signal sensitivity and confounds, acquisition and denoising methods for BOLD improvements in real-time, and finally multi-echo fMRI and its application in real-time use cases. We show from reviewed sources that multi-echo fMRI is promising for improving real-time BOLD sensitivity due to its ability to separate BOLD and non-BOLD effects and to provide optimal brain-wide T2*-weighting.

2.1 Functional magnetic resonance imaging of the human brain

During rest or when performing a mental task, the neurons in our brains need to metabolise oxygen in order to generate energy to support their function. Oxygen molecules are transported to where they are required through a vast array of cerebral arteries and capillaries by a paramagnetic protein known as hemoglobin. During this process, physiological changes in the brain such as metabolic rate, blood flow, and blood volume all influence relative local concentrations of oxygenated and deoxygenated blood, which subsequently give rise to local magnetic susceptibility gradients. Using functional magnetic resonance imaging (fMRI), and T2*-weighted acquisition sequences in particular, we can capture these brain-wide, physiologically induced, magnetic perturbations over time and at millimeter-level spatial resolution. Since the inception of fMRI into brain research around 1990, this blood oxygen level-dependent (or BOLD) signal has been characterised as a proxy for brain activity, which allowed researchers to study its relation to fundamental brain function in typical and disease-stricken human brains. Importantly, our ability to infer accurate information about neuronal processes is influenced by the sensitivity with which we can capture these BOLD changes and by how we subsequently delineate its sources of variance. This requires a thorough understanding of the BOLD signal, its constituents, and their influences on sensitivity.

The MRI scanner is a large permanent magnet that has a base magnetic field strength which causes the protons in water molecules in our blood and brain tissue to become magnetised in the scanner. These protons are also referred to as ”spins”, since they rotate at an atomic level around an axis positioned along the magnetic field. To acquire a single fMRI image of a human brain, a short transverse radio frequency pulse is applied while the person is lying longitudinally inside the scanner. The resulting transverse magnetic field disturbs the base magnetisation of the spins, essentially turning their direction sideways, which then requires time once the transverse pulse is removed for the spins to revert to their equilibrium magnetisation state. This process is called relaxation or decay. Decay relates to how the spins dissipate their energy with regards to the main magnetic field (called T1, or spin-lattice, decay), but also with regards to other local spins (called T2, or spin-spin, decay). In a human brain there are tissue differences on micro- and macroscopic level that cause magnetic field inhomogeneities which in turn influence the local spin-spin decay rate. This leads to an observed or effective T2 decay rate, termed T2* decay. Different tissue types have different proton densities and contain different levels of local field inhomogeneities, thus leading to varying decay rates across the brain and across tissue types. Taking a snapshot of the tissue magnetisation at a given time point after transverse excitation allows us to capture differences in decay rates, which we then translate into differences in image contrasts at distinct spatial positions on an MRI image. Additionally, taking repeated snapshots over time, each time after a repeated transverse excitation, allows us to capture time-dependent changes in decay rates such as those relating to changes in oxygenated and deoxygenated blood, i.e. the T2*-weighted BOLD signal. That is the core principle behind T2*-weighted imaging, further explained

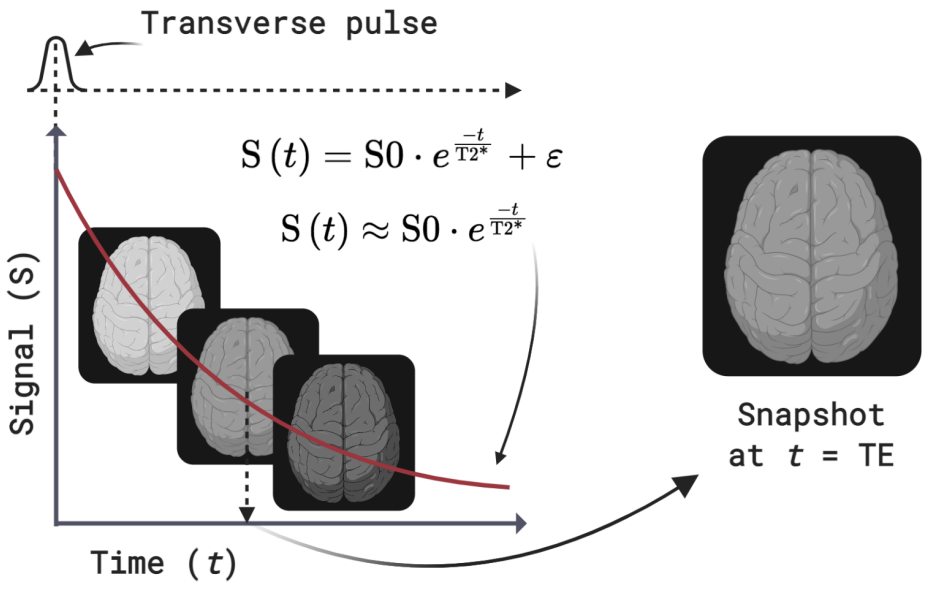

Figure 2.1 — *Diagram of a transverse excitation pulse, followed by mono-exponential T2*-decay of the magnetised tissue, and lastly acquisition of a single functional MRI volume at echo time TE*

by the depiction in Figure 2.1.

2.2 Real-time fMRI

Most functional, T2*-weighted imaging datasets are acquired as a single time series, also called a functional run, that consists of tens or hundreds of three-dimensional T2*-weighted images, termed volumes. These runs, whether it is acquired during a resting state or task-based experiment, are typically preprocessed, denoised and analysed some time after the acquisition session, i.e. offline. However, online analysis of each fMRI volume as it is acquired from the person lying in the scanner is also possible, as depicted in Figure 2.2. This advancement of acquiring and analysing data in a matter of seconds has made real-time fMRI a viable tool for real-time data quality monitoring, functional activation mapping and adaptive experimentation since its development by Cox, Jesmanowicz, and Hyde, 1995. Since then, the ensuing two decades saw a substantial increase of research interest and activity in this field. Advancements in MRI technology, computational algorithms, and computer processing power have also allowed increasingly faster processing of functional images and have given researchers and clinicians access to data in real-time that would otherwise only be available hours, days or weeks after scanning.

Applications of real-time fMRI include real-time data quality assurance and patient compliance checking (Voyvodic, 1999), pre-experimental and pre-surgical functional localisation and intraoperative guidance (see for example Hirsch et al.,

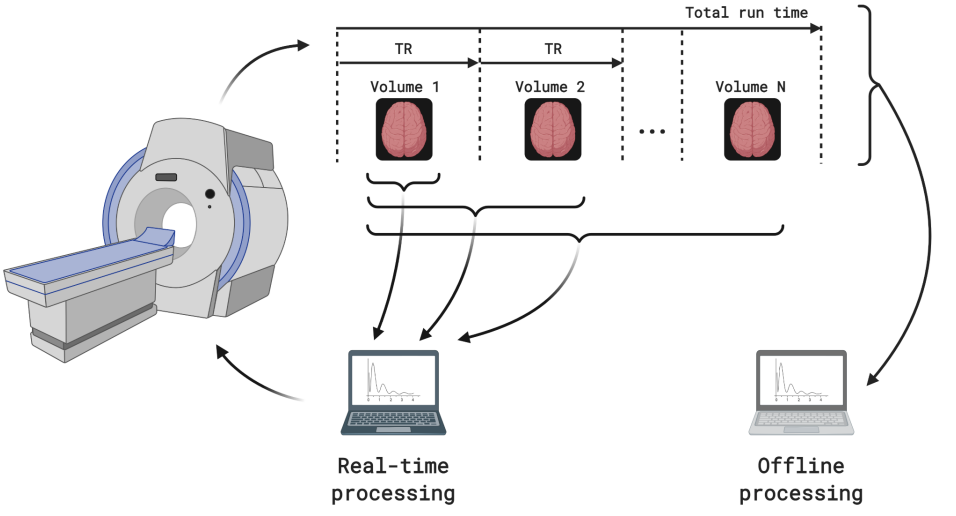

Figure 2.2 — *A depiction of a full fMRI run consisting of N volumes each acquired at a specific repetition time, with offline processing indicated as the processing of all acquired data after the run has finished. Real-time processing involves processing each volume as it is acquired, together with all previously acquired volumes.*

2000, and Binder, 2011), real-time functional activity mapping (as is available in the software accompanying all major MRI vendors), brain computer interfaces (e.g. Sorger et al., 2012), brain state decoding (LaConte, 2011), real-time neurofeedback training (Sitaram et al., 2017), and even as an interactive teaching tool (Weiskopf et al., 2007b).

From the perspective of understanding and treating mental health conditions, learned brain activity regulation through neurofeedback training has been used in neuropsychological and -psychiatric disorders and other subject groups to test for behavioural and symptomatic correlates. If successful and robust, such findings would make non-invasive real-time fMRI a viable alternative to more invasive treatment modalities like pharmaceuticals, surgery or deep brain stimulation. Several studies have reported significantly beneficial behavioural, symptomatic or experiential changes after fMRI neurofeedback training in a variety of clinical or other populations, including major depressive disorder (Linden et al., 2012), tinnitus (Emmert et al., 2017), attention deficit and hyperactivity disorder (Alegria et al., 2017), (Spetter et al., 2017), and nicotine cravings (Canterberry et al., 2013).

However, with this rapid expansion of real-time fMRI applications, especially in clinical settings, similar attention has not been given to the fundamentals of BOLD sensitivity and the implementation of steps to improve it in real-time. There are core differences between offline and real-time analysis that make real-time data quality an essential step for online experiments. For one, real-time fMRI analysis does not have access to the same full dataset that allows advanced statistical analysis to be conducted offline. In real-time processing the algorithm can only

access each data point acquired up to a specific point in time, resulting in less statistical power to draw valid real-time inferences from and less data with which to calculate useful metrics of brain function or artefacts. Additionally, real-time analysis typically expects each acquired volume to be processed by the time the following volume in the time series is acquired, which leaves seconds for the real-time code to execute. Conversely, available offline processing time is essentially limitless.

Consequently, real-time denoising and analysis algorithms typically include simplistic versions of offline fMRI processing steps, even when taking advancements in computational power into account. As a result of these restrictions and simplifications, the real-time BOLD signal might still contain confounding fluctuations or artefacts that would otherwise have been removed with offline analysis, lowering its quality and casting doubt on the implementation and results of real-time fMRI applications. The exploration of acquisition and analysis methods that aim to improve real-time data quality can therefore be seen as an important and necessary investigative route, and it is the core focus of this thesis.

2.3 BOLD sensitivity and confounds

A variety of aspects influence the sensitivity with which we can capture BOLD signal changes: at the levels of the magnet, the T2*-weighted sequence and the person being scanned. By controlling or correcting for these influences, we can diminish their effect on the measured BOLD fluctuations and improve our ability to relate BOLD changes to neuronal changes, thus increasing BOLD sensitivity and improving our inferences.

To understand this, let us focus first on the drawbacks of T2*-weighted sequences. Conventionally, a single-echo fMRI image is acquired (i.e. a single snapshot is taken after transverse excitation) at one echo time specifically selected to optimise BOLD sensitivity. This optimum is typically achieved at an echo time close to the average baseline T2*-value (Menon et al., 1993), which at 3T is around TE = 30 ms for the cortex. This brain-wide optimisation leads to suboptimal location-specific BOLD sensitivity since the single echo time is selected to optimise BOLD contrast for an average T2*-value, while it is known that T2* varies across tissue types and brain regions (Peters et al., 2007). This can result, amongst others, in spatial variability in the detection of task-related activation patterns or in resting state metrics such as functional connectivity.

Furthermore, while T2*-weighted imaging specifically exploits decay differences due to local magnetic susceptibility gradients on a microscopic level, this can be detrimental at a larger spatial scale. For example, macroscopic magnetic susceptibility effects in areas with air/tissue boundaries result in more severe image defects such as signal dropout and image distortion, leading to a loss of potentially valuable brain activity information. Signal dropout is known to be more pronounced in the inferior frontal, the medial temporal and the inferior temporal lobes (Devlin et al., 2000).

Lastly, even if region-specific BOLD sensitivity is optimised and signal dropout is diminished, the BOLD signal results from a complex interplay of blood flow, blood volume and magnetic susceptibility effects that can be influenced strongly by system- and participant-level noise sources. Scanner instabilities, field inhomogeneities, head movement, respiration, cardiac activity, and blood pulsatility can all confound the BOLD signal and diminish our ability to relate BOLD changes to neuronal activity.

The implications of not correcting sufficiently for (or ignoring) such noise sources, confounds and artefacts have also been studied widely. Head motion, for example, is well known to diminish the signal-to-noise ratio of fMRI and 3D volume realignment is a standard correction step implemented in fMRI preprocessing to account for this. Even so, head motion has still been shown to result in false activity patterns when coupled to the timing of the task paradigm (Hajnal et al., 1994), to cause simultaneous decreases in long-distance correlations and increases in short-distance correlations within functional connectivity networks (Power et al., 2012), and to cause problems in interpretations of functional connectivity measures across groups (Van Dijk, Sabuncu, and Buckner, 2012). Another source of variability is caused by our assumptions about the hemodynamic response of brain tissue. A typical step in fMRI analysis is to model the hemodynamic response by convolving the task design with a standard hemodynamic response function that is assumed to be constant, while it is known that this varies spatially across the brain and across individuals, especially with age. Rangaprakash et al. (2018) found that hemodynamic response function variability, if not accounted for, could lead to identification of false functional connectivity measures. Yet more noise sources include respiratory and cardiac cycles that influence blood flow and oxygen concentration and can result in global brain signal fluctuations that are not necessarily related to neuronal activity. These have been shown to lead to incorrect attribution of signal to brain activity if regional BOLD fluctuations are considered in isolation (Noll and Schneider, 1994), i.e. without regard to possibly confounding global signal correlations.

Given these aspects, it remains a continuous challenge to increase BOLD sensitivity and thus requires continuous and persistent efforts to find innovative solutions or mitigators. This is especially true for real-time fMRI analysis, where similar efforts to investigate denoising methods and the behaviour of the BOLD signal in their absence is sorely lacking.

2.4 Acquisition and denoising methods for BOLD improvements

Improvements to BOLD sensitivity can be approached via hardware, acquisition sequences, data processing and training or interventions. With hardware changes being the most expensive and cumbersome to implement, researchers often focus on more pragmatic options. Intervention methods are mostly implemented prior to or during an fMRI session and aim to minimise artefacts or prevent them from

adding noise to the data. This includes physical intervention such as the use of bite bars, foam pads or restraints to minimise motion (Green et al., 1994), training subjects to minimise movement and breathing fluctuations, or using end-tidal forcing systems to help subjects maintain stable breathing rates (Wise et al., 2004).

By far the most widely reported methods for improving BOLD sensitivity involve offline data processing, or "cleaning". Such methods typically take the form of model-based or model-free methods. Typical examples of model-based denoising or artefact removal steps include: slice-time correction, 3D motion correction, frequency band filtering, spatial smoothing, distortion correction, outlier removal/scrubbing (Siegel et al., 2014) , regression of movement parameter residuals (Friston et al., 1996), global signal regression (Power et al., 2017), and physiological noise regression (Glover, Li, and Ress, 2000; Birn et al., 2006). Model-free methods mainly include the identification and removal of artefacts through the use of region-based principal component analysis (PCA; Behzadi et al., 2007), and spatial independent component analysis (ICA; Perlbarg et al., 2007; Griffanti et al., 2014). Real-time fMRI denoising pipelines often prioritise processing time over gains in BOLD sensitivity resulting from all of the mentioned offline processing steps. As a result, real-time implemented steps typically only include those that are seen as essential, such as: 3D motion correction, frequency filtering, temporal filtering, and some forms of signal modeling and regression.

We can also improve BOLD sensitivity by adapting various parameters of the MRI acquisition sequence with which we acquire T2*-weighted images. Such examples include ways to address B0 field inhomogeneities (Gelderen et al., 2007; Balteau, Hutton, and Weiskopf, 2010; Bollmann et al., 2017), implementing sequences to reduce susceptibility-induced artefacts (Glover and Law, 2001; Deichmann et al., 2002; Weiskopf et al., 2006), increasing BOLD sensitivity through parameter optimisations or alternative acquisition sequences (Posse et al., 1999; Mathiak et al., 2002; Triantafyllou et al., 2005; Bodurka et al., 2007), and optimising for imaging of specific regions (Bellgowan et al., 2006; Weiskopf et al., 2007a; Morawetz et al., 2008).

An acquisition (and accompanying analysis) method that has received increasing attention over the past decade due to its proven benefits for BOLD sensitivity in offline use cases, and one which we explore in-depth in this thesis, is multi-echo fMRI.

2.5 Multi-echo fMRI

Fundamentally, multi-echo fMRI allows improved brain-wide BOLD sensitivity by sampling multiple T2*-weighted images at distinct echo times following a single transverse excitation pulse, i.e. once per repetition time (TR), as depicted in Figure 2.3. This theoretically allows the optimum BOLD contrast to be achieved for a range of baseline T2*-values, as opposed to standard single echo fMRI which optimises its single snapshot for an average grey matter T2*-value.

In offline analysis, echo combination is a critical step that has been imple-

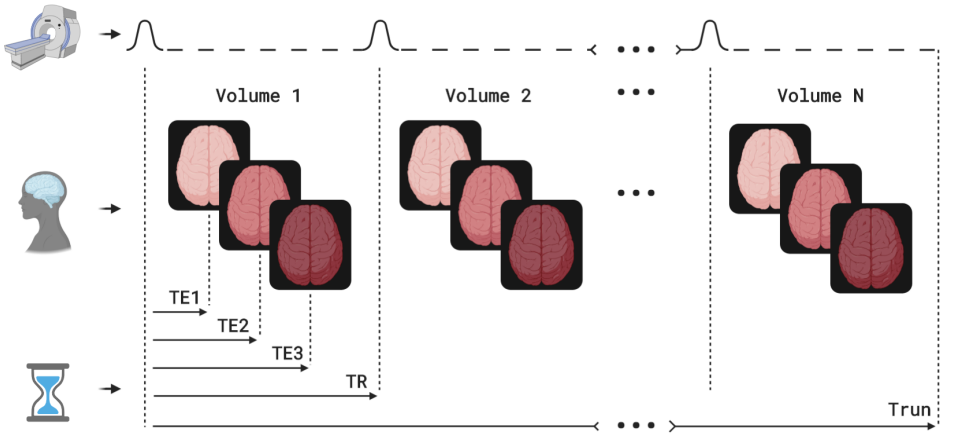

Figure 2.3 — *A depiction of three echo images acquired at distinct echo times (TE1, TE2, TE3) per volume, i.e. within a single repetition time (TR). Transverse pulses are repeated per volume, leading to a multi-echo fMRI time series with amount of volumes = N and run time = Trun.*

mented since the inception of multi-echo fMRI. It uses (weighted) summation or averaging to combine all the echoes following a single excitation, which generally increases temporal signal-to-noise ratio and decreases signal drop-out in highly affected regions, and has been reported to improve activation extent for task-analysis (Poser et al., 2006). Data driven methods such as multi-echo independent component analysis (MEICA) introduced by Kundu et al. (2012), have shown promise in separating BOLD and non-BOLD effects for time series denoising purposes. Several studies have shown benefits of MEICA-based denoising for both resting state (e.g. Olafsson et al., 2015; Dipasquale et al., 2017) and task-based fMRI data (e.g. Lombardo et al., 2016; Gonzalez-Castillo et al., 2016).

With access to multiple data samples along the decay curve, multi-echo also allows quantification of relaxation parameters T2* (the decay time constant) or R2* (its inverse, decay rate), and S0 (initial net magnetisation). This form of quantitative T2*-mapping, such as described by Weiskopf et al. (2013), is a known technique that uses a gradient-echo echo planar imaging (EPI) sequence to acquire multiple closely spaced echoes, followed by a data fitting procedure that yields a static, baseline T2*-map. In the context of functional MRI, temporal or per-volume T2*-mapping adds the benefit of quantifying T2* and S0 changes (from baseline) during stimulated neuronal activation. This estimation and separation enables us to distinguish fluctuations in local T2* relaxation effects, that are largely (although not completely) influenced by neuronal activity, from other fluctuating magnetisation factors such as hardware instabilities, subject head motion, or inflow effects that are not of interest, thus improving BOLD sensitivity. Importantly, the ability to quantify and separate T2* and S0 changes per volume (see Figure 2.4) makes multi-echo analysis, and the benefits that it holds, a promising option in real-time analysis.

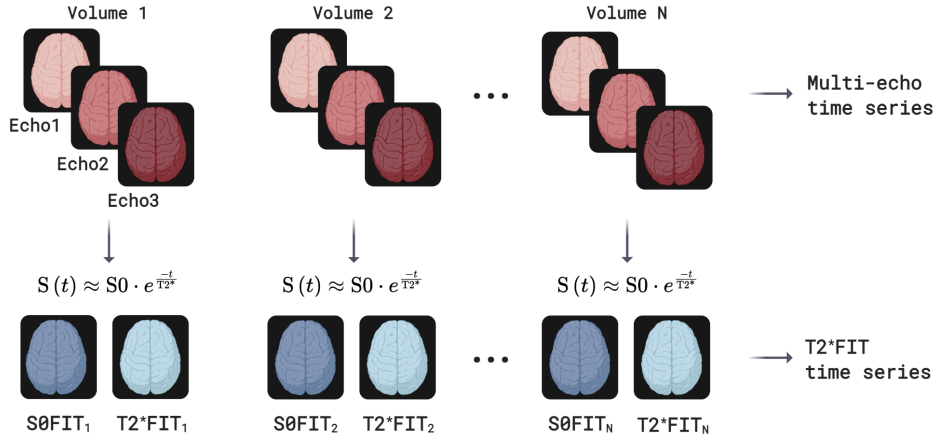

Figure 2.4 — *The rapid mapping of T2*FIT and S0FIT parameters (bottom row) per volume of a full multi-echo fMRI time series (top row). For each volume (and within the span of a single TR for real-time use cases) the decay parameters are calculated via log-linear regression of the three echoes to the mono-exponential decay equation. This allows tracking the per-volume fluctuations of T2*, yielding potential improvements in real-time BOLD sensitivity.*

Initial implementations of multi-echo fMRI sequences had to manage trade-offs with spatial resolution, temporal resolution and an adequate field of view due to earlier hardware or software restrictions and the strain on resources caused by acquiring extra echoes. As such, multi-echo images often had lower spatial resolution, longer repetition times and smaller brain coverage compared to conventional single-echo images, and were not prone to wide implementation in real-time use cases. However, with technological advancements over the past decade such as increased processing power incorporated into scanner hardware, faster image reconstruction algorithms, image acceleration methods, and parallel imaging techniques, whole-brain multi-echo fMRI has become as feasible as standard single-echo acquisition at comparable spatial and temporal scales.

2.6 Real-time multi-echo fMRI

Real-time use cases of multi-echo data have also been reported in literature. Posse et al. (1998) developed a single-shot, multi-echo spectroscopic imaging sequence that quantified region-specific T2* changes during olfactory and visual tasks, and which reported a larger functional contrast (up to 20% increase in the visual cortex) compared to standard EPI data. Several developments followed course, including measuring single-event related brain activity (Posse et al., 2000), whole brain T2*-mapping at 1.5T using a linear combination of echoes (Hagberg et al., 2002), later with added gradient compensation (Posse et al., 2003b), and a multi-echo EPI sequence at 3T with real-time distortion correction (Weiskopf et al., 2005). Rapid T2*-mapping has also been a useful tool in studying the interplay between cerebral blood flow, blood volume and blood oxygenation, particularly in

combination with contrast agents (see, for example: Scheffler et al., 1999; Schulte et al., 2001; Pears et al., 2003). In real-time fMRI neurofeedback, some examples of multi-echo use are reported specifically for improving signal gains in regions such as the amygdala, including Posse et al. (2003b) which uses T2*-weighted echo summation and Marxen et al. (2016), which uses scalar TE-dependent weights pre-selected to yield an average T2*-value of 30ms in the amygdala.

Apart from the mentioned examples, multi-echo developments and their benefits for real-time data quality remain underexplored. Consequently, the exploration of real-time multi-echo fMRI acquisition and analysis methods forms a core part of this thesis.

Chapter 3 Quality and denoising in real-time fMRI neurofeedback: a methods review

Abstract

Neurofeedback training using real-time functional magnetic resonance imaging (rtfMRI-NF) allows subjects voluntary control of localised and distributed brain activity. It has sparked increased interest as a promising non-invasive treatment option in neuropsychiatric and neurocognitive disorders, although its efficacy and clinical significance are yet to be determined. In this work, we present the first extensive review of acquisition, processing and quality control methods available to improve the quality of the neurofeedback signal. Furthermore, we investigate the state of denoising and quality control practices in 128 recently published rtfMRI-NF studies. We found: (i) that less than a third of the studies reported implementing standard real-time fMRI denoising steps; (ii) significant room for improvement with regards to methods reporting; and (iii) the need for methodological studies quantifying and comparing the contribution of denoising steps to the neurofeedback signal quality. Advances in rtfMRI-NF research depend on reproducibility of methods and results. Notably, a systematic effort is needed to build up evidence that disentangles the various mechanisms influencing neurofeedback effects. To this end, we recommend that future rtfMRI-NF studies: (i) report implementation of a set of standard real-time fMRI denoising steps according to a proposed COBIDAS-style checklist (Appendix B; `https://osf.io/kjwhf/`); (ii) ensure the quality of the neurofeedback signal by calculating and reporting community-informed quality metrics and applying offline control checks; and (iii) strive to adopt transparent principles in the form of methods and data sharing and support of open-source rtfMRI-NF software.

This chapter has been peer reviewed and published as: Heunis, S., Lamerichs, R., Zinger, S., Caballero-Gaudes, C., Jansen, J.F.A., Aldenkamp, B., Breeuwer, M., 2020. Quality and denoising in real-time functional magnetic resonance imaging neurofeedback: A methods review. Hum Brain Mapp hbm.25010. https://doi.org/10.1002/hbm.25010

3.1 Introduction

Real-time fMRI: Real-time functional magnetic resonance imaging (rtfMRI) involves the dynamic processing, analysis and visualisation of a subject's changing blood oxygen level-dependent (BOLD) signal and related information while the subject is inside the MRI scanner. It was initially proposed and developed by Cox, Jesmanowicz, and Hyde (1995) as a tool for real-time data quality monitoring, functional activation mapping and interactive experimental design. Since its inception this technology has expanded to include a variety of software tools that allow pre-experimental and pre-surgical functional localisation (Hirsch et al., 2000; Binder, 2011), real-time functional activity mapping (as is available in the software accompanying MRI systems from all major vendors), brain computer interfacing (e.g. Sorger et al., 2012), brain state decoding (LaConte, 2011), real-time neurofeedback (Sitaram et al., 2017), and interactive demonstrations for educational purposes (Weiskopf et al., 2007b).

3.1.1 BOLD self-regulation through neurofeedback

Neurofeedback training as an application of real-time fMRI (rtfMRI-NF) has gained much interest in the past decade due to its ability to help subjects achieve learned regulation of regional brain activation, as was initially demonstrated by Yoo and Jolesz (2002) in a motor task experiment. Interested readers are referred to Sitaram et al. (2017) for a recent review of rtfMRI-NF functionality, technology and applications. Shortly, by feeding a representation of quantified brain activity back to the subject in the scanner in near-real-time, and asking subjects to increase or decrease the presented metric by adopting one of several possible training strategies (or none at all), subjects have been able to regulate their own BOLD signal. This is evidenced by increased activation levels and cluster sizes in the areas of interest measured over multiple training sessions (see for example deCharms, 2007).

3.1.2 Clinical applications

In further steps, learned brain activity regulation through neurofeedback training has been used in neuropsychological and psychiatric disorders to test for behavioural correlates, aiming to investigate non-invasive rtfMRI-NF as an alternative to more invasive treatment modalities like pharmacological interventions, surgery or deep brain stimulation. Several studies have reported significantly beneficial behavioural, symptomatic or experiential changes after rtfMRI-NF training in a variety of clinical or other populations, including major depressive disorder (Linden et al., 2012), tinnitus (Emmert et al., 2017), attention deficit and hyperactivity disorder (Alegria et al., 2017), obesity (Spetter et al., 2017), and nicotine cravings (Canterberry et al., 2013).

3.1.3 Criticism and open questions

In order for rtfMRI-NF to show proven clinical utility and efficacy, reproducibility of methods, of results and of inferences are imperative[1] (Goodman, Fanelli, and Ioannidis, 2016; Munafò et al., 2017). Evidence for widespread and clinically significant effects of rtfMRI-NF training has however been called into question by recognising a lack of replication studies (Sulzer et al., 2013a), of blinded placebo-controlled study designs (Thibault et al., 2018) and of reproducible methods (Stoeckel et al., 2014). As an example, deCharms et al. (2005) showed in a pilot study that 8 out of 12 chronic pain patients (total N=36 subjects) could learn to regulate the BOLD response in the rostral anterior cingulate cortex, leading to significant changes in pain perception in this group.

However, their subsequent study assessing adverse events associated with repeated fMRI scanning (Hawkinson et al., 2012) found no significant changes with regards to baseline in adverse event reporting in pain patients undergoing multiple rtfMRI neurofeedback sessions (69 out of total N=114 patients). This apparent inability to replicate pilot findings in a larger sample size, which featured as a prominent discussion at the first Swiss rtfMRI Neurofeedback Conference (Decharms, 2012), suggests the need to re-evaluate current small-sample positive findings and incentivise the publication of null results, so as to counteract publication bias in neurofeedback literature.

Ongoing debate in the field still focuses on important and unanswered questions and challenges, many previously highlighted by Sulzer et al. (2013a). For example: how is neurofeedback learning and its success quantified, and is this quantification consistent enough to allow generalisation across studies? How do outcomes of active neurofeedback training perform compared to that of alternative and conventional treatment methods, and compared to outcomes of sham neurofeedback? Are perceived clinical benefits specific to certain populations, individual learning strategies, feedback calculation, feedback display, study design, data analysis, or other sources of variance? Widespread evidence to support specific, robust and reproducible findings for these research questions is still lacking, which should be seen as an incentive to improve methods reproducibility and to conduct large-scale replication studies investigating specific effects of rtfMRI-NF.

3.1.4 Methods reproducibility and quality

Central to several aspects influencing the reproducibility of both methods and results in rtfMRI-NF is the concept of quality, which pertains to real-time fMRI data, to the neurofeedback signal and to methods reporting. Take the assumption that the neurofeedback signal calculated from the real-time fMRI data aims to represent brain activity relating to the subject's ongoing cognitive processes (Koush et al., 2012). It is well-known that the resting state or task-induced BOLD

[1] To prevent ambiguous interpretations of the more general terms "reproducibility", "replicability" and "repeatability", in this work we adhere to the definitions for methods-, results- and inferential reproducibility in the biomedical sciences proposed by Goodman, Fanelli, and Ioannidis (2016)

signal contains several scanner-, sequence-, subject- or experiment-related nuisance signals and artefacts (Murphy, Birn, and Bandettini, 2013; Power et al., 2014; Caballero-Gaudes and Reynolds, 2017; Liu, 2016). If such confounding factors are not sufficiently accounted for during acquisition or minimised through real-time processing, the feedback signal will remain confounded and will thus not sufficiently reflect brain activity of interest. This may lead to sham learning or to a nuisance signal being trained instead of the subject's BOLD response (LaConte, 2011; Koush et al., 2012), which affects reproducibility of results and inferences. Similarly, doubts about the quality of the feedback signal can exist due to the as yet unknown influences of feedback presentation (e.g. the widely used thermometer display versus a more naturalistic display or virtual environment) and feedback signal calculation (e.g. temporal smoothing parameters, signal scaling, and the way in which percentage signal change is calculated). Few studies in this field have meticulously investigated such detail. This, added to the lack of methods standardisation and best practices for methods reporting, hinders reproducibility and generalisability.

3.1.5 Research goal

The mentioned open questions, methodological uncertainties and lack of standardisation should guide efforts to move towards improved reproducibility in the field of fMRI neurofeedback. Specifically, a systematic effort is needed to build up evidence that disentangles neurofeedback training outcomes from placebo effects, that clarifies the efficacy of neurofeedback compared to existing treatments, and that demonstrates the specificity of neurofeedback effects while accounting for other sources of variance.

To support this effort, this work reviews the methods currently available to the researcher to improve the data quality and signal-to-noise ratio (SNR) of the rtfMRI-NF signal and of real-time fMRI data and studies in general. Specifically, we investigate three research questions:

1. What are challenges to effective denoising and improving quality in rtfMRI-NF?

2. Which steps have recent rtfMRI-NF studies taken to improve data quality and SNR?

3. Which methods for denoising data and improving data quality and SNR are available to the researcher studying rtfMRI-NF?

To preface addressing these questions, a background on the BOLD signal and its confounds and on the details of the calculated neurofeedback signal is provided. Although both acquisition and processing methods are covered in this work, focus is given to the latter. We conclude with a general discussion and future recommendations based on the reviewed literature.

3.2 Background

3.2.1 The BOLD signal, noise, artefacts and correction methods

A. The noisy BOLD signal

The T2*-weighted BOLD signal typically acquired using standard gradient-echo echo-planar imaging (EPI) in fMRI represents hemodynamic and metabolic responses, through a neurovascular coupling, to alterations in neuronal activity (Ogawa et al., 1998). It results from a complex interaction between neural metabolism, blood oxygen concentration (specifically the local concentration of paramagnetic deoxyhemoglobin), cerebral blood flow (CBF) and cerebral blood volume (CBV) (Logothetis, 2003).

Given its dependence on neuronal metabolism, cerebral blood flow/volume and the inherent properties of MRI (and the EPI sequence in particular), it should be no surprise that the BOLD signal has several confounds and remains difficult to isolate as a proxy for true neuronal activity (Diedrichsen and Shadmehr, 2005). fMRI is typically plagued by a variety of noise fluctuations and artefacts originating either from the subject, from the experimental conditions, from the inherent properties of the acquisition sequence, or from the scanner and its (interfering) environment.

B. Denoising the BOLD signal

Much research effort has been given to ridding fMRI of noise. These efforts can be divided into two main categories: acquisition and data processing. Acquisition methods typically entail pulse sequence alterations or MRI parameter choices that improve the BOLD sensitivity, increase SNR, or preempt and minimise the effects of artefacts that may occur during scanning. Data processing methods to remove noise have been widely reported and typically take the form of model-based or model-free methods. Examples of model-based denoising or artefact removal steps in fMRI preprocessing pipelines include: slice-time correction, 3D volume realignment, frequency band filtering, spatial smoothing, distortion correction, outlier removal/scrubbing (Siegel et al., 2014), regression of movement parameter residuals (Friston et al., 1996), global signal regression (Power et al., 2017), and physiological noise regression (Glover, Li, and Ress, 2000; Birn et al., 2006). Model-free methods mainly include the identification and removal of artefacts through the use of spatial independent component analysis (ICA; Perlbarg et al., 2007; Griffanti et al., 2014). For a thorough understanding of fMRI noise and denoising methods, readers are referred to in-depth reviews by Murphy, Birn, and Bandettini (2013), Power et al. (2014), Caballero-Gaudes and Reynolds (2017), Liu (2016), Kundu et al. (2017) and Power et al. (2018).

C. In the absence of noise correction

Studies have investigated the implications of not correcting sufficiently for (or ignoring) fMRI noise, confounds and artefacts. Head motion, for example, has been shown to result in false activity patterns when coupled to the timing of the task paradigm (Hajnal et al., 1994), to cause simultaneous decreases in long-distance

correlations and increases in short-distance correlations within functional connectivity networks (Power et al., 2012), and to cause problems in interpretations of functional connectivity measures across groups (Van Dijk, Sabuncu, and Buckner, 2012). The hemodynamic response function (HRF) is known to vary spatially across the brain, as well as between subjects and between studies (Huettel and McCarthy, 2001; Handwerker et al., 2012), but the time-to-peak in standard task-fMRI experiments is typically assumed to be 4-6s brain-wide. Gitelman et al. (2003) investigated this assumption and showed the importance of deconvolution prior to modeling psychophysiologic interactions when considering functional/effective connectivity measures across the brain. HRF variability was further explored in a recent study by Rangaprakash et al. (2018) which found that, if not accounted for, it could lead to identification of false functional connectivity measures. Noise sources resulting in global signal fluctuations (e.g. respiratory cycles) can also lead to incorrect attribution of signal to brain activity if regional BOLD fluctuations are considered in isolation (Noll and Schneider, 1994), i.e. without regard to possibly confounding global signal correlations.

Noise sources remain problematic whether fMRI data are considered in real-time or offline. It is therefore important when considering real-time fMRI to address these known noise fluctuations and artefacts so as to increase the BOLD SNR, and to consider the implications of not correcting for these nuisances.

3.2.2 Real-time fMRI

The vast majority of real-time fMRI implementations use single echo echo-planar imaging (EPI) as the preferred acquisition method, likely due to its prevalence in conventional functional imaging. Acquired slices are reconstructed on the MRI scanner hardware, and upon completion each functional image volume is typically exported and shared on a local network from where it is accessible by the real-time fMRI application software. Figure 3.1 illustrates a standard real-time fMRI setup, including components of a neurofeedback application.

A. Time frame definitions

The 'real-time' time frame is loosely defined to be the interval between two successive functional image scans, i.e. the repetition time (TR), indicating that the concept 'real-time' varies according to the application. Ideally, all required reconstruction, export and processing steps for each functional image should be completed sufficiently prior to or by the time the next image in the session is acquired, thus allowing the presentation of up-to-date image information to the researcher and/or subject. Given the nature of the HRF, real-time fMRI not only includes a delay of one TR typically used for data processing (reported to be 1-3s in standard rtfMRI-NF applications), but also a substantial delay due to the indirect measurement of neuronal activity (4-6s). As such, typical implementations of real-time fMRI often only allow a representation of brain activity about 5s or more after such changes occurred on a neuronal level, leading to the term 'near-real-time'. This definition is distinct from the same term used by some studies

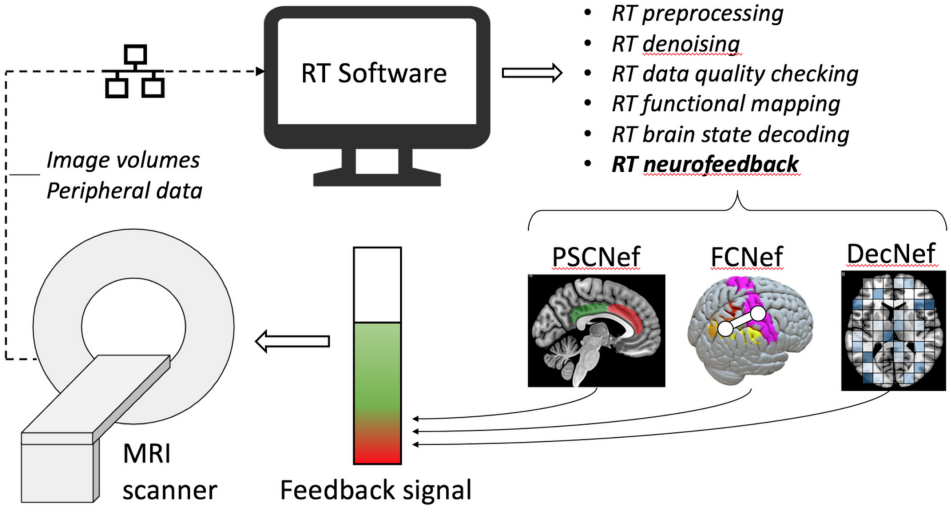

Figure 3.1 — *A typical real-time fMRI technical setup, showing detailed components of a neurofeedback application. DecNef, decoded neurofeedback; FCNef, functional connectivity neurofeedback; RT, real-time; PSCNef, percentage signal change neurofeedback.*

to refer to a real-time fMRI processing stream that delivers brain activity and other information within minutes after completing the functional scan session (e.g. Voyvodic, 1999). These time frame definitions assume a streamlined infrastructure for real-time fMRI volume reconstruction and export with negligible latency issues, which in reality will vary and could result in potentially serious synchronisation challenges.

Note that neurofeedback presentation does not have to be synchronised with image acquisition and can be updated continuously or intermittently depending on the fMRI acquisition rate, software implementation and experimental design. Differences between continuous and intermittent feedback can also influence the selection of online preprocessing and analysis strategies, as well as training goals and assumptions about the involved cognitive and neural processes. For such considerations, evidence from studies including Johnson et al. (2012), Oblak, Lewis-Peacock, and Sulzer (2017), Emmert et al. (2017), and Hellrung et al. (2018b) could be useful when selecting between feedback types. Real-time processing steps: The data processing steps necessary to derive a near-real-time representation of brain activity vary according to the application and implemented toolset, but typically follow the course of conventional task-based or resting state fMRI analysis, where data are first preprocessed to remove artefacts or noise fluctuations and then analysed with model-based or model-free statistical methods to extract information of interest. Real-time fMRI neurofeedback preprocessing typically consists of 3D volume realignment, spatial smoothing, linear or polynomial trend removal and temporal filtering, while few applications report the use of slice-timing correction, physiological noise correction methods or real-time distortion correction. These reported preprocessing steps are delineated further in Section 3.4 in this chapter.

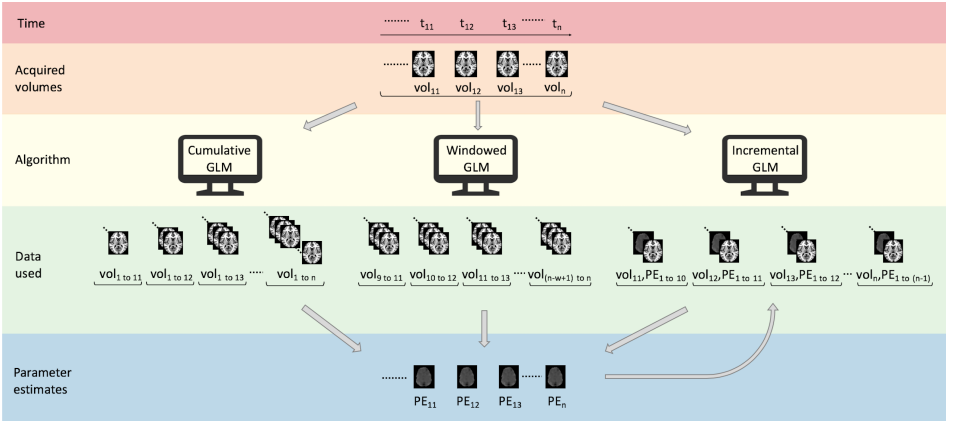

Figure 3.2 — *A representation of the three most commonly used real-time general linear model (GLM) algorithms, indicating the differences in how data available for each iteration are incorporated into the algorithms. A cumulative GLM (cGLM) uses all available data at each iteration to calculate the parameter estimates per iteration. A windowed GLM (wGLM) uses a window size of the most recent w (=3 in this example) volumes to calculate parameter estimates for a specific iteration. An incremental GLM (iGLM) incorporates volume data for each new iteration into an existing state. PE, parameter estimate; t, time; vol = volume.*

Univariate statistical analysis methods implemented in real-time include recursive correlation between voxel time-series and a reference vector (Cox, Jesmanowicz, and Hyde, 1995), t-tests (Voyvodic, 1999), multiple linear regression (Smyser et al., 2001), and general linear model (GLM; Bagarinao et al., 2003). Multivariate methods applied to real-time fMRI are less common, with the real-time implementation of a support vector machine classifier (SVM; LaConte, Peltier, and Hu, 2007) being the first example, and sparse logistic regression (Shibata et al., 2011) and sparse multinomial or linear regression (Shibata et al., 2016) being used for recent real-time pattern decoding.

B. Algorithmic adaptations

To decrease the required per-volume processing time, algorithms generally make use of sliding window (Gembris et al., 2000) or incremental approaches (Bagarinao et al., 2003) when analysing time-series data (see Figure 3.2). While time-windowed algorithms allow more sensitivity to temporal brain activity fluctuations by only analysing a recent subset of the acquired data, they are characterised by a decrease in statistical power (Weiskopf et al., 2007a), the converse being the case for incremental or cumulative algorithms that analyse all acquired data. A distinction is made here between incremental methods that use the data in each new iteration to update a growing statistical model so as to avoid recomputation (e.g. the incremental GLM developed by Bagarinao et al., 2003, that incrementally estimates and updates the coefficients of a GLM), and cumulative methods that repeat the operation during each iteration on all data acquired up to that iteration.

C. Computational advances

In general, real-time fMRI preprocessing and statistical analysis pipelines are simplified and/or optimised versions of their standard offline counterparts because priority is given to fast algorithms (those that converge in as few as possible iterations) and to the inclusion of the minimum sufficient steps to achieve an acceptable level of data quality, so as to decrease per-volume processing time. This trade off between maintaining a high level of method accuracy and minimising the required per-volume processing time has initially been a large constraint to expanding the complexity of real-time fMRI processing steps, but has become increasingly easier to manage with advances in modern computing technology and algorithm development. The use of parallel computing using clusters (e.g. Bagarinao et al., 2003), multiple processing cores (e.g. Koush et al., 2017a), and parallel cloud computing (Wang et al., 2016; Cohen et al., 2017), as well as the use of graphical processing units (GPUs; Eklund, Andersson, and Knutsson, 2012; Scheinost et al., 2013; Misaki et al., 2015), allow substantial decreases in required per-volume processing times and could accordingly afford real-time fMRI tools a comparative level of complexity and accuracy as that of their offline counterparts. New research avenues become possible like whole-brain real-time fMRI (Misaki et al., 2015), full correlation matrix analysis (Wang et al., 2016), and complex processing for more effective noise removal (Misaki et al., 2015). With such computing power advancements, research outputs become more dependent on how the researcher selects MRI sequence parameters and signal processing steps, and less so on per-volume time restrictions. This shift enables increases in real-time BOLD quality.

3.2.3 Real-time fMRI Neurofeedback

The rtfMRI-NF signal presented to the subject varies per study, but has been based on measures derived through three main computing methods: (1) BOLD activity percentage signal change typically in a single or differential region of interest (PSCNef), (2) functional connectivity between BOLD activity in multiple ROIs (FCNef), and (3) multivariate (or multivoxel) pattern analysis (MVPA), typically within a single ROI (DecNef).

A. Percentage signal change neurofeedback

The majority of volunteer and patient rtfMRI-NF studies have used a single or multiple ROI approach to calculate the feedback signal, specifically using the percentage signal change (PSCNef) of the spatially averaged signal obtained from all voxels within the defined ROI(s), as illustrated in Figure 3.3. Various regions of interest have been selected for different reasons, with the insula, amygdala, and the cingulate, auditory, visual and motor cortices often forming the basis for neurofeedback (Thibault et al., 2018). Regions of interest are most often acquired using a subject-based functional localiser run before neurofeedback commences (Weiskopf et al., 2007a), although template based or anatomical ROIs have also been used. Several important factors need to be accounted for when using single

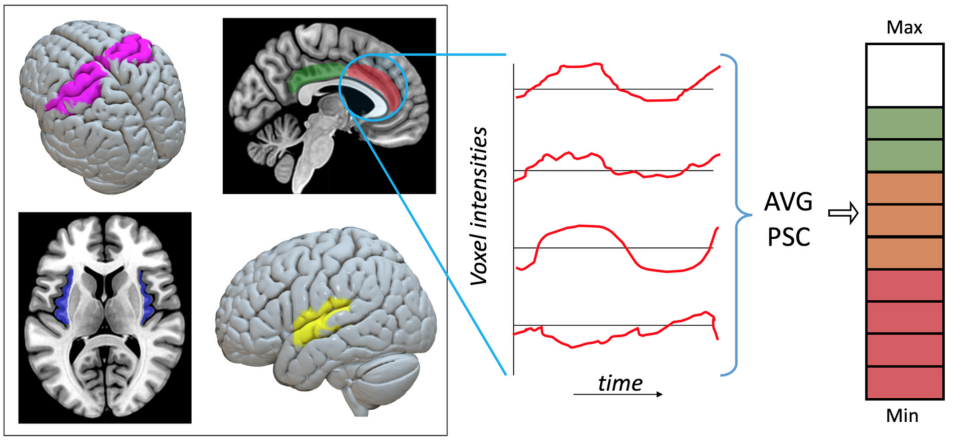

Figure 3.3 — *A linear neurofeedback signal (right) calculated as the average percentage signal change within the anterior cingulate cortex. Examples of other regions of interest are also displayed (left).*

ROIs as the feedback target. This includes increased signal dropout resulting from EPI imaging of lower or mid-brain regions (e.g. the limbic system or medial temporal region) due to increased magnetic susceptibility gradients near air/tissue borders, leading to lower BOLD SNR.

B. Functional connectivity neurofeedback

FCNef (Watanabe et al., 2017) was introduced to target applicable brain networks and their correlation rather than isolated activity in specific ROIs (Ruiz, Birbaumer, and Sitaram, 2013), and it has shown promise as an alternative to PSCNef. The principle is explained in Figure 3.4, where the average signal from different ROIs (in this case the motor and parietal cortices) are correlated across a moving time window to calculate the feedback signal. Various connectivity measures can be used as a basis for the neurofeedback signal, including Pearson's Correlation (Zilverstand et al., 2014) and Dynamic Causal Modeling (Koush et al., 2013). When using FCNef, care has to be taken to prevent global signal fluctuations from biasing the calculated connectivity measure (and thus the feedback signal), based on concerns raised by Power et al. (2012) and Van Dijk, Sabuncu, and Buckner (2012) that were highlighted earlier.

C. Decoded neurofeedback

Real-time fMRI multivoxel pattern analysis (also known as brain state decoding, decoded neurofeedback or DecNef, Watanabe et al., 2017) applies multivariate techniques to fMRI data, first by constructing a decoder using pre-neurofeedback session data with known task-modulation or states, which is then used in real-time to decode each acquired volume for similarity to the target brain state pattern (see Figure 3.5). Support vector machine (SVM) algorithms for real-time classification

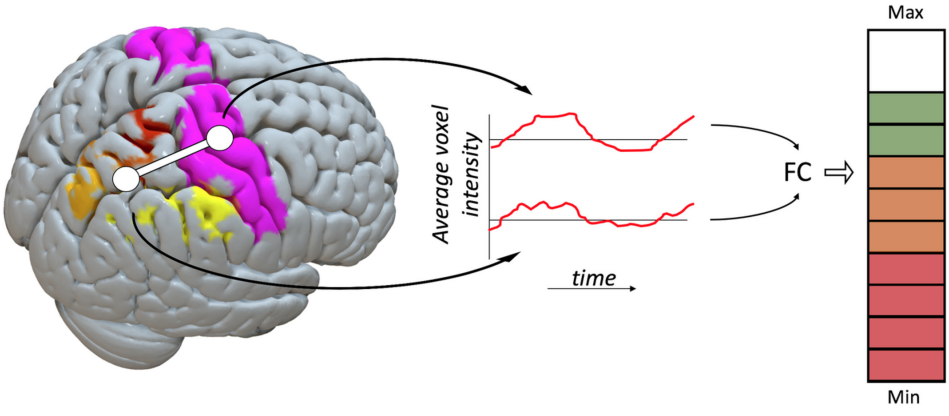

Figure 3.4 — *A linear neurofeedback signal (right) calculated as the functional connectivity (e.g. windowed Pearson's correlation) level between the motor and parietal cortex ROIs.*

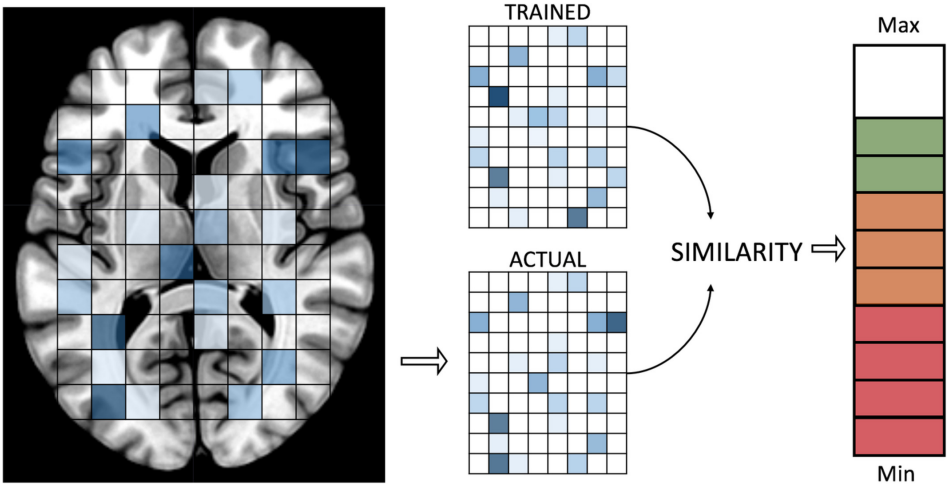

Figure 3.5 — *A linear neurofeedback signal (right) decoded as a representation of the similarity between voxel intensities in the trained pattern (resembling some known brain state) and the real-time brain voxel pattern.*

have been incorporated into several rtfMRI-NF toolboxes (AFNI - LaConte, Peltier, and Hu, 2007; Turbo-BrainVoyager - Sorger et al., 2010; FRIEND - Basilio et al., 2015). In addition, sparse logistic, sparse multinomial and sparse linear regression algorithms have been often used as decoders, depending on both the software implementation and the nature of the required neurofeedback signal (e.g. binary or linear). For further detail, LaConte (2011) and Watanabe et al. (2017) provide reviews of methodology and studies, respectively, using real-time fMRI DecNef.

For more examples of studies using these neurofeedback methods, readers are referred to Watanabe et al. (2017) and Thibault et al. (2018). Watanabe et al. (2017) explored advances in FCNef and DecNef based real-time fMRI, providing a list

of 9 studies using these methods, explaining concepts and listing new challenges and possible solutions in the realm of FCNef and DecNef methods. Thibault et al. (2018) conducted a critical systematic review of 99 rtfMRI-NF studies (mostly PSCNef) to evaluate the effectiveness of reported experimental protocols to train subjects to self-regulate their BOLD signal.

Apart from the feedback type and target region, several aspects of rtfMRI-NF can influence the ability of subjects to learn self-regulation of the neurofeedback signal (Kadosh and Staunton, 2019). Experiments need to take account of the advantages or disadvantages of, amongst others, the regularity of neurofeedback presentation (continuous vs intermittent), external rewards for learning outcomes, simultaneous visual display of task and feedback information, instructions given to subjects on learning strategy, variability in individual learning strategy of subjects, real-time data quality measures, and the use of control groups and blinding in order to reach the full potential of a rigorously designed and reproducible rtfMRI-NF experiment. Importantly, studies need to clarify these decisions (based on available evidence, pilot results, or sound reasoning) and report their choices transparently, in aid of the effort to delineate the multiple mechanisms and influences leading to neurofeedback learning and accompanying behavioural effects.

3.3 Quality in real-time fMRI neurofeedback

Quality is an umbrella term that is applicable to real-time fMRI data, to the neurofeedback signal and to the methods reporting process. Generally, fMRI data quality is a measure of how well the acquired BOLD data reflects the signal of interest, i.e. neural activity, and it is influenced by variability in multiple factors including the subject, the experimental design and acquisition (spatial resolution, image contrast, field strength, etc). If fMRI data quality is high, the implication is that signals that are not of interest (i.e. noise) are either absent from or not biasing our interpretation of the processed data, and there is lower possibility of making false inferences. This improves results and inferential reproducibility, and thus scientific progress. As an extension of fMRI data, high quality of the real-time fMRI neurofeedback signal implies that a signal closely reflective of brain activity (and not of noise or artefacts) is fed back to the subject in real-time. Quality in methods reporting implies that a published study contains enough information about the applicable experimental-, acquisition- and data processing steps that would allow different researchers to reproduce the methods. Here, high quality has a direct and beneficial influence on methods reproducibility.

When aiming to improve quality in real-time fMRI neurofeedback it is therefore advised to (1) separate the effects of noise (measurement-, system-, or subject-based) from true BOLD fluctuations, (2) quantify and report the quality of real-time fMRI data and the calculated neurofeedback signal, and (3) accurately and sufficiently report the use of applicable real-time fMRI denoising methods.

3.3.1 Measuring, comparing and reporting rtfMRI data quality

Traditionally, apart from expert visual inspection of fMRI datasets to identify low quality volumes / sessions / subjects / sites (as evidenced by visible artefacts in fMRI images like excessive motion, RF interference, or ghosting), the temporal signal-to-noise ratio (tSNR) has been an important quantitative measure of fMRI data quality and the ability of an experiment to find effects of interest (Parrish et al., 2000; Welvaert and Rosseel, 2013; Murphy, Bodurka, and Bandettini, 2007). tSNR gives an indication of the per-voxel signal fluctuations rated against the background noise fluctuations, with an example equation being:

$$\mathrm{tSNR} = \frac{\bar{\mathrm{S}}}{\sigma} \tag{3.1}$$

Here, $\bar{\mathrm{S}}$ and σ refer to the (per-voxel) mean and standard deviation of the fMRI time series, respectively. A variation of tSNR is the temporal contrast-to-noise ratio (tCNR; Geissler et al., 2007), which investigates the difference between functional contrast conditions (e.g. task activity vs. baseline activity) rather than considering signal fluctuations at all times. As such, tCNR could be defined as (Koush et al., 2012):

$$\mathrm{tCNR} = \frac{\bar{\mathrm{S}}_{\text{contrast}}}{\sigma_{\text{all}}} = \frac{\bar{\mathrm{S}}_{\text{condition}} - \bar{\mathrm{S}}_{\text{baseline}}}{\sqrt{\sigma^2}} = \left(\frac{\Delta \mathrm{S}}{\bar{\mathrm{S}}} * \mathrm{tSNR}\right) \tag{3.2}$$

The part of Equation 3.2 in brackets provides a common definition of CNR (Krüger and Glover, 2001), where ΔS is the signal change due to an experimental condition. Equation 3.2 thus assumes that $\bar{\mathrm{S}}_{\text{condition}} = \Delta \mathrm{S}$ and that $\bar{\mathrm{S}}_{\text{baseline}} = 0$

A simple fMRI quality inspection approach could be to compare the tSNR or tCNR values calculated before and after denoising to see if the change brings about a data quality increase. It should be noted that, depending on how noise and signal sources are defined spatially and on the type of condition and baseline choices, tSNR and tCNR values could vary and are not automatically standardised. Importantly, there is little consensus on a standard definition of tSNR and tCNR (Welvaert and Rosseel, 2013), which could hinder comparability between different sites and studies. Additionally, a single metric is unlikely to provide a full quantitative view of the quality of a complex signal such as fMRI, and further measures could be insightful.

A. Quality tools and methods

Historically, AFNI's real-time fMRI module (Cox, Jesmanowicz, and Hyde, 1995) supported the ability to display motion parameters to the subject in order the suppress head motion (Yang et al., 2005) and to feed back a display of variability in areas affected by physiological noise (e.g. ventricles) in order to reduce the standard deviation of the fMRI signal (Bodurka, Gonzales-Castillo, and Bandettini, 2009). These parameters can inherently also serve as real-time quality indicators.

More recent real-time quality tools include Framewise Integrated Real-time fMRI Monitoring (FIRMM; (Dosenbach et al., 2017)), which focuses on real-time motion tracking and related quality metrics, and rtQC, a recently presented open-source collaborative framework for quality control methods in real-time (Hellrung et al., 2017; Heunis et al., 2019b). rtQC currently focuses on highlighting quality issues between the offline and real-time variants of fMRI data as well as real-time visualisation of quality control metrics, including a real-time display of a grayplot (a 2D representation of voxel intensity fluctuations over time; Power, 2017).

B. Quality reporting practices

In further rtfMRI-NF literature, studies employing data quality checks focus on pre- and post-real-time application of quality control processes. Stoeckel et al. (2014) propose the calculation and use of tSNR and the concordance correlation coefficient on pilot data to determine, respectively, whether the rtfMRI-NF signal is detectable and reproducible between runs. They also proposed a list of seven high-level guidelines to help optimise real-time fMRI neurofeedback for therapeutic discovery and development: (i) the rtfMRI signal is accurate and reliable, (ii) rtfMRI neurofeedback leads to learning, (iii) the training protocol is optimised for rtfMRI-based neurofeedback and learning, (iv) there is an appropriate test of training success, (v) rtfMRI neurofeedback leads to behavioral change, (vi) an appropriate rtfMRI neurofeedback-based clinical trial design is in place, and (vii) sharing resources and using common standards. Sorger et al. (2018) provided a list of five criteria used for selection of custom feedback ROIs per subject: including (i) robust and typical hemodynamic response shown in ROI, (ii) high tSNR and tCNR, (iii) ample evidence for the ROI's involvement in the selected activation strategy, (iv) insensitivity to susceptibility artefacts, and (v) the ROI should consist of 10-15 neighbouring voxels spanning three fMRI slices. As post-real-time quality control, Koush et al. (2012) report the use of four quality metrics to evaluate their real-time denoising algorithms (tSNR, event-related tSNR, tCNR and statistical t-values), while Zilverstand et al. (2017) used mean displacement and tSNR to investigate offline data quality differences between control and test groups. Thibault et al. (2018) suggested a list of best practices for rtfMRI-NF studies spanning the whole process from study design to outcome measurement, including suggestions for: (i) study pre-registration, (ii) sample size justification, (iii) inclusion of control neurofeedback measures, (iv) inclusion of control groups, (v) collection and reporting of the BOLD neurofeedback signal, (vi) collection and reporting of behavioural data, and (vii) outcome measure definitions and reporting.

In this work, we propose both wider adoption of such best practices in rtfMRI-NF, as well as more granular specification of data quality measurement and reporting concerning the processing steps that could influence the quality of the signal being regulated.

3.3.2 Data quality challenges in rtfMRI-NF

Real-time fMRI is plagued by the same noise fluctuations and artefacts present in conventional task-based and resting state fMRI with the main difference being the required real-time removal of these confounds per volume, versus offline otherwise. This has to be achieved with an altered technical setup compared to the conventional approach. This time-constrained and technically novel scenario brings about a range of challenges, discussed subsequently.

A. Inseparability of data measures and subject regulation effects

A major challenge in assessing neurofeedback signal quality is the inherent mediation of the real-time signal by the process of neurofeedback training. This mediation effect, and in fact neurofeedback learnability itself, is highly variable within and between subjects and unlikely to be estimated or predicted accurately. This is known from neurofeedback based on electroencephalography (EEG), is referred to as the inefficacy problem (Alkoby et al., 2018), and appears to generalise across neuroimaging modalities. An estimated 15-30% of subjects are unable to learn control over brain computer interfaces (BCIs; Vidaurre and Blankertz, 2010), while in a review of psychological factors influencing neurofeedback learning outcomes, Kadosh and Staunton (2019) found attention, among other factors, to be crucial for neurofeedback learning success. The inability to reliably separate the rtfMRI signal into BOLD regulation effects versus noise (or noise-absent signal) makes standard quantitative measures like tSNR ill-suited to granularly assess the quality of the neurofeedback signal. Alternative measures or procedures become necessary, an example being the framework for offline evaluation and optimisation of real-time neurofeedback algorithms recently put forward by Ramot and Gonzalez-Castillo (2019).

Decreased statistical power

In offline fMRI denoising, data for the whole session is available and there is effectively no time limit on the processing, which respectively allows improved statistical power for noise detection and the execution of complex algorithms to model and remove noise fluctuations. Conversely, in rtfMRI-NF the statistical power is decreased, specifically in a moving window approach or during the start of a cumulative approach due to the small amount of data samples available. Additionally, the available calculation time in real-time is limited to the span of a single TR (in the standard case of continuous feedback), albeit mostly with fewer data to process. This means that rtfMRI algorithms can less likely detect true BOLD effects (or noise effects) as they occur, resulting in diminishing quality control of the rtfMRI-NF signal.

B. Lack of readily available peripheral measurements

Most scanner setups require custom modifications to hardware and/or software in order for extra physiological information to be transferred in real-time. For example, to our knowledge few reports exist of physiological data (respiration and heart rate) being transferred and incorporated into a rtfMRI-NF software pipeline

to remove physiological noise in real-time (e.g. Bodurka, Gonzales-Castillo, and Bandettini, 2009; Misaki et al., 2015; Hamilton et al., 2016). Addressing this challenge (technologically and algorithmically) could potentially be of substantial benefit to the quality of the neurofeedback signal, as it would diminish the possibility of subjects being trained on physiological nuisance signals (e.g. respiration effects) and would thus increase the contingency of the signal on actual brain activity.

C. Difficulty of real-time visual quality control

The neurofeedback signal is calculated and fed back to the subject immediately after the relevant preprocessing and analysis has been completed within a single TR, i.e. there is no time for an expert to inspect the volume, to assess its quality, and to perform conditional denoising steps, as opposed to offline fMRI quality control. However, this challenge provides an opportunity for rtfMRI-NF to improve computational/methods reproducibility, because a potential solution would be to have automated data quality inspection and control per volume. An example would be calculating framewise displacement (FD; Jenkinson et al., 2002; Power et al., 2012) per volume using real-time volume realignment (or head motion) parameters and automatically classifying the volume as a motion outlier or not based on some predetermined FD threshold. These outliers, in turn, could be added to a real-time motion outlier regressor in a cumulative or incremental GLM, to achieve real-time scrubbing, the results of which could be inspected and compared to offline counterparts after the rtfMRI experiment. Such functionality is currently available in rtQC (Heunis et al., 2019b).

D. Differences in quality between real-time and offline fMRI

Differences can occur in fMRI data that are reconstructed and transferred in real-time compared to offline exported data, including changes to spatial, image orientation, image intensity and temporal information. Whereas per-volume reconstruction and export timing (and related latency and jitter) are not critical for conventional fMRI analysis, they can cause substantial delays in real-time processing and feedback presentation. However, specific details such as the tools and software versions used for data export and the real-time latencies are rarely reported, which complicates reproducibility of methods. Additionally, differences in voxel intensity scaling, image orientation and image header information have been reported (Hellrung et al., 2017). Such issues, if known about at all, are hardly reported by rtfMRI-NF studies, even though it could lead to potential differences of interpretation when analysing online vs. offline data. Most rtfMRI-NF studies process data offline in order to show the effects of neurofeedback training over time, often looking at the t-statistic and clustering of significantly activated voxels in a region of interest. If this analysis is carried out on different datasets because of online-offline quality control issues, conclusions could vary.

Several methods, applied during acquisition and data processing phases as

well as offline, have been reported to decrease the detrimental effects of known fMRI noise and artefacts on the quality and SNR of the real-time BOLD signal. The next section investigates a set of 128 rtfMRI-NF studies to determine the prevalence of a variety of preprocessing steps in real-time fMRI pipelines, while the section thereafter focuses on the methods that address, at least in part, some of the mentioned challenges.

3.4 Denoising in real-time fMRI neurofeedback studies

A recent critical systematic review by Thibault et al. (2018) assessed 99 rtfMRI-NF studies in order to evaluate the effectiveness of reported experimental protocols to train subjects to self-regulate their BOLD signal and to induce behavioural improvements. The list featured a prominent set of the most recent rtfMRI-NF studies spanning a variety of patient groups and feedback signal types, and also included all 12 studies used by Emmert et al. (2016) in one of the only rtfMRI-NF meta-analyses conducted to investigate the mechanism of brain regulation resulting from neurofeedback. Apart from its main findings, the review by Thibault et al. (2018) showed that 62 out of 99 studies did not report any account being taken of respiratory confounds, that 19 studies subtracted activity in a background region to account for so-called global effects, and that 9 studies regressed out respiration-related noise signals in real-time. Respiration is known to be a source of global BOLD fluctuations and its removal is seen as a recommendable preprocessing step in conventional resting state fMRI processing (Bright and Murphy, 2013).

To facilitate further meta-analyses and systematic reviews, studies should not only ensure a high level of data quality (in terms of the real-time BOLD and neurofeedback signals) but also have to consistently and comprehensively report their use of acquisition and processing methods. A further search of rtfMRI-NF literature (including methods reviews) showed that rtfMRI-NF processing methodology has been covered in some detail (e.g. Weiskopf et al., 2004a; Bagarinao, Nakai, and Tanaka, 2006; Caria, Sitaram, and Birbaumer, 2012), but that real-time fMRI denoising methods have not received similar attention on a more granular level. To quantify the extent to which rtfMRI-NF studies report correcting for commonly known fMRI noise sources and artefacts, we investigated whether 128 recent studies[2] reported the use of a standard list of real-time preprocessing steps. We conducted a Web of Science search across All Databases on 9 April 2019 using the same search terms and selection criteria as provided by Thibault et al. (2018), and found another 29 studies in addition to the original 99. The list of preprocessing steps was selected based on established practices in conventional task-based and resting state fMRI (Poldrack, Mumford, and Nichols, 2011), as well as through identifying steps specific to rtfMRI-NF during the process of reviewing the 128 studies and further literature. The full text of each article, including supplementary material, were searched and coded for the following key terms: *averag**,

[2]Available at: `http://bit.ly/rtfmri-nf-zotero-library`

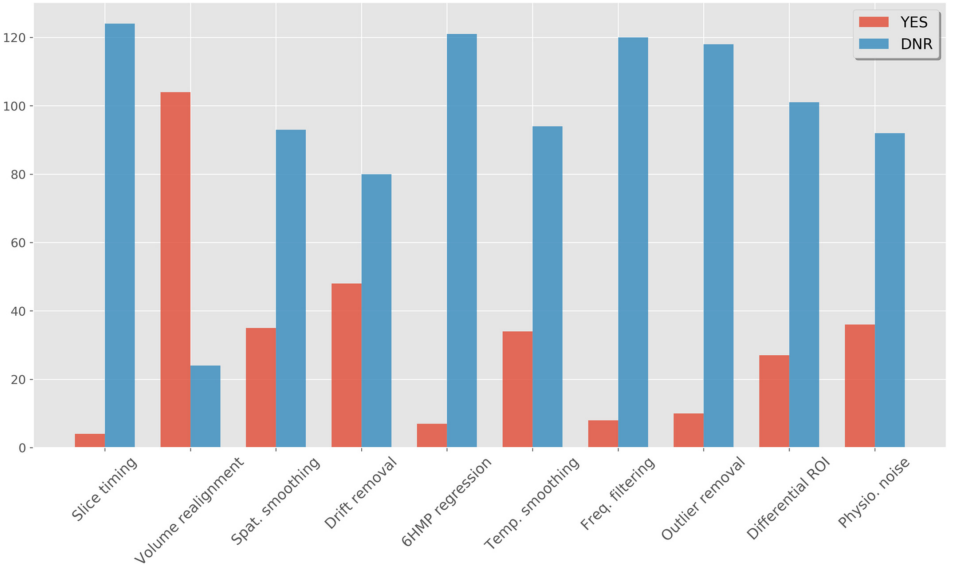

Figure 3.6 — *A list of real-time pre-processing and denoising steps used in 128 recent rtfMRI neurofeedback studies. (All bars are indicated as YES/red and DNR/blue while the breakdown for the bar 'Differential ROI' is 27 YES, 100 'DNR' and 1 'No', Marins et al., 2015). DNR, did not report.*

band, cutoff, difference, differential, drift, filter, frequency, heart, high, linear, low, motion, movement, nuisance, outlier, parameter, pass, physiol, respir*, retroicor, scale, scrub, slice, smooth, spike, trend*. All study DOIs and coded preprocessing steps are available as part of the accompanying Supplementary Material (JSON file, Tab Delimited Text files and Notes). Data and code necessary to reproduce Figure 3.6 and Figure 3.7 are available on Github[3], which also links to an interactive environment allowing exploration and visualisation of the study data.

Figure 3.6 shows the list of preprocessing and denoising steps and the amount of studies that report employing these methods. Importantly, we classified studies as Did Not Report (DNR) if no mention of the particular method was made in the article or supplementary material, and if we could not confidently infer its use from studying the particular article's content. A possible exception to this rule is volume realignment, which could reasonably be expected to be used in almost all recent rtfMRI-NF studies. Figure 3.6 shows that 24 out of 128 studies did not report applying volume realignment, and through investigating toolbox use (for a full distribution see Figure 3.7E) it was found that the majority of these used Turbo-BrainVoyager (TBV; Brain Innovation, Maastricht, The Netherlands), which does allow including this as a standard real-time preprocessing step. Similar discrepancies could be expected in the classification of studies as DNR for any of

[3] https://github.com/jsheunis/quality-and-denoising-in-rtfmri-nf

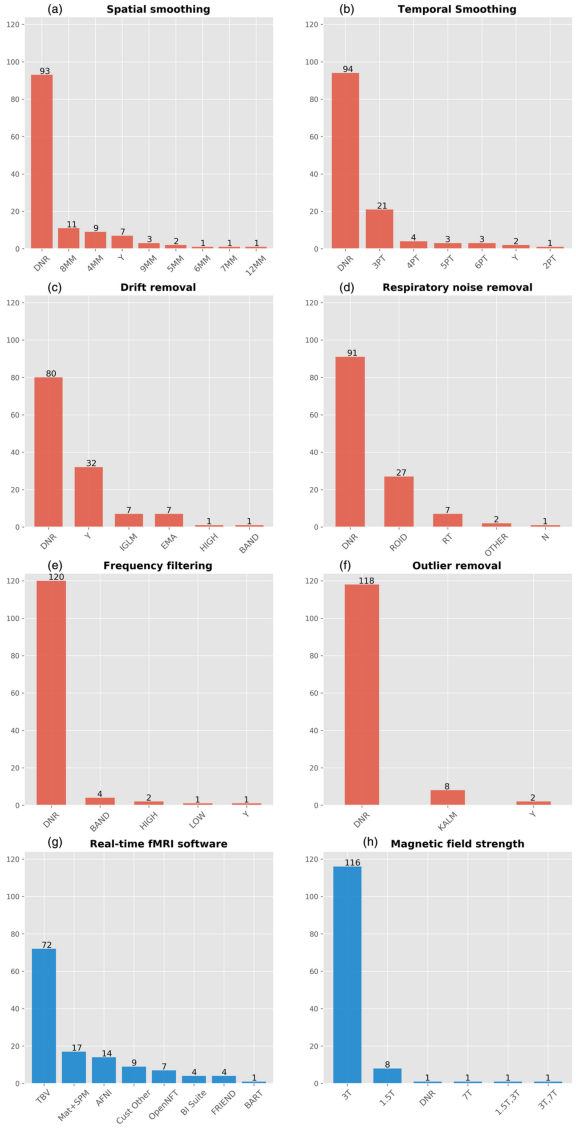

Figure 3.7 — *Bar graphs showing a breakdown of methods used for specific pre-processing and/or denoising steps in the 128 studies compiled in this work (red). The last two bar graphs (blue) indicate a breakdown of other features of the studies. (a) Spatial smoothing (4,5,6,7,8,9,12MM = FWHM size of Gaussian smoothing kernel). (b) Temporal smoothing through time point averaging (2,3,4,5,6PT = number of time points used). (c) Drift removal (EMA = exponential moving average filter; IGLM = incremental general linear model; BAND, HIGH = filter types). (d) Respiratory noise removal (ROID = differential region of interest; RT = real-time; OTHER = other methods including averaged compartment signal regression, e.g. white matter and/or ventricle signals). (e) Frequency filtering in addition to drift removal (BAND, HIGH, LOW = filter types). (f) Outlier removal (KALM = modified Kalman filter implemented in OpenNFT). (g) rtfMRI-NF software toolboxes (TBV = Turbo-BrainVoyager). (h) Magnet field strengths. DNR, did not report; N, no; Y, yes, but no further detail reported.*

the other denoising steps, although such discrepancies are expected to decline with the reported use of more non-standard or novel techniques (e.g. real-time physiological noise regression). To account further for possible discrepancies in the reporting of assumed default processing steps, we recoded the dataset such that studies that used mature and widely used software packages reflected default options where particular steps were not reported. The motivation for this step, the resulting figures, and accompanying limitations can be viewed in the Supplementary Notes. These findings highlight the importance of correctly reporting rtfMRI-NF denoising methods, so as to promote methods reproducibility.

Further results in Figure 3.6 show that volume realignment is the only step reported to be used by over half of the studies, while less than half report implementing linear drift removal and less than a third report the use of spatial smoothing, temporal smoothing and outlier removal. A special case of real-time denoising is correction for physiological noise, where multiple approaches have been used (Figure 3.7E). An often-used method is differential feedback (Weiskopf et al., 2004a), based on the assumption that global effects caused by respiration will be cancelled out when subtracting the averaged signal in a task-unrelated ROI from the main ROI used for neurofeedback. This also assumes that global respiration effects in both areas are identical. Still, two thirds of the studies do not report any correction for physiological noise (either in real-time or offline), while six studies use modeled physiological noise regression or data driven methods to remove noise fluctuations possibly caused by subject physiology (Thibault et al., 2018, reported nine due to a mischaracterisation of offline physiological noise regression as real-time regression in some cases). Additionally, it was also found that while several studies reported the use of optimised acquisition sequences to reduce susceptibility-induced image distortion (e.g. the spiral-in/out sequence by Glover and Law, 2001), only one study from the 128 reported incorporating post-acquisition distortion correction into their real-time algorithm (Marxen et al., 2016).

Finally, Thibault et al. (2018) noted a lack of both preregistration of rtfMRI-NF study designs and registered report type publications, as well as a lack of adoption of general open science principles. Although open source software solutions like AFNI's real-time plugin (Cox, Jesmanowicz, and Hyde, 1995), BART (Hellrung et al., 2015), FRIEND (Basilio et al., 2015) and OpenNFT (Koush et al., 2017a) counter some of these concerns, we find additionally that minimal evidence exists for open data and methods sharing. Specifically, apart from a large dataset on default-mode-network neurofeedback shared publicly by McDonald et al. (2017), a useful single-subject dataset for testing OpenNFT functionality and general methods development (Koush et al., 2017b), and further useful supplementary data shared in some cases (e.g. Zilverstand et al., 2017), we found no other publicly available rtfMRI-NF datasets related to the investigated studies.

3.5 Methods to improve signal quality and denoising

This section addresses the third research question of this review: *which methods for denoising data and improving data quality and SNR are available to the researcher studying rtfMRI-NF?* We consider acquisition methods and processing methods, focusing on the latter, and investigate current rtfMRI-NF algorithms and their capabilities with regards to the reported noise mitigation or denoising methods. Some offline methods for neurofeedback signal quality checking, although not strictly real-time, are also considered.

3.5.1 Acquisition methods

As with conventional fMRI, it is recommended that researchers take the necessary precautions to mitigate the introduction of any unwanted noise sources into the data. This includes the possibility of using physical interventions - e.g. individualised head restraints[4], bite bars, foam pads or end-tidal forcing systems - to counter head motion or respiratory rate variation artefacts, respectively, but also extends to tweaking pulse sequence parameters or implementing alternative sequences to increase BOLD sensitivity. Several pulse sequences, hardware changes and other acquisition steps are highlighted in the next section.

EPI, acceleration and high field imaging

The gradient echo EPI sequence still remains the most widely used technique for real-time fMRI, as it allows fast acquisition of volumes covering the whole brain. The main disadvantages of the EPI sequence are that it is sensitive to susceptibility effects and machine instabilities, although all major vendors offer techniques that compensate (partly) for these scanner effects.

The EPI sequence also allows for the acquisition of multiple echoes. The basic advantage of multi-echo over standard single-echo EPI is that it allows more data to fit an assumed mono-exponential decay curve, which can yield voxel-wise estimations of S0 (initial signal intensity, i.e. magnetisation) and T2* (transverse relaxation time, Posse et al., 1998). Increased BOLD sensitivity results when these spatially varying T2*-values are combined so as to leverage optimal BOLD contrast at each voxel, as opposed to assuming a single T2* for all grey matter voxels as per single-echo EPI processing. Posse et al. (1999) incorporated this advantage into their "TurboPEPSI" imaging technique for spectroscopic imaging, and later adapted it into the FIRE software toolbox for use in real-time fMRI (Posse et al., 2000), using linear echo summation. Further improvements led to the development of a method, using TurboPEPSI, for quantitative T2*-mapping as well as compensation of susceptibility related signal losses in multiple brain regions at different echo times (Posse et al., 2003b). Later, Weiskopf et al. (2005) implemented a real-time multi-echo EPI acquisition sequence that corrected for dynamic distortions along the phase-encoding direction without the need for additional reference scans (as per standard static B0 field correction techniques).

[4] `https://caseforge.co/`

The EPI sequence can also be combined with various accelerations techniques. The introduction of parallel imaging techniques, e.g. SENSE and GRAPPA, has contributed significantly to improved spatial resolution in fMRI, and has become standard in recent imaging applications. Also, advancements in acquisition speed using multi-band or 3D EPI techniques can improve temporal resolution as well as real-time SNR characteristics, e.g. as demonstrated by the multi-slab echo volumar imaging techniques of Posse et al. (2012) implemented in real-time. It should be noted, however, that the possible improvement in temporal resolution resulting from multi-band sequences must be balanced with the possible increase in image reconstruction time required if implemented on default scanner hardware.

Lastly, imaging at higher field strengths can improve SNR and BOLD sensitivity (Triantafyllou et al., 2005), both of which is beneficial to real-time fMRI neurofeedback. High field imaging at 7T could be particularly useful to overcome the lower SNR provided by 1.5T and 3T imaging in sub-cortical regions, as demonstrated by Sladky et al. (2013) for the amygdala, and by Hahn et al. (2013) for the insula. However, an important consideration for neurofeedback at 7T is that physiological noise increases with field strength and may dominate the BOLD signal of interest (Krüger and Glover, 2001), necessitating an appropriate denoising procedure. If accurately accounted for, however, the increased BOLD sensitivity at 7T could improve the quality of the neurofeedback signal, which would allow closer examination of the hypothesised coupling between learning effects and the neurofeedback signal. rtfMRI-NF at 7T has been implemented (e.g. Hollmann et al., 2008; Andersson et al., 2011) and compared to rtfMRI-NF at 3T (Gröne et al., 2015). The latter study found slightly greater increases in post-neurofeedback ROI activation in the 3T subject group compared to the 7T group. The difference was ascribed to a decrease in tSNR in the 7T group compared to the 3T group, due to several contributing factors including shimming conditions, B1-field inhomogeneities, phase-encoding polarity and physiological noise.

Alternative sequences and shimming

Alternative sequences or shimming practices have also been used to minimise the real-time image distortion or dropout artefacts related to local susceptibility gradients or other causes. A sequence developed by Glover and Law (2001) follows a spiral in/out readout trajectory of k-space that reduces signal dropout and increases BOLD contrast. Spiral-in has the advantage that it allows for higher temporal resolution, while spiral-out allows for short echo times which could also be an advantage in multi-echo denoising applications (e.g. when regressing the short echo signal out of the acquired data to remove proximal S0 effects;Bright and Murphy, 2013). Spiral in/out acquisition has been implemented by a number of rtfMRI-NF studies (Hamilton et al., 2010; Greer et al., 2014; Hamilton et al., 2016). Real-time shimming to account for geometric distortion has also been implemented. Here, Ward, Riederer, and Jack (2002) implemented a sequence to detect and correct for linear shim changes in real-time, while Gelderen et al. (2007) used a reference B0 scan and chest motion data to apply respiration-compensating

B0 shims in real-time.

Prospective motion correction and motion feedback

In addition to various MRI acquisition methods, prospective motion correction is another step that could increase SNR of the rtfMRI BOLD signal during the acquisition phase. Image-based motion detection (Thesen et al., 2000), field cameras (Dietrich et al., 2016) or external optical tracking methods (Zaitsev et al., 2006) have been used to estimate rigid body transformations and subsequently update pulse sequence parameters in real-time, such that the imaging volume essentially "follows" the subject's movement (Maclaren et al., 2012). Another method to curtail subject head motion is to feed back the head motion parameters (HMPs), derived from real-time head motion correction algorithms, to the subject. This in itself is a form of biofeedback training, and has been shown to reduce subject motion during scanning. In the case of Yang et al. (2005), head motion parameters resulting from real-time motion correction of functional image volumes were presented to subjects in the form of a composite 'head motion index', similar to framewise displacement. Greene et al. (2018) used FD as the feedback measure in their implementation using FIRMM software. Importantly, the implications of feeding back several measures to the subject and displaying them together with task instructions have to be properly understood and weighed before deciding on its use.

Adaptive paradigms

Adaptive paradigms provide interventions at a variety of stages in the acquisition and processing pipeline and allow selective data acquisition or presentation based on subject-specific measures and a predefined set of criteria. For example, Wilms et al. (2010) developed a system where real-time eye-tracking data could be used to generate gaze-contingent stimuli during fMRI experiments, while Hellrung et al. (2015) created an integrated, open-source framework for adaptive paradigm design, which also allows the dynamically updated design (based on a gaze direction-contingent assessment in their pilot experiment) to be transferred to the real-time GLM for adaptive processing. Such interventions could improve data quality and SNR by earmarking the volumes during which the subject adhered to selected quality control criteria.

Peripheral data collection

Lastly, the collection of peripheral subject data (e.g. heart rate, respiration rate, motion/eye tracking) for denoising purposes is strongly recommended. While it may not always be possible to correct for physiological noise or motion in real-time using these measures (given technical constraints or other reasons, see the following section) they should at least be used offline to calculate and comment on correlations with BOLD fluctuations, task design or other subject-related or experimental confounders.

3.5.2 Processing methods

As previously mentioned, real-time denoising methods tend to follow the course of standard offline fMRI preprocessing, although reports on the use of individual steps vary. Section 3.4 provided a list of real-time preprocessing or denoising steps employed by recent rtfMRI-NF studies, with Figures 3.6 and 3.7 indicating their relative usage. These methods are presented next together with other techniques identified through further literature search.

To aid the reader's understanding and guide future use of these methods, Table A.1 in Appendix A summarises the most often reported real-time processing methods. In addition, Table A.1 provides context for analogous methods in conventional fMRI analysis, how the real-time methods differ from their offline counterparts, and recommendations for deciding on implementation. Table A.1 focuses on processing methods since there would mostly be no differences between acquisition methods implemented to improve data quality for real-time versus conventional fMRI. It should be noted, however, that some artefacts like electromagnetic spikes or shimming errors could be of greater importance for real-time analysis compared to conventional fMRI analysis, since they could possibly be compensated for offline. This possibility does not exist for neurofeedback applications, hence extra care should be taken at the acquisition stage to try and avoid such artefacts. Table A.1 also lists possible approaches to this challenge using real-time processing methods.

Distortion correction

Geometric distortion effects, if addressed, are mostly accounted for using specialised acquisition methods as presented in the previous section, although correction through real-time processing is possible. An example is the point spread function (PSF) mapping approach developed by Zaitsev, Hennig, and Speck (2004) that is used in combination with parallel imaging techniques to allow fast and fully automated distortion correction of EPI. Note that this was implemented on scanner infrastructure and not as part of an external real-time fMRI software toolbox, and that it requires a reference PSF map scan. This method was used in a rtfMRI-NF study at 3T with multi-echo EPI by Marxen et al. (2016). Another example is the dynamic, multi-echo distortion correction sequence implemented by Weiskopf et al. (2005), also implemented on scanner infrastructure.

Slice timing correction

Slice timing correction interpolates the data of different 2D slices acquired at slightly different time points along the hemodynamic response, such that the resulting 3D image represents brain activity sampled at the same time point (Sladky et al., 2011). It has been suggested that event-related analysis in fMRI is relatively robust to possible slice timing problems in sequences with a TR 2 s (Poldrack, Mumford, and Nichols, 2011). With dynamic causal modeling (DCM), whose initial formulations assumed a single time point sampling of all 2D slices in an fMRI volume, Kiebel et al. (2007) showed with simulations that exclusion of slice tim-

ing correction leads to larger deviations from the true connectivity parameters. They showed further that this problem is easily overcome by including information about temporal sampling in the dynamic causal model (explicitly as an extra model level). While Koush et al. (2017a) do not include slice-timing correction in their pipeline, they specifically mention selecting a short repetition time (1100 ms) to limit the effects of slice-timing differences in their implementation of DCM-based neurofeedback.

Although some rtfMRI-NF toolboxes allow real-time slice timing correction through plugin or additionally developed functionality (e.g. OpenNFT, TurboBrainVoyager), few rtfMRI-NF studies report its use (Harmelech et al., 2013; Harmelech, Friedman, and Malach, 2015), which might be explained by reporting discrepancies or by the generally short TR used in typical neurofeedback studies. To our knowledge, no studies have been conducted to determine its usefulness in rtfMRI-NF.

3D volume realignment

As one of the major noise sources in fMRI, head motion received much attention during initial algorithm development in real-time fMRI. Cox and Jesmanowicz (1999) developed a fast method for 3D image registration in real-time that was incorporated into AFNI's real-time fMRI module (Cox, Jesmanowicz, and Hyde, 1995), while Mathiak and Posse (2001) developed the EMOTIONAL FIRE algorithm to perform 3D rigid body realignment as part of the FIRE rtfMRI package (Gembris et al., 2000). Most other rtfMRI-NF toolboxes or custom software implementations allow some form of 3D volume realignment, e.g. OpenNFT (Koush et al., 2017a) which uses a faster version of SPM12's *spm_realign* routine[5], or FRIEND (Basilio et al., 2015) that incorporates FSL's MCFLIRT algorithm[6].

Regression of the six head motion parameter time courses (and their framewise derivatives and/or squares derived by Volterra expansion) is a typical step used in conventional fMRI preprocessing to correct for residual motion effects (Friston et al., 1996). This can be implemented in the incremental or cumulative GLMs typically used in real-time fMRI, and some studies have reported its use (Hamilton et al., 2016; Harmelech et al., 2013; Harmelech, Friedman, and Malach, 2015; Kim et al., 2015; Yamashita et al., 2017).

Spatial smoothing

Spatial smoothing of fMRI volumes with a Gaussian kernel is typically recommended to increase the SNR for detection of signals with a spatial extent larger than a few voxels (Poldrack, Mumford, and Nichols, 2011). Given that the neurofeedback signal is typically derived (per volume) from averaging the signal intensity over multiple voxels within an ROI, a basic form of spatial smoothing is inherently applied. It could be argued that this negates the need for an extra spa-

[5]See SPM: `www.fil.ion.ucl.ac.uk/spm`

[6]See FSL: `https://fsl.fmrib.ox.ac.uk/fsl`

tial smoothing step in the real-time fMRI processing pipeline, but further research is necessary to determine this argument's validity. Numerous rtfMRI-NF studies report spatially smoothing their fMRI data before calculating the neurofeedback signal, while in some cases it might be explicitly excluded, e.g. neurofeedback based on MPVA of voxels within an ROI, or for small regions of interest like the amygdala imaged at high field strengths (Sladky et al., 2018).

Linear detrending / drift removal

Correcting for signal drift is a relatively standard step in real-time fMRI and could form part of the real-time GLM procedure, where a linear term and/or basis set of low frequency drift terms are included as regressors, acting as a high-pass filter. An inherent correction for baseline drift is also executed in some percentage signal change neurofeedback paradigms during feedback signal calculation, due to the cumulative global mean being subtracted from the averaged ROI BOLD signal (e.g. deCharms et al., 2005; Garrison et al., 2013). Most major rtfMRI-NF toolboxes allow some form of low-frequency drift correction. In a recent study, Kopel et al. (2019) compared the performance of commonly used online detrending algorithms with regards to their ability to eliminate drift components and artefacts without distorting the signal of interest. They found performance to be similar for exponential moving average (EMA), incremental general linear model (iGLM) and sliding window iGLM (iGLMwindow), although the latter option was proposed for future studies.

Temporal filtering or averaging

Further filtering of real-time fMRI data is possible, for example with the exponential moving average filter employed by Koush et al. (2012) to remove both high frequency noise and low frequency drift from the BOLD signal, or by including regressors relating to a specific frequency pass-band in the real-time GLM. Averaging of timepoints before calculating the neurofeedback signal, using a moving window approach, is another step implemented in several rtfMRI-NF studies (e.g. Young et al., 2014).

Outlier or spike removal

Removal or replacement of outlier volumes or data based on some quality criteria (whether defined visually or according to data calculations) is a method employed in conventional fMRI analysis to improve SNR (Power et al., 2014). Similar steps have been taken in real-time fMRI, for example in the BioImage Suite and custom MATLAB implementation of Garrison et al. (2013), where a volume is classified as an outlier and replaced by the previous volume if mean activation in the ROI differed by more than 10% from the previous measurement. Koush et al. (2012) implemented an adapted Kalman filter, by applying nonlinear modifications, that define outliers by their irregular statistical properties in order to achieve spike detection and high frequency filtering. This algorithm has been incorporated into the open-source OpenNFT toolbox as part of its standard real-time processing pipeline (Koush et al., 2017a). Additionally, the Kalman filter requires only the

current datapoint and previous state information, as opposed to all previous data points (or a subset thereof), and therefore does not add much latency to the real-time pipeline. Lastly, outlier rejection based on a standardised voxel intensity threshold has also been reported by McCaig et al. (2011), in which they exclude voxels with a standardised intensity of $z<2.0$ from the real-time ROI analysis in order to reduce noise associated with out-of-brain voxels and signal dropout.

Accounting for global effects through differential feedback

Feedback on the difference signal between ROIs has been motivated as a way to cancel out global effects like global intensity changes caused by respiration-induced artefacts (Weiskopf et al., 2004a; Weiskopf et al., 2004b; deCharms et al., 2004). In addition to the main ROI selected for neurofeedback, a reference or background ROI is typically defined as a task-unrelated axial slice or 3D ROI, in which the average signal is calculated and subtracted from the main ROI. Alternatively, defining the reference ROI as another task-related region allows subjects to attempt more specific bidirectional control of brain activity due to general regulation effects being cancelled out, for example using both the supplementary motor area and the parahippocampal place area as ROIs for PSCNef (Weiskopf et al., 2004b). These points have motivated several studies to opt for differential feedback over standard (non-differential) feedback, although a limitation would be that global effects may in fact vary substantially across the brain and that differential feedback might actually decrease SNR if activation related information is contained within the reference ROI (Marins et al., 2015). To our knowledge, no experiments have been conducted and published that investigate the relationship between differential feedback and SNR of the feedback signal, thus further research would benefit this area.

Physiological noise correction (respiration and heart rate)

Denoising physiological confounds has been approached in a variety of ways in rtfMRI-NF, even though most studies do not report any correction for physiological noise. In those that do, differential feedback is most often used as a potential correction method for global effects caused by respiration (although accompanied by previously mentioned caveats). Filtering can also remove some physiology-induced variance, with the modified Kalman filter by Koush et al. (2012) being a special case where high-frequency spikes resulting from changes in head position or breathing can be filtered out with no prior assumption about the specific noise model. Another option to remove physiology-related variance is to regress the spatial-averaged time course of compartments like white matter or the ventricles from the signal of interest, i.e. a real-time version of tissue-based nuisance regression as conventionally used in offline analyses. Spetter et al. (2017) calculated partial correlation of areas of interest with white matter and used these results to regress out any unwanted fluctuations before the neurofeedback signal was calculated, and Yamashita et al. (2017) included averaged signals from white matter, grey matter and CSF as nuisance signals in their real-time regression analysis.

Model-based approaches follow the work done by Glover, Li, and Ress (2000), Birn et al. (2006) and Chang, Cunningham, and Glover (2009) on retrospective image correction (RETROICOR), respiratory volume per time (RVT) and heart rate variability (HRV), respectively, where concurrent recordings of the subject's breathing and heart rate are used to create nuisance regressors used in subsequent real-time linear modeling. With physiological signal monitoring built into AFNI's real-time plugin (Bodurka, Gonzales-Castillo, and Bandettini, 2009), Misaki et al. (2015) implemented the first real-time RETROICOR and RVT physiological regression as an extension, using a GPU to denoise over 100k voxels (i.e. whole brain data) in under 300ms per volume. Hamilton et al. (2016) reported including two physiological noise regressors in their real-time regression analysis implemented in custom C/C++ and MATLAB, with no further detail provided.

Time synchronisation of peripheral recordings and fMRI data is a legitimate challenge to model-based correction of breathing and heart rate variability artefacts in real-time, unless the challenge is avoided altogether by using advanced processing power and full recalculation of all available data for every iteration, as was done by Misaki et al. (2015). Some global time-stamping solutions have been implemented to allow synchronisation of concurrent physiology and fMRI recordings (Smyser et al. (2001); Voyvodic (2011); Hellrung et al. (2015)). This typically requires a custom-programmed software package dedicated to managing time-synchronisation of multiple concurrent inputs and outputs, for example the CIGAL software (Voyvodic, 1999) which could run modules in parallel for the main stimulus event, a button-press hardware input, an analog data input for physiological recordings, the scanner trigger, eye-tracker recordings of eye position and pupil diameter, and more.

Lastly, we found no examples of studies investigating and comparing the efficacy of different real-time physiological noise removal strategies or their effect on the neurofeedback signal in rtfMRI-NF, although regarding offline correction, it has been suggested that motion or physiological fluctuations do not drive neurofeedback learning effects (Hellrung et al., 2018a).

Other real-time processing methods

Global signal regression, although a controversial denoising step in offline fMRI processing (Murphy and Fox, 2017), can be used in real-time to remove global fluctuations common to large areas of the brain and hypothesised to be of non-neuronal origin. This would typically involve including the cumulative global mean signal in the real-time GLM and regressing that out of the averaged ROI BOLD signal of interest, similar to CSF and white matter compartment regression.

Independent component analysis (ICA) has been a very effective tool in finding nuisance networks in resting state fMRI, which can be regressed out of the fMRI time series for effective denoising. Esposito et al. (2003) were the first to implement a real-time ICA algorithm using a sliding-window approach on a limited amount of axial brain slices, as a plugin to Turbo-BrainVoyager. Although this was used to generate quasi-stationary activation maps and accompanying time

courses, this demonstration sufficed to highlight the possibility of generating the spatiotemporal characteristics of nuisance signals for real-time denoising. This functionality, however, has not extended towards wider exploration or adoption.

Voxel efficiency scaling was proposed and implemented by Hinds et al. (2011) in their software toolbox Murfi as a way to avoid the undesired noise weighting resulting from standard direct averaging of all voxels within the neurofeedback region of interest. Rather, a z-score weighted average of the ROI voxels were used for neurofeedback signal calculation, which they found to result in increased SNR of the neurofeedback signal compared to a post-hoc calculation method as well as the standard direct averaging method.

Lastly, *multi-echo EPI processing* methods in real-time have also shown promise in increasing the SNR of the real-time BOLD signal, specifically in areas of the brain where the local T2* is not close to the standard EPI echo time of 30 ms selected for optimal BOLD contrast at 3T. The multi-echo acquisition methods reviewed earlier are typically accompanied by echo summation schemes that allow real-time increases in BOLD sensitivity. Posse et al. (2003a) implemented a fixed, linear, TE-weighted summation of echo signals, a processing scheme later also used by Marxen et al. (2016) in their neurofeedback study of the amygdala. After multi-echo image acquisition and real-time distortion correction of all echo images, Weiskopf et al. (2005) used a BOLD sensitivity curve for weighted combination. Several other combination schemes are possible (e.g. Poser et al. (2006)), and in related work we have investigated the comparative performance of various real-time combination schemes in terms of tSNR distributions (Heunis et al., 2019a). Further work is necessary to determine their comparative efficacy in terms of extended quality metrics important to rtfMRI-NF.

Further quality control of the feedback signal

Some methods do not consist of efforts to denoise the real-time BOLD signal of specific nuisance fluctuations, but rather to improve the quality of data acquisition or feedback presentation in real-time. Offline methods are also used as post-hoc data quality checks.

Temporally averaging and scaling the feedback signal are often used to prevent abrupt changes to the signal presented to the subject in real-time. For example, Garrison et al. (2013) used a sliding window of 5 volumes for temporal smoothing of the mean ROI activation intended for neurofeedback. OpenNFT (Koush et al., 2017a) uses a dynamic range, defined by the average of the 5% highest and lowest acquired activity time points, to scale the dynamic feedback signal.

Lastly, several quality control methods have been proposed to determine whether respiration or heart rate fluctuations may have had any significant effect on the neurofeedback signal calculation that could bias the data. These should be separated from real-time denoising algorithms which aim to remove the noise/artefact before the feedback signal is calculated and displayed to the subject. For example, Sorger et al. (2018) collect real-time cardiac and respiratory traces and analyse them after the neurofeedback session to investigate possible correlations

with the task design or other BOLD fluctuations. Physiological traces can also be incorporated into offline physiological denoising (e.g. RETROICOR) when assessing the BOLD signal for neurofeedback-induced changes over time (e.g. Sulzer et al., 2013b). In a 7T study investigating the influences of motion, heart rate, heart rate variability, and respiratory volume on amygdala self-regulation learning effects, Hellrung et al. (2018a) found that neither physiological fluctuations nor motion artefacts were driving factors in learning success. Even so, they did find notable differences in physiological measures between rest and regulation conditions within participants, and recommended the clear reporting of these measures alongside offline physiological noise correction.

3.6 Reporting practices revisited

Apart from summarising the processing methods used in 128 recent rtfMRI-NF studies, Figures 3.6 and 3.7 in Section 3.4 highlighted the likelihood that many of the studies' implemented methods remain unreported.

This challenge is not limited to the field of real-time fMRI neurofeedback and has indeed been described more generally for MRI, including efforts to address it. Nichols et al. (2017) aimed at understanding and improving good practice and reporting standards by creating the COBIDAS guidelines for conducting and reporting all aspects of MRI-based neuroimaging studies. Related approaches exist in fMRI neurofeedback research, e.g. in the form of the TIDieR checklist (Randell et al., 2018) for describing studies in standard terms of "diagnostic groups, dose/duration, targeted areas/signals, and psychological strategies and learning models". The CRED-nf checklist (Ros et al., 2020) is another laudable example that proposes a standardised checklist that outlines best practices for experimental design and reporting of neurofeedback studies.

Using our improved understanding of real-time fMRI neurofeedback processing methods from Section 3.5, as well as building on the existing work to improve reporting practices, we have created a COBIDAS-inspired template to aid researchers in reporting the methods used when calculating their feedback signals. This template checklist should act as a guideline, and we acknowledge that this is not an exhaustive list but one that could mature over time with community input. It was compiled in the vein of the COBIDAS best practice effort and would best be interpreted as an addition to the COBIDAS reporting guidelines for real-time fMRI. This template is displayed in Table B.1 in Appendix B, and an online version is also available[7].

3.7 Discussion, recommendations and future perspective

In this work, our goal was to shed light on the status of data quality challenges, denoising practices and methods reporting in the field of real-time fMRI neurofeedback. Prior studies in conventional fMRI have shown the implications of not

[7] https://osf.io/kjwhf/

sufficiently removing noise signals or not accounting for confounding effects (e.g. Gitelman et al., 2003; Van Dijk, Sabuncu, and Buckner, 2012; Power et al., 2012; Rangaprakash et al., 2018). We aimed to investigate this in the domain of real-time fMRI neurofeedback and present our findings such that researchers can be thoroughly informed about the quality of their neurofeedback signal of interest. The aim is to assist researchers in designing rtfMRI-NF studies that avoid (as far as possible) sham learning and, subsequently, incorrect inferences, and improves (as much as possible) the methods reproducibility of their work through transparent reporting.

3.7.1 Existing denoising methods: acquisition and processing

Literature showed that methods development during the past two decades has delivered multiple acquisition and processing methods to the researcher conducting a rtfMRI-NF study, implemented in the form of custom sequences and tools including Turbo-BrainVoyager, AFNI, OpenNFT, FRIEND and BART. For acquisition real-time shimming, spiral-in/out and multi-echo EPI (including multi-band) approaches show promise in reducing susceptibility induced geometric distortion and increasing BOLD sensitivity, and are recommended for future implementation.

From a processing perspective, real-time denoising pipelines showed high similarity to offline counterparts, although some tradeoffs are made because of the time limitation and the iterative nature of real-time processing. The effects of inclusion or exclusion of specific denoising steps in the real-time pipeline on the quality of the neurofeedback signal were found to be unexplored except for a single study (Kopel et al., 2019). Table A.1 summarised the available real-time processing methods and made conservative recommendations based on the available evidence, mostly commenting that methods should be piloted to determine their validity for each specific study. At a minimum, 3D volume realignment, drift removal, and signal scaling could be applied, while time-point smoothing, frequency filtering, and simple nuisance regression using an iGLM could be considered, provided that these methods are first piloted and their effects understood. Researchers are advised against implementing a real-time iGLM with too many nuisance regressors to avoid overfitting, regressor collinearity and noisy parameter estimates.

It remains difficult to make further empirically supported recommendations for specific denoising pipelines, apart from such general recommendations that are mostly based on evidence from conventional fMRI. This highlights the need for new methodological studies to quantify denoising step effects and compare pipelines. Collection of peripheral physiological data (e.g. heart rate, respiration rate, eye movements) is always recommended when possible, either to be used for real-time denoising or otherwise to rule out as confounds during offline analysis.

3.7.2 Quality control in real-time fMRI neurofeedback

Quality control and best practices in rtfMRI-NF is markedly unexplored and unreported compared to conventional fMRI, where initiatives like MRIQC (Esteban

et al., 2017), QAP (Project, 2014), COBIDAS (Nichols et al., 2017) support improved quality control and methods reproducibility. Although some studies report the use of best practices and data quality metrics to assess their neurofeedback signal (Koush et al., 2012; Stoeckel et al., 2014; Sorger et al., 2018; Zilverstand et al., 2017), it is unreported in the majority of the literature. Furthermore, other potential data quality issues like differences between offline and real-time acquired data, or geometric distortion unaccounted for during acquisition or real-time processing, could further skew the data, yet they remain unreported. It is our perspective that a concerted effort is necessary to establish a practical set of rtfMRI-NF quality metrics and methods that allow their calculation, visualisation, comparison and reporting. This could expand on the work proposed by Stoeckel et al. (2014) and Thibault et al. (2018).

3.7.3 Methods reporting and best practice adoption

Figure 3.6 showed that less than a third of the studies reported implementing slice timing correction, spatial smoothing, regression of head motion parameters, temporal averaging or filtering, outlier or spike removal, using a differential ROI to account for global effects, and further physiological noise correction. While this in itself is not necessarily indicative of insufficient data quality (recall the general absence of empirical evidence for methods recommendations), this low percentage of studies could still raise concern about the general quality of the real-time fMRI neurofeedback signal. Furthermore, it does indicate a problem with how methods are typically reported, which is an effective hindrance to methods reproducibility.

Ultimately, we should aim for future studies to have the required methodological rigour that allows delineation of the various mechanisms that could drive neurofeedback effects. This creates the imperative that we report accurately and transparently on acquisition, processing and any other steps taken to remove noise fluctuations from and improve the quality of real-time fMRI and the neurofeedback signal. As a starting point, studies could include a checklist reporting the implementation of the real-time processing steps listed in this work, as summarised in Appendix B. An online version of this COBIDAS-inspired checklist is also available[8].

3.7.4 Future perspective

Moving towards a scenario where the hypothesised usefulness of rtfMRI-NF in a clinical environment can be investigated and demonstrated transparently will require studies with reproducible methods and results. In light of this, we echo the recommendations made by Thibault et al. (2018) regarding reproducible science. Where possible, rtfMRI-NF studies with a clear hypothesis should be preregistered or follow a registered report submission process. Additionally, the continued use and development of open source software solutions based on widely used neuroimage processing tools, like OpenNFT (SPM), FRIEND (FSL) or AFNI's

[8] https://osf.io/kjwhf/

real-time plugin, are recommended together with data sharing on platforms like OpenNeuro[9]. In this way, both published data and methods can be queried by multiple researchers, paving the way for reproducible methods, results and inferences.

[9] https://openneuro.org/

Chapter 3

Part II: Hardware and software for real-time fMRI analysis and quality control

Chapter 3

Chapter 4 Neu3CA-RT: A Framework for Real-Time fMRI Analysis

Abstract

Real-time functional magnetic resonance imaging (rtfMRI) allows visualisation of ongoing brain activity of the subject in the scanner. Denoising algorithms aim to rid acquired data of confounding effects, enhancing the blood oxygenation level-dependent (BOLD) signal. Further image processing and analysis methods, like general linear models (GLM) or multivariate analysis, then present application-specific information to the researcher. These processes are typically applied to regions of interest but, increasingly, rtfMRI techniques extract and classify whole brain functional networks and dynamics as correlates for brain states or behaviour, particularly in neuropsychiatric and neurocognitive disorders.

In this chapter, we present Neu3CA-RT: a MATLAB-based rtfMRI analysis framework aiming to advance scientific knowledge on real-time cognitive brain activity and to promote its translation into clinical practice. Design considerations are listed based on reviewing existing rtfMRI approaches. The toolbox integrates established SPM preprocessing routines, real-time GLM mapping of fMRI data to a basis set of spatial brain networks, correlation of activity with 50 behavioural profiles from the BrainMap database, and an intuitive user interface. The toolbox is demonstrated in a task-based experiment where a subject executes visual, auditory and motor tasks inside a scanner. In three out of four experiments, resulting behavioural profiles agreed with the expected brain state.

The experience gained and algorithms generated through the process of developing this tool also allows further signal processing advancements such as real-time fMRI quality control, which is elaborated on in Chapter 5. This work also forms the baseline for the transfer and processing of multi-echo fMRI data in real-time, discussed in Chapters 6 and 7.

This chapter has been peer reviewed and published as: Heunis, S., Besseling, R., Lamerichs, R., de Louw, A., Breeuwer, M., Aldenkamp, B., Bergmans, J., 2018. Neu3CA-RT: A framework for real-time fMRI analysis. Psychiatry Research: Neuroimaging 282, 90–102. https://doi.org/10.1016/j.pscychresns.2018.09.008

4.1 Introduction

Real-time functional magnetic resonance imaging (rtfMRI) involves the online measurement of a subject's neural activity, indirectly, through the measurement of the blood oxygenation level-dependent (BOLD) signal. After preprocessing and analysing these data within the repetition time (TR) the researcher has access to these dynamic results while the subject is inside the scanner. This stands in contrast to conventional fMRI, where image processing is applied after the full set of fMRI scans has been acquired. Since the first published implementation of rtfMRI in 1995 (Cox, Jesmanowicz, and Hyde, 1995) the ensuing two decades saw a substantial increase of research interest and activity in this field. Advancements in medical imaging technology (reviewed by Cohen, 2001, Weiskopf et al., 2007b), computational algorithms (reviewed by Cohen, 2001, Weiskopf et al., 2007b, deCharms, 2007) and computer processing power allow increasingly faster and more advanced acquisition and processing of functional images and give researchers and clinicians access to data and results in real-time that would otherwise only be available hours, days or weeks after scanning (Weiskopf, 2012).

The application of rtfMRI, initially proposed as a tool to monitor data quality, to easily develop new task and stimulus protocols, and for use in interactive neurological experiments (Cox, Jesmanowicz, and Hyde, 1995), has expanded to include: real-time data quality assurance and patient compliance checking (Voyvodic, 1999), pre-experimental or pre-surgical functional localisation and intraoperative guidance (see for example Hirsch et al., 2000; Binder, 2011), neurofeedback studies and treatment (see Weiskopf, 2012; Christopher deCharms, 2008, Sulzer et al., 2013a, Sitaram et al., 2017, for extensive reviews), and teaching (Weiskopf et al., 2007b). Increasingly, applied rtfMRI is viewed as a useful diagnostic and treatment (navigation) tool in psychoradiology, a growing field described as the use of radiologic approaches for diagnosis, treatment planning and monitoring of patients with major neuropsychiatric disorders (Lui et al., 2016).

Apart from the basic real-time processing capabilities integrated into the hardware of all major MRI vendors, several proprietary, custom in-house and open-source rtfMRI solution sets or toolboxes have been developed at various locations worldwide. These include FIRE (Gembris et al., 2000) and TurboFIRE (Gao and Posse, 2003), scanSTAT (Cohen, 2001), AFNI's[1] real-time plugin (Cox, 1996), TurboBrainVoyager (Brain Innovation, Maastricht, the Netherlands; Goebel, 2012), STAR (Magland, Tjoa, and Childress, 2011), FRIEND (Sato et al., 2013), the FieldTrip toolbox's rtfMRI extension[2] (Oostenveld et al., 2011), BART (Hellrung et al., 2015) and more recently OpenNFT (Koush et al., 2017a). While these toolboxes allow a wide range of rtfMRI processing and neurofeedback signal calculation capabilities, most clinical studies reporting the use of rtfMRI (in particular most neurofeedback studies) have focused on analysing, visualising and feeding back activation changes for particular ROIs in the brain that are associated with the disorder or condi-

[1] See: `https://afni.nimh.nih.gov/`

[2] See: `http://www.fieldtriptoolbox.org/development/realtime/fmri`

tion being studied (see for example Alegria et al., 2017; Young et al., 2017; Ruiz, Birbaumer, and Sitaram, 2013; Subramanian et al., 2011; Nicholson et al., 2017). In most neuropsychiatric conditions, however, an array of complex brain functions such as cognition are affected, processes that are increasingly regarded as being mediated by synchronous activity across multiple brain regions (Mišić and Sporns, 2016). To improve learning effects in neurofeedback training experiments conducted in subjects with these conditions, the operant conditioning model requires feedback to be contingent on the brain mechanism believed to underlie the condition (Weiskopf et al., 2004a). Thus, it is hypothesised that a feedback signal calculated based on a model that reflects a richer understanding of the underlying neural mechanism could be an improved approach over ROI-based methods in cases where complex brain function is involved. To enable further development and testing of this hypothesis, rtfMRI toolsets and neurofeedback studies should expand to include a particular focus on the analysis of dynamic and spatially distributed brain activity, in addition to ROI-based approaches.

The dynamics and spatial distribution of functional brain networks at rest have been widely investigated and reported. Resting state networks tend to show separable spatial patterns with distinct temporal characteristics during rest- or task-based experimental paradigms (Beckmann et al., 2005). Differences in resting state network characteristics between subjects with neuropsychiatric disorders and healthy subjects have also been studied and used as the basis for potential biomarkers (see e.g. Whitfield-Gabrieli and Nieto-Castanon, 2012, for a review focusing on the default mode network). Recently, Karahanoğlu and Van De Ville (2015) applied temporal deconvolution and clustering techniques to resting state fMRI time series to yield spatially and temporally overlapping co-activation patterns. These iCAPs form dynamically assembling building-blocks for resting state networks, and each pattern has been associated with a consistent behavioural profile using the Brainmap database[3] (Laird, Lancaster, and Fox, 2005). These aspects, that is the spatially distributed and dynamic nature of the iCAPs patterns as well as their relation to behavioural brain state interpretations, suggest that they could be useful as targets for neurofeedback calculation in rtfMRI neurofeedback experiments relating to neuropsychiatric conditions.

In this article we introduce Neu3CA-RT, a MATLAB-based framework for rtfMRI analysis developed at the Neu3CA research group[4] at the Eindhoven University of Technology. Based on design considerations obtained from reviewing previous and current state of the art rtfMRI solutions and methodologies, we describe the experimental setup and image (pre)processing steps central to the framework. We present an exploratory rtfMRI analysis implementation, which is based on a dynamic spatial general linear model (GLM) fit of Karahanoğlu and Van de Ville's innovation-driven coactivation patterns (iCAPs) (Karahanoğlu and Van De Ville, 2015) to real-time fMRI data and the subsequent mapping to

[3] Available at: `http://www.brainmap.org/`

[4] `http://neu3ca.org/background/neu3ca/`

behavioural brain states. The method is demonstrated by subjecting a healthy control to several known behavioural paradigms and comparing the data-driven network analysis and behavioural interpretation to the expected brain state(s). We conclude by discussing the results and future work.

4.1.1 Design considerations for a rtfMRI toolbox

Several aspects of existing rtfMRI toolsets influence their performance and area of application. These include the particular technical infrastructure and imaging parameters, pre-real-time processing, pre-processing, image analysis, program execution time and software design. When assessing the performance of real-time toolsets, specific attention should be given to latency, i.e. the total delay of the real-time processing chain between image acquisition and availability of the analysis results, and the achievable throughput, i.e. the quantified output per time period (in our case, analysed images per second or, similarly, TR).

Particulars of how rtfMRI aspects have been implemented in existing toolsets, especially artefact correction and ROI and whole-brain processing algorithms, have been reviewed extensively elsewhere (Weiskopf et al., 2007a; LaConte, 2011; Caria, Sitaram, and Birbaumer, 2012). For the purpose of this work, important design considerations (and, where applicable, their influence on latency and throughput) are described in this section.

A. rtfMRI technical setup

The specifics of the MRI scanner, processing hardware and the accompanying rtfMRI software package are considered. In principle, rtfMRI should be achievable with any modern MRI scanner that has online image reconstruction and network communication capabilities, although custom development is typically necessary to facilitate transporting or sharing image data between scanner hardware and the device used for real-time processing, whether this is the scanner console or a network location. Dedicated development has also been done to integrate rtfMRI processing directly into scanner hardware 1995 (Cox, Jesmanowicz, and Hyde, 1995; Cohen, 2001; LaConte, Peltier, and Hu, 2007). Ideally, all major MRI vendor hardware should be able to export acquired images in real-time to a network location, from which the preferably vendor-agnostic rtfMRI software package would then collect and process the data. Both the Turbo-BrainVoyager and OpenNFT toolboxes employ such a server-client setup and are compatible with scanners from multiple MRI vendors. Neu3CA-RT has been implemented similarly, facilitated by real-time data transfer software developed in collaboration with Philips.

The technical setup extends from the scanner to external hardware and software. Firstly, rtfMRI packages need to be easily understood and easily adaptable to facilitate widespread use. As reported by Koush et al. (2017a), interpreted languages like MATLAB (MathWorks, Natick, Massachusetts, United States) and

Python[5] allow intuitive understanding and easier sharing of code and continued collaborative tool development by a wide-ranging and large user base. This is strengthened further by the existence of SPM [6], FSL [7] and AFNI [8], three of the most widely used platform-independent and freely available fMRI analysis libraries that can readily be incorporated into interpreted language programs. When optimising for widespread use and whenever possible, rtfMRI toolboxes should exploit these libraries and frameworks. While acknowledging that commercial tools like MATLAB provide barriers to unconditional dissemination of software tools and knowledge, our familiarity with the programming environment and its widespread use in research and educational institutions led to the initial version of Neu3CA-RT being based in MATLAB and using SPM12.

Secondly, the central or graphical processing unit (CPU or GPU) of a designated image processing computer needs to have enough power so as to minimise real-time latency while managing a trade-off between processing speed and all factors restricting increased processing power (these might include cost, logistical impediments and site-specific restrictions). To facilitate ease of implementation, a personal computer (PC) with 16GB RAM and a 4-core GHz-range processor is recommended for a rtfMRI setup like Neu3CA-RT. Increased processing power could be warranted if the resulting latency is too high for the desired throughput, while more complicated pipelining and parallelisation of real-time processes could be considered (either at application-level, computationally on a single PC or at hardware level on multiple machines) if throughput needs to be increased.

B. rtfMRI image quality considerations

Echo-planar imaging (EPI) is widely used in fMRI imaging sequences and provides a sound, although not exclusive, basis for rtfMRI. The use of multi-echo imaging sequences in real-time (Posse et al., 1999; Weiskopf et al., 2005) has been reported to remove image distortion artefacts and increase BOLD contrast sensitivity through weighted combination of multi-echo images. More recently, Kundu et al. (2012) implemented an independent component analysis algorithm (ME-ICA) on full multi-echo EPI datasets to yield significant gains in BOLD CNR. Importantly, imaging parameters like the field-of-view (FOV), voxel resolution, voxel matrix size, repetition time (TR) and echo time (TE) have to be refined so as to manage the tradeoff between increased spatial resolution, increased BOLD sensitivity, and shortened TR, while keeping the specific application in mind. Increased spatial resolution is beneficial when requiring rtfMRI output that is highly spatially localised, but this in turn requires more acquisition and processing time and thus increases latency. Similarly, a short TR (in reviewed literature, typically in the order of 2 s for ROI-based acquisition and real-time processing) is beneficial for more frequent real-time data visibility and neurofeedback, but simultaneously

[5] `https://www.python.org/`
[6] `www.fil.ion.ucl.ac.uk/spm`
[7] `https://fsl.fmrib.ox.ac.uk/fsl`
[8] `https://afni.nimh.nih.gov/`

compromises spatial resolution and constrains the amount of available dynamic calculation time, essentially requiring the real-time latency to be less than 2 s if the throughput is to be one analysed image per TR and no pipelining is used.

Selection of a short TR is further motivated by the need to identify distributed changes in BOLD signal response (from a predefined baseline) as soon as they occur. In a task paradigm the general haemodynamic response function characteristics are well established: an initial post-stimulus delay of 1–2 s and a peak at 4–6 s, reaching a plateau if the stimulus is sustained (Bandettini et al., 1992). For a controlled task time course with an expected response, less incentive exists for shortening the TR, but for the comparatively unknown dynamics of resting state fMRI data this is not the case. Here, more frequent sampling enables a real-time description of dynamic data, which is especially useful if this description needs to be acted on in real-time.

Real-time denoising or preprocessing is required to provide further image quality improvements. Previously implemented algorithms include those for image distortion correction, prospective or retrospective 3D motion correction, temporal filtering and spatial smoothing (reviewed by Weiskopf et al., 2007a). Prospective motion correction typically incorporates real-time data from optical motion tracking systems, such as described by Zaitsev et al. (2006), or is implemented to estimate and apply a 3D transformation during reconstruction of each EPI image. Other confounders of real-time BOLD activation are artefacts resulting from subject physiology like heartbeat and respiration, as well as EPI artefacts resulting from gradient coil heating and other scanner instability effects. Technical setup allowing, physiological data should be sent dynamically to the applicable rtfMRI toolbox for continuous monitoring (for example Voyvodic, 1999) and correction (for example Smyser et al., 2001).

In general, any imaging parameters or preprocessing approaches (such as those described here) that fundamentally improve the signal-to-noise-ratio (SNR) are important to improve spatiotemporal resolution and hence to reduce latency for a specified spatial resolution. However such approaches should themselves have limited latency to ensure that there is a net improvement in overall latency.

With the aim of acquiring and describing distributed BOLD activity in specific (sub)networks of the brain, the imaging parameters for current Neu3CA-RT experiments were selected to favour increased spatial resolution ($1.75 \times 1.75 \times 3$ mm per voxel, see Data Acquisition in the Materials and Methods section) over a short TR, resulting in a TR of 3 s which can be considered standard in a task-based paradigm.

C. rtfMRI image analysis considerations

Reviewed literature shows a wide variety of mass univariate and multivariate analysis algorithms being implemented in rtfMRI. Historically, statistical methods like t-tests, correlation analysis (Voyvodic, 1999), GLMs and multiple regression (for example Bagarinao et al., 2003) formed the basis of analysing single ROI activation or identifying artefacts in real-time. Thus researchers and clinicians

are able to view, for example, real-time ROI activation maps or real-time subject motion estimations.

In clinical applications, multiple rtfMRI studies have reported benefits of specific ROI-based neurofeedback as a treatment option in neurological and psychiatric conditions, such as ADHD, depression, schizophrenia, Parkinson's disease and PTSD (see Sitaram et al., 2017, for a review). For studying cognition-related aspects related to whole-brain networks, however, the methodological focus should include analysing spatially distributed and temporally dynamic brain activity. Accordingly, an increasing amount of rtfMRI algorithms using functional connectivity and multivariate pattern analysis (MVPA, also referred to as multi-voxel pattern analysis) have been published and made available in rtfMRI toolsets, including: windowed correlation (Zilverstand et al., 2014); dynamic causal modelling (Koush et al., 2013); spatial GLMs; independent component analysis (ICA) (Esposito et al., 2003); support vector machines (SVMs) (LaConte, Peltier, and Hu, 2007); and neural networks (reviewed by LaConte, 2011). Reviewed literature shows that, in the case of machine learning algorithms, the focus is increasingly on quantifying intuitive and interpretable brain states through classification, as opposed to quantifying the lower-level BOLD activation level of specific ROIs and using that for biomarker development or neurofeedback.

In the current version of our Neu3CA-RT framework, we implemented an exploratory functional network-based fMRI analysis pipeline that aims to quantify the real-time brain state of the subject by mapping dynamic and spatially distributed brain activity onto known co-activation patterns that relate to certain behavioural profiles. In a recent study, Karahanoğlu and Van De Ville (2015) developed the iCAP model of functional brain networks, which is based on a spatio-temporal regularisation of resting state fMRI data from healthy volunteers. It decomposes fMRI data into a set of 13 generic co-activation patterns (see Figure 2 of Karahanoğlu and Van De Ville, 2015) that can be used as spatially and temporally minimally overlapping building blocks to describe a variety of dynamic brain network states. These iCAPs have in turn been associated with the set of 50 behavioural domains as defined by the Brainmap database[9] (Laird, Lancaster, and Fox, 2005), a vast online repository of activation maps from fMRI studies (in the order of 3000 papers, 70000 subjects, 15000 experiments and 122000 reported brain locations). This allows for the interpretation of observed networks in terms of constituents of interpretable behavioural categories Action, Cognition, Emotion, Introception and Perception (see Figure 6 of Karahanoğlu and Van De Ville, 2015). The implementation in the current version of our Neu3CA-RT framework thus allows for a real-time (every 3 s) mapping of dynamic whole-brain activity to the 13 innovation-driven co-activation patterns through a spatial GLM (i.e. calculating how well the dynamic brain activity pattern can be explained by known "building block" patterns) and the subsequent association to behavioural profiles through correlation (i.e. how the subject's dynamic brain activity pattern, as explained

[9] `http://www.brainmap.org/`

by the iCAP networks, relates to known behavioural states. This analysis adds real-time throughput steps of voxel masking, executing two GLM calculations, and calculating correlation coefficients to the Neu3CA-RT pipeline. These steps add minimal latency to the real-time process, in the order of 0.3 s (see Results section).

In exploring the use of whole-brain activity patterns in real-time, we aim to provide a framework that allows the rtfMRI neurofeedback signal to be calculated from a more representative data sample, which could lead to improved neurofeedback learning effects. Additionally, the access to real-time brain state interpretations in terms of behavioural profiles allows a more intuitive look at dynamically changing brain activity.

D. rtfMRI program execution considerations

The statement by Cox, Jesmanowicz, and Hyde (1995) that dynamically increasing calculation time in rtfMRI applications is unacceptable remains valid, although improvements in computer processing power can be a mitigating factor. Where possible, new rtfMRI developments should aim to avoid cumulative algorithms (processing larger amounts of data for every iteration) that could lead to problematic increases in calculation time, while taking experiment-specific constraints in terms of TR and number of acquired volumes into account. This applies to all preprocessing and image analysis steps applied to fMRI data during the course of a single TR. Sliding-window approaches (Gembris et al., 2000), recursive algorithms (Cox, Jesmanowicz, and Hyde, 1995) and approximations can be implemented to contain the required calculation time.

To minimise real-time program latency, a rtfMRI processing pipeline can be constructed such that real-time processing occurs in the native functional stereotactic space. This removes the real-time preprocessing step of normalisation to a standard space, but necessitates the pre-real-time mapping of standard space model components (if applicable) to the native functional space. This might add time (to the order of 10–20 min) to the overall experiment, but could easily be incorporated into the functional localiser pipeline that is part of a typical neurofeedback experiment. It was thus selected as the desired method for Neu3CA-RT.

Furthermore, standard software programming best practices should be implemented to ensure efficient code execution (for example, in MATLAB, vectorisation and preallocation of memory). Ultimately, if the desired throughput is to be 1 analysed image per TR, all real-time preprocessing and image analysis steps should result in a total dynamic calculation time less than the selected TR, and with an increasing need to shorten the TR for resting state real-time applications, future rtfMRI toolbox developments should optimise algorithms for speed.

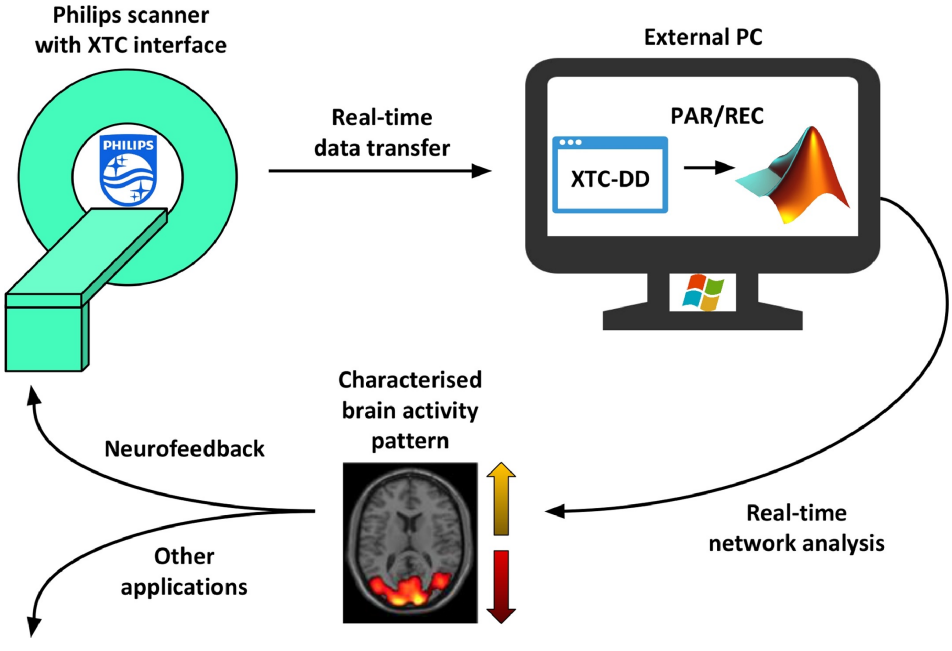

Figure 4.1 — *The experimental setup of Neu3CA-RT.*

4.2 Methods

4.2.1 Experimental setup

Neu3CA-RT was developed and tested using a Philips Achieva MRI scanner (3T) interfaced with an external PC (16GB RAM, 3.2 GHz single core processor) running Windows 7 and MATLAB. The program retrieves data from a user-specified location on the processing PC, which could in principle be served by NIfTI data[10] from any network-enabled MRI scanner (provided the ability for real-time fMRI data transfer and conversion to NIfTI format), thus allowing implementations with other MRI vendors. The experimental setup is shown in Figure 4.1.

4.2.2 Data Acquisition

As a preliminary step to real-time image acquisition and processing, both an anatomical and a functional image are acquired. These images are used in the pre-real-time processing steps described shortly. Anatomical data are recorded using a three dimensional T1-weighted gradient echo sequence (T1 TFE) with scanning parameters: TR=8.2 ms, TE=3.75 ms, flip angle 8°, FOV 240 × 240 × 180 mm, resolution 1x1x1 mm^3, total scan time=6:02 min.

Functional whole brain data are recorded using a gradient echo EPI sequence with scanning parameters: TR=3000 ms; TE=30 ms; 45 transverse slices with a

[10]For detailed information, see: `https://nifti.nimh.nih.gov/`

slice thickness of 3 mm (no gap); in plane resolution=1.75 × 1.75 mm; voxel matrix size 128 × 128 × 45; flip angle=90°; total scan time=8 min.

4.2.3 Data transfer

An integral part of the technical rtfMRI setup is having access to functional scans for processing as soon as they are acquired. This is achieved by real-time TCP/IP data transfer from the MRI scanner to an external processing PC through the Philips scanner's eXTernal Control (XTC) interface and the XTC-datadumper application installed on the processing PC (Smink J et al., 2011). These packages were implemented with support from the vendor. The XTC interface allows reconstructed image data to be retrieved from the scanner, which the XTC-datadumper then receives and converts to Philips PAR/REC files (one pair per functional image) before storing it in a pre-specified location on the processing PC, ready for import by the rtfMRI toolbox.

4.2.4 Image processing

All image processing is done in MATLAB using a combination of adapted SPM12 routines and self-developed scripts. The pre-real-time and real-time processing pipelines are illustrated in Figure 4.2 and Figure 4.3.

4.2.5 Pre-real-time processing

To minimise real-time program execution time, the full pipeline is constructed such that real-time processing occurs in the native functional stereotactic space. Prior to real-time processing, the initial structural image is coregistered to the initial functional image using SPM12's coregister functionality. The coregistered structural image is then segmented into grey matter, white matter and cerebrospinal fluid (CSF) tissue classes using SPM12's unified segmentation procedure. This segmentation process also implicitly normalises the coregistered structural image to the standard MNI space (Montreal Neurological Institute; Collins et al., 1994), generating forward and inverse transformations. The inverse transformation is subsequently applied to the 13 iCAPs networks/images to transform them from MNI to the native functional space. Finally, the tissue probability maps and native-space iCAPs images are all resliced to the native functional space grid, thus allowing for direct comparison of voxels.

4.2.6 Real-time processing

For every functional dynamic (i.e. once every TR), the XTC-datadumper sends a PAR/REC file pair to a prespecified location on the external PC. These files are converted to NIfTI format using a modified version of r2agui[11]. Once converted, the dynamic functional NIfTI image is realigned to the first functional image (which can be user-specified as the initial pre-real-time functional image,

[11] See: `http://r2agui.sourceforge.net/`

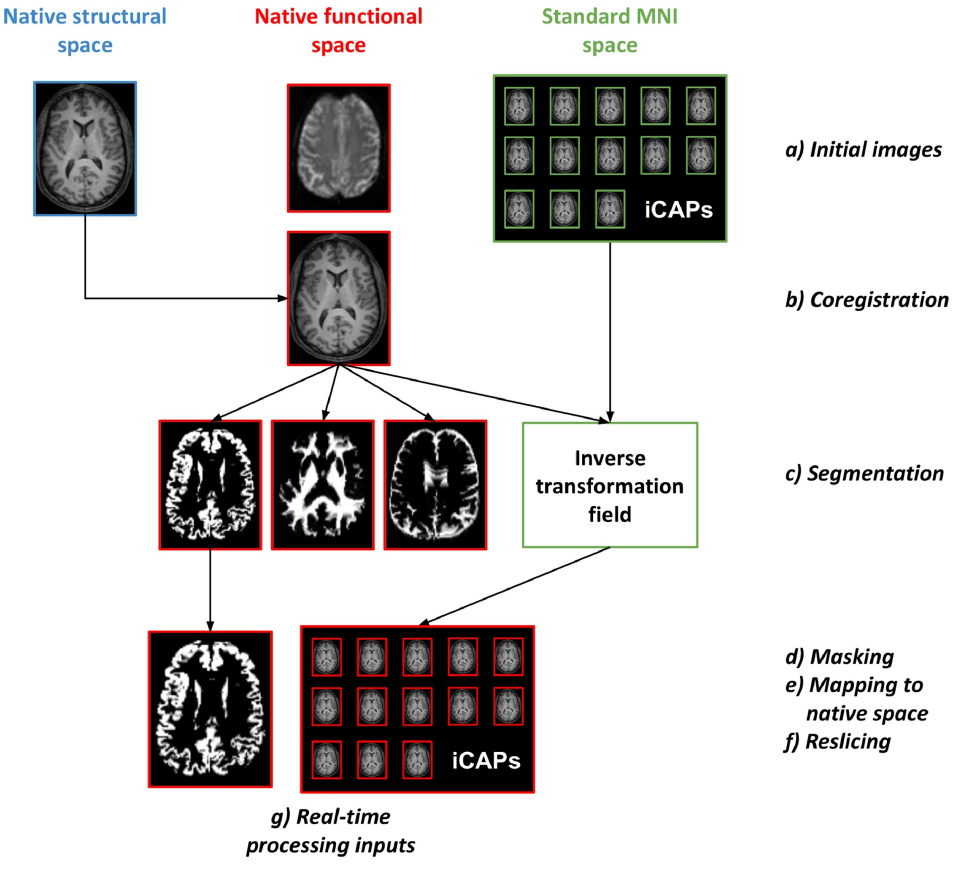

Figure 4.2 — *The pre-real-time processing pipeline.*

or the first image in the real-time series) using a least squares approach and a 6 parameter rigid body transformation. The algorithms for the motion correction steps were adapted from the *spm_realign_rt* and *spm_reslice_rt* routines of the OpenNFT codebase[12], which were originally adapted from SPM12 to minimise execution time. A binary mask derived from the grey matter tissue class image is then applied to the realigned functional image. From this point onward, standard matrix calculations are done from in MATLAB on matrix data retrieved from each dynamic NIfTI image.

To determine how the iCAPs model of network-building-blocks fits the dynamic fMRI data, a spatial GLM containing the iCAPs spatial maps is subsequently applied, with the 13 most frequently occurring iCAP images (as the desired model) and the mean functional image (derived from the full 4D fMRI dataset) as the spatial design matrix regressors. As the model aims to describe spatial activity differences in terms of distinct co-activation patterns, the image mean is included

[12] `https://github.com/OpenNFT/OpenNFT`

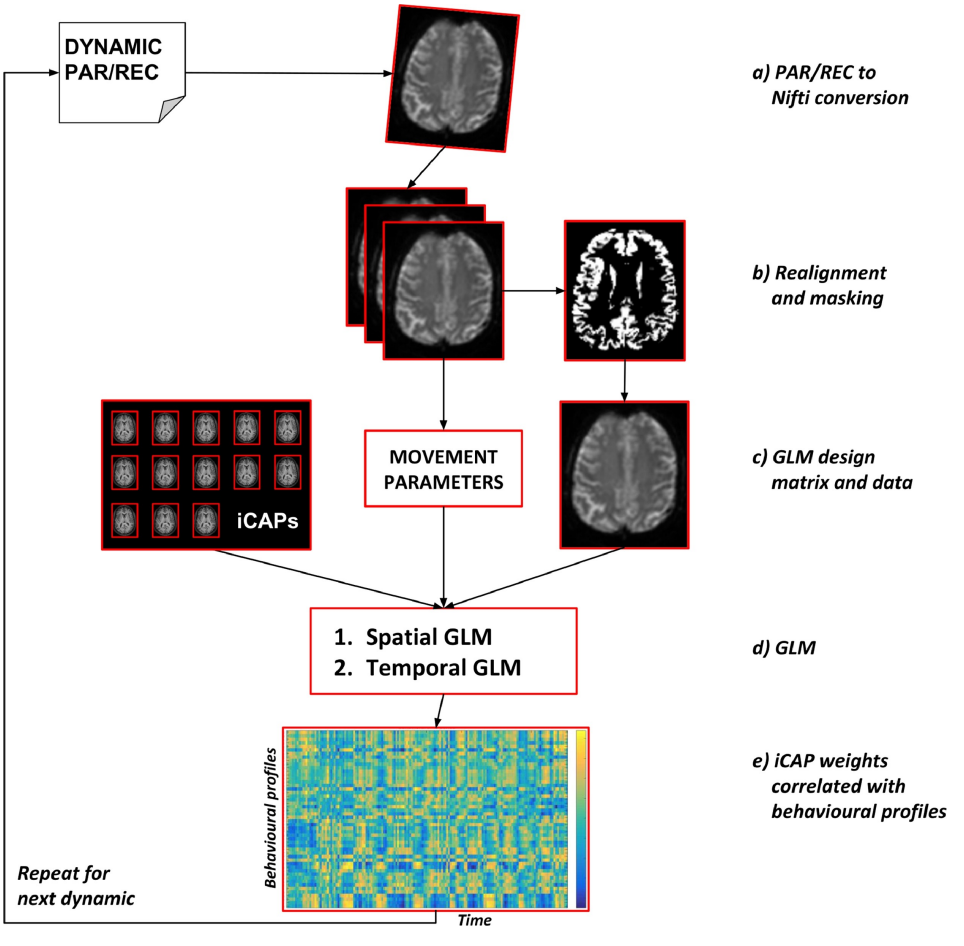

Figure 4.3 — *The real-time processing pipeline.*

so as to describe the majority of the observed signal in the dynamic functional image. This allows the 13 iCAP regressors to describe any additional up- or down-regulated activity across grey matter. Beta values resulting from the spatial GLM are corrected for drift and for realignment residuals by applying a temporal GLM with the 6 realignment movement parameters and linear and quadratic drift terms as regressors.

The GLM steps generate a list of iCAP network weights (beta values) that indicate in which relative proportion the iCAP network building blocks best describe the current fMRI activity with respect to the image mean. To convert these weights into interpretable information, they are correlated (using Pearson's linear correlation) with the 50 behavioural profiles from the BrainMap database that fall into 5 behavioural categories: Action, Cognition, Emotion, Introception and Perception. These profiles can then be used as a means to interpret the real-time brain state of the subject.

In summary, once a dynamic image has been realigned and masked, the real-time processing entails mapping the current spatial activity pattern to a set of iCAP building blocks, yielding a set of beta weights that are subsequently detrended and then correlated with the 50 BrainMap behavioural profiles. This translates spatial patterns into possible brain states experienced by the subject in the scanner.

4.2.7 Experimental task design

With a set of 13 iCAPs beta-weights and a correlated set of 50 behavioural correlation coefficients being generated for each functional dynamic image, a full functional imaging run essentially contains a time series of BrainMap-database-interpreted behavioural activity fluctuations. To demonstrate our dynamic fMRI network modelling approach, i.e. to map real-time distributed brain activity to underlying iCAP patterns and subsequently to a behavioural interpretation, experiments were done with a single healthy, right-handed, male volunteer. Conditions of known block task paradigms were chosen such that the calculated behavioural activity time series could be compared with the variation in brain state expected to be induced by the stimulus or task. Controlled task paradigms included visual stimulus (watching movie clips of underwater sea life), auditory stimulus (listening to Bach) and motor task execution (finger tapping), each with a box-car design. In addition, auditory data from SPM's so-called Mother of All Experiments (MoAE, released as part of the SPM user manual) were also analysed off-line. Experimental task paradigms for both the visual stimulus and motor task were: 16 interleaved rest and task periods of 30 s each (starting with rest), totalling an experiment run-time of 8 min. The paradigm for the auditory stimulus experiment was: 5 task periods of 60 s each, interleaved with rest periods of 30 s each (starting with rest), totalling an experiment run-time of 8 min. For the MoAE auditory data, the paradigm was: 14 interleaved rest and task periods of 42 s each (7 periods each, starting with rest), totalling an experiment run-time of 9 min 48 s.

4.2.8 Results Analysis

For each experiment, the behavioural time series resulting from Neu3CA-RT processing was correlated with the expected (haemodynamic response function - HRF - convolved) task time course to generate a set of Pearson's linear correlation coefficients (R) and corresponding p-values. Bonferroni correction was applied for multiple comparisons (i.e. 50 behavioural profiles); consequently, correlations with a corrected p-value below 0.001 were deemed significant. Correlations with a corrected p-value above 0.001 and below 0.002 (i.e. 0.1/50) were regarded as displaying a trend towards significance.

To investigate how well the iCAPs model described the real-time fMRI data fluctuations, the dynamic estimation error was calculated and the sum of squared estimation errors (SSE) for each experimental run was compared to the sum of squared fMRI signal (SSS) for the run. While the SSE gives an indication of the model error that can be compared between runs (by subtracting the model fit, i.e. the matrix product of the design matrix and the estimated beta weights, from

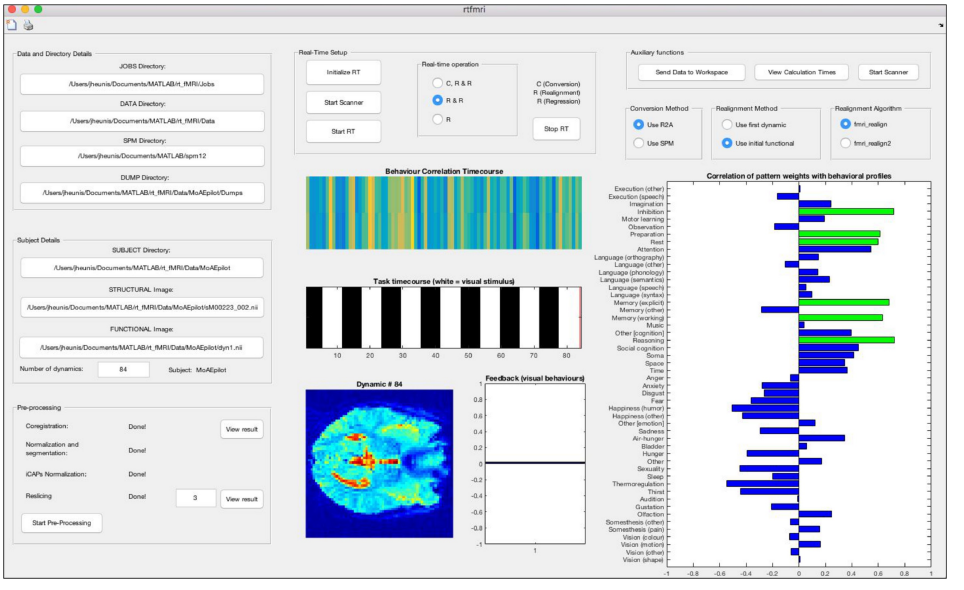

Figure 4.4 — *A screenshot of the Neu3CA-RT graphical user interface.*

the data and calculating the square of the residual), the SSE to SSS ratio gives an indication of how large the error is compared to the actual signal (i.e. the real-time fMRI data).

4.3 Results

4.3.1 Technical results

All pre-real-time and real-time processing functionality was combined into a MATLAB graphical user interface (GUI), known as Neu3CA-RT (displayed in Figure 4.4), a video demonstration of which can be accessed on the Neu3CA website[13] and for which the basic functionality is available on Github[14]. The GUI allows for the specification of relevant file locations (particularly the location where real-time images are stored), the selection of pre-real-time acquired images, controlling the MRI scanner via a START/STOP command, display of real-time acquired and processed data (functional activity, task paradigm, iCAP weights and behavioural profile correlation values), as well as offline (re)processing of real-time acquired data.

Regarding timing considerations, the calculation time was logged in real-time for all processing steps of each dynamic. This included real-time file format conversion ($\sim$0.4 s), image realignment ($\sim$0.55 s), spatial GLM calculations ($\sim$0.08 s), temporal GLM calculations ($\sim 2.7 \times 10^{-4}$ s) and correlations and visualisations

[13] `http://neu3ca.org/project/rtfMRINF/`

[14] `https://github.com/jsheunis/Neu3CA-RT`

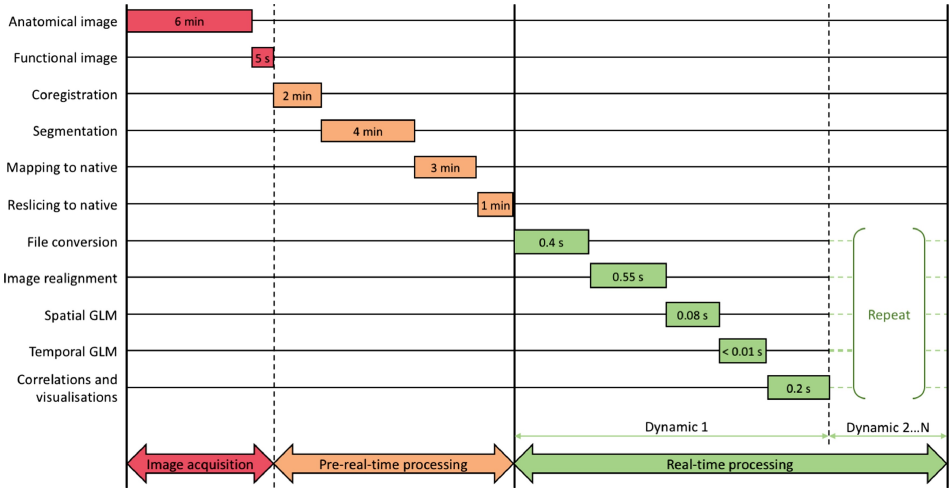

Figure 4.5 — *Neu3CA-RT's real-time latency. Real-time latency (green, totalling less than 2 s) is indicated on a scale with all processing steps (vertical axis). The time scale has been selectively adapted for ease of reading. (For interpretation of the references to colour in this figure legend, the reader is referred to the web version of this article.)*

(~0.2 s), totalling ~1.5 s on average. These averaged values were calculated for the three experiments with TR=3 s. For the MoAE-SPM data, which had a considerably lower in-plane resolution with a 64 × 64 matrix size, the image realignment duration was ~0.3 s and the total real-time latency amounted to less than 1 s on average.

4.3.2 Throughput and latency

After image acquisition and pre-real-time processing steps, the current throughput of Neu3CA-RT amounts to 1 analysed fMRI image per TR (3 s). Pre-real-time steps include, as described, anatomical and functional image acquisition, coregistration, segmentation, mapping of the iCAPs framework to the functional space and reslicing all relevant images to the functional space resolution. During a single real-time dynamic, the throughput includes file format conversion, functional image realignment, masking, spatial and temporal GLM calculations, correlation calculations and visualisations. In Neu3CA-RT's current experimental setup, the actual time required for initial image acquisition and pre-real-time processing is about 6 min and 10 min respectively. These are indicated together with the real-time latency in Figure 4.5.

4.3.3 Experimental results

Experimental results are shown in Figure 4.6 for all four experiments (auditory, visual, motor and auditory-MoAE), with the 50 BrainMap behavioural profiles located on the vertical axes and Pearson's linear correlation coefficient defining the unit for the horizontal axes. The correlation results are colour coded according

Table 4.1 — *Top four positive correlations between HRF-convolved task time course and behavioural profiles for multiple task paradigms*

Task Paradigm	Behavioural profile	R-value	p-value
Visual stimulus	1. Vision (other)	0.3927	0.0028×10^{-4}
	2. Vision (shape)	0.3669	0.0183×10^{-4}
	3. Hunger	0.3215	0.3384×10^{-4}
	4. Vision (colour)	0.3212	0.3485×10^{-4}
Auditory stimulus	1. Anger	0.4103	0.0071×10^{-5}
	2. Audition	0.3977	0.0192×10^{-5}
	3. Music	0.3876	0.0410×10^{-5}
	4. Somesthesis (pain)	0.3618	0.2583×10^{-5}
Motor task execution	1. Execution (speech)	0.2690	0.0006
	2. Language (other)	0.2677	0.0006
	3. Somesthesis (other)	0.2530	0.0012
	4. Execution (other)	0.2202	0.0051
Auditory (MoAE-SPM)	1. Audition	0.4056	0.0001
	2. Anger	0.3757	0.0004
	3. Music	0.3415	0.0015
	4. Language (phon.)	0.3236	0.0027

to their corresponding corrected p-values: blue shows p >0.002, cyan shows 0.001 <p <0.002), and green indicates significant correlation (p <0.001).

For improved interpretation, the top four positively correlated behavioural profiles from each experiment are displayed in Table 4.1, together with their R- and corrected p-values.

Additionally, to investigate how well the iCAPs model described the real-time fMRI data, the sum of squared estimation errors for each experimental run was compared to the sum of squared fMRI signal for the run. The results are shown in Figure 4.7, which indicates the median (red line), 25th percentile (lower bound of blue box), 75th percentile (upper bound of blue box), upper and lower adjacent values (upper and lower black lines) and outlier values (red markers) for each of the four experimental runs. In all four cases, the sum of squared error to sum of squared signal ratio is between 0.9:1 and 1:1.

4.4 Discussion

4.4.1 Technical aspects

The importance of minimising rtfMRI calculation times has been stressed. Regarding Neu3CA-RT's latency performance, averages of real-time processing step calculation times indicated that image realignment had the longest duration: about 0.55 s of the available 3 s (i.e. 1 TR). In contrast, the data analysis and visualisation steps total about 0.28 s, although it must be added that the current visualisation

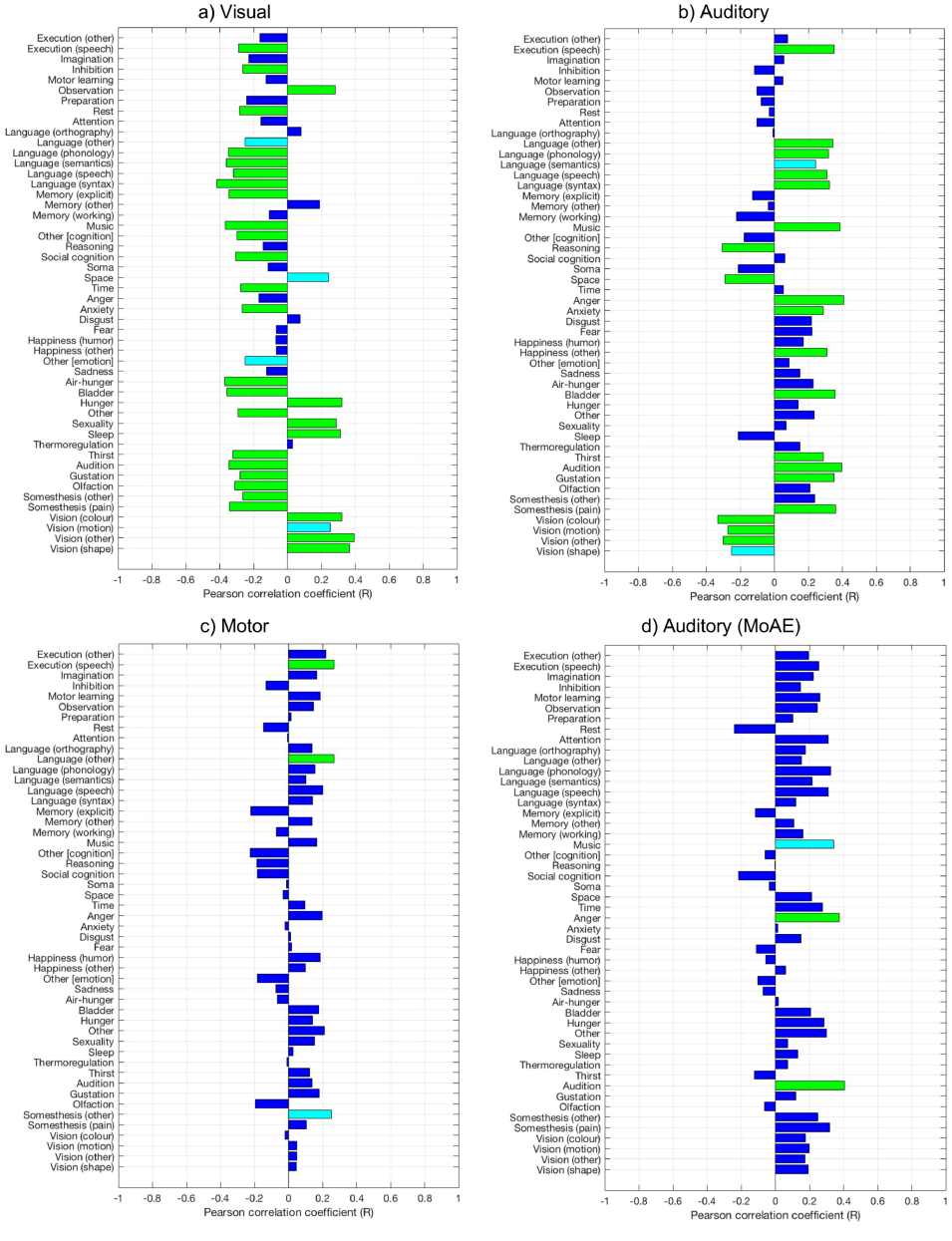

Figure 4.6 — *Correlation results (colour-coded for p-values) for behavioural time series datasets (resulting from real-time processing) for different experimental task paradigms. (a) Visual stimulus, (b) Auditory stimulus, (c) Motor task execution and (d) Auditory stimulus (SPM's "Mother of All Experiments"). Colour code: Blue shows p >0.002, cyan shows 0.001 <p <0.002, and green indicates significant correlation (p <0.001). (For interpretation of the references to colour in this figure legend, the reader is referred to the web version of this article.)*

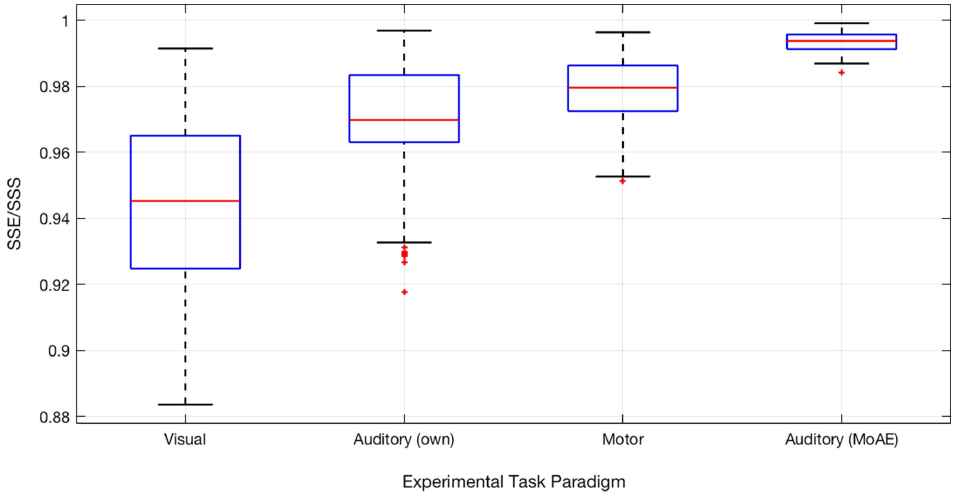

Figure 4.7 — *Sum of squared errors (SSE) divided by sum of squared signal (SSS). SSE/SSS (on the vertical axis, lowest value at 0.88 for easier comparability) is shown for each of the four experimental runs (on the horizontal axis).*

options of Neu3CA-RT are not complex or resource-intensive. Considering the likely future increase of real-time processing steps (e.g. additional denoising steps and analysis algorithms, e.g. functional connectivity or MVPA methods) while keeping the throughput constant, steps should be taken to optimise for speed. It should be noted that the incorporated SPM realignment routine has several parameters (including estimation quality, interpolation techniques and reslicing options) that can be optimised for calculation speed, however the tradeoff in data quality will have to be investigated.

The real-time latency could be decreased further if no processing time is required for conversion of PAR/REC files to NIfTI by the external PC, i.e. if the vendor-supplied software exported functional images already converted to the standard NIfTI or DICOM format. However, if this conversion is handled by the vendor (either as part of the online reconstruction process or by peripheral software responsible for transporting the data) it should necessarily have a shorter execution time than the current conversion latency.

Another option worth investigating towards decreasing latency is the functional masking. Calculation time increases with the number of voxels being processed, which could be of concern given that we focus on whole-brain analysis (as opposed to ROIs with limited voxels, assuming comparable spatial resolution) and given that increased spatial resolution could lead to improved spatial localisation. For our own experiments, the grey matter voxels of interest amounted to about 100k out of a possible 740k. Different masking methods should be investigated to minimise this number while maintaining enough multivariate data for accurate network analysis. Similarly, lower in-plane matrix sizes could be considered (as evidenced by the lower latency for the SPM-MoAE data vs the experimental data)

if high spatial resolution is not particularly important for the specific analysis.

Considering overall experiment duration, Figure 4.5 and the Data Acquisition section indicated that the typical experiment lasted about 25 min, with the initial image acquisition time being 7 min (taking time between scans into account), the pre-real-time processing time being 10 min, and the real-time latency being $\sim$1.5 s per dynamic and 8 min in total. This is within the clinically acceptable total scan duration of 30 min to 1 h. Even so, processing steps will need to be addressed for improved data quality. More denoising steps or denoising steps with increased efficiency could lead to a latency increase, which should be restricted as far as possible. Apart from the discussed options, more promising additional time savers would be to optimise the program structure, algorithm selection and processing equipment for decreased latency of all processing steps. In this regard, apart from optimising MATLAB code for speed by incorporating accepted best practices, no further in-depth consideration was given to improving program execution in the current implementation of Neu3CA-RT. Future work should also investigate the use of graphical processing units (GPUs), parallel computing architectures or multi-platform shared memory multiprocessing programming APIs towards decreasing real-time latency.

Finally, concerning the software infrastructure, as displayed in Figure 4.1 and described previously, vendor specific software is necessary (on the scanner itself and on the external processing PC) for real-time transfer of functional images. However, Neu3CA-RT was created with the requirement of a server-client infrastructure, allowing future integration with scanners from vendors other than Philips. In the case that scanners from other vendors output data in a proprietary file format (i.e. not NIfTI), conversion plugins will be necessary to serve data in a compatible format.

4.4.2 Data quality

The model estimation error investigation showed a significant difference between the actual rtfMRI data and the data described by the iCAPs model: in the order of 90%–100%, which means the error and the signal are almost equal in size. This is an undesirable outcome for a model attempting to describe as large a percentage as possible of the measured signal fluctuations. Several factors could influence this error, including: insufficient noise regressors or confounding regressors in the spatial GLM (for example, real-time physiological data were unavailable and thus not corrected for in the current Neu3CA-RT implementation); not accounting for other possible artefacts like EPI signal dropout or scanner induced distortion; processing fMRI data at suboptimal BOLD contrast; and incorrect model definition. If it can be established that said artefacts have significant detrimental effects on the quality of these experimental rtfMRI data, they should first be corrected for before further analysis iterations can shed light on the remaining error and the resulting performance of the iCAPs model. Thus, although realignment residuals and signal drift were already corrected for in the current implementation, improved noise modelling and removal techniques should be investigated. Because masks were

calculated in the functional space for grey matter, white matter and CSF, the latter two could be used to generate averaged noise compartment signals to be used as extra regressors in the denoising GLM.

Whether improved preprocessing steps result in an improved fit of the iCAPs model to the experimental data or not, or if completely different models or analysis techniques are applied in future, accurate preprocessing for improved data quality remains of utmost importance.

4.4.3 Network-based analysis

In the real-time fMRI analysis method explored in this work, a brain-wide multi-voxel approach was used to characterise modulation of distributed brain activity during a known task paradigm as a set of innovation-driven co-activation pattern fluctuations, which were in interpretable as correlated behavioural profile fluctuations. The main aim was to develop a toolbox that allows the analysis of whole-brain networks as the basis for eventually calculating a neurofeedback signal, as networks are hypothesised to contain richer information about the underlying condition being studied (as compared to ROI-based analysis). Measures of brain network fluctuation and interaction could thus serve as contingent neurofeedback signals with the aim of increasing training effects in rtfMRI neurofeedback studies.

Our proof-of-concept network-based analysis consisted of fitting a model of temporally and spatially overlapping co-activation patterns, regarded as building-blocks of standard resting state networks (Karahanoğlu and Van De Ville, 2015), to real-time denoised fMRI data using a spatial GLM. For each time point in a functional time series, the beta weights resulting from the GLM were transformed to correlation values with 50 behavioural profiles from the BrainMap database, essentially yielding a real-time behavioural interpretation of the subject's brain state. These behavioural time series were then correlated with their respective experimental task designs to find specific behavioural profiles that correlated with the task or stimulus time series. This was compared against expected behaviours given the task or stimulus.

The results indicated expected effects in three out of the four experiments, where the most significant positive correlation between a BrainMap behavioural profile time course and the experimental task design was shown for an expected brain state. 4.1 summarised this result: for a visual stimulus, Vision had the most significant correlation; for an auditory stimulus (MoAE-SPM data), Audition; and for a motor task, Execution (speech). It should be noted that the Execution (speech) profile might detract from the results' accuracy, as Execution (other) seems like a more logical expectation, although it is known that speech involves complex articular movement and that the sensorimotor and language networks involve common anatomy (Besseling et al., 2013). Unexpected results in the top four positively correlated behavioural profiles are also noted for each experiment: for the visual experiment, Hunger is unexpected; and for both auditory experiments, Anger is unexpected. This occurrence of unexpected effects was not limited to within-behavioural-category profiles, as is demonstrated by the Hunger profile

(from the category, Introception) being significantly correlated with the visual experiment task design. The fact that more significant effects (and trends towards such effects) were found than were expected indicates a lack of specificity of the analysis method. Furthermore, the observed correlation values in all experiments were relatively low, reaching a maximum of 0.4103 for behavioural profile Anger in the auditory stimulus experiments.

For the experiments under consideration, the investigation was limited to task-positive correlations in a single subject in an attempt to identify significant up-regulated behaviour for a given task paradigm. This design decision, however, posited no claims as to the importance of significant and simultaneous task-negative correlations, nor to simultaneous but unexpected up-regulations, nor to the relative correlation values. An example of strong negative correlation between behavioural profiles and the task design was found in all language profiles for both the visual and auditory experiment. Further investigation, with an increase in statistical power, is required into the dynamics of simultaneous and opposing behavioural profile fluctuations to shed light on this observation, specifically given the known spatially distributed and dynamic nature of human brain networks.

Furthermore, the iCAPs and BrainMap behavioural profile model used in this study was selected as an exploratory method based on their hypothesised usefulness as targets for neurofeedback in neuropsychiatric conditions, given the spatially distributed and dynamic nature of the patterns and the intuitive relation to brain state interpretations. This, however, does not preclude the use of other network-based analysis methods in Neu3CA-RT. With some updates to the code, it is possible to use the framework with different network models hypothesised to underlie whichever whole-brain mechanism is being studied and used for neurofeedback training.

4.4.4 Future work

Although the current implementation of Neu3CA-RT serves as a successful proof of concept of a network analysis driven rtfMRI framework, the discussion items indicate that further development and testing is required, especially with regards to improving technical implementation, network analysis and data quality.

Regarding Neu3CA-RT's technical implementation and software design, aside from adding improved artefact monitoring and visualisation options to the toolbox, particular attention will be given to: minimising the latency of each step in the real-time processing pipeline; minimising the latency added by the MATLAB GUI infrastructure (either by using a compiled version of MATLAB or a different programming framework); investigating increased processing power and parallelisation options; and updating the GUI for intuitive user experience.

To improve the network analysis presented in this study, the first aim should be to use a better understanding of the behavioural profile dynamics to propose an efficient model that increases the specificity of the results, an aspect that the Neu3CA-RT framework currently lacks. With increased specificity, more complete and intuitive interpretations can be made from the results about the dynamic brain

state of the subject and hence about the validity of the iCAPs/BrainMap network analysis model in a rtfMRI framework. In future, network analysis need not be limited to the iCAPs model and should be expanded to include other network models as well as MVPA, data-driven and/or machine learning methods known in literature to yield improved results.

Envisaged steps to investigate and improve data quality include: adding real-time white matter and CSF nuisance regressors to the denoising GLM; correcting for physiological noise in real-time (heart beat and breathing); correcting for scanner induced artefacts in real-time; improving software options to display subject movement and other noise in real-time (i.e. quality checking); and optimising BOLD contrast and sensitivity with the use of real-time multi-echo EPI acquisition and processing.

Finally, while this work reported the development and explorative use of a real-time fMRI analysis tool based on whole-brain networks, the ultimate goal of Neu3CA-RT is for it to be used as a tool in rtfMRI neurofeedback training experiments. In this regard, several data processing steps should be added to the real-time pipeline, including neurofeedback signal calculation, scaling and presentation. Once future developments with regards to rtfMRI data denoising and quality improvements have been accomplished, a neurofeedback experiment could investigate the effects of neurofeedback-driven modulation of one or a set of the behavioural profiles, as these profiles provide a simple representation of complex network-based and dynamic brain activity.

Chapter 5

rtQC: An open-source toolbox for real-time fMRI quality control

Abstract

While recent literature shows an increase in the availability and use of standardised quality control metrics for conventional functional magnetic resonance imaging (fMRI) studies, a comparative lack exists for real-time fMRI use cases. In an effort to explore real-time fMRI quality metrics and to facilitate a community effort of standardisation and practice adoption, we introduce the newly developed *rtQC*: an open source, MATLAB and SPM12-based toolbox for real-time quality control. The user-friendly graphical user interface allows three domains of quality control: Pre-QC, Online-QC and Post-QC. Pre-QC provides functionality to select defaults, template images, and regions of interest, and ensures the consistency of real-time volume acquisitions. Online-QC includes real-time computation and monitoring of quality metrics including framewise displacement, motion outliers, global Z-score, temporal signal-to-noise ratio and real-time carpet plots. Post-QC triggers established quality control pipelines and provides summary data and visualisations. *rtQC*'s functionality is demonstrated and validated using two open fMRI datasets.

By formalising and validating algorithms for real-time quality metrics that have until recently only been available as offline measures, and by making these algorithms available publicly, *rtQC* facilitates real-time quality control as a standard practice in fMRI research. The real-time algorithms developed for *rtQC* also lay the foundation for the algorithms used in further developments of real-time multi-echo fMRI analysis as well as automated quality control pipelines, which are elaborated on in Chapter 6 of this thesis. Extensive validation of these and further algorithms are then demonstrated in Chapter 8, using the real-time multi-echo fMRI dataset that was collected and curated for this purpose (Chapter 7).

rtQC is available publicly at `https://github.com/rtQC-group/rtQC`, which includes installation and usage instructions, as well as sample use cases

This chapter and the related software have been presented at an international conference as: Heunis, S., Hellrung, L., Meer, V.D., Bergert, S., Sladky, R., Pamplona, G.S.P., Scharnowski, F., Koush, Y., Mehler, D., Falcon, C., Gispert, J.D., Molinuevo, J.L., Skouras, S., 2019. rtQC: an open-source toolbox for real-time fMRI quality control. Proceedings of the 2019 annual meeting of the Organization for Human Brain Mapping. Rome, Italy. https://doi.org/10.5281/zenodo.3239084

5.1 Introduction

It is well-known that the resting state and task-based blood oxygen level-dependent (BOLD) signal acquired with functional magnetic resonance imaging (fMRI) contains several scanner-, sequence-, subject- or experiment-related nuisance signals and artefacts (Murphy, Birn, and Bandettini, 2013; Power et al., 2014; Caballero-Gaudes and Reynolds, 2017; Liu, 2016). If such confounding factors are not sufficiently accounted for during acquisition or minimised through real-time or offline processing, resulting fMRI measures can bias our inferences and our consequent conclusions about brain function. Conversely, if such issues are isolated during acquisition, even to the extent that bad quality data can be flagged and discarded as they are acquired, this can lead to both cost/time savings as well as decreased bias in the data and its derivative measures. Quality control (QC) should therefore be an integral part of the fMRI acquisition and analysis procedures. However, standardised fMRI data quality control and reporting has not received widespread attention as an adopted experimental practice nor in reported literature, perhaps until the recent advent of interoperable data structures and automated workflows that gave rise to open tools such as fmriprep[1] (Esteban et al., 2019), MRIQC[2] (Esteban et al., 2017) and PCP-QAP (Project, 2014). While this advances our ability to calculate and report standardised quality measures, offline quality control presents only one dimension to the quality control process, and only after acquisition. Standardisation of methods and tools to report quality control measures in real-time, i.e. as the data are acquired, would be another particularly useful dimension.

Existing tools have previously introduced novel ways of minimising quality issues and reporting quality metrics in real-time. Originally, AFNI's real-time fMRI module (Cox, Jesmanowicz, and Hyde, 1995) supported the ability to display motion parameters to the subject in order the suppress head motion (Yang et al., 2005) and to feed back a display of variability in areas affected by physiological noise (e.g. ventricles) in order to reduce the standard deviation of the fMRI signal (Bodurka, Gonzales-Castillo, and Bandettini, 2009). More recent real-time quality tools include Framewise Integrated Real-time fMRI Monitoring (FIRMM; Dosenbach et al., 2017), which focuses on real-time motion tracking and related quality metrics, and Turbo-BrainVoyager (Lührs and Goebel, 2019) which added functionality for inspecting read/processing times, motion parameters, and region of interests overlaid on functional or anatomical data. In recent work we reviewed the quality and denoising practices in 128 real-time fMRI neurofeedback studies, and found a variety of examples for offline and real-time quality control. Stoeckel et al. (2014), for example, proposed the calculation and use of tSNR and the concordance correlation coefficient on pilot data to determine, respectively, whether the fMRI neurofeedback signal is detectable and reproducible between runs. And Sorger et al. (2018) suggested a list of five criteria used for selection

[1] https://fmriprep.org/

[2] https://mriqc.readthedocs.io/

of custom feedback regions per subject, including that the ROI should consist of 10-15 neighbouring voxels spanning three axial slices.

In an effort to explore real-time fMRI quality metrics extensively and to facilitate a community effort of standardisation and quality practice adoption, we introduce *rtQC*: an open source, MATLAB and SPM12-based toolbox for real-time quality control. While *rtQC* originated previously as a set of scripts and guidelines for post-hoc identification of quality issues between offline and real-time exported versions of the same data (Hellrung et al., 2017), this new work documents the results of a major refactoring process. The new version of *rtQC* consists of a graphical user interface that is capable of accessing, preprocessing and denoising fMRI data in real-time, calculating real-time quality control metrics, providing real-time visualisations of the acquired data and quality metrics, and highlighting quality issues between the offline and real-time variants of fMRI data. Additionally, performance improvement recommendations from Chapter 4 (**heunis˙neu3ca-rt:˙2018**) have been considered to minimise per-volume processing time. The ability of *rtQC* to calculate quality metrics in real-time makes it practical for data collectors to identify data quality issues as they occur (versus hours, days or weeks after data collection), leading to time and cost savings.

5.2 Overview

The version of *rtQC* that was developed as part of this thesis takes the form of a graphical user interface that allows three levels of data entry, processing, and visualisation (depicted in Fig. 1): Pre-QC, Online-QC and Post-QC. Pre-QC defines anatomical data, regions of interest, template information, and ensures the consistency of real-time versus offline volume acquisitions. Online-QC includes real-time monitoring of quality metrics, including temporal signal-to-noise ratio (tSNR), Z-score, region-based signals, and a real-time carpet plot which displays per-voxel signal intensity fluctuations over time. Post-QC provides summary quality control data and visualisation, with the further potential of triggering established quality control software pipelines. *rtQC* can operate on both pre-acquired datasets or incoming volumes in real-time.

5.3 Core features

5.3.1 Focus on functional MRI

rtQC has a core focus on subject-specific, single-echo functional MRI. A principled step in this regard is to process all functional data in subject-specific functional space, i.e. without transformation of the acquired data to a standard stereotactic space (such as the MNI152 or Talairach spaces) which is typically done for conventional fMRI studies. This saves per-volume processing time, which is particularly useful for real-time use cases, and limits the amount of data transformations and interpolations so as to keep the image data as similar as possible to the raw acquired data.

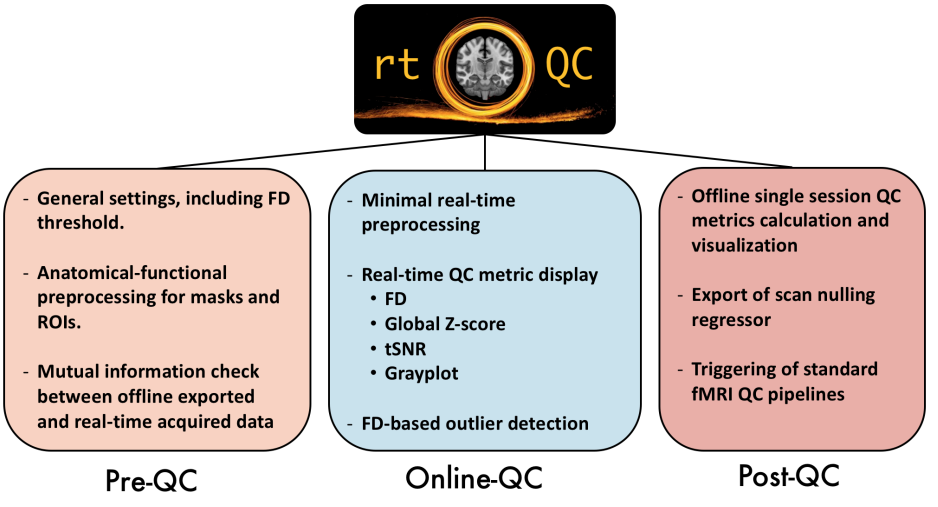

Figure 5.1 — *Overview of the architecture of rtQC.*

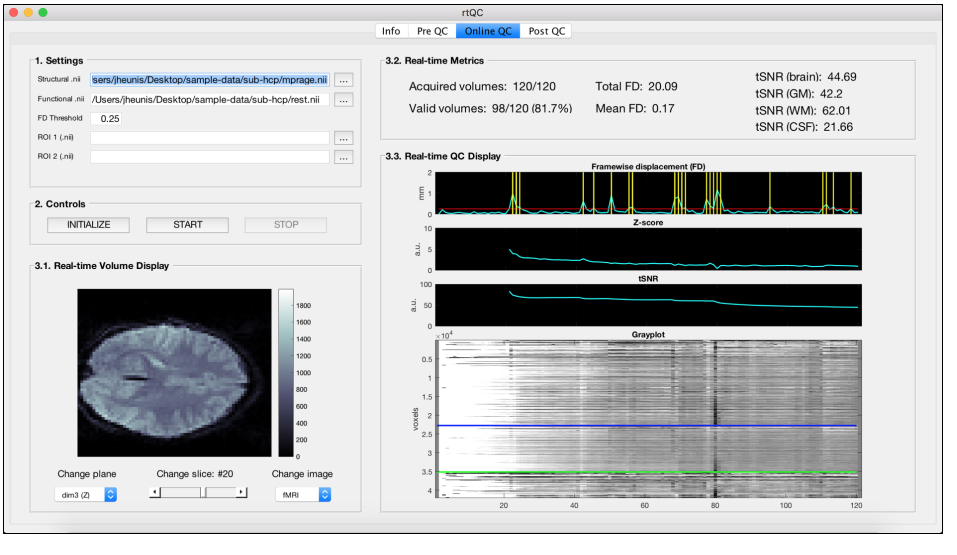

Figure 5.2 — *The "Online QC" tab of the rtQC graphical user interface.*

5.3.2 Graphical user interface

The user-friendly toolbox was created as a MATLAB graphical user interface (GUI) that allows data setup, preprocessing, real-time processing, visualisation of quality metrics and offline pipelines. For real-time use, the GUI enables the user to easily start, pause and resume processing at any moment, as shown in the snapshot of the GUI in Fig. 2.

5.3.3 Pre-QC, Online-QC and Post-QC

rtQC provides the required functionality to set up fMRI data prior to online (or simulated online) experiments (Pre-QC), to process and visualise quality metrics for these data in real-time (Online-QC), and to view summary information and trigger further pipelines after all data have been collected (Post-QC).

In the Pre-QC tab, users are expected to upload a pre-acquired T1-weighted image and a template functional volume of the subject. This is then followed by minimal preprocessing in preparation for online quality control, which includes:

- Coregistration of the T1-weighted anatomical image to the template functional image using SPM12's coregister/estimate functionality.
- Segmenting the coregistered T1-weighted image using tissue probability maps and SPM12's unified segmentation algorithm (Ashburner and Friston, 2005), yielding subject-specific probability maps for gray matter, white matter, CSF, soft tissue, bone and air in the subject functional space.
- Resampling the coregistered T1-weighted image and all tissue segmentations to the subject functional resolution using SPM12's coregister/write functionality.
- Generating binary masks for gray matter, white matter, CSF, and the whole brain (a combination - logical OR after thresholding - of the previous three masks).

Pre-QC also allows the comparison of data that were acquired offline versus in real-time, since these can result in differences (e.g. due to altered image reconstructions or file format conversions) that would otherwise go unnoticed. A mutual information check can be performed on two images, with a high-valued result indicating a close match and a low-valued result suggesting that further inspection and appropriate corrective measures should be performed.

Online-QC includes all controls for running an online quality control procedure and plots for visualising the output. Before the calculation and display of all quality metrics, functional MRI data are preprocessed per-volume, which includes 3D volume realignment using a 6 degree of freedom transformation, and linear detrending.

Post-QC functionality is similar to Online-QC in the sense that quality control and visualisation is executed for the same dataset. However, this is done offline during the Post-QC step and calculated metrics will therefore resemble standardised values that can be compared across datasets. Additionally, Post-QC includes the calculation and display of metrics that are only possible using a full functional dataset, such as visualisations of time series mean, standard deviation, and tSNR.

5.3.4 Calculation and visualisation of standardised quality control metrics

The Online-QC functionality calculates and displays several metrics per volume:

Functional volume visualisation, which can be viewed along each axis (coronal, axial, sagittal) and any slice in order to detect visual quality issues as the data are acquired. This can be set to view a functional volume or the cumulative temporal signal-to-noise ratio.

Framewise displacement (FD), which is an estimation of linear, volume-to-volume head movement in milliliters (Power et al., 2012). For each acquired volume, framewise displacement can be used to classify motion-outliers based on a predefined threshold (typically 0.2 to 0.5 mm) and to consequently store ascan-nulling regressor for both online or offline denoising.

Global Z-score, reflecting the number of standard deviations that the global intensity of an incoming volume deviates from the temporal mean. Z-score peaks can indicate movement or scanner artifacts, and will typically reflect the same peaks seen in framewise displacement.

Temporal signal-to-noise ratio (tSNR), indicating overall data quality and the ability to detect small signal changes (Parrish et al., 2000; Welvaert and Rosseel, 2013). It is computed within the whole brain mask and, if prespecified, within ROIs as the ratio of the temporal mean over temporal standard deviation. These entities are calculated cumulatively per-volume, using all volumes up to and including the volume being processed at any given moment.

Carpet plot (or grayplot), providing a compact display of image intensity fluctuations in terms of percentage signal change (PSC) across all voxels in time. This serves to visualise sudden intensity changes and slow (task-related or breathing-related) fluctuations (Power, 2017).

Summary values, which are text displays of the listed measures and their means as they are updated per-volume. These values include: the number of volumes that have been processed; the umber of volumes that have passed the quality control threshold for which the default is a framewise displacement value of maximum 0.25 mm; the total and mean framewise displacement; and the temporal signal-to-noise ratio of the whole brain, grey matter, white matter and cerebrospinal fluid.

5.4 Installation, requirements, usage and support

rtQC can be installed from its GitHub repository[3], and requires MATLAB 2016b or later to run. Its only dependency is SPM12 (r7771[4]; Friston et al., 2007). Both *rtQC* and SPM12 have to be available locally and added to the MATLAB path to

[3] `https://github.com/rtQC-group/rtQC`

[4] `https://github.com/spm/spm12/releases/tag/r7771`

allow the use of the graphical user interface.

Further installation and usage instructions are provided in the README file located in the project's GitHub repository[5]. Specific instructions for all of the core featuresare also provided in the graphical user interface as the user progresses through the Pre-QC, Online-QC and Post-QC steps.

The use of *rtQC* is demonstrated and validated in a pilot using two existing and publicly available datasets: one resting state dataset (subject 05120) from the UCLA site of the Autism Brain Imaging Data Exchange consortium (ABIDE; Di Martino et al., 2014), and one task-based dataset made available together with OpenNFT (Koush et al., 2017b). The outputs of *rtQC* during and after being run on these data, all deemed to be accurate compared to offline metrics, can be reproduced using the "Demo" functionality embedded in the *rtQC* GUI.

Support is provided via the project's GitHub repository, where issues can be logged when users experience problems, want to report bugs or feature requests, or want to start contributing to the toolbox.

5.5 Discussion

The *rtQC* toolbox, available as open-source software, offers important functionality for real-time fMRI quality control to clinicians and technicians alike. The user-friendly GUI implementation facilitates quick and effective assessment of acquisitions in order to exclude bad datasets and shed light on irregularities in the data. It offers a platform for standardisation of real-time quality metrics, including real-time framewise displacement (FD), temporal signal-to-noise ratio (tSNR), voxel-based and spatially averaged Z-scores, region-based signals, and real-time 2D representations of voxel intensity fluctuations over time. As such, it is intended as a community tool to promote the use and continued development of best practice.

Suggestions for additional features include real-time DVARS, global signal, global signal correlation, and more metrics and visualisations from widely used community tools such as fmriprep (Esteban et al., 2019) and MRIQC (Esteban et al., 2017). Additionally, improvements to code structure and documentation will make the tool more accessible and will encourage further use.

[5] `https://github.com/rtQC-group/rtQC/blob/master/README.md`

Chapter 5

Chapter 6

fMRwhy: BIDS-compatible fMRI analysis with SPM12

Abstract

Features in functional magnetic resonance imaging (fMRI) analysis like standardised data manipulation, interoperability, workflow automation, and reproducible analysis pipelines have experienced increased development growth in the Python ecosystem, but are lacking in MATLAB-based functional neuroimaging projects, even though MATLAB use is still predominant. Similar restrictions hold for the introduction of new methods for improving the quality of fMRI and its derivative measures, with multi-echo fMRI and its application in real-time use cases being a core example. While Python toolboxes exist to make multi-echo processing pipelines available to the research community, similar advancements are not seen elsewhere, effectively excluding MATLAB users from access to state-of-the-art methods for increased quality in real-time fMRI. To address these drawbacks, we developed *fMRwhy*: a MATLAB- and SPM12-based toolbox with a variety of helper functions and BIDS-compatible workflows to assist researchers with their reproducible fMRI analysis journey.

fMRwhy's goal is to make open workflow developments and novel methods available to fMRI researchers using SPM12 and MATLAB. This new functionality includes a focus on functional MRI, BIDS-compatibility, automated fMRI data quality reporting workflows, support for reproducible SPM12-based scripting, and importantly for this thesis, support for real-time and multi-echo fMRI analysis. This chapter presents an overview of *fMRwhy* and details its core functionality, particularly detailing the implementation and usage of quality control and reporting pipelines and multi-echo analysis pipelines. For comprehensive information about the software's installation and usage, readers are referred to the software documentation and API (`https://fmrwhy.readthedocs.io/`) and the project code base (`https://github.com/jsheunis/fMRwhy`), both of which were created and curated alongside *fMRwhy*. With this toolbox and the accompanying resources, the practical groundwork is laid to allow the detailed exploration and validation of new real-time multi-echo fMRI methods, which is the focus of Chapters 7 and 8 in this thesis.

6.1 Introduction

Recent developments in open source neuroimaging software have given researchers unprecedented and widespread access to state of the art methods for functional magnetic resonance imaging (fMRI) analysis. Examples include community maintained data structure standards (such as the Brain Imaging Data Structure; Gorgolewski et al., 2016), software pipelining tools (for example nipype; Gorgolewski et al., 2011), automated preprocessing and quality reporting workflows (such as fmriprep and MRIQC, respectively; Esteban et al., 2019; Esteban et al., 2017), and packages for analysing new fMRI acquisition types (such as tedana for multi-echo fMRI; DuPre et al., 2020). Data standards like BIDS allow for interoperability and the consequent generation of automated workflows (fmriprep, MRIQC), which can be constructed using pipelining tools that ensure methods reproducibility (nipype) and can interface with a wide range of neuroimaging tools. New acquisition or analysis packages that have built-in compatibility with these tools and standards then provide users with easier and quicker access to advancements in the field of fMRI.

A common aspect of these examples is the open source Python programming language, possibly reflecting similar implementation and usage trends seen in the wider software development and data science fields. Another driver behind widespread adoption could be that open source programming languages and accompanying development frameworks allow increased community participation by lowering entry cost. Ideally, the lower cost and community adoption allowed by open source tools would be integral to the improvement of inclusivity in the field of neuroimaging research. However, it cannot be the exclusive platform for future developments. Several established neuroimaging analysis packages and software tools use or are based on proprietary software such as MATLAB, including SPM12 (Friston et al., 2007), Anatomy Toolbox (Eickhoff et al., 2005), and qMRlab (Karakuzu et al., 2020), while still having open source code and wide user bases. Poldrack, Gorgolewski, and Varoquaux (2019) showed that the MATLAB and SPM12 user base in neuroimaging research maintains a substantially higher proportion than all current alternatives. Moving continued support and developments away from these tools on the basis of a strict idealisation of open source software would result in a significant number of users being excluded from access to the aforementioned advancements and from the fMRI community.

A more inclusive solution would be to build tools that extend advancements like interoperability, workflow generation, quality reporting practices, and new analysis methods across programming languages and development platforms. An example is the bids-matlab package[1] that aims to make a BIDS dataset easier to interact with for those scripting in MATLAB, similar to the pyBIDS Python package (Yarkoni et al., 2019). Another is qMRLab, a MATLAB-based and Octave-compatible toolbox for quantitative MRI analysis that makes methods for data fitting, simulation and protocol optimisation more transparent and accessible

[1] https://github.com/bids-standard/bids-matlab

across vendors and to non-specialist users. More work is needed to bring new and continued developments in the open source space into existing MATLAB tools and frameworks, such that users of these tools can gain equal access to the same state of the art advancements.

Here, we present *fMRwhy* as an option to address, in part, the mentioned challenges, specifically those relating to reproducible scripting, automated quality control, and multi-echo fMRI analysis. By developing *fMRwhy* as an open toolbox, we have made several novel contributions that, to the best of our knowledge, have previously been lacking in MATLAB-based neuroimaging projects and can now form an inclusive basis for community use. These new developments include: (1) built-in compatibility with standard neuroimaging data structures such as BIDS; (2) modularised wrapper-functions for SPM12 processes that allow the creation of reproducible analysis scripts; (3) an automated software pipeline for quality control and metrics reporting of fMRI data; and (4) modularised functionality for the processing of real-time and offline multi-echo fMRI data. The accompanying open code base[2] and comprehensive API documentation[3], contribute strongly to the accessibility and reuse of *fMRwhy*.

6.2 Overview

Development of *fMRwhy* started over the course of this work as a new collection of MATLAB- and SPM12-based scripts created to reproduce useful quality control measures and interesting visualisations as reported in journal articles, such as calculating the temporal signal-to-noise ratio of an fMRI time series or creating a carpet plot (Power, 2017) from fMRI data. The core idea behind this was: if the results of our research are supported by useful processing and quality control methods, why not implement these in a reproducible and extensible way so that the greater community can benefit from and contribute to it? This evolved over time into a modular set of SPM12 batch process wrapper functions that simplified the process of creating reproducible fMRI preprocessing and quality reporting scripts. With the goal of allowing automated quality reporting workflows, partial BIDS-compatibility was added using bids-matlab as a dependency. Additionally, work inspired by the benefits of multi-echo fMRI analysis and its possible utility in real-time use cases led to added functionality in those domains.

At the time of writing this overview, *fMRwhy* has several core features, depicted in Figure 6.1, including: a focus on standard functional MRI, BIDS-compatibility, automated fMRI data quality reporting workflows, support for real-time and multi-echo fMRI analysis, and support for reproducible SPM12-based scripting. Importantly, while *fMRwhy* aims to make these features and future developments available to a wider community of MATLAB users under an open license, it is not (nor is it intended to be) a fully-fledged fMRI analysis package. It would not suffice

[2] `https://github.com/jsheunis/fMRwhy`

[3] `https://fmrwhy.readthedocs.io/`

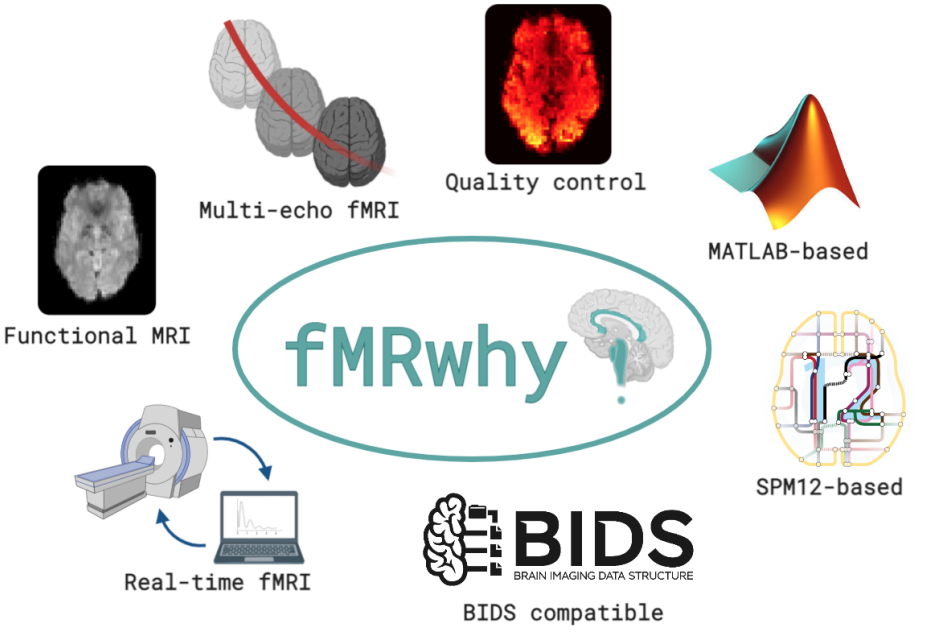

Figure 6.1 — *A depiction of the core features of the fMRwhy software package.*

nor should it be used as a replacement tool for the likes of SPM12, FSL, fmriprep, AFNI, or their constituent functionality. It is better positioned as an auxiliary tool for MATLAB and SPM12 users who work with BIDS-formatted fMRI datasets and who want to: 1) generate automatic, user-friendly quality reports, 2) build reproducible SPM12-based processing pipelines, 3) preprocess multi-echo fMRI data, 4) build/test real-time analysis pipelines, or 5) use auxiliary tools for fMRI visualisation and image manipulation.

6.3 Core features

6.3.1 Focus on functional MRI

fMRwhy was created with a core focus on subject-specific functional MRI and basic structural (i.e. T1-weighted) preprocessing applications. A principled step in this regard is to process all functional data in subject-specific functional space, and only to apply transformations into standard space if required for calculating group-summary measures or based on user preferences.

6.3.2 BIDS compatibility

fMRwhy aims to stay compatible with the Brain Imaging Data Structure, at least in terms of the functionality and data-types that it supports. This includes understanding the structure of a BIDS-compliant fMRI dataset, such as the number and

names of subjects, sessions, tasks, runs, and more. This compatibility allows automated workflows to be run for a BIDS-compliant dataset, such as visual quality control and reporting. Additionally, *fMRwhy* outputs relevant derivative data in a BIDS-compliant fashion.

6.3.3 Visual fMRI quality control

This is currently the core functionality of *fMRwhy*. *fmrwhy_workflow_qc* is an automated, BIDS-compatible quality checking and reporting workflow that generates subject-specific fMRI quality reports in interactive HTML format, easily viewable in a browser application. It can run on a multi-subject fMRI dataset with T1-weighted and BOLD data, and will automatically derive the structure of the data (tasks, sessions, runs, etc) in order to process all BOLD data correctly. Default settings and user preferences are provided as input to this function in the form of a settings file, requiring users to specify a number of parameters prior to running the workflow.

The workflow entails minimal preprocessing of T1-weighted and functional MRI data, and generating quality metrics in both cases.

For anatomical MRI:

- Coregistered T1-weighted segmentations (grey matter, white matter, CSF, and a whole-brain mask) are overlaid onto the subject functional space, for visual inspection of the registration and segmentation quality.
- Coregistered anatomical regions of interest (if specified) are mapped from MN152 space and overlaid onto the subject functional space, for visual inspection.

For functional MRI:

- A summary table provides values for all runs per subject for mean framewise displacement (FD), total FD, FD outliers, and mean tSNR in all tissue compartments. This allows quick inspection per subject, but is better understood when referenced to the whole dataset.
- Several image montages are generated per run, including the time series mean, the standard deviation and the tSNR map. The time series mean gives a quick view of the general quality of the time series and can indicate spike or interference artefacts. The standard deviation map shows areas with high signal fluctuation that can often be related to movement (e.g. close to the eyes). The tSNR maps are useful for investigating general signal quality, to indicate signal dropout and comparing signal quality across regions.
- A carpet (time series) plot is generated per run, which displays voxel intensity in percentage signal change from the mean over time. The vertical axis (voxels) is either grouped per tissue type (compartment ordered) or ordered

from top to bottom according to the voxel's time series correlation strength to the global signal. Signal traces above the carpet plot are also shown, including tissue compartment signals, respiration, heart rate, and framewise displacement. These plots are useful quality checking tools as they make it easy to visualise wide scale signal fluctuations across voxels, which can then be related visually to changes in physiological signals or subject movement.

- If cardiac and respiratory recordings are available, images generated by the dependency TAPAS PhysIO during basic preprocessing are included to check the quality of these recordings. Images include a plot of the temporal lag between derived heart beats within thresholds for outliers, and a plot showing the breathing belt amplitude distribution that can be inspected for unexpected shapes.

After the calculation of these QC metrics and visualisations, a browser-based HTML report is generated per subject, which can be used to interactively explore the data quality of all fMRI runs. Excerpt images from the report can be viewed in Fig. 6.2 and a full report example can be viewed online[4].

Further planned development for the quality reporting workflow includes added quality metrics and associated visualisations (such as DVARS, ghost-to-signal ratio and more), as well as group-level quality plots and summary reports.

6.3.4 Multi-echo fMRI preprocessing

Multi-echo fMRI has known benefits for improving fMRI signal recovery, increasing the temporal signal-to-noise ratio, and separating BOLD and non-BOLD fluctuations, with the Python package tedana being a leading open source implementation allowing wide use and community contributions. However, similar support does not currently exist in MATLAB, which is why *fMRwhy* aims to make multi-echo processing methods accessible to researchers using SPM12 and MATLAB.

Multi-echo analysis support currently includes:

- Estimating 3D realignment parameters from the time series of a single echo and applying these to the time series of the other echoes in the same run.
- Estimating baseline T2* and S0 parameter maps from the time series mean of a multi-echo run, using log-linear regression and assuming a mono-exponential decay model.
- Estimating per-volume T2*FIT and S0FIT parameter maps for (simulated) real-time use.
- Combining multi-echo time series using various echo combination schemes:

[4] `https://jsheunis.github.io/fmrwhy_sample_QCreport.html`

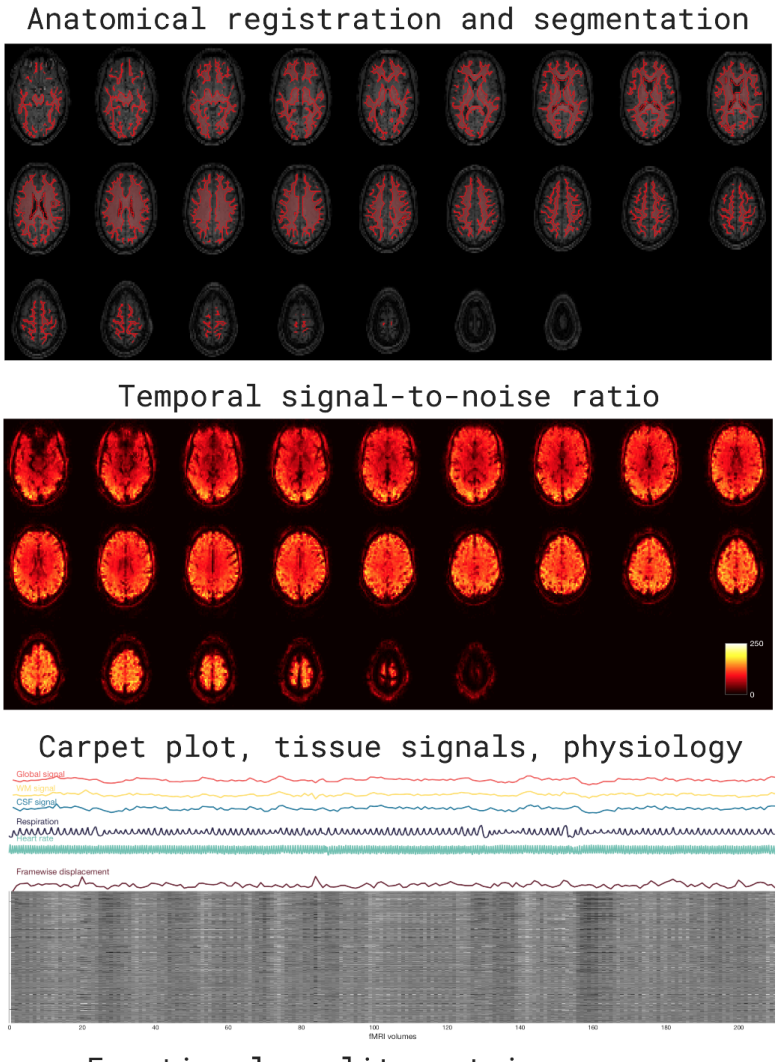

Functional quality metric summary

Functional run	Mean framewise displacement (mm)	Total framewise displacement (mm)	FD outliers (thresh 0.2mm)	FD outliers (thresh 0.5mm)	Mean Zscore	Global correlation	Mean tSNR (GM)	Mean tSNR (WM)	Mean tSNR (CSF)	Mean tSNR (brain)
task-rest_run-1	0.16	33.22	43	0	0.79	0.00	80.44	100.63	32.44	75.13
task-fingerTapping	0.14	29.71	22	0	0.76	0.00	87.75	108.04	36.51	81.85
task-emotionProcessing	0.13	27.44	21	0	0.76	0.00	89.16	110.19	37.87	83.45
task-rest_run-2	0.16	34.48	43	0	0.77	0.00	84.82	106.57	34.35	79.50
task-fingerTappingImagined	0.13	27.39	11	0	0.76	0.00	91.05	111.39	38.54	84.88
task-emotionProcessingImagined	0.15	31.08	27	0	0.76	0.00	87.59	107.41	36.92	81.58

Figure 6.2 — *Excerpt images from the quality report generated by the fmrwhy_workflow_qc pipeline. This includes overlays to check anatomical registration and segmentation (top row), temporal signal-to-noise-ratio slice montages (second row), carpet plots of voxel intensity and other time series fluctuations over time (third row) and a summary table of functional data quality metrics per run (bottom row).*

- tSNR-weighted
- T2*-weighted
- TE-weighted
- Scalar-weighted
- T2*FIT-weighted

Planned future developments for multi-echo support include automated comparison of multi-echo combined data (using various combination schemes) with single-echo data, as well as a standardised multi-echo report similar to the described quality report.

6.3.5 Real-time fMRI preprocessing

Several real-time processing functions were ported and adapted into *fMRwhy* from the open sourced code base of OpenNFT (Koush et al., 2017a), mainly as a means to support the development of real-time multi-echo fMRI analysis scripts. These new developments for real-time multi-echo analysis includes the following functionality:

- Per-volume image preprocessing functions to support 3D volume realignment and spatial smoothing.
- Real-time estimation of T2*FIT and S0FIT as previously explained
- Real-time combination of multi-echo data using various combination schemes
- Real-time calculation of region-based signals
- Cumulative GLM-denoising functionality, including,
- Kalman filtering
- Signal scaling

A pilot real-time workflow allows testing of new or altered real-time denoising or other preprocessing steps. Future work includes expanding this workflow to generate comparison metrics and visualisations for real-time signals and 3D time series, both in real-time and offline.

6.3.6 Accessible and extensible SPM12 batch processing

In an attempt to assist users in moving from click-through graphical user interfaces to building reproducible SPM12-based analysis scripts, *fMRwhy* has several wrapper functions for SPM12 batch processes and other functionality. This includes standard SPM12 preprocessing functions such as coregistration, segmentation, slice timing correction, realignment, reslicing, smoothing, and normalisation, as well as subject-level statistical analysis and thresholding. In conjunction with the utilities, these wrappers allow the modular use of functions to build custom yet reproducible processing pipelines, and to extend these pipelines with ease.

6.3.7 Utilities for (pre)processing, visualisation and file I/O

A variety of utility functions are also available to assist with preprocessing, image calculation, visualisation, and file input/output (I/O) tasks. These are all documented as part of the API.

6.4 Installation, requirements, usage and support

Detailed information about *fMRwhy*'s features, installation process, usage instructions, and API is available via the documentation[5].

fMRwhy can be installed from its GitHub repository[6] and requires MATLAB 2016b or later to run. It has the following dependencies:

- SPM12 (r7771[7]; Friston et al., 2007)
- Anatomy Toolbox (v3.0; Eickhoff et al., 2005)
- bids-matlab (v.0.0.1[8])
- dicm2nii (v0.2 from a forked repository[9])
- TAPAS PhysIO (v3.2.0[10]; Kasper et al., 2017)
- Raincloud plots (v1.1[11]; Allen et al., 2019)

fMRwhy and all dependencies have to be available locally and added to the MATLAB path.

Usage instructions for all of the core features are described in detail in the project documentation, and a fully documented API is available for further understanding. Scripted examples are available for (amongst others) running QC workflows, processing multi-echo data, and using utility and visualisation functions.

Further support is provided via the project's GitHub repository, where issues can be logged when users experience problems with *fMRwhy*, want to report bugs or feature requests, or want to start contributing to the toolbox.

6.5 Discussion

fMRwhy is a MATLAB- and SPM12-based toolbox with helper functions and BIDS-compatible workflows to assist researchers with their reproducible fMRI analysis

[5] https://fmrwhy.readthedocs.io/

[6] https://github.com/jsheunis/fMRwhy

[7] https://github.com/spm/spm12/releases/tag/r7771

[8] https://github.com/jsheunis/bids-matlab/releases/tag/fv0.0.1

[9] https://github.com/jsheunis/dicm2nii/releases/tag/v0.2

[10] https://github.com/translationalneuromodeling/tapas/releases/tag/v3.2.0

[11] https://github.com/RainCloudPlots/RainCloudPlots/releases/tag/v1.1

journey. It makes aspects such as standardised data manipulation, interoperability, workflow automation, and reproducible analysis pipelines more accessible to researchers working on MATLAB-based neuroimaging projects. Novel features of the tool include modularised functionality for the processing of real-time and offline multi-echo fMRI data as well as full-length automated pipelines for quality control and reporting. Additional strong features of *fMRwhy* that contribute to its accessibility and reuse are its comprehensive and open code base[12] and API documentation[13]. Next steps for the *fMRwhy* toolbox should focus on uptake, accessibility and community contribution, without which its impact and usefulness will be difficult to quantify. To further this cause, established software engineering and project maintenance principles should be implemented, such as: comprehensive and automated documentation, automated testing, continuous integration, avenues for issue logging and resolution, open contribution guidelines, and open communication platforms.

[12] `https://github.com/jsheunis/fMRwhy`
[13] `https://fmrwhy.readthedocs.io/`

Part III: Real-time multi-echo fMRI

Chapter 6

Chapter 7

rt-me-fMRI: A task and resting state dataset for real-time, multi-echo fMRI methods development and validation

Abstract

A multi-echo fMRI dataset (N=28 healthy participants) with four task-based and two resting state runs was collected, curated and made available to the community. Its main purpose is to advance the development of methods for real-time multi-echo functional magnetic resonance imaging (*rt-me-fMRI*) analysis with applications in neurofeedback, real-time quality control, and adaptive paradigms, although the variety of experimental task paradigms supports a multitude of use cases. Tasks include finger tapping, emotional face and shape matching, imagined finger tapping and imagined emotion processing. This work provides a detailed description of the full dataset; methods to collect, prepare, standardise and preprocess it; quality control measures; and data validation measures. A web-based application is provided as a supplementary tool with which to interactively explore, visualise and understand the data and its derivative measures: `https://rt-me-fmri.herokuapp.com/`. The dataset itself can be accessed via a data use agreement on DataverseNL at `https://dataverse.nl/dataverse/rt-me-fmri`. Supporting information and code for reproducibility can be accessed at `https://github.com/jsheunis/rt-me-fMRI`.

This chapter is currently undergoing peer review and a preprint has been published as: Heunis, S., Breeuwer, M., Gaudes, C.C., Hellrung, L., Huijbers, W., Jansen, J.F., Lamerichs, R., Zinger, S., Aldenkamp, A.P., 2020. rt-me-fMRI: A task and resting state dataset for real-time, multi-echo fMRI methods development and validation. bioRxiv 2020.12.07.414490. https://doi.org/10.1101/2020.12.07.414490

7.1 Background and summary

Real-time functional magnetic resonance imaging (fMRI) is a brain imaging method where functional brain signals are acquired, processed, and used during an ongoing scanning session. Applications include real-time data quality control (Dosenbach et al., 2017), adaptive experimental paradigms (Hellrung et al., 2015), and neurofeedback (Sitaram et al., 2017). Neurofeedback is a cognitive training method where the real-time feedback signal is presented back to the participant to allow self-regulation of their blood oxygen level-dependent (BOLD) signal, prompting researchers to investigate it as an intervention for patients with neurological or psychiatric conditions. Work by Ros et al. (2020) and Haugg et al. (2020) show an absence of standardisation in experimental design and outcome reporting restricts the synthesis of evidence to determine the efficacy of fMRI neurofeedback. Further, it remains a major challenge to delineate the sources of variance in the brain and in neurofeedback signals and their eventual effects on neurofeedback training outcomes. Similar challenges exist for separating BOLD and non-BOLD variations and their influences on data quality, and subsequently on all real-time fMRI applications.

In recent work (see Chapter 3; Heunis et al., 2020c) we investigated the available acquisition and processing methods for improving real-time fMRI signal quality, and identified an absence of methodological denoising studies and a need for community-driven quality control standards. Here, we aim to advance this process by curating a multi-echo fMRI dataset (*rt-me-fMRI*). It builds on known benefits of multi-echo fMRI for increasing BOLD sensitivity both in resting state and task fMRI (Olafsson et al., 2015; Gonzalez-Castillo et al., 2016; Kundu et al., 2017; Dipasquale et al., 2017; Moia et al., 2020). Potential benefits of multi-echo fMRI in the real-time context have been reported before (Posse et al., 2000; Posse et al., 2003a; Weiskopf et al., 2005; Marxen et al., 2016), but real-time multi-echo processing methods remain underexplored. By releasing the *rt-me-fMRI* dataset, we aim to facilitate a community effort to advance the development of methods and standards in this domain.

The *rt-me-fMRI* dataset includes multi-echo resting state and task-based fMRI data from 28 healthy participants. Figure 7.1 provides an overview, including the task types: finger tapping, emotion processing, imagined finger tapping, and imagined emotion. Several factors influenced the experimental and acquisition protocols:

Multi-echo fMRI

To facilitate the development of real-time multi-echo methods, all functional acquisitions have multiple echoes. The first resting state run allows calculation of quantitative multi-echo parameters such as baseline T2* or S0 maps, which can in turn be used for echo combination during subsequent runs.

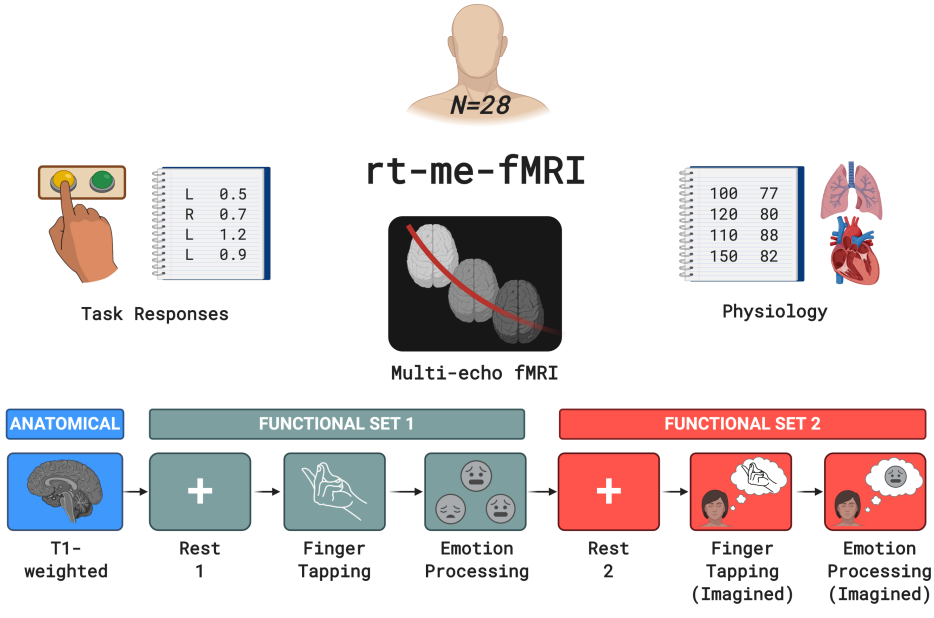

Figure 7.1 — *A depiction of the rt-me-fMRI dataset collected for 28 healthy participants. Acquired data include anatomical MRI, resting state and task-based multi-echo fMRI, task responses and physiology data. The bottom row indicates the order and type of acquired MRI scans. Colour-coding separates the anatomical scan from functional set 1 and from functional set 2. Functional set 1 includes resting state, fingerTapping and emotionProcessing acquisitions, while functional set 2 includes resting state, fingerTappingImagined, and emotionProcessingImagined acquisitions.*

Task and resting state

The motor cortex, amygdala, and visual system were selected as representative regions based on frequency of studies in fMRI and neurofeedback literature (Thibault et al., 2018), and tasks were selected to elicit appropriate BOLD responses. The *fingerTappingImagined* and *emotionProcessing* tasks respectively allow investigations into mental imagery and visual shape/face processing. Since these structures are located at distinct anatomical regions that experience different levels of noise (e.g. the amygdala suffers from more severe image dropout and physiological noise; Boubela et al., 2015), this allows investigation of spatially distinct effects of real-time denoising. Resting state scans allow comparison of the effects of processing steps in the absence and presence of a task.

Template data

In real-time fMRI applications, anatomical and functional scans are typically acquired before the main session to generate registration, segmentation, and localisation templates. This assists real-time realignment and extraction of region-based signals, and minimises per-volume processing time.

No neurofeedback

To keep the setup applicable to a range of real-time scenarios without introducing additional confounds, no neurofeedback was provided. Instead, to approximate similar mental states, the second functional set of scans were structured as imagined versions of the first functional set. This is a common approach in neurofeedback training: amygdala neurofeedback participants have been asked to think about an emotional event in their past (e.g.Young et al., 2014; Misaki et al., 2018), while motor cortex neurofeedback participants have been asked to think about performing physical exercises (e.g. Subramanian et al., 2011).

Physiology data

To facilitate the development and exploration of real-time physiological denoising methods and their relation to multi-echo-derived data, cardiac and respiratory signals were acquired.

The *rt-me-fMRI* is available in BIDS format via the DataverseNL repository[1], while a browser-based environment[2] allows interactive exploration of the data quality and derivatives.

7.2 Methods

7.2.1 Ethics and data privacy

The data described here was collected as part of a study for which ethics approval was granted by two ethics review boards. To confirm that the study protocol is in accordance with the Dutch national law on medical-scientific research conducted on human participants (see WMO[3]), the medical ethical review board at the Máxima Medisch Centrum (Veldhoven, NL) granted ethics approval. Secondly, the local ethics review board at Kempenhaeghe Epilepsy Center (Heeze, NL; where the data was collected) approved the study protocol.

All participants provided informed and written consent to participate in the study and for their maximally de-identified data (also referred to as limited data) to be shared publicly under specific conditions (see GDPR considerations in the following paragraph). Participants were provided with an electronic version of a "Participant Information Letter" which contained, in addition to standard information about the study protocol, clear information about their personal data privacy and the risks and benefits involved in sharing maximally de-identified versions of their data. They were asked to read it thoroughly and to discuss it with friends and family if they wished to do so. They were granted an opportunity to discuss any questions or concerns about their voluntary participation in the study with the lead researcher, both via email and in person. If they decided to continue

[1] https://dataverse.nl/dataverse/rt-me-fmri

[2] https://rt-me-fmri.herokuapp.com/

[3] https://wetten.overheid.nl/BWBR0009408/2020-01-01

with participation, participants signed the consent form and were provided with an electronic copy.

The dataset was collected, processed and shared in accordance with the European Union's General Data Protection Regulation (GDPR) as approved by Data Protection Officers (DPOs) at Kempenhaeghe Epilepsy Center (Heeze, NL) and the Eindhoven University of Technology. Of particular note is the procedure that was followed to enable sharing of the dataset under specific conditions that allow personal data privacy to be prioritised while adhering to FAIR data standards ("findable, accessible, interoperable, reusable"; see Wilkinson et al., 2016), with this being the first documented implementation. It followed from the collaborative effort of the Open Brain Consent Working Group (Bannier et al., 2017), a group of researchers, data experts, and legal practitioners that aim to provide globally standardised templates for informed consent and data privacy statements that allow for brain research data to be shared while prioritising personal data privacy. Steps to accomplish this include following best practices to de-identify brain images (e.g. removing personally identifiable information from image filenames and metadata and removing facial features from T1-weighted images), converting the data to BIDS format, employing a Data Use Agreement, and keeping participants fully informed about each of these steps and the associated risks and benefits. The Data Use Agreement can be accessed in this manuscript's GitHub repository[4].

7.2.2 Participants

The *rt-me-fMRI* dataset consists of MRI and physiology data from 28 healthy, right-handed (self-report) adults recruited from the local student population: 20 male, 8 female; age = 24.9 ± 4.7 (mean ± standard deviation). During recruiting, possible participants were excluded if they reported prior or current (at the time of the study) indications of neurological or psychiatric conditions, or any other standard contraindications for MRI scanning. 31 participants were initially recruited for the dataset, but three were excluded because of technical and administrative challenges. All anatomical scans were inspected by a trained radiologist and no incidental findings were reported.

7.2.3 Experimental protocol

A. Preparation and instructions

A single experimenter interacted with all participants. Data for each participant was collected during a single scanning session of approximately 1 hour, preceded by a 30 min onboarding procedure and followed by a 15 min offboarding procedure. Onboarding included a tour of the scanner and related equipment, detailed instructions for the participant to follow during each scan, and time for additional questions.

To minimise participant motion during scans so as to improve spatial and temporal image quality, participants were asked to remain as still as possible

[4] `https://github.com/jsheunis/rt-me-fMRI`

inside the scanner. Additionally, a length of tape was fixed across the participants' foreheads to the stationary part of the head coil. This provided tactile feedback which has been demonstrated as a simple and effective way to reduce head motion during fMRI scanning (Krause et al., 2019).

Lights in the scanner room were dimmed during the experiment. Participants viewed instructions projected on a screen at the back of the scanner bore via a head coil-mounted mirror. For resting state functional scans, participants were instructed to keep their eyes open and fixate on the cross on the screen.

B. Experimental design

All functional scans have 210 volumes and exactly the same sequence parameters. All task scans follow a block design with 10 volumes (i.e. 20 s) per block, and with blocks alternating between control and task conditions. All task designs start and end with a control condition. These block design aspects are depicted in Figure 7.2 for all task runs. Take note that the depictions do not necessarily agree with the exact stimuli as seen by the participants, as the depictions are purely illustrative.

For the *fingerTapping* task, participants were instructed to execute finger tapping with their right hand by steadily tapping the tip of the thumb to the tip of each other finger in succession, reversing the tapping order until the end of the task block is reached. For the *fingerTappingImagined* task, participants were instructed to imagine doing exactly the same as in the actual finger tapping task, but without actually moving their right fingers. For the control condition during the *fingerTappingImagined* task, participants were asked to count backwards in multitudes of 7.

The *emotionProcessing* task was an adapted "Hariri" task from the emotion processing task used in the Human Connectome Project (Van Essen et al., 2012; Hariri et al., 2002; Manuck et al., 2007). Materials were implemented to suit the paradigm for this *rt-me-fMRI* dataset. During each 20 s task block, participants were presented with a task cue (3 s duration), followed by a trial with three pictures of faces where the participant had to select one of the bottom figures (left or right) that resembled the top one, by pressing a left or right button (2 s duration). The inter-trial interval was 1 s duration (see Figure 7.3). Each 20 s block had 6 trials. The same design timing was used for the control condition blocks, i.e. matching shapes, as for the trial condition blocks depicted in Figure 7.3. Participants used an MRI-compatible button box with their right hand to complete the task. Participants were asked to press the left button with their right index finger if selecting the bottom left image (shape or face) on the screen, and to conversely press the right button with their right middle finger if selecting the bottom right image.

For the *emotionProcessingImagined* task, participants were instructed prior to the scanning session to identify an emotional event in their past that involved a person or people, and to think about this event and also try to mentally experience the identified emotion during the task blocks. For the control condition during this

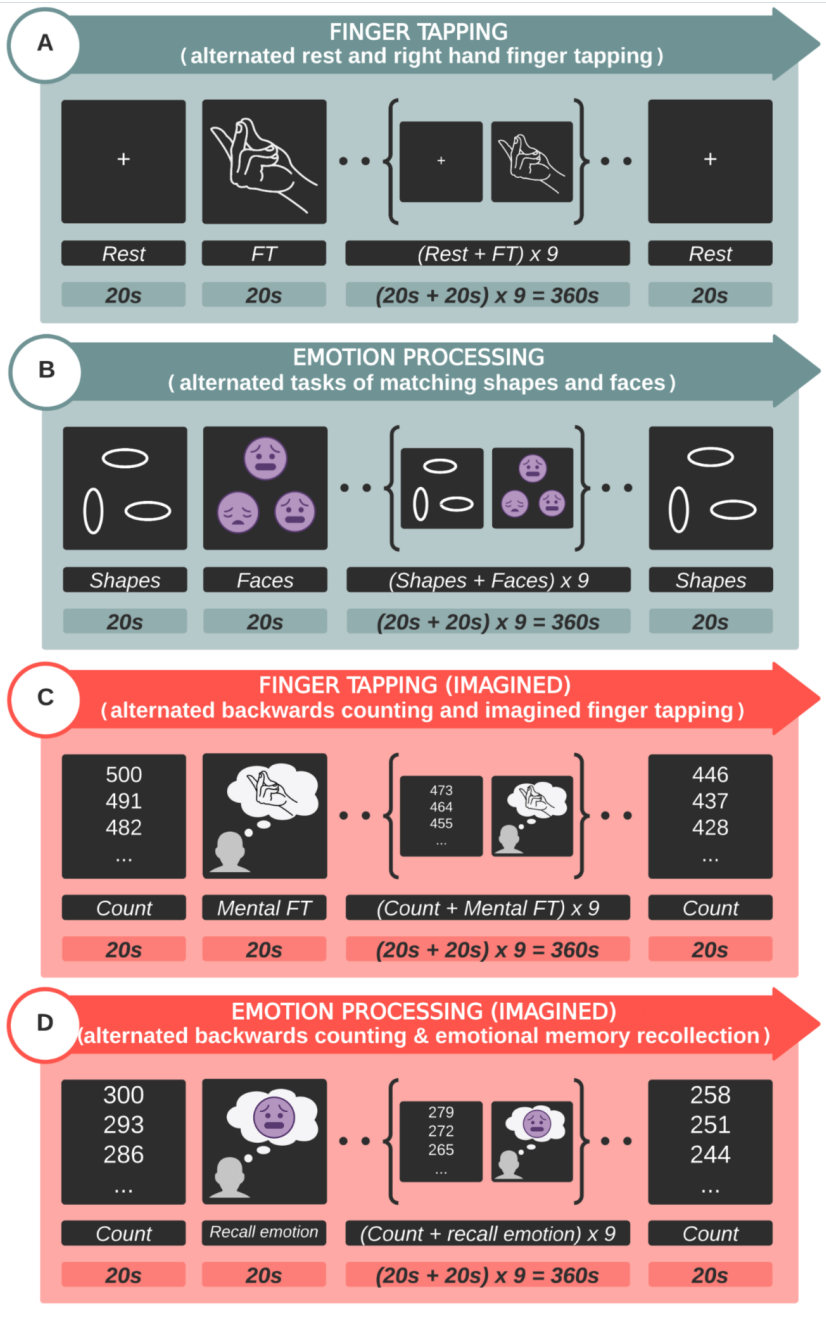

Figure 7.2 — *Depictions of the experimental designs for all tasks. Subfigures include: (A) fingerTapping - right hand finger tapping, (B) emotionProcessing - matching shapes and faces, (C) fingerTappingImagined - imagined finger tapping, and (D) emotionProcessingImagined - emotional memory recollection. All designs follow a block paradigm with 10 volumes (i.e. 20 s) per block, and with blocks alternating between control and task conditions. All task designs start and end with a control condition. Color code: functional set 1 = Green; functional set 2 = Red. FT = finger tapping.*

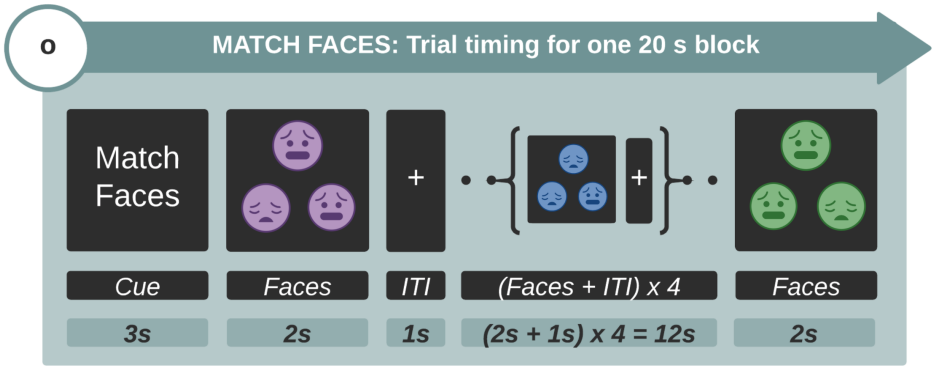

Figure 7.3 — *The task timing for the emotionProcessing task. Times are provided for the cue, trials and inter-trial interval during a single block (20 s) of the face matching condition. The same design timing was used for the control condition blocks.*

mental emotion task, participants were asked to count backwards in multitudes of 9.

Participants were interviewed after the scanning session about their experiences during the MRI acquisition and the tasks. None reported detrimental issues with regards to their ability to focus on the task or with task-switching.

Tasks and instructions were programmed and presented to the participants using E-Prime Studio version 2.0.10.248. The programmed E-prime files used for each task (".es2" format), as well as all presented images for trials, conditions, cues and instructions (.jpg format), can be accessed in the supplementary code repository[5]. The exact timing information for the presented material (for all functional runs) and the button presses (for *emotionProcessing*), as well as the actual button press responses, were exported from E-prime (in .dat and .txt format) at the end of each session[6].

7.2.4 MRI acquisition parameters

MRI data was acquired on a 3 Tesla Philips Achieva scanner (software version 5.1.7) and using a Philips 32-channel head coil.

A. Anatomical MRI

A single T1-weighted anatomical image was acquired using a 3D gradient echo sequence (T1 TFE) with scanning parameters: TR = 8.2 ms; TE = 3.75 ms; flip angle

[5] `https://github.com/jsheunis/rt-me-fMRI`

[6] For the majority of participants, the presentation timing for the *emotionProcessing* task was delayed by tens of milliseconds for each trial (planned versus actual timing). This resulted in the full task presentation running on for about 5 s after the scan acquisition stopped. This is not deemed a problem, mainly since the exact presentation time was captured and is available in the BIDS dataset. However, users should take note not to use the planned timing parameters as that would ignore the delay that occurred.

= 8°; field of view = 240×240×180 mm^3; resolution = 1×1×1 mm^3; total scan time = 6:02 min.

B. Functional MRI

All six functional MRI scans were acquired using a multi-echo, echo-planar imaging sequence with scanning parameters: TR = 2000 ms; TE = 14, 28, 42 ms (3 echoes); number of volumes = 210 (excluding 5 dummy volumes discarded by the scanner); total scan time = 7:00 min (excluding 5 dummy volumes); flip angle = 90°; field of view = 224×224×119 mm^3; resolution = 3.5×3.5×3.5 mm^3; in-plane matrix size = 64×64; number of slices = 34; slice thickness = 3.5 mm; interslice gap = 0 mm; slice orientation = oblique; slice order/direction = sequential/ascending; phase-encoding direction = A/P; SENSE acceleration factor = 2.5; parts of the cerebellum and brainstem were excluded for some participants to ensure full motor cortex and amygdala coverage.

The echo times, spatial resolution, and SENSE factor were tuned with the aim of improving spatial resolution and coverage while limiting the TR at maximum 2000 ms, including a maximum number of echoes, and keeping the SENSE factor low to prevent SENSE artefacts.

7.2.5 Physiology data acquisition parameters

Breathing fluctuations were recorded with the use of a pressure-based breathing belt strapped around the participant's upper abdomen. Heart rate was recorded using a pulse oximeter fixed to the participant's left index finger. Both of these recording devices were wired directly to the scanner, sampled at 500 Hz, synchronised internally to the start/stop pulses of each functional scan, and data were written to Philips's standard "scanphyslog" log file type.

7.2.6 Standardisation: Brain Imaging Data Structure

To adhere to FAIR data principles, the full dataset was curated into the standardised and community-maintained Brain Imaging Data Structure (BIDS; Gorgolewski et al., 2016). This involved the use of several software packages and custom scripts to assist in file format conversion and data structuring. A Jupyter notebook containing Python code and descriptions for each of the steps in this section can be accessed at the project's code repository[7].

A. MRI data

Anatomical and functional MRI data were converted from the Philips PAR/REC format to BIDS using the Python package bidsify (v0.3[8]) This package has dcm2niix (v1.0.20190410[9]) as a dependency to convert the PAR/REC files to NIfTI. It also structures the data into the directory system specified by the BIDS standard.

[7] https://github.com/jsheunis/rt-me-fMRI

[8] https://github.com/NILAB-UvA/bidsify

[9] https://github.com/rordenlab/dcm2niix/releases/tag/v1.0.20190410

Anatomical files were additionally de-identified using pydeface (v2.0.0[10]; Omer Faruk Gulban et al., 2019), which removes facial features from the T1w NIfTI image. Further anonymisation steps included removing time and date stamps and any identifiable information related to the acquisition location or system from the files output from bidsify.

Since PAR/REC files do not contain slice timing information, the converted NIfTI files did not contain it either. Slice timing information was calculated using available parameters and added with a script to the BIDS-specific JSON sidecar files.

B. Physiology data

Heart rate and breathing traces were converted from the Philips "scanphyslog" format to BIDS format using the Python package scanphyslog2bids (v0.1[11]).

C. Task presentation and response data

Presentation timing, button presses and button press response timing information were all converted to the BIDS format using a combination of custom Python scripts and the convert-eprime package (v0.0.1[12]; Salo, 2020).

7.2.7 Preprocessing

Raw data was preprocessed using the open source MATLAB-based and Octave-compatible *fMRwhy* toolbox (see Section 7.4 for details). The basic anatomical and functional preprocessing pipeline applied to all data is depicted in Figure 7.4.

As a first step, the T1-weighted anatomical image was coregistered to the template functional image (task-rest_run-1_echo-2, volume 1) using SPM12's *coregister/estimate* functionality, which maximises normalised mutual information to generate a 12 degree-of-freedom transformation matrix. Before resampling to the functional resolution, this coregistered T1-weighted image was segmented using tissue probability maps and SPM12's *unified segmentation* algorithm (Ashburner and Friston, 2005). This yielded subject-specific probability maps for gray matter, white matter, CSF, soft tissue, bone and air in the subject functional space. All of these probability maps were then resampled (using *coregister/write*) to the subject functional resolution. Masks were generated for gray matter, white matter, CSF, and the whole brain (a combination - logical OR after thresholding - of the previous three masks). These were overlaid on the coregistered and resampled T1w image, to allow visual inspection of segmentation and registration quality.

Anatomical regions of interest were then taken from the cytoarchitecture-based atlases in the SPM Anatomy Toolbox (Eickhoff et al., 2005). For the motor cortex, regions 4a and 4p were used. For the amygdala, regions LB, IF, SF, MF, VTM, and

[10] https://github.com/poldracklab/pydeface/releases/tag/2.0.0

[11] https://github.com/lukassnoek/scanphyslog2bids

[12] https://github.com/tsalo/convert-eprime/releases/tag/0.0.1

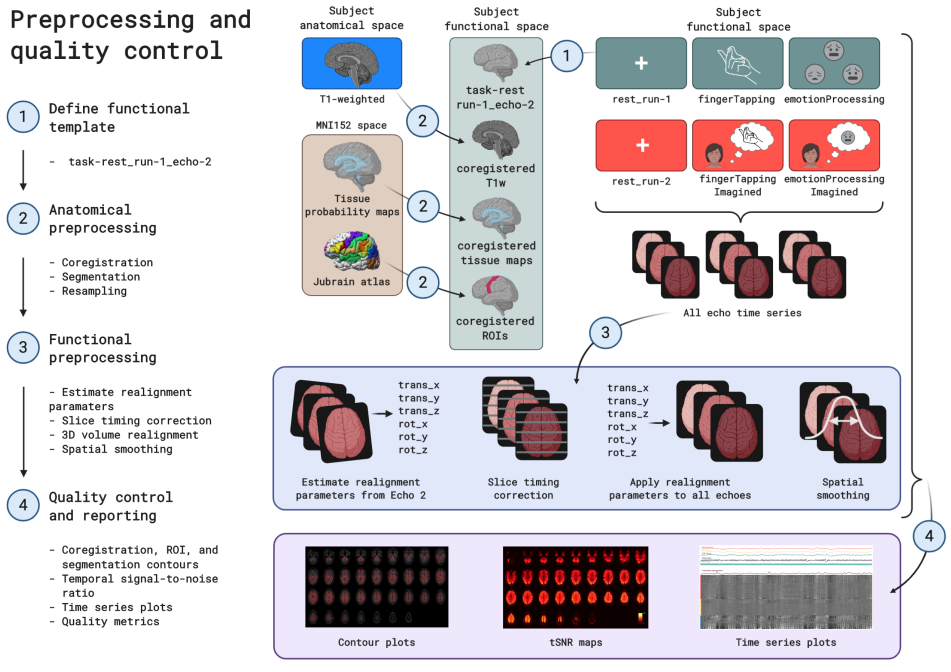

Figure 7.4 — *A diagram depicting the preprocessing steps conducted on the rt-me-fMRI dataset in chronological order. Steps include: (1) defining a functional template image from the first resting state run; (2) mapping the anatomical image and atlas-based regions of interest to the functional template space; (3) estimating realignment parameters from the template echo time series, running slice timing correction, applying realignment parameters to all echo time series, and applying spatial smoothing, and (4) generating quality control metrics and visualisations for anatomical and functional data.*

CM were used. For the fusiform gyrus, regions FG1, FG2, FG3, and FG4 were used. Regions of interest were transformed from MNI152 space to the subject functional space using SPM12 normalise/write, as well as the inverse transformation field that was saved as part of the segmentation procedure. The regions of interest for this study include the left motor cortex (for the motor processing tasks), the bilateral amygdala (for the emotion processing tasks) and the fusiform gyrus (for the *emotionProcessing* task). These ROIs are overlaid on the coregistered and resampled T1-weighted image, to allow visual inspection of normalisation quality.

Functional data were preprocessed, starting with estimating realignment parameters for each functional time series using SPM12's realign/estimate, which performs a 6 degree-of-freedom rigid body transformation that minimises the sum of squared differences between each volume and the template volume. Realignment parameters were estimated for the second-echo time series of each run. Then, slice timing correction was done with SPM12, which corrects for differences in image acquisition time between slices. Each echo time series of all functional runs were slice time corrected. 3D volume realignment followed, which applied spatial transformation matrices derived from the previously estimated realign-

ment parameters to all echo time series of all functional runs. Both raw time series and slice time corrected time series were realigned. Lastly, all echo time series of all functional runs were spatially smoothed using a Gaussian kernel filter with FWHM = 7 mm (i.e. double the voxel size). Smoothing was performed on raw, slice time corrected and realigned time series data.

Next, several signal time series were calculated or extracted for use as possible GLM regressors in functional task analysis, or for quality control. From the realignment parameters (3 translation and 3 rotation parameters per volume), a Volterra expansion yielded derivatives, squares and squares of derivatives (Friston et al., 1996). Framewise displacement (FD; Power et al., 2012) was also calculated from the realignment parameters, and volumes were marked as outliers based on different thresholds of, respectively, 0.2 mm and 0.5 mm. RETROICOR regressors (Glover, Li, and Ress, 2000) were generated from the cardiac and respiratory signals using the TAPAS PhysIO toolbox, which yielded 6 cardiac regressors, 8 respiratory regressors, 4 interaction regressors, and additionally a cardiac rate regressor (CR; the cardiac rate time series convolved with the cardiac response function; Chang, Cunningham, and Glover, 2009) and a respiratory volume per time regressor (RVT; respiratory volume per time convolved with the respiratory response function; Birn et al., 2006; Birn et al., 2008). From the slice time corrected and realigned time series data (of all functional runs), signals were extracted per voxel and spatially averaged within the previously generated tissue masks to yield tissue compartment signals for gray matter, white matter, cerebrospinal fluid (CSF) and the whole brain.

The last set of preprocessing steps included calculation of image quality metrics and visualisations, using the BIDS-compatible *fmrwhy_workflow_qc* pipeline from the *fMRwhy* toolbox. Operations on functional time series data were all done on detrended (linear and quadratic trends) realigned data, except where otherwise specified. Temporal signal-to-noise ratio (tSNR) maps were calculated for all runs by dividing the voxel-wise time series mean by the voxel-wise standard deviation of the time series. Tissue compartment averages were then extracted from these tSNR maps. Percentage difference maps (from the time series mean) were calculated per volume for use in carpet plots (or gray plots).

7.3 Dataset validation

7.3.1 BIDS validation

The full dataset was validated for BIDS compatibility with the use of the web-based "BIDS validator" tool (v1.5.4[13]). A log of the BIDS validator output can be found in the project's code repository[14].

[13] https://bids-standard.github.io/bids-validator/

[14] https://github.com/jsheunis/rt-me-fMRI

7.3.2 COBIDAS reporting

Data acquisition and experimental protocol parameters for this study were reported according to the community-formulated COBIDAS guidelines (Nichols et al., 2017). A modular version of this information is available in the project's GitHub repository.

7.3.3 Data quality assessment

Image and data quality of this dataset was assessed using the *fMRwhy* toolbox. This allowed quality to be assessed for raw and minimally (pre)processed versions of the data, and also for interim steps on which the validity of eventual study outcomes might depend. A BIDS-compatible workflow in the *fMRwhy* toolbox, *fmrwhy_workflow_qc*, runs initial preprocessing and quality control of the raw data and outputs a quality report per subject, which includes metrics and visualisations for anatomical and functional MRI data and for peripheral data.

For anatomical MRI:

- Coregistered T1w segmentations (gray matter, white matter, CSF, and a whole brain mask) were overlaid onto the subject functional space, for visual inspection of the registration and segmentation quality.

- Coregistered anatomical regions of interest (in this case the left motor cortex, bilateral amygdalae and bilateral fusiform gyri) were overlaid onto the subject functional space, for visual inspection.

For functional MRI (all runs):

- A summary table provides values for all runs per subject for mean framewise displacement (FD), total FD, FD outliers, and mean tSNR in all tissue compartments. This allows quick inspection per participant, but is better understood when referenced to the whole dataset.

- Several image montages were generated per run, including the time series mean, the standard deviation and the tSNR map. The time series mean gives a quick view of the general quality of the time series and can indicate spike or interference artefacts. The standard deviation map shows areas with high signal fluctuation that can often be related to movement (e.g. close to the eyes). The tSNR maps are useful for investigating general signal quality, to indicate signal dropout and comparing signal quality across regions.

- A carpet (time series) plot was generated per run, which displays voxel intensity in percentage signal change from the mean over time. The vertical axis (voxels) is either grouped per tissue type (compartment ordered) or ordered from top to bottom according to the voxel's time series correlation strength to the global signal. Signal traces above the carpet plot are also shown, including tissue compartment signals, respiration, heart rate, and framewise displacement. These plots are useful quality checking tools as they make it easy to visualise wide scale signal fluctuations across voxels, which can then be related visually to changes in

physiological signals or subject movement.

- Checking the quality of the recorded cardiac and respiratory traces is made possible with images generated by TAPAS PhysIO during the process of calculating RETROICOR, CR and RVT regressors. Images include a plot of the temporal lag between derived heart beats within thresholds for outliers, and a plot showing the breathing belt amplitude distribution that can be inspected for unexpected shapes.

All functional quality metrics of the full dataset, generated by the *fmrwhy_workflow_qc* workflow, are summarised in Table C.1 [15] in Appendix C. This includes, per run, mean framewise displacement, total framewise displacement, framewise displacement outliers (based on a conservative 0.2 mm threshold, and a liberal 0.5 mm threshold), z-score, and mean tSNR in all tissue compartments (grey matter, white matter, cerebrospinal fluid, whole brain). This allows possible data users to inspect the quality measures and to set personalised thresholds and exclusion criteria.

Figure 7.5 displays summarised quality metrics for the *rt-me-fMRI* dataset, and examples of single-subject quality images. Individual quality reports can be downloaded together with the dataset.

7.3.4 Task validation

The slice timing corrected, 3D realigned and spatially smoothed Echo 2 time series of all task runs underwent individual- and group-level statistical analysis using a general linear model with SPM12. Task regressors included the main "ON" blocks for the *fingerTapping*, *fingerTappingImagined*, and *emotionProcessingImagined* tasks, and both the separate "SHAPES" and "FACES" trials for the *emotionProcessing* task. Regressors not-of-interest for all runs included six realignment parameter time series and their derivatives, the CSF compartment time series, and RETROICOR regressors (both cardiac and respiratory to the 2nd order, excluding interaction regressors, selected based on common implementation procedures in literature). Additional steps executed by SPM12 before beta parameter estimation include high-pass filtering using a cosine basis set and AR(1) autoregressive filtering of the data and GLM design matrix.

Contrasts were then applied to the single task-related beta maps for the fingerTapping, *fingerTappingImagined*, and *emotionProcessingImagined* tasks, and to the FACES, SHAPES, and FACES¿SHAPES beta maps for the *emotionProcessing* task. Statistical thresholding, consisting of familywise error rate control with $p < 0.05$ and a voxel extent threshold of 0, was then applied on a per-subject basis to identify task-related clusters of activity. Unthresholded subject-level contrast maps were normalised to MNI152 space and then fed into a group-level one-sided

[15] Online version: `https://github.com/jsheunis/rt-me-fMRI/blob/master/data/sub-all_task-all_desc-allQCmetrics.tsv`

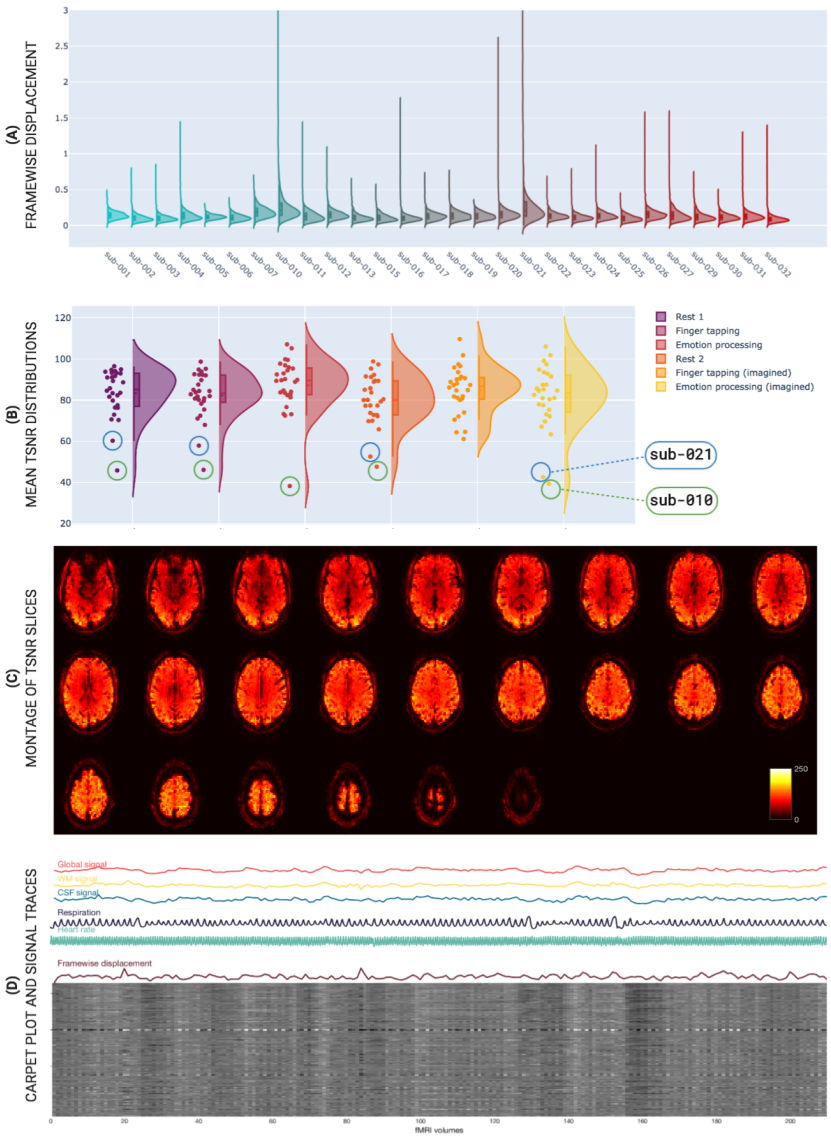

Figure 7.5 — *Representative quality checking information for the rt-mf-fMRI dataset. Sub-figures include group level summary plots (A and B) and examples of subject level quality metric figures (C and D): (A) Vertical distribution (violin) plots of framewise displacement per subject, covering all functional runs. sub-010, sub-020 and sub-021 show comparatively high means and more outliers. (B) Vertical distribution (violin) plots of mean grey matter temporal signal-to-noise ratio (tSNR) per functional run, covering all subjects. Head movement results in higher signal fluctuations and hence lower tSNR, which is exemplified in the circled high mover data points: sub-021 (blue) and sub-010 (green); (C) An axial slice montage of temporal signal signal-to-noise ratio. (D) A time series "carpet plot" showing the global, white matter, CSF, respiration, and cardiac signals, as well as the calculated framewise displacement time series; (B) an axial slice montage of temporal signal signal-to-noise ratio.*

Table 7.1 — *Neurosynth-decoded terms*

Task	10 highest correlated decoded terms
fingerTapping	motor, premotor, finger, premotor cortex, movements, movement, hand, supplementary, execution, finger movements
emotionProcessing	face, fusiform, faces, fusiform face, fusiform gyrus, face ffa, ffa, occipital, inferior occipital, visual
fingerTappingImagined	theory mind, medial prefrontal, social, mind, mind tom, mental states, tom, primary, primary motor, junction
emotionProcessingImagined	medial, medial prefrontal, autobiographical, social, default, posterior cingulate, theory mind, mind, default mode, autobiographical memory

t-test, for which the t-statistic maps were subsequently thresholded at $p < 0.001$ and an extent threshold of 20 voxels. Unthresholded individual- and group-level t-statistic maps can be accessed as a NeuroVault collection[16].

Figure 7.6 shows the resulting thresholded group t-statistic maps for all four task runs. Figure 7.6A clearly shows activity clusters in the left motor cortex and right cerebellum, as expected for a finger tapping task as well as a negative activation pattern in the default mode network. Figure 7.6C shows activation in the visual cortex commensurate with a face/shape matching task, specifically in the left and right fusiform gyri. Additional clusters are found in the amygdalae and hippocampi, as expected for an emotion processing task. For both imagined tasks, similar but weaker activation clusters are found in the expected regions (respectively the motor cortex in Figure 7.6B, and amygdalae in Figure 7.6D) but both wide scale activation patterns are consistent with mental tasks including imagery and memory recollection. Additionally, Figure 7.6B and Figure 7.6D show negative activation patterns in the dorsal attention network. The activation results in Figure 7.6 are further evidenced by the resulting highest correlated terms when decoding the unthresholded group t-statistic images with the web-based Neurosynth tool[17] (Yarkoni et al., 2011). Table 7.1 shows the resulting terms[18].

[16] `https://neurovault.org/collections/XWDGUJHD/`

[17] `www.neurosynth.org`

[18] Task names of the *rt-me-fMRI* dataset were selected based on the desired activation response for the given use cases, e.g. *emotionProcessing* to elicit a response in regions involving emotion processing, with the knowledge that the tasks might yield varied responses and have varied use cases. This can lead to the activation analysis and Neurosynth decoding process yielding patterns and terms that do not necessarily reflect the task name, e.g. activation of the fusiform face area and related terms ("face", "fusiform", "occipital") for the *emotionProcessing* task.

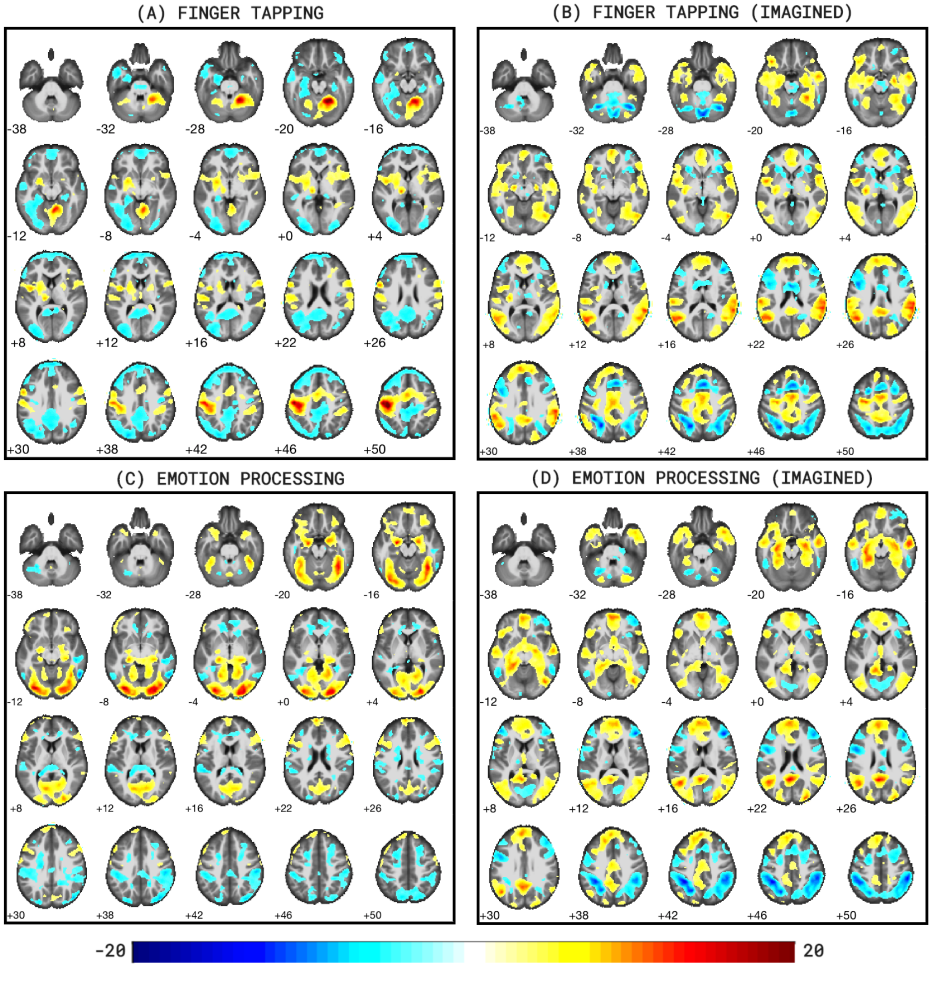

Figure 7.6 — *Group-level t-statistic maps for all tasks of the rt-me-fMRI dataset. Subfigures include: (A) fingerTapping, (B) fingerTappingImagined, (C) emotionProcessing, and (D) emotionProcessingImagined ($p<0.001$, voxel extent=20). Images were generated with bspmview. Figure 7.6A clearly shows activity clusters in the left motor cortex and right cerebellum, as expected for a finger tapping task. Figure 7.6C shows activation in the visual cortex commensurate with a face/shape matching task, specifically in the left and right fusiform gyri. For both imagined tasks, similar but weaker activation clusters are found in the expected regions (respectively the motor cortex in Figure 7.6B, and amygdalae in Figure 7.6D) but both wide scale activation patterns are consistent with mental tasks including imagery and memory recollection.*

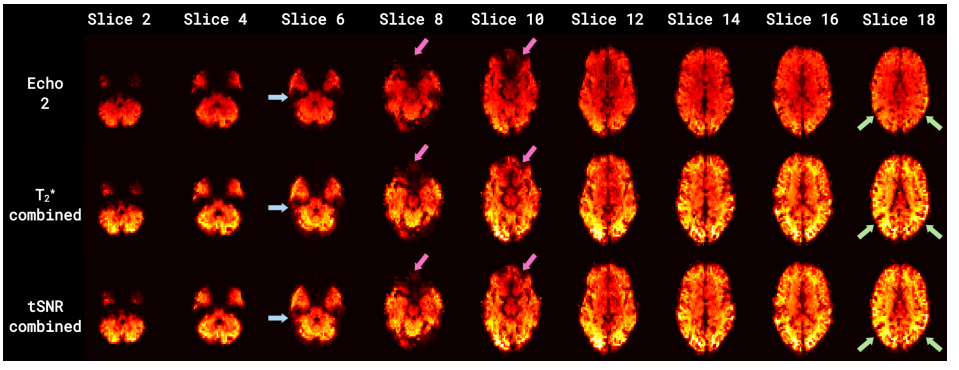

Figure 7.7 — *Axial slice montages of temporal signal-to-noise ratios (tSNR) in single and multi-echo combined time series. Time series include: the 2nd echo time series (top row) and two combined time series (middle row = T2*-combined; bottom row = tSNR-combined). Blue and magenta arrows indicate areas of signal dropout and recovery (including, respectively, the medial temporal and inferior temporal lobes, and the inferior frontal lobe). Light green arrows indicate areas with substantial increases in tSNR (in the lateral cortex and towards the anterior cortex as the slices increase in a superior direction). Combined multi-echo time series result in both substantially higher tSNR and signal recovery compared to Echo 2.*

7.3.5 Multi-echo data validation

A core contribution of this *rt-me-fMRI* dataset lies in the multi-echo acquisition. Multi-echo fMRI samples multiple T2*-weighted images at a range of echo times along the decay curve following a single transverse magnetic excitation, which theoretically allows the optimum BOLD contrast to be optimised for a range of baseline tissue T2* values. Subsequently, echo combination through weighted summation or averaging is a typical processing step that generally increases temporal signal-to-noise ratio and contrast-to-noise ratio and decreases signal dropout in regions with high susceptibility artefacts and signal dropouts (Menon et al., 1993; Posse et al., 1999; Posse et al., 2012). Echoes can be combined using a variety of weights, including baseline voxelwise tSNR and T2* maps.

Figure 7.7 and Figure 7.8 illustrate that such combination procedures improve tSNR and signal dropout, hence validating the use of multi-echo fMRI for improved quality data. Representative signal recovery is demonstrated in the tSNR maps of Figure 7.7 for a single run of a single subject, particularly by the blue and magenta arrows showing areas of signal dropout in the Echo 2 time series (including, respectively, the medial temporal and inferior temporal lobes, and the orbitofrontal lobe) and subsequent recovery in the combined time series. The light green arrows indicate substantial increases in tSNR in areas close to the bilateral temporal-occipital junction and towards the occipital lobe as the slices increase in a superior direction. Figure 7.8 shows distribution plots of the mean grey matter tSNR for the single (2nd) echo and two combined echo (tSNR-combined and T2*-combined) time series, covering all functional runs and all subjects. The two combined echo time series clearly have improved tSNR values, increasing by 30%

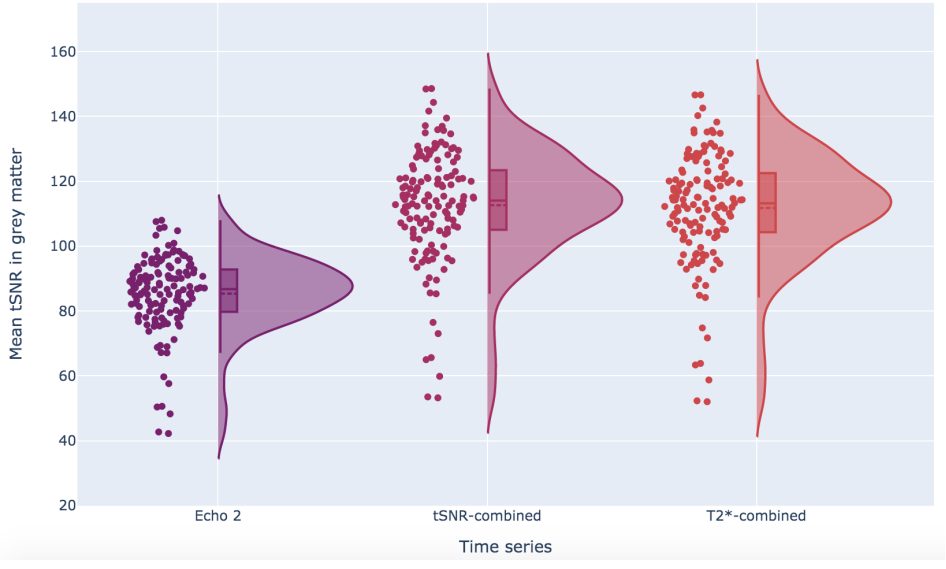

Figure 7.8 — *Vertical distribution (violin) plots of mean grey matter temporal signal-to-noise ratios (tSNR) in single and multi-echo combined time series. Distributions are shown for three time series: Echo 2, tSNR-combined and T2*-combined. A single distribution plot covers all subjects and all runs excluding rest_run-1. The two combined echo time series show clear increases in mean tSNR values.*

from 85 (2nd echo) to 112 (tSNR-combined).

Further benefits of multi-echo over conventional single-echo fMRI exist (see for example Olafsson et al., 2015; Dipasquale et al., 2017; Lombardo et al., 2016; Gonzalez-Castillo et al., 2016; Moia et al., 2020; Caballero-Gaudes et al., 2019), but such analyses are beyond the scope of this validation step and can be explored further with this publicly available dataset. In complementary work using this dataset we evaluate the use of several combination and T2*-mapping procedures for both offline and real-time BOLD sensitivity (see Chapter 8; Heunis et al., 2020a).

7.3.6 Data inclusion/exclusion

To be a possible participant in this study, individuals had to be healthy, right-handed volunteers with no prior or current (at the time of the study) indications of neurological or psychiatric conditions. They also had to report the absence of any other standard contraindications for MRI scanning. 32 participants were initially recruited for the study, and the datasets of three participants were excluded due technical and one due to administrative challenges. No further datasets were excluded, even in cases of more than average or severe motion (e.g. sub-010 and sub-021), since it was decided that such data could still be useful for future methods development or related insights. Table C.1 (also available in the project's

GitHub repository[19]) provides a list of all functional quality metrics for all participants and runs, which allows possible data users to inspect the quality measures and to set personalised thresholds and exclusion criteria.

7.4 Data and Software Availability

7.4.1 Data

The *rt-me-fMRI* dataset is available in BIDS format via the Dutch research data repository DataverseNL[20]. This repository includes the raw BIDS data, descriptive metadata, and derivative data including quality reports.

Apart from the dataset README file, all core files are available in one of 3 formats: NIfTI, TSV and JSON. Functional and anatomical data are stored as uncompressed NIfTI files (with the ".nii" extension), which contain image and header data and can be handled/viewed by all major neuroimaging analysis packages and programming languages. Tabular data such as participants, task events, response timing and physiology data are stored in tab-separated value text files (with the extension ".tsv", or if compressed ".tsv.gz") and can be handled by text or spreadsheet reading/editing software on all major operating systems, or alternatively by all major software programming languages. Metadata about the dataset, tasks, events and more are stored as key-value pairs in text-based JSON files (with the extension ".json") that can be handled/viewed using all major software programming languages.

All data files are organised according to the BIDS convention for dataset participants, MRI data type (anatomical or functional), and derivatives, as depicted in Figure 7.9.

Each participant directory contains two subdirectories: "anat" and "func", respectively containing all anatomical and functional images and metadata. Different data types can be distinguished based on BIDS identifiers, e.g. "_bold" for functional and "_T1w" for anatomical MRI data. The full list of data acquisitions with their data types, descriptions, and formats are provided in Table 7.2. Note that for functional data, each resting state and task run consists of three separate image files, one per echo (i.e. "_echo-1_bold.nii", "_echo-2_bold.nii", and "_echo-3_bold.nii"). JSON sidecar files accompany all BOLD and physiology data files on the participant level, while the accompanying JSON sidecar files for the four types of task event files are on the dataset level. Other files on the dataset level include the README, the dataset description (JSON) and the participant list (TSV).

[19] https://github.com/jsheunis/rt-me-fMRI

[20] https://dataverse.nl/dataverse/rt-me-fmri

Figure 7.9 — *A diagram showing the content of the rt-me-fMRI dataset. The top level directory includes metadata about the dataset, participants and task events, as well as a directory per participant and lastly a derivatives directory. The expansion of "sub-001" (top right) shows subdirectories "anat" and "func", each with neuroimages and metadata related to anatomical and functional scans, respectively. The expansion of the "derivatives" directory (bottom right) shows subdirectories "fmrwhy-dash" and "fmrwhy-qc". The former contains all derivative data required to run the interactive browser-based application accompanying this dataset. The latter includes a quality report per participant in HTML format.*

Table 7.2 — *rt-me-fMRI core dataset acquisitions, types, descriptions and formats.*

Acquisition	BIDS identifier (extension)	Data Type	Description	Acquired Data Format(s)	BIDS Format
T1-weighted	_T1w (.nii)	Anatomical MRI	Standard high-resolution	NIfTI	NIfTI
Resting data: task-rest_run-1	_bold (.nii)	Functional MRI	Resting state	PAR/REC, DICOM	NIfTI
Task data: fingerTapping	_bold (.nii)	Functional MRI	Right-hand finger tapping	PAR/REC, DICOM	NIfTI
Task data: emotionProcessing	_bold (.nii)	Functional MRI	Matching shape and faces	PAR/REC, DICOM	NIfTI
Resting data: rest_run-2	_bold (.nii)	Functional MRI	Resting state	PAR/REC, DICOM	NIfTI
Task data: fingerTapping-Imagined	_bold (.nii)	Functional MRI	Mental motor task - imagined finger tapping	PAR/REC, DICOM	NIfTI
Task data: emotionProcessing-Imagined	_bold (.nii)	Functional MRI	Mental emotion task - emotional memory recollection	PAR/REC, DICOM	NIfTI
Task responses and timing	_events (.tsv.gz)	Peripheral measure	Stimulus and response timing for all tasks, i.e. x4	Eprime 'dat' and 'txt' files	TSV
Physiology data	_physio (.tsv.gz)	Peripheral measure	Cardiac and respiratory traces for all runs, i.e. x6	Philips scanphyslog.log	TSV
n/a	n/a	Metadata	JSON sidecar files for all files of type _bold and _physio	Philips scanphyslog.log	JSON

7.4.2 Software

An interactive environment[21] was created alongside this study to allow users to interactively explore summaries of the data derivatives and quality control aspects.

All software scripts and self-developed tools used to prepare, preprocess and quality check the data are openly available at the project's code repository [22]. This includes instructions to download, extract, and understand the data; the data preparation script; the preprocessing script; the quality reporting script; and the script to reproduce the figures for this manuscript.

[21] `https://rt-me-fmri.herokuapp.com/`

[22] https://github.com/jsheunis/rt-me-fMRI

Dependent software and toolboxes/packages used for these preparation, preprocessing and quality reporting steps include:

- Python 3.7+
- bidsify (v0.3[23])
- scanphyslog2bids (v0.1[24]).
- dcm2niix (v1.0.20190410[25])
- pydeface (v2.0.0[26]; Omer Faruk Gulban et al., 2019)
- convert-eprime (v0.0.1[27]; Salo, 2020)
- MATLAB R2016b or later (9.1.0.441655; The MathWorks Inc)
- fMRwhy (v.0.0.1[28])
- SPM12 (r7771[29]; Friston et al., 2007)
- Anatomy Toolbox (v3.0; Eickhoff et al., 2005)
- bids-matlab (v.0.0.1[30])
- dicm2nii (v0.2 from a forked repository[31])
- TAPAS PhysIO (v3.2.0[32]; Kasper et al., 2017)
- Raincloud plots (v1.1[33]; Allen et al., 2019)
- bspmview (v20180918[34]; Spunt, 2016)

[23] https://github.com/NILAB-UvA/bidsify
[24] https://github.com/lukassnoek/scanphyslog2bids
[25] https://github.com/rordenlab/dcm2niix/releases/tag/v1.0.20190410
[26] https://github.com/poldracklab/pydeface/releases/tag/2.0.0
[27] https://github.com/tsalo/convert-eprime/releases/tag/0.0.1
[28] https://github.com/jsheunis/fMRwhy
[29] https://github.com/spm/spm12/releases/tag/r7771
[30] https://github.com/jsheunis/bids-matlab/releases/tag/fv0.0.1
[31] https://github.com/jsheunis/dicm2nii/releases/tag/v0.2
[32] https://github.com/translationalneuromodeling/tapas/releases/tag/v3.2.0
[33] https://github.com/RainCloudPlots/RainCloudPlots/releases/tag/v1.1
[34] https://github.com/spunt/bspmview/tree/20161108

Chapter 7

Chapter 8

The effects of multi-echo fMRI combination and rapid T2*-mapping on offline and real-time BOLD sensitivity

Abstract

A variety of strategies are used to combine multi-echo functional magnetic resonance imaging (fMRI) data, yet recent literature lacks a systematic comparison of the available options. Here we compare six different approaches derived from multi-echo data and evaluate their influences on BOLD sensitivity for offline and in particular real-time use cases: a single-echo time series (based on Echo 2), the real-time T2*-mapped time series (T2*FIT) and four combined time series (T2*-weighted, tSNR-weighted, TE-weighted, and a new combination scheme termed T2*FIT-weighted). We compare the influences of these six multi-echo derived time series on BOLD sensitivity using a healthy participant dataset (N=28) with four task-based fMRI runs and two resting state runs. We show that the T2*FIT-weighted combination yields the largest increase in temporal signal-to-noise ratio across task and resting state runs. We demonstrate additionally for all tasks that the T2*FIT time series consistently yields the largest offline effect size measures and real-time region-of-interest based functional contrasts and temporal contrast-to-noise ratios. These improvements show the promising utility of multi-echo fMRI for studies employing real-time paradigms, while further work is advised to mitigate the decreased tSNR of the T2*FIT time series. We recommend the use and continued exploration of T2*FIT for offline task-based and real-time region-based fMRI analysis. Supporting information includes: a data repository (`https://dataverse.nl/dataverse/rt-me-fmri`), an interactive web-based application to explore the data (`https://rt-me-fmri.herokuapp.com/`), and further materials and code for reproducibility (`https://github.com/jsheunis/rt-me-fMRI`).

This chapter is currently undergoing peer review and a preprint has been published as: Heunis, S., Breeuwer, M., Caballero-Gaudes, C., Hellrung, L., Huijbers, W., Jansen, J.F., Lamerichs, R., Zinger, S., Aldenkamp, A.P., 2020. The effects of multi-echo fMRI combination and rapid T2*-mapping on offline and real-time BOLD sensitivity. bioRxiv 2020.12.08.416768. https://doi.org/10.1101/2020.12.08.416768

8.1 Introduction

In functional magnetic resonance imaging (fMRI), T2*-weighted MRI sequences use the blood oxygen level-dependent (BOLD) signal as a proxy for neuronal activity. Our ability to infer accurate information about neuronal processes is influenced by the sensitivity with which we can capture these BOLD changes and subsequently delineate its sources of variance. Improved sensitivity is particularly important for real-time use cases, such as adaptive experimental paradigms, real-time quality control, or fMRI neurofeedback, where BOLD changes are quantified and used as they are acquired without the benefit of a full dataset or the requisite amount of post-processing time. It is well known that optimum sensitivity of single-echo fMRI is achieved at an echo time (TE) close to the apparent tissue T2*-value at baseline (Menon et al., 1993), which also underlies an inherent drawback of T2*-weighted sequences. Location-specific BOLD sensitivity is suboptimal since T2* varies across tissue types and brain regions (Peters et al., 2007), which can result in spatial variability in the detection of task-related activation patterns. Furthermore, magnetic susceptibility gradients on a macroscopic level result in image defects such as signal dropout and distortion, which is pronounced in the ventromedial prefrontal, orbitofrontal, the medial temporal and the inferior temporal lobes (Devlin et al., 2000). Additionally, the complex interplay of blood flow, blood volume and magnetic susceptibility effects can be influenced strongly by system- and participant-level noise sources, thus confounding the BOLD signal.

An advancement that has shown promise in making inroads into these drawbacks is multi-echo fMRI. Several studies have shown benefits of offline denoising based on multi-echo independent component analysis (MEICA; Kundu et al., 2012) for both resting state (e.g. Olafsson et al., 2015; Dipasquale et al., 2017) and task-based fMRI data (e.g., Lombardo et al., 2016; Gonzalez-Castillo et al., 2016; Moia et al., 2020). Echo combination via weighted summation is a critical step in multi-echo post-processing that has been reported to increase temporal signal-to-noise ratio, decrease signal drop-out, and improve activation extent for task-analysis (Poser et al., 2006). Posse et al. (1999) proposed several echo combination schemes, including simple echo summation (i.e. equal weights) and weighting echoes by their relative expected BOLD contrast contribution (i.e. T2*), which would require a numerical or fitted estimation of T2*. Other possible weighting schemes include optimised scalar weights, TE-weighted combination, and tSNR-weighted combination (also termed the PAID method) proposed by Poser et al. (2006). A theoretical framework for optimising multi-echo combination has also been proposed by Gowland and Bowtell (2007). However, the relative benefits of all available combination schemes remain unclear.

With access to multiple data samples along the decay curve, multi-echo allows quantification of the effective transverse relaxation parameter T2* (decay time) or R2* (its inverse, decay rate), and S0 (initial net magnetisation). This form of quantitative T2*-mapping (such as described by Weiskopf et al., 2013) acquires multiple closely spaced echoes followed by a data fitting procedure that yields a static, baseline T2*-map. In the context of functional imaging, however, tempo-

ral or per-volume T2*-mapping is also feasible, with the core benefit being the separation and quantification of T2* and S0 changes (from baseline) during stimulated neuronal activation. Such real-time use cases of multi-echo data have been reported, starting with Posse et al. (1998) who developed a single-shot, multi-echo spectroscopic imaging sequence that quantified region-specific T2* changes during olfactory and visual tasks, and which reported a larger functional contrast (up to 20% increase in the visual cortex) compared to standard EPI data. Several developments followed, including measuring single-event related brain activity (Posse et al., 2000), whole brain T2*-mapping at 1.5T using a linear combination of echoes (Hagberg et al., 2002), later with added gradient compensation (Posse et al., 2003a), and a multi-echo EPI sequence at 3T with real-time distortion correction (Weiskopf et al., 2005). Rapid T2*-mapping has also been a useful tool in studying the interplay between cerebral blood flow, blood volume and blood oxygenation, particularly in combination with contrast agents (see, for example: Scheffler et al., 1999; Schulte et al., 2001; Pears et al., 2003). In real-time fMRI neurofeedback, some examples of multi-echo use are reported specifically for improving signal gains in regions such as the amygdala, including Posse et al. (2003a) which uses T2*-weighted echo summation and Marxen et al. (2016), which uses scalar TE-dependent weights pre-selected to yield an average T2*-value of 30ms in the amygdala.

Although methodological studies have reported the benefits of multi-echo fMRI combination, a comprehensive evaluation of its practical benefits is lacking. Specifically, a variety of combination methods exist that can lead to both offline and real-time improvements in BOLD sensitivity, but there has been no systematic comparison between such methods. Additionally, per-volume T2*-mapping forms a necessary step in established multi-echo-based methods, but recent literature has not explored its value for task fMRI analysis. Consequently, this study has two main goals: (1) to explore the differences in BOLD sensitivity, both offline and per-volume, between time series of standard single echo EPI, per-volume estimated T2*FIT, and multi-echo-combined time series (including tSNR-weighted, T2*, TE-weighted, and T2*FIT-weighted); and (2) to explore the T2*FIT time series as an alternative to single-echo or multi-echo-combined time series for offline and real-time fMRI analysis. We investigate these aims for whole brain data in separate task paradigms, eliciting responses to motor and emotion processing tasks and mental versions thereof, and during resting state. To quantify differences, we employ several metrics such as tSNR, task activity effect size, region-of-interest based temporal percentage signal change (tPSC), functional contrast, and temporal contrast-to-noise ratio (tCNR).

8.2 Multi-echo fMRI relaxation and combination

Multi-echo fMRI sequences acquire a slice or multiple slices of a functional image at discrete echo times (TE) after a single transverse excitation pulse of the scanner. All slices of a whole brain image are acquired within the standard repetition time (TR) which then yields multiple echoes per volume. The relaxation of the fMRI

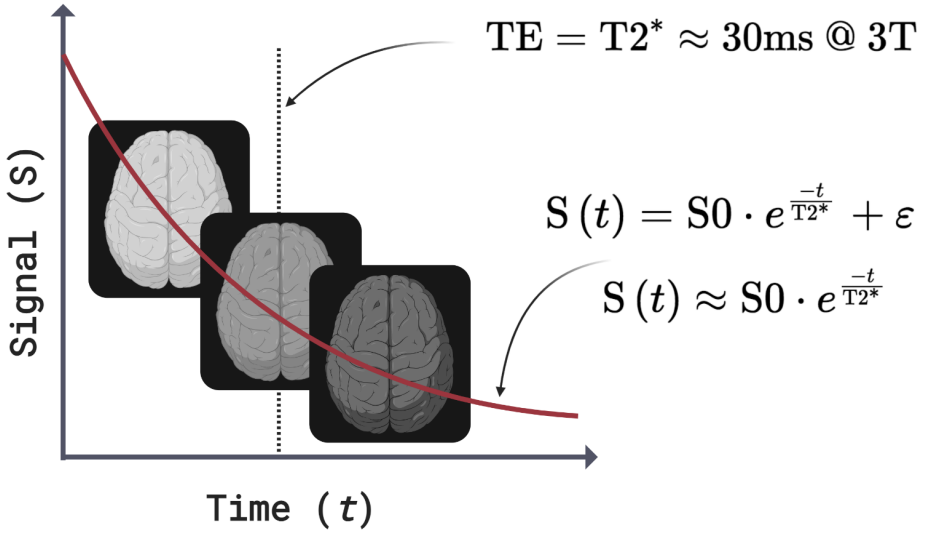

Figure 8.1 — *A representation of mono-exponential signal decay showing diminishing image intensity along three echoes. The second echo is sampled at the optimum echo time equal to average grey matter T2*, standard for single echo fMRI. The equation for the red, mono-exponential decay curve is provided (Equation 8.1).*

signal in a given voxel after transverse excitation, assuming a mono-exponential decay model, is given as:

$$\mathrm{S}\left(t\right) = \mathrm{S0} \cdot e^{\frac{-t}{\mathrm{T2}^*}} + \varepsilon = \mathrm{S0} \cdot e^{-t \cdot \mathrm{R2}^*} + \varepsilon \tag{8.1}$$

with S(t) being the time-decaying fMRI signal, S0 being the tissue magnetisation directly after transverse excitation, and T2* being the local tissue transverse relaxation (i.e. decay time) constant (the inverse of the decay rate, R2*). Per-voxel estimates of S0 and T2* (depicted in Figure 8.1) can be derived using a log-linear regression estimation and the available echo times (t_1 to t_N, where *pinv* is the pseudo-inverse log the natural logarithm):

$$\begin{bmatrix} \log\left(\mathrm{S0}\right) \\ \mathrm{R2}^* \end{bmatrix} = pinv\left(\begin{bmatrix} 1 - t_1 \\ 1 - t_2 \\ \vdots \\ 1 - t_\mathrm{N} \end{bmatrix}\right) * \begin{bmatrix} \log\left(\mathrm{S}\left(t_1\right)\right) \\ \log\left(\mathrm{S}\left(t_2\right)\right) \\ \vdots \\ \log\left(\mathrm{S}\left(t_\mathrm{N}\right)\right) \end{bmatrix} \tag{8.2}$$

The mathematics of all widely used multi-echo combination schemes are based on the underlying concepts of data weighting, summation and averaging. In Appendix D, we provide a background of these concepts along with explanatory Equations D.1 through D.6. Importantly, the multi-echo combination schemes presented here use the convention of weighted summation with normalised weights.

This implies that (1) all weights are normalised such that their sum equals 1, then (2) each normalised weight is multiplied by its corresponding data point, then (3) these products are summed to produce the weighted summation.

Simple echo summation

Simple echo summation assumes equal weights for all echoes (totalling N), which is calculated for an individual echo *n* as:

$$w_n^{\mathrm{SUM}} = \frac{1}{\mathrm{N}} \tag{8.3}$$

tSNR-weighted combination

The PAID method put forward by Poser et al. (2006) uses the voxel-based tSNR measured at each echo (tSNR_n) as the weights:

$$w_n^{\mathrm{tSNR}} = \frac{\mathrm{tSNR}_n \cdot \mathrm{TE}_n}{\sum_{i=1}^{\mathrm{N}} \mathrm{tSNR}_i \cdot \mathrm{TE}_i} \tag{8.4}$$

TE-weighted combination

Purely using each echo's echo time, TEn, as the weight for that echo has also been suggested (Posse et al., 1999). In this case, the same scalar value is used as the weighting factor for all voxels of a specific echo:

$$w_n^{\mathrm{TE}} = \frac{\mathrm{TE}_n}{\sum_{i=1}^{\mathrm{N}} \mathrm{TE}_i} \tag{8.5}$$

Similarly, a range of scalar values can be used as echo-dependent weighting factors, usually optimised according to study-specific criteria. For example, Marxen et al. (2016) selected scalar weights in order to yield an average T2* value of 30 ms in their region of interest (the amygdala). In such a case, the predefined scalar weights SW_1, SW_2, . . ., SW_N can be normalised as:

$$w_n^{\mathrm{SW}} = \frac{\mathrm{SW}_n}{\sum_{i=1}^{\mathrm{N}} \mathrm{SW}_i} \tag{8.6}$$

T2*-weighted combination

The T2*-weighted combination scheme used by Posse et al. (1999) and termed "optimal combination" by Kundu et al. (2012), calculates the individual echo weights w_n per voxel as:

$$w_n^{\mathrm{T2^*}} = \frac{\mathrm{TE}_n \cdot \exp\left(-\mathrm{TE}_n/\mathrm{T2^*}\right)}{\sum_{i=1}^{\mathrm{N}} \mathrm{TE}_i \cdot \exp\left(-\mathrm{TE}_i/\mathrm{T2^*}\right)} \tag{8.7}$$

T2*FIT-weighted combination

Finally, as proposed in the introduction, real-time T2*-mapping is made possible when using multi-echo fMRI. Here, the per-volume estimation of T2* at each voxel, termed T2*FIT(t), can also be used as the weighting factor in a per-volume echo combination scheme:

$$w_n^{\mathrm{T2^*FIT}}(t) = \frac{\mathrm{TE}_n \cdot \exp\left(-\mathrm{TE}_n/\mathrm{T2^*FIT}(t)\right)}{\sum_{i=1}^{\mathrm{N}} \mathrm{TE}_i \cdot \exp\left(-\mathrm{TE}_i/\mathrm{T2^*FIT}(t)\right)} \tag{8.8}$$

The per-volume nature of this echo combination scheme makes it ideal for use in both offline and real-time applications, when an a priori T2*-map is not available or not preferred. To the best of our knowledge, this T2*FIT-weighted combination approach has not been described previously in the literature

In the methods and results presented in this work, we compare metrics derived from standard single echo fMRI analysis to metrics derived from analysing T2*-weighted, tSNR-weighted, TE-weighted, T2*FIT-weighted, and the T2*FIT parameter time series, in both offline and per-volume scenarios.

8.3 Methods

8.3.1 Participants

MRI and physiology data were collected from N=28 participants (male=20; female=8; age = 24.9 ± 4.6 mean + standard deviation). The study was approved by the local ethics review board and all participants gave written consent for their data to be collected, processed and shared in accordance with a GDPR-compliant procedure.

8.3.2 Experimental design

A total of seven MRI acquisitions were collected during a single scanning session per participant. These acquisitions include, in order of acquisition:

1. A T1-weighted anatomical scan
2. *rest_run-1*: the first resting state run, eyes fixated on a white cross
3. *fingerTapping*: a right hand finger tapping functional task
4. *emotionProcessing*: a matching-shapes-and-faces functional task
5. *rest_run-2*: the second resting state run, eyes fixated on a white cross
6. *fingerTappingImagined*: an imagined finger tapping functional task
7. *emotionProcessingImagined*: a functional task to recall an emotional memory

All four task paradigms followed an ON/OFF boxcar design, starting with the OFF condition, with both conditions lasting 10 volumes (= 20 s at TR = 2

s). The control (i.e. OFF) condition for the *fingerTapping* task was to focus on a small white cross on a black screen; for the *emotionProcessing* task the control condition was the shape-matching block; and for the *fingerTappingImagined* and *emotionProcessingImagined* tasks the control conditions were counting backwards, respectively, in multitudes of 7 and 9.

8.3.3 MRI protocol

MRI data were acquired on a 3 Tesla Philips Achieva scanner (software version 5.1.7) and using a Philips 32-channel head coil. A single T1-weighted anatomical image was acquired using a 3D gradient echo sequence (T1 TFE) with scanning parameters: TR = 8.2 ms; TE = 3.75 ms; flip angle = 8°; field of view = 240×240×180 mm; resolution = 1×1×1 mm; total scan time = 6:02 min.

All six functional MRI scans were acquired using a multi-echo, echo-planar imaging sequence with scanning parameters: TR = 2000 ms; TE = 14,28,42 ms (3 echoes); number of volumes = 210 (excluding 5 dummy volumes discarded by the scanner); total scan time = 7:00 min (excluding 5 dummy volumes); flip angle=90°; field of view = 224×224×119 mm; resolution = 3.5×3.5×3.5 mm; in-plane matrix size = 64×64; number of slices = 34; slice thickness = 3.5 mm; interslice gap = 0 mm; slice orientation = oblique; slice order/direction = sequential/ascending; phase-encoding direction = A/P; SENSE acceleration factor = 2.5. Parts of the cerebellum and brainstem were excluded for some participants to ensure full coverage of the cortex and subcortical areas of interest. Echo times, spatial resolution, and the SENSE factor were tuned with the aim of improving spatial resolution and coverage while limiting the TR to maximum 2000 ms, including a maximum number of echoes, and keeping the SENSE factor low to prevent SENSE artefacts.

In addition, cardiac and respiratory fluctuations were recorded during the functional scans, respectively using a pulse oximeter fixed to the participant's left index finger, and a pressure-based breathing belt strapped around the participant's upper abdomen. These were sampled at 500 Hz.

8.3.4 Data analysis

Data analysis consists of anatomical and functional preprocessing, definition and calculation of echo combination weights, multi-echo combination, time-series processing and calculation of comparison metrics. All analyses are done on an individual basis (i.e. participant-specific), unless otherwise stated, to describe the effects and facilitate the use of these methods in real-time fMRI use cases.

All processing steps were done using the open source MATLAB-based and Octave-compatible *fMRwhy* toolbox (v0.0.1[1]), which has conditional dependencies:

- SPM12 (r7771[2]; Friston et al., 2007)

[1] `https://github.com/jsheunis/fMRwhy`

[2] `https://github.com/spm/spm12/releases/tag/r7771`

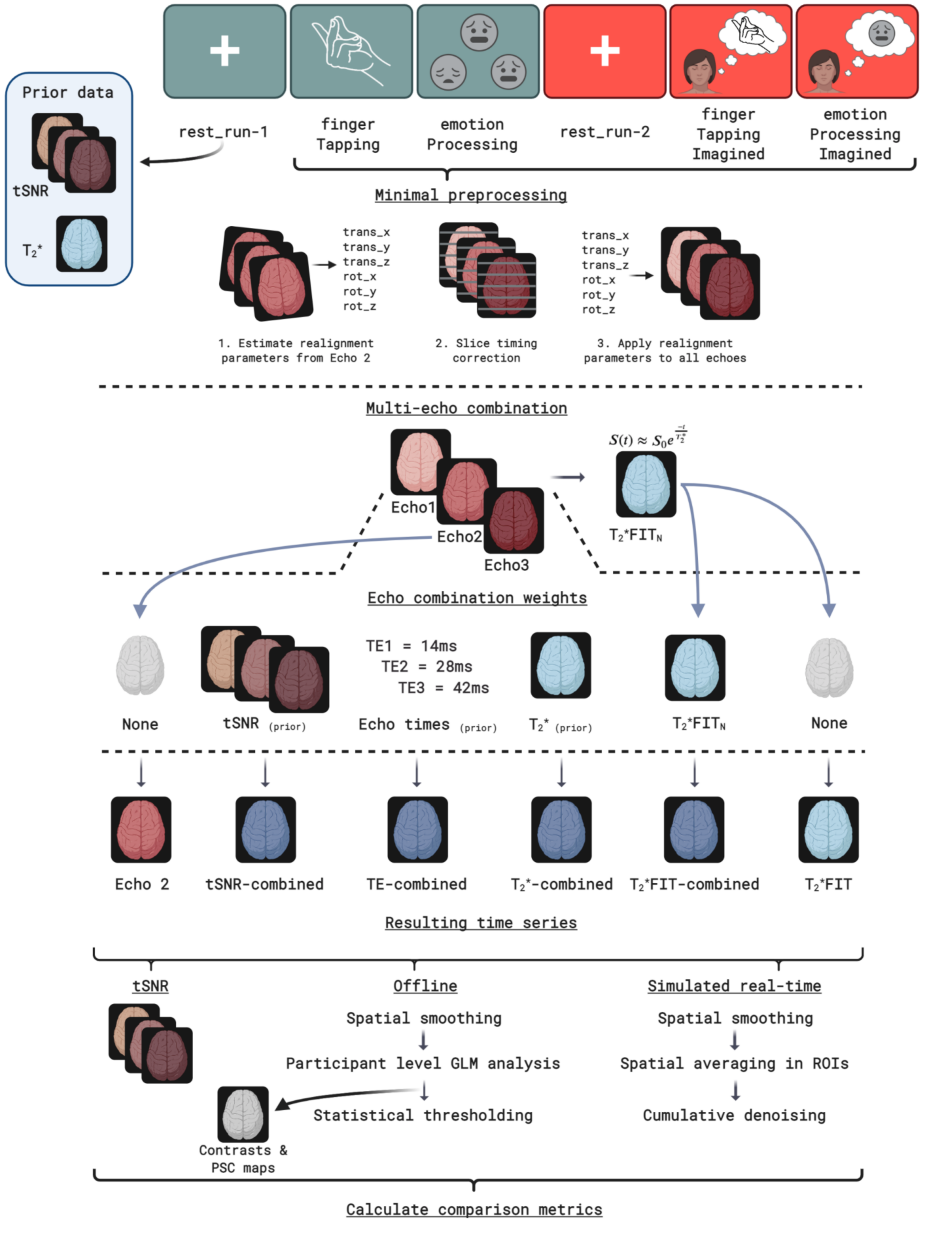

Figure 8.2 — *The analysis pipeline applied to the rt-me-fMRI dataset. Prior tSNR and T2* maps are derived from the first resting state run. For all other functional runs (top row), six steps are executed per volume after minimal preprocessing in order to yield resulting multi-echo-derived time series for comparison: (1) the 2nd echo time series is extracted without processing, (2) the prior tSNR-weighted combination, (3) the TE-weighted combination, (4) the baseline T2*-weighted combination, (5) the T2*FIT-weighted combination, and (6) T2*FIT time series. Following this, each of the six time series then undergoes offline and simulated real-time processing pipelines. The offline pipeline includes (in order): tSNR calculation, spatial smoothing, participant-level task analysis, calculation of percentage signal change effect sizes, and statistical thresholding of the participant-level contrast maps. The simulated real-time pipeline is run per volume for each time series and includes (in order): spatial smoothing, spatial averaging of the appropriate region-of-interest signals, and cumulative denoising (including detrending using linear and quadratic regressors).*

- Anatomy Toolbox (v3.0; Eickhoff et al., 2005)
- bids-matlab (v.0.0.1[3])
- dicm2nii (v0.2 from a forked repository[4])
- TAPAS PhysIO (v3.2.0[5]; Kasper et al., 2017)
- Raincloud plots (v1.1[6]; Allen et al., 2019)

All data analysis scripts can be accessed online for reproducibility or reuse with attribution[7].

A. Preprocessing
The basic anatomical and functional preprocessing pipeline applied to all data is described in detail in the data article, and in included:

1. Defining a functional template from Echo 2 of the first volume of the first resting state run. Echo 2 is selected in order to apply the same pipeline and allow a fair comparison of multi-echo to single-echo data, since for the latter only a single time series similar to Echo 2 would be available.
2. Mapping prior data to the subject functional space, including:
    a) Coregistration of the anatomical image and atlas-based regions of interest (available in MNI152 space; Eickhoff et al., 2005) to the functional template space, and resampling these to the functional resolution.
    b) Tissue-based segmentation of the coregistered anatomical image (after coregistration but before downsampling) and subsequent definition of binary maps for grey matter, white matter, cerebrospinal fluid (CSF) and the whole brain.
3. Basic functional preprocessing steps, including: estimating realignment parameters from the Echo 2 time series, running slice timing correction on all echo time series, applying realignment parameters to all echo time series, and applying spatial smoothing (7 mm isotropic, i.e. twice the voxel width) to all echo time series.
4. Generating data quality control metrics and visualisations to allow inspection of the quality of anatomical and functional data and their derivatives.

[3] https://github.com/jsheunis/bids-matlab/releases/tag/fv0.0.1
[4] https://github.com/jsheunis/dicm2nii/releases/tag/v0.2
[5] https://github.com/translationalneuromodeling/tapas/releases/tag/v3.2.0
[6] https://github.com/RainCloudPlots/RainCloudPlots/releases/tag/v1.1
[7] https://github.com/jsheunis/rt-me-fMRI

Two aspects of the preprocessing and analyses pipelines are worth highlighting in the context of this study. Firstly, while an important focus for this work is its application and utility in real-time scenarios, all processing was done offline, either on the full dataset or on a per-volume (i.e. simulated real-time) basis. This was viable since the study did not include any neurofeedback or real-time adaptive paradigms that would have required real-time computation and interaction. Secondly, in order to use a standardised pipeline (across multiple runs of multi-echo and single-echo data) that can compute derivative measures that are aligned across analyses and therefore comparable on a per-voxel basis, we followed the concept of "minimally processed" data as described by (DuPre et al., 2020). This means that minimal steps including slice timing correction and 3D volume realignment are applied to multi-echo data before decay parameter estimation or multi-echo combination.

B. Data quality control

The *fMRwhy* toolbox has a BIDS-compatible data quality pipeline for functional and anatomical MRI, *fmrwhy_workflow_qc*, that can be run automatically for a full BIDS-compliant dataset. After running minimal preprocessing steps it generates a subject-specific HTML-report with quality control metrics and visualisations to allow inspection of the data and its derivatives. Individual reports can be accessed in the derivatives directory of the shared BIDS-compliant dataset of this study (see Chapter 7 for details; Heunis et al., 2020b). Additionally, a web-application named *rt-me-fMRI* is provided along with this work[8]. It can be used interactively to explore various summaries of data quality metrics, including distributions of framewise displacement (FD) and tSNR, and physiology recordings, as well as the results of this study.

None of the participant datasets were excluded after inspection of the included quality metrics, even in cases of more than average or severe motion (specifically sub-010, sub-020, and sub-021), since such data could still be useful for data quality related insights or for future denoising methods validation. In addition, for all participant data the alignments of the anatomical mask, the derived tissue segmentation masks, and the EPI data were visualised, inspected and the overlap was found acceptable.

C. Multi-echo combination

Existing weighting parameters or parameter maps are required to allow both offline and per-volume combination of multi-echo data. Of the previously reported options for weighting schemes given in Section 8.2, the simplest option used in this study is the echo time (Equation 8.5) derived from the functional MRI protocol, which yields a TE-weighted combination. Other prior weighting parameters are calculated using the first resting state functional scan. For each minimally preprocessed echo time series of the resting state run, the time series mean and

[8] https://rt-me-fmri.herokuapp.com/

standard deviation are calculated. The mean divided by the standard deviation yields the temporal signal-to-noise ratio (tSNR), per echo, that is used as another weighting parameter (Equation 8.4) described as the PAID method by Poser et al. (2006). Additionally, the mean images from the three echo time series are used to derive the per-voxel estimates of S0 and T2* assuming a mono-exponential decay model and using a log-linear regression estimation (Equation 8.2). This baseline T2* map can be used for T2*-weighted combination (Equation 8.7), described as optimal combination by Kundu et al. (2012). Lastly, the same log-linear regression that is applied to the time series mean images can also be applied to a single volume of any multi-echo data. This implies that the three echo images of any volume can be used as data points to estimate per-volume and per-voxel parameter maps, S0FIT(t) and T2*FIT(t), which in turn can be used for per-volume multi-echo combination (Equation 8.8), hereinafter referred to as T2*FIT-combination.

Multi-echo combination schemes are applied to all functional data excluding the first resting state run, from which prior baseline weight maps are derived. In sum, six time series are computed per functional run (as described in Figure 8.2): Echo 2, tSNR-combined, TE-combined, T2*-combined, T2*FIT-combined, and the T2*FIT time series.

D. Time series processing

After computing the six time series per functional run (excluding the first resting state run), each resulting time series is processed as summarised in the bottom row of Figure 8.2).

First, the tSNR of each time series is calculated prior to any further processing. Then, each time series is spatially smoothed using a Gaussian kernel with FWHM at 7 mm (i.e. double the voxel size). This is followed by participant-level GLM-based analysis of the four task runs. Task regressors included the main "ON" blocks for the *fingerTapping*, *fingerTappingImagined* and *emotionProcessingImagined* tasks, and both the separate "SHAPES" and "FACES" trials for the *emotionProcessing* task. Regressors not-of-interest for all runs included six realignment parameter time series and their derivatives, the CSF compartment time series, and RETROICOR regressors (both cardiac and respiratory to the 2nd order, excluding interaction regressors). Additional steps executed by SPM12 before beta parameter estimation include high-pass filtering using a cosine basis set and AR(1) autoregressive filtering of the data and GLM design matrix. Contrasts are applied to the task-related beta maps for the *fingerTapping*, *fingerTappingImagined* and *emotionProcessingImagined* tasks, and to the FACES, SHAPES, and FACES¿SHAPES beta maps for the *emotionProcessing* task. In order to yield a standard measure of effect size, the parameter estimates or contrast maps are then used to calculate percentage signal change (PSC) using the method described by Pernet (2014) and given by:

$$\mathrm{PSC} = \frac{\hat{\beta}_{condition} * \mathrm{SF} * 100}{\hat{\beta}_{constant}} \tag{8.9}$$

where condition and constant are parameter estimates corresponding to the relevant GLM regressors that are scaled with regards to the actual BOLD magnitude. To account for this the scaling factor, SF, is determined as the maximum value of a reference trial taken at the resolution of the super-sampled design matrix X_ss (where supersampling is typically done before convolution with the hemodynamic response function):

$$\mathrm{SF} = max(TrialX_{ss}) \tag{8.10}$$

Statistical thresholding was applied to identify task-related regions of activity by controlling the voxel-wise familywise error rate (FWE), with pFWE ¡ 0.05, and a voxel extent threshold of 0.

E. Real-time analysis

Minimally processed time series are also analysed per-volume (using data acquired up to each volume in time) in order to explore multi-echo related BOLD sensitivity changes for real-time applications. Real-time analysis typically involves minimal processing (including 3D realignment), spatially averaging the signal within given ROIs, and additional per-volume denoising steps on the averaged signal. Here, we run a per-volume denoising process adapted from OpenNFT (Koush et al., 2017a) on all task time series. This process is depicted in the bottom row of Figure 8.2 and includes, in order: 1) Spatial smoothing using a Gaussian kernel with FWHM at 7 mm, 2) Spatial averaging of voxel signals with defined ROIs, and 3) Cumulative GLM-based detrending of the ROI signals, including linear and quadratic trend regressors. This then yields per-volume minimally denoised ROI-signals from which percentage signal change or another calculation can be used as the basis for the neurofeedback or real-time ROI signal.

F. Comparison metrics

To explore the differences between various multi-echo combinations and standard single echo data, and to investigate the usefulness of the former over the latter, we employ several comparison metrics:

- **Temporal signal-to-noise ratio (tSNR)** calculated as the voxel-wise time series mean divided by voxel-wise time series standard deviation. tSNR is an indicator of the amount of signal available from which to extract potentially useful BOLD fluctuations. Additionally, tSNR maps can be a robust visual indicator of increases or decreases in signal dropout.
- **Percentage signal change (PSC)** of task-based contrast maps resulting from participant-level GLM analysis. PSC represents a standardised measure of effect size (which beta or contrast values are not) and is an indicator of the BOLD sensitivity of the data based on GLM analysis.
- **T-statistic values** related to the task based contrast maps resulting from participant-level GLM analysis.

- **Temporal percentage signal change (tPSC)** of the single echo, combined-echo and derived time series data of the task runs. This is calculated per voxel on minimally processed task data as the per-volume signal's percentage signal change from the time series mean (or, for real-time scenarios, from the mean of the preceding baseline "OFF" block or the cumulative mean). These are then spatially averaged within the regions listed shortly to yield ROI-based time series. These time courses are similar to what would be calculated in real-time as the ROI-based neurofeedback signal, and their amplitudes can be an indicator of BOLD sensitivity.

- **Functional contrast** of the ROI-based tPSC signals. To calculate the functional contrast in ROIs, the average tPSC in volumes classified as being part of "OFF" condition blocks are subtracted from the average signal in volumes classified as being part of each "ON" condition block. Visually, this corresponds to the average amplitude difference between conditions in the tPSC signal. The functional contrast is an indicator of the BOLD sensitivity of a signal based on both minimally processed and denoised data.

- **Temporal contrast-to-noise ratio (tCNR)** of the single echo, combined-echo and derived time series data of the task runs. To calculate the tCNR, the functional contrast in an ROI is divided by the time series standard deviation of the tPSC signal in the same ROI. This is related to both the tSNR and BOLD sensitivity. Where tPSC consists of time courses, tCNR provides a single summary value per voxel or region.

Extracting and spatially averaging voxel time series from specific regions is a common approach to exploring patterns of task-based activity in fMRI (Poldrack, 2007). This can be done both offline on a full dataset, and in real-time on the data as they are acquired. In this work, we explore and compare the above-mentioned metrics on both whole-brain and region-specific levels. Regions include:

- Grey matter (GM), white matter (WM) and cerebrospinal fluid (CSF) compartments. This allows quantifying, for example, whether combined multi-echo data changes a given metric similarly or differently across tissue types.

- A binary map of the voxels surviving voxel-wise pFWE ¡ 0.05 statistical thresholding (FWE). These maps vary spatially per time series of a given task run and they represent the functionally most responsive voxels based on the underlying data but assuming shared criteria (i.e. statistical threshold).

- A binary map resulting from a logical OR of the FWE-thresholded maps of all six time series of a given task run (FWE-OR). This allows the comparison of metrics in a region that includes the voxels that are judged to be significantly active in any time series, thus removing time series-specific spatial bias.

- Atlas-based anatomical regions of interest (Atlas-based ROI), derived from templates in MNI152 space (Eickhoff et al., 2005) that have been mapped

to individual anatomical scans and coregistered and resampled to the individual functional space. This allows quantification of the above metrics within an a priori defined ROI, thus excluding spatial bias introduced by statistical thresholding. The Atlas-based ROIs include the left motor cortex (for right-hand finger tapping), and the bilateral amygdala (for emotion processing).

The focus of this work is on exploring, quantifying and describing differences and on generating data that allows deriving clear hypotheses for future confirmatory follow-up. While null hypothesis significance testing is used where necessary in task-based analysis, overall differences in the above-mentioned comparison metrics are not significance tested and are rather described in terms of means and percentage change from a reference.

8.4 Results

A web-application named *rt-me-fMRI* is provided alongside this work[9]:. This browser-based application can be used interactively to explore the summary and participant-specific results presented here, and is intended to serve as supplementary material to this work.

8.4.1 Multi-echo decay

To illustrate signal decay and dropout as a function of echo time, a simple plot of the inferior slices of a single subject is given in Figure 8.3. Signal decay can be seen clearly as the signal intensity diminishes from Echo 1 to Echo 3 (top to bottom) in all displayed slices. Signal dropout from Echo 1 through Echo 3 is particularly evident in the areas of the orbitofrontal and ventromedial prefrontal cortices, and the inferior and anterior temporal lobe (magenta arrows; slices 8, 10, 12) and the cerebellum (light blue arrows; slices 2, 4, 6).

8.4.2 Signal intensity, dropout, and temporal signal-to-noise ratio

We can visually inspect the effect on signal intensity and dropout when combining multi-echo data or deriving time series from it. Figure 8.4A shows the mean of each of the six time series: Echo 2, tSNR-weighted combination, TE-weighted combination, T2*-weighted combination, T2*FIT-weighted combination, and T2*FIT.

It is evident that most echo combination schemes, with the exception of TE-weighted combination, recover some signal lost due to dropout in the orbitofrontal and ventromedial prefrontal regions (magenta arrows; slices 8, 10) and inferior and anterior temporal regions (light blue arrows; slices 6, 8). This signal recovery is further demonstrated in the tSNR maps provided in Figure 8.4B, particularly by the magenta arrows showing areas of signal dropout in Echo 2 and subsequent recovery in combined and derived time series tSNR maps. Even the T2*FIT, for

[9] https://rt-me-fmri.herokuapp.com/

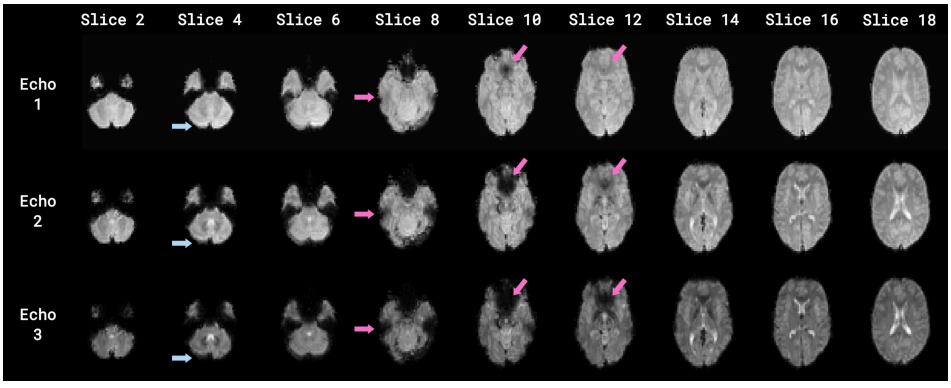

Figure 8.3 — *Signal decay along the three echoes (top to bottom) of a single volume. Signal decay is displayed across a selection of slices (horizontal axis). Signal dropout is clearly evident in the orbitofrontal and ventromedial prefrontal cortices and inferior and anterior temporal lobes (magenta arrows; slices 8, 10, 12) and the cerebellum (light blue arrows; slices 2, 4, 6).*

which the tSNR is evidently much lower than all other time series including Echo 2, recovers some of the signal that is lost due to low BOLD sensitivity in the affected areas, although signal loss is also more evident (slice 10). Additionally, tSNR in areas close to the bilateral temporal-occipital junction and towards the occipital lobe (Figure 8.4B, green arrows) appears to increase substantially for all combined time series vs. Echo 2. This is more pronounced in the T2*FIT-weighted compared to the T2*-weighted and tSNR-weighted combinations, and less so in the TE-weighted combination.

To provide a more quantified view than these visualisations of signal intensity (Figure 8.4A) and tSNR (Figure 8.4B), distribution plots were created for grey matter tSNR values, both for the whole group and for subjects individually. These are accessible in the supplementary web-application, which shows (for example) for for sub-001_task-rest_run-2 a mean tSNR increase for all combined time series compared to Echo 2, with the T2*FIT-weighted combination showing the largest increase (36.14%) and the T2*FIT time series showing a substantial decrease (-55.89%). This generalises to the whole group (see Figure 8.5A), i.e. a mean tSNR increase for all combined time series compared to Echo 2, with the T2*FIT-weighted combination showing the largest increase (a comparable 36.95%). This increase in the tSNR of T2*FIT-weighted combination replicates results that we previously reported on a different dataset (Heunis et al., 2019a). This relationship also repeats for different regions, as can be seen for the left motor cortex (Figure 8.5B) and the bilateral amygdala (Figure 8.5C).

Note, however, that the mean tSNR values increase differentially based on the region. For the T2*FIT-weighted combination, for example, whole brain data show a mean tSNR increase of 36.95%; the left motor cortex shows a mean tSNR increase of 31.63%; and the bilateral amygdala shows a mean tSNR increase of

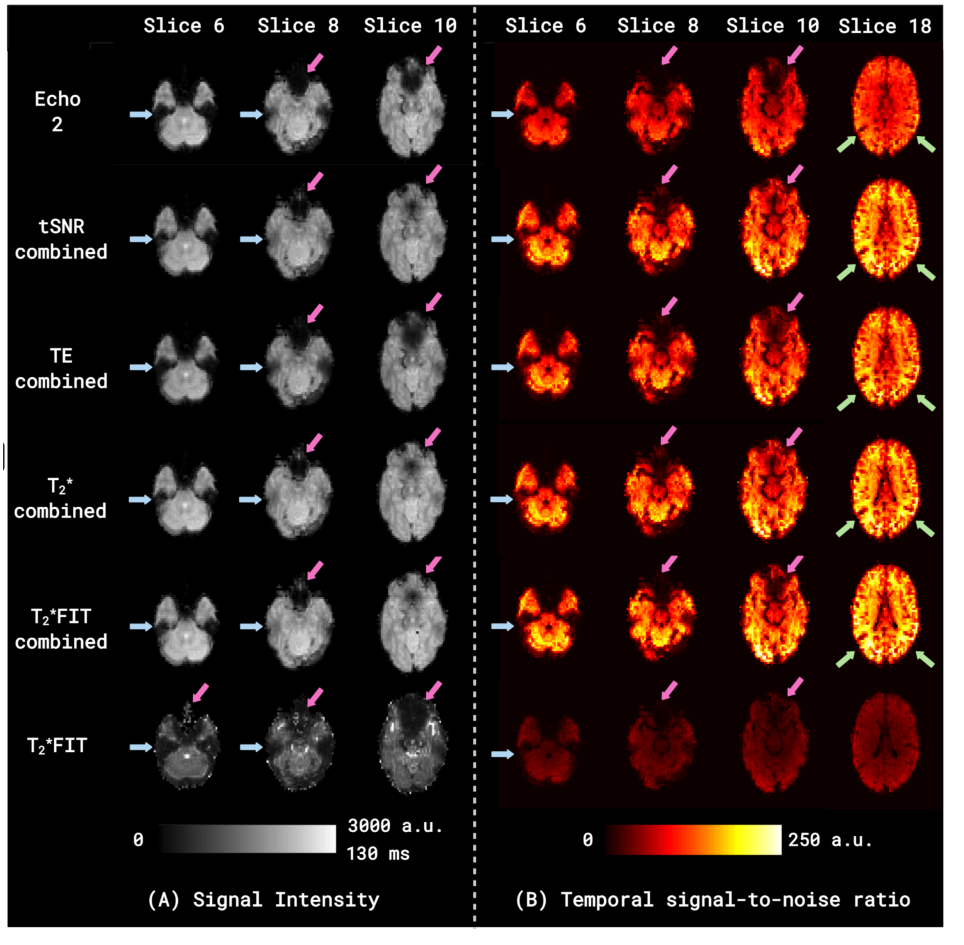

Figure 8.4 — *Signal intensity (Figure 8.4A) and Temporal signal-to-noise ratio (Figure 8.4B) shown in mean images for the time series in rows from top to bottom: Echo 2, tSNR-weighted combination, TE-weighted combination, T2*-weighted combination, T2*FIT-weighted combination, and T2*FIT. Scaling for Figure 8.4A is given both for the T2*FIT signal (0-130 ms) and for all the other signals (0-3000 a.u.). All echo combination schemes, with the exception of TE-weighted combination, recover some signal lost due to dropout in the orbitofrontal and ventromedial prefrontal regions (magenta arrows; slices 8, 10) and inferior and anterior temporal regions (light blue arrows; slices 6, 8). Slight signal recovery in T2*FIT is visible in the orbitofrontal and ventromedial prefrontal regions (slice 6) although signal loss is more evident in slice 10. In Figure 8.4B, all time series apart from T2*FIT show increases in tSNR (from Echo 2) in areas close to the bilateral temporal-occipital junction and towards the occipital lobe (green arrows; slice 18), which is more pronounced in the T2*FIT-weighted compared to the T2*-weighted and tSNR-weighted combinations, and less so in the TE-weighted combination.*

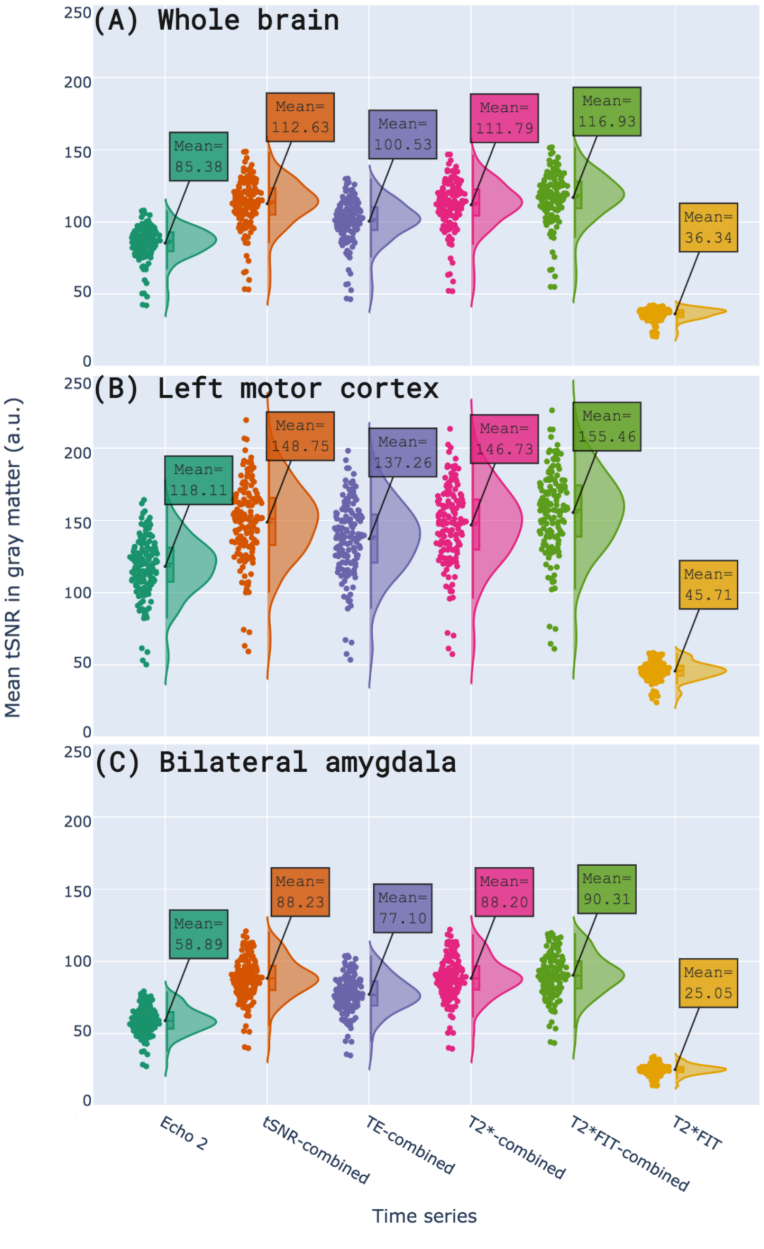

Figure 8.5 — *Distribution / ridge plots of mean grey matter temporal signal-to-noise ratio (tSNR) over all participants and all runs. Plots are shown for (A) the whole brain, (B) the left motor cortex, and (C) the bilateral amygdala, each displaying a distribution for the six time series from left to right: Echo 2, tSNR-weighted combination, TE-weighted combination, T2*-weighted combination, T2*FIT-weighted combination, and T2*FIT. In all regions, the mean T2*FIT tSNR decreases from Echo 2 while the tSNR of all other time series increase, with the T2*FIT-weighted combination showing the largest increase in all regions. Notably, tSNR increases for all the combined echo time series are more substantial in the amygdala (C) than the other regions (A, B).*

53.35%. Other combined time series show percentage increases following the same pattern, i.e. a larger tSNR increase for the amygdala than for the whole brain or motor cortex. This could be explained by the baseline T2*-values in the motor cortex and the whole brain being closer to the time Echo 2 (28 ms) than the T2*-values in the amygdala, i.e. that the T2*-weighting of Echo 2 in those regions is already closer to optimal than the weighting of Echo 2 in the amygdala. This suggests that the amygdala and similarly affected areas with T2*-values that are different from the average have more to gain from the multi-echo combination process.

Another noteworthy aspect is the low signal intensity and low tSNR of the T2*FIT time series. The low signal intensity is explained by the fact that T2*FIT values correspond to quantified units (ms) that are expected to be in a certain range (0 to 120 ms for the human brain at 3T; Peters et al., 2007), while the intensity of the standard single and combined echo images are in analogue units determined by MRI hardware and software. The low tSNR of the T2*FIT time series could be explained by an increase in time series standard deviation resulting from the log-linear fitting procedure on noisy data and only using the three echoes to fit the mono-exponential decay model per volume. This increase in time series noise becomes evident when investigating T-statistic values related to task-analysis, and temporal percentage signal change.

Distributions of grey matter tSNR values are useful for inspecting differences in signal increases and dropout recovery between single-echo, multi-echo combined, and derived timeseries, and enable identifying new voxels or regions with adequate signal for task (or other) analysis. However, tSNR does not provide a direct measure of task sensitivity, i.e. it does not directly tell us whether newly recovered signal/regions would be usefully related to the underlying task. For that reason, further measures derived from task analyses like the effect sizes, T-statistic values, and contrast to noise ratios are important to explore.

8.4.3 Effect sizes and T-statistics

Figure 8.6 shows distribution plots (over all subjects) of the mean PSC values within the respective FWE-OR clusters for all task runs: *fingerTapping* (Figure 8.6A), fingerTappingImagined (Figure 8.6B), *emotionProcessing* (Figure 8.6C), and *emotionProcessingImagined* (Figure 8.6D). It is evident from Figure 8.6A through 8.6D that the effect sizes show a substantial increase for the T2*FIT time series (from Echo 2) in all tasks (respectively 87.91%, 67.86%, 13.51%, and 43.28%), while displaying a similar or decreased mean effect size for all combined times series. Data in the supplementary browser-based application also shows that this increase for T2*FIT is more pronounced when looking at the effect sizes within their respective FWE regions (i.e. different activated voxels for each multi-echo derived time series, although mostly overlapping), which one should be wary of overinterpreting given the inherent circularity of re-analysing data in voxels that previously passed a significance threshold using the same data. On the other hand, this result is less pronounced for the time series effect sizes within their respective

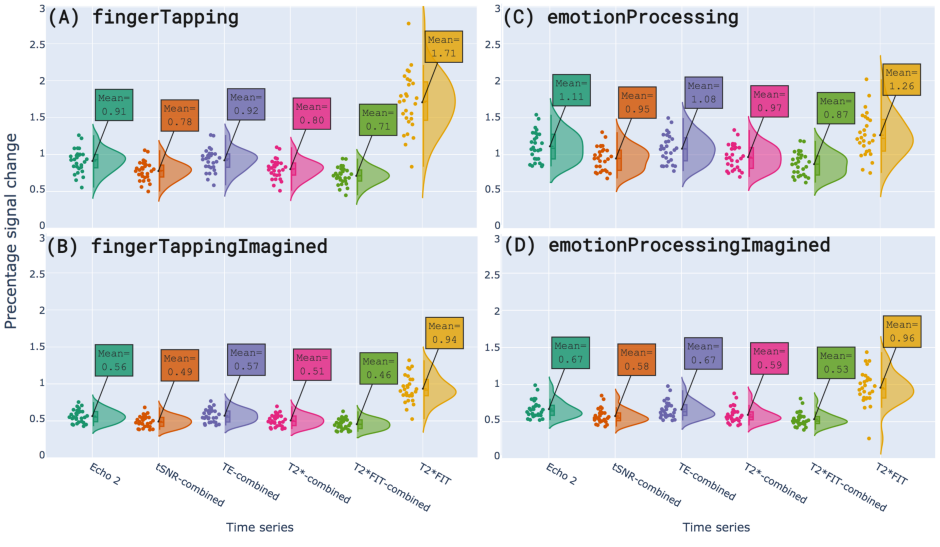

Figure 8.6 — *Distribution plots of mean percentage signal change (PSC) values in the FWE-OR region for each of the four task runs. Plots from top to bottom are: (A) fingerTapping, (B) fingerTappingImagined, (C) emotionProcessing, and (D) emotionProcessingImagined. PSC values are shown for all six time series, from left to right: Echo 2, tSNR-weighted combination, TE-weighted combination, T2*-weighted combination, T2*FIT-weighted combination, and T2*FIT. For all tasks, the T2*FIT time series effect sizes show mean increases above the effect sizes of the Echo 2 time series, while all multi-echo combined time series effect sizes show similar or decreased means.*

atlas-based regions of interest, mainly resulting in a longer tailed distribution of mean PSC values for the T2*FIT time series. In some participants the mean PSC values of the T2*FIT time series even show a slight decrease. These decreases in PSC disappear when looking at peak effect sizes, as opposed to mean effect sizes, in all regions of interest. Further differences can be inspected in depth using the supplementary browser-based application.

To accompany these effect size values, Figure 8.7 shows distribution plots (over all subjects) of the mean T-statistic values in the respective FWE-OR regions for all task runs: *fingerTapping* (Figure 8.7A), *fingerTappingImagined* (Figure 8.7B), *emotionProcessing* (Figure 8.7C), and *emotionProcessingImagined* (Figure 8.7D). For all tasks, it is evident that resulting T-values for the combined echo time series are very similar in size and distribution to that of the Echo 2 time series, while T-values for the T2*FIT time series are notably lower. The low mean T-values of T2*FIT are due to the noise captured when estimating T2* per-volume using only three data points, where noisy data would increase standard deviation and decrease the resulting T-values. This is substantiated by the large decrease in tSNR we saw for the T2*FIT time series compared to that of the Echo 2 time series in Figures 8.4 and Figure 8.5. Additionally, the TE-combined time series show slightly higher T-values for all tasks compared to other combined time series. However, this slight increase does not persist when analysing other regions (e.g. FWE or atlas-based)

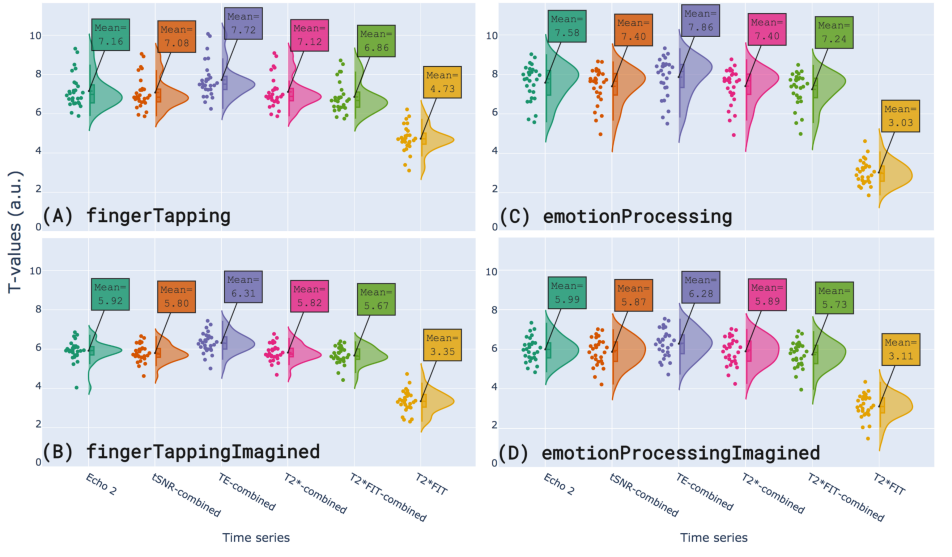

Figure 8.7 — *Distribution plots of mean statistical T-values in the FWE-OR region for each of the four task runs. Plots from top to bottom are: (A) fingerTapping, (B) fingerTappingImagined, (C) emotionProcessing, and (D) emotionProcessingImagined. T-values are shown for all six time series, from left to right: Echo 2, tSNR-weighted combination, TE-weighted combination, T2*-weighted combination, T2*FIT-weighted combination, and T2*FIT. For all tasks, T-values of the combined echo time series are very similar in size and distribution shape to that of the Echo 2 time series, while T-values for the T2*FIT time series are notably lower.*

as can be viewed with the supplementary browser-based application.

8.4.4 Temporal percentage signal change and functional contrast

Temporal percentage signal change is useful to inspect the per-volume fluctuations of signal in task-related regions. This can be done for both offline and real-time scenarios but is particularly important for the latter in applications like region-based neurofeedback. tPSC in the offline scenario is calculated per volume from minimally processed data, yielding a per-voxel tPSC time series that can be depicted in a carpet plot for quality inspection or used for ROI analyses. tPSC for real-time scenarios is calculated from real-time minimally denoised *ROI-averaged signal* (with regards to the mean of the preceding baseline "OFF" block or with regards to the cumulative total or baseline mean) yielding the real-time ROI-signal typically used in region-based neurofeedback.

Here we focus on exploring tPSC and functional contrast for the real-time scenario. While offline tPSC is useful for post-hoc inspection of signal quality and task activity, it reflects similar data already presented above in the PSC and T-statistic distributions. Additionally, offline tPSC does not accurately reflect the effects seen for real-time scenarios where per-volume calculations can only use information available up to the most recently acquired volume. For that purpose,

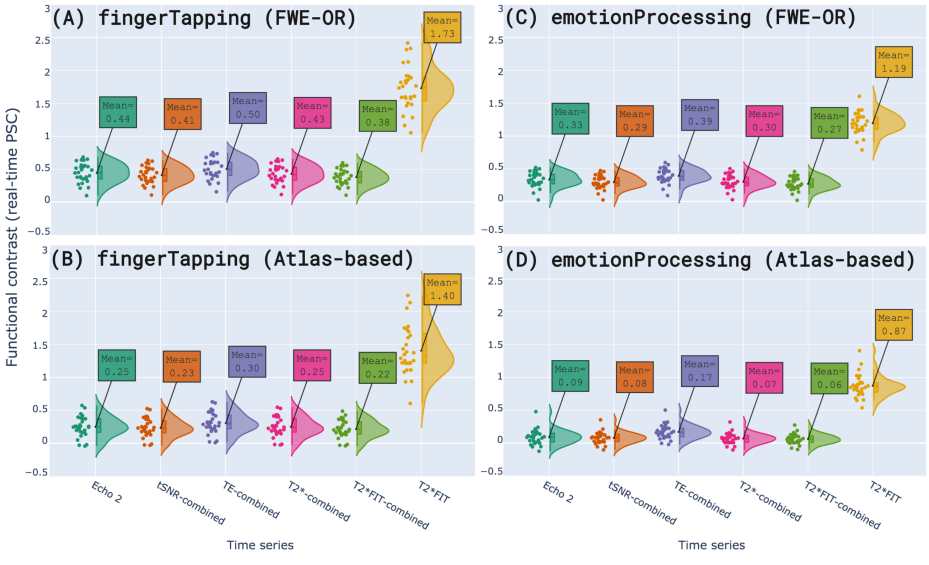

Figure 8.8 — *Distributions of functional contrasts calculated from real-time temporal percentage signal change of the fingerTapping and emotionProcessing tasks. Contrast distributions are shown for both tasks within the FWE-OR region (A and C) and within the atlas-based region (B and D). Signals are colour coded for Echo 2, tSNR-weighted combination, TE-weighted combination, T2*-weighted combination, T2*FIT-weighted combination, and T2*FIT. Similar to the offline tPSC case, the functional contrast (in both tasks) for the T2*FIT time series is greater than the contrasts for all other time series, in both regions, although this is less pronounced for the emotionProcessing task than for the fingerTapping task. Notably, functional contrast for the real-time T2*FIT time series is substantially increased compared to its offline counterpart (see supplementary web-application). Functional contrast is presented as differences in percentage signal change (y-axes).*

minimally processed data are cumulatively detrended and real-time tPSC is then calculated with regards to a cumulative baseline mean.

Figure 8.8 shows functional contrast for all subjects calculated from real-time tPSC signals for the *fingerTapping* and *emotionProcessing* tasks, in the FWE-OR and atlas-based regions (the corresponding offline metrics can be inspected in detail in the supplementary web-application). The T2*FIT signal clearly has a larger functional contrast (higher tPSC during task blocks and lower tPSC during resting blocks) than all other signals, for which the functional contrasts are very similar. For example, the minimum percentage increase of T2*FIT functional contrast over Echo 2 functional contrast is 260.61% (from 0.33 to 1.19) in the FWE-OR region of the *emotionProcessing* task. Taking supplementary data into account, there is also an increased functional contrast for the real-time T2*FIT time series compared to its offline counterpart.

A caveat here is that the T2*FIT time series has the lowest tSNR of all time series, as noted in Figure 8.5. In real-time scenarios, this could diminish the benefit of the high functional contrast in that the improved sensitivity to detect brain

activity in an ROI would not necessarily be temporally stable. To take this into account, the functional contrasts are divided by the standard deviation of the tPSC time series to yield the temporal contrast-to-noise ratio (tCNR). This is shown for the FWE-OR regions in the *fingerTapping* and *emotionProcessing* tasks in Figure 8.9 below, along with examples of single-participant real-time tPSC signals for the same tasks and regions. These plots highlight both functional contrast and volume-to-volume fluctuations.

Notably, the distributions in Figures 8.9A and B show a substantial increase in tCNR for the T2*FIT time series versus Echo 2 (97.78% for *fingerTapping* and 172.31% for *emotionProcessing*), while the distributions of all other multi-echo combined time series are very similar in shape and size to Echo 2. These promising results suggest that the decreased voxel-wise tSNR of the T2*FIT time series is less detrimental on the level of the ROI-averaged signal. Offline tCNR calculations (accessible in the supplementary web-application) however show very similar tSNR distributions for all time series including T2*FIT and Echo 2. On the level of individual ROI-averaged signals, Figures 8.9C and D show tPSC signals in the FWE-OR regions, with higher amplitude differences for the T2*FIT time series compared to all other time series, echoing the increased functional contrast seen for the group in Figure 8.8. While a slight increase in volume-to-volume fluctuations relative to the signal amplitude is also visible, this does not substantially affect tCNR measures.

Another note regarding the tPSC signals shown in Figures 8.9C and D is that these visualisations reflect temporally smoothed data, using a moving 3-point average. In real-time analysis it is common to apply a windowed averaging filter to the ROI time series in order to increase the tSNR, which improves the contrast and stability of the neurofeedback signal. This also improves our ability to classify individual volumes as a detected or undetected event of activity in cases where binary decision making is an important step for the specific real-time application. In the case of Figure 8.9 it highlights the functional contrast improvement of the T2*FIT time series. Note that the tCNR calculations that yielded the data of Figure 8.8 were executed on temporally unsmoothed data. The supplementary web-application can be used to change views of the tPSC time series between temporally smoothed and unsmoothed visualisations.

8.5 Discussion

In this work we presented a comprehensive exploration and evaluation of existing and novel multi-echo combination and T2*-mapping methods for both real-time and offline BOLD sensitivity improvements. A resting state and task-based healthy participant dataset was collected, curated and made available to the community for future investigations. In this dataset, we investigated five time series derived from multi-echo data and their differences from a single echo time series (Echo 2): tSNR-weighted combination, TE-weighted combination, T2*-weighted combination, T2*FIT-weighted combination, and the T2*FIT time series. These

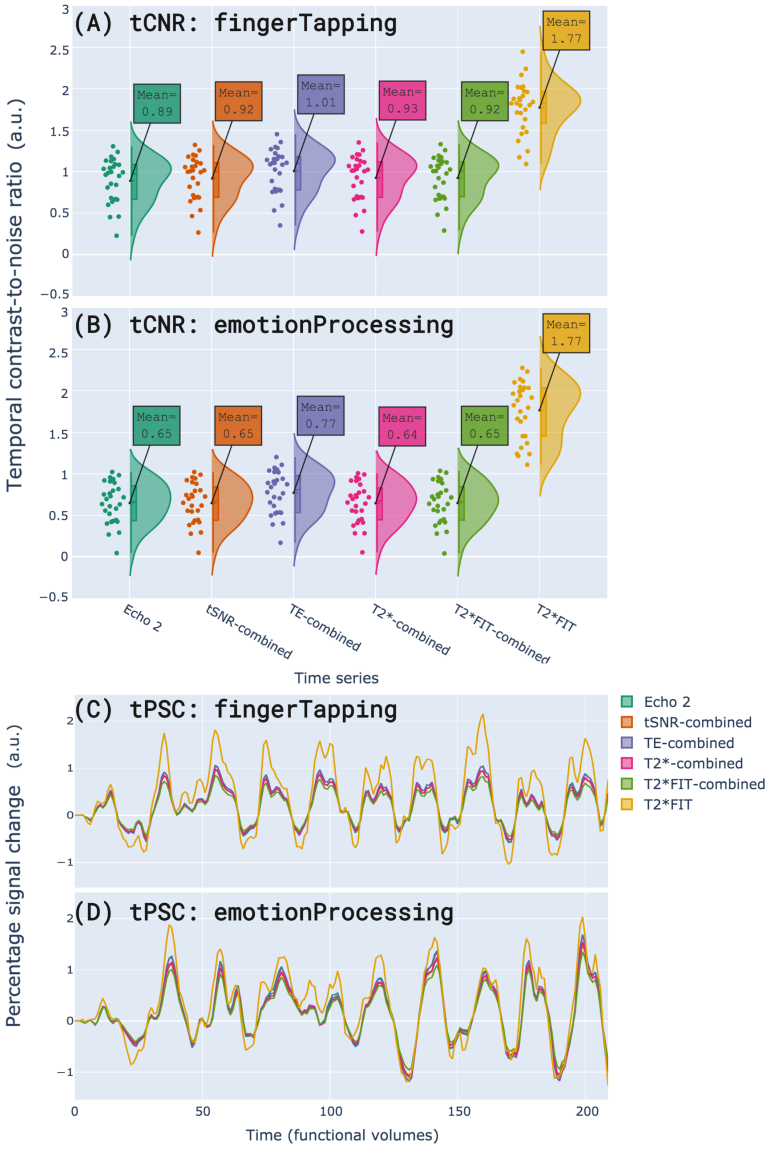

Figure 8.9 — *Distributions of mean functional contrast-to-noise ratio (calculated from real-time temporal percentage signal change) of the (A) fingerTapping and (B) emotionProcessing tasks within the FWE-OR region. Subplots (C) and (D) show individual subject tPSC time series for the same tasks as mentioned, respectively, for (A) and (B). Signals are colour coded for Echo 2, tSNR-weighted combination, TE-weighted combination, T2*-weighted combination, T2*FIT-weighted combination, and T2*FIT. Since tCNR is computed from tPSC time series, the tCNR values computed from (C) and (D) represent a single data point per time series in subplots (A) and (B). The time series visualisations in (C) and (D) reflect temporally smoothed data, using a moving 3-point average. Transient fluctuations for the first two volumes in (C) and (D), ascribed to differences in calculating real-time tPSC (using the cumulative baseline mean) versus offline tPSC (using a full time series mean) were zeroed across all six time series in order to remove their biasing effects on tCNR calculations.*

differences were explored in terms of: temporal signal-to-noise ratio, percentage signal change as task-based effect size measure, offline and real-time temporal percentage signal change in regions of interest, functional contrast in ROIs, and temporal contrast-to-noise ratio in ROIs.

8.5.1 Results

Our results, across 28 participants, are summarised as follows. Dropout recovery is more pronounced (in orbitofrontal, ventromedial prefrontal regions as well as inferior and anterior temporal regions) for the T2*-weighted, tSNR-weighted, and T2*FIT-weighted combinations than for the TE-weighted combination. All multi-echo combined time series yield increases in tSNR compared to Echo 2, with the newly-proposed T2*FIT-weighted combination resulting in the largest increase in mean tSNR. For the T2*FIT-weighted combination, increases in mean tSNR are larger for the amygdala than for the left motor cortex or the whole brain. In contrast, the T2*FIT time series results in a substantial mean decrease in tSNR from Echo 2. Alternatively, the T2*FIT time series yields the largest effect size measures across all investigated functional tasks and regions, whereas the effect size measures derived from combined echo time series tend to decrease slightly from those of Echo 2, for all functional tasks. Based on temporal percentage signal change calculated offline from minimally processed data, the T2*FIT time series yields the highest functional contrast for all tasks. Similarly, based on temporal percentage signal change calculated in simulated real-time from cumulatively denoised data, the T2*FIT time series also yields the highest functional contrast for all tasks, although this increase is substantially more than the increase seen for its offline counterpart. For real-time scenarios, the temporal contrast-to-noise ratio of the T2*FIT time series is notably higher than all other time series, which are very similar in size and distribution.

The fact that multi-echo combined time series yields increased tSNR compared to single echo data has been widely demonstrated in previous research, and has been repeated here for all combined time series with respect to Echo 2. Additionally, we show that the novel T2*FIT-weighted combination yields the largest increase, replicating our previous results from a different dataset (Heunis et al., 2019a). In the amygdala, a mean increase in tSNR of 53.35% was calculated across participants, while the mean increases for the left motor cortex and the whole brain were respectively 31.63% and 36.95%. These differences suggest that multi-echo combination, and in particular T2*FIT-weighted combination, could prove more useful in terms of tSNR for areas traditionally suffering from suboptimal BOLD sensitivity due to their lower local baseline T2*-values. On the other hand, improving tSNR in individual regions could also benefit whole-brain methods where spatially distributed ROIs or networks are used as the neurofeedback substrate (e.g. connectivity-based neurofeedback employed by Megumi et al., 2015, or default mode network-based neurofeedback employed by McDonald et al., 2017), since this would decrease spatial variability in BOLD effects and could lead to more accurate brain-wide estimates of interest. Note that we did not explore the

approach of averaging the echoes (i.e. simple summation) as for instance originally proposed in Posse et al. (2000), but this approach has proven reduced BOLD sensitivity than the rest of combination approaches investigated here.

While not novel, an important aspect demonstrated here was the decrease in tSNR for the T2*FIT time series, reported before by others including Kundu et al. (2017). Importantly, the fitting procedure used to estimate per-volume T2*- and S0-values (assuming a mono-exponential decay curve) yields noisy results that influence the amplitude of the signal fluctuations with respect to the mean, thus increasing the standard deviation and decreasing tSNR. The pitfalls of assuming mono-exponential (as opposed to multi-compartment) decay and using a fitting procedure with few data points (three in this case) have been described before (Whittall, MacKay, and Li, 1999) and remain applicable here. Future work should aim to exploit technical advances such as simultaneous multi-slice imaging to increase the number of echoes acquired per volume, while investigating more robust models of T2*-decay.

While tSNR is a useful quantifier of relative spatial signal increases and dropout recovery, it does not directly measure or represent BOLD sensitivity. To investigate how multi-echo derived data could improve our ability to link BOLD changes to neuronal effects, we employed statistical task-analysis to yield effect size measures to show the benefits of rapid T2*-mapping over single echo fMRI. For all tasks, the T2*FIT time series consistently yielded the largest standardised effect size measures in terms of percentage signal change calculated offline from contrast maps after participant-level GLM analysis, while the effect sizes for multi-echo combined data decreased slightly. This phenomenon of decreased effect sizes has been reported before for both optimally combined as well as MEICA-denoised data by Gonzalez-Castillo et al. (2016). This was reported for five subjects performing an auditory task in a 20 s ON/OFF block paradigm similar to the one in this work. Gonzalez-Castillo et al. (2016) calculated per-volume T2*-maps (i.e. T2*FIT time series) using the same log-linear fitting approach but with only two echoes (TE = 31.7 ms and 49.5 ms), also in accordance with Beissner et al. (2010), and found that the activation extent, effect sizes and T-statistic values all decreased for the T2* time series compared to the original single echo time series. In contrast, we observe that the effect sizes calculated from the T2*FIT time series increase, while the related T-statistic values decrease (indirectly preempted by the decrease in tSNR). This difference in the change of the effect size with respect to Echo 2 might be explained by the use of three echoes in our calculation of the T2*FIT time series, instead of two echoes, that could result in reduced accuracy of the T2* estimates. This hypothesis can, in fact, be tested using the current *rt-me-fMRI* dataset, although that is considered beyond the scope of this work.

The T2*FIT time series also consistently yielded the largest functional contrasts in terms of differences in task vs. baseline amplitudes in tPSC signals calculated from offline and real-time data. As an example, we observe an 87.91% increase in mean PSC (T2*FIT compared to Echo 2) for the FWE-OR region of the *fingerTapping* task, and increases in functional contrast for the same task and region of 100%

and 293%, respectively for offline and real-time scenarios. Interestingly, functional contrast for the real-time calculated tPSC signal showed an increase above the functional contrast calculated from offline data. The main mathematical difference in real-time vs offline approaches that this could be ascribed to is the cumulative calculation vs offline calculation, especially as regards the mean (cumulative baseline mean vs full time series mean). Beyond the functional contrast, the temporal contrast-to-noise ratio of the real-time tPSC signals were calculated to control for relative signal fluctuations, especially considering the low tSNR of T2*FIT. Even so, the T2*FIT time series consistently yielded the largest tCNR increase above Echo 2 for all tasks (e.g. 97.78% for the *fingerTapping task*), suggesting its benefits for improving BOLD sensitivity in real-time use cases.

This apparent contradiction of low tSNR versus high offline PSC and high real-time tCNR is worth exploring. Theoretically, we should expect an increase in BOLD sensitivity when analysing quantified T2* fluctuations versus fluctuations in single echo image intensity, since the separation of T2* and S0 should remove (to a considerable extent) system-level, inflow, and subject-motion effects from the T2*-signal. What is left in the form of voxel-based T2*FIT-values would then theoretically be more indicative of local neuronal activity than information derived from single echo data, assuming noise from the fitting procedure and other confounding factors do not attenuate this contrast substantially. Kundu et al. (2017) suggested that, even given a noisy fitting procedure, direct T2* and S0 fitting can be valid for separating low-frequency BOLD changes, while not ideal for higher frequency modulations that could alias with fitting error variations. In the task and ROI signal analyses presented here, as well as in the intended offline and real-time use cases of the presented methods, ON/OFF block paradigms generate slow BOLD changes where volume-to-volume fluctuations are averaged out to generate summary measures. This could explain, in part, the absence of detrimental effects resulting from the low tSNR. We also note that several levels of spatial smoothing applied to the real-time use case (whole volume spatial smoothing, followed by in-ROI voxel averaging) are bound to increase the tSNR of the ROI signal from which the tCNR is calculated. This likely counteracts the low tSNR of the T2*FIT time series that conversely attenuates T-values in the offline use case. Additionally, acquisition parameters can have important influences on signal noise and parameter fitting error. Large voxel sizes (in this case 3.5 mm isotropic) are known to increase SNR and can be a contributing factor to the promising result reported in this work.

In terms of practical applicability to real-time fMRI research, we have shown the usefulness of multi-echo for real-time use cases in a 28-person dataset with several functional task designs. We demonstrate that real-time T2*FIT-weighted combination yields brain wide mean tSNR increases and improves signal recovery in regions affected by dropout, compared to single echo and other combined multi-echo time series. We show additionally that the real-time T2*FIT time series yields large functional contrast and tCNR increases compared to single echo or combined multi-echo time series. These improvements could benefit both real-time

brain wide connectivity measures and real-time region-based signals, respectively, showing the possible utility for studies on adaptive paradigms and neurofeedback.

Lastly, we have shown that real-time multi-echo processing, specifically rapid T2*-mapping and subsequent multi-echo combination is technically viable and practically supported. The software tools generated through this work (and shared with the community) support several per-volume or real-time multi-echo processing operations, including real-time 3D realignment of multi-echo data, real-time estimation of multi-echo decay parameters, real-time multi-echo combination using several weighting schemes, and multiple standard real-time preprocessing steps. It provides a practical toolkit for exploring real-time multi-echo fMRI data and for comparing the effects of acquisition and processing settings on BOLD sensitivity in individuals. Additionally, the interactive browser application allows easy access to the results[10], while the provision of supporting material and code[11] allows the presented results to be reproduced and allows replication attempts to be conducted on future datasets.

8.5.2 Limitations and future work

It remains important to consider caveats before further implementations and in order to direct future work. To start, we note that the *rt-me-fMRI* dataset does not include field maps and consequently no field map-based distortion correction steps were applied. To counter this absence, the alignments of the anatomical mask, as well as the derived tissue segmentation masks, and the EPI data were visualised, inspected and the overlap was found acceptable.

As regards the acquisition of a resting-state run from which to estimate T2* before the start of a real-time session, future work could look into other acquisition types to improve the quality of prior T2*-maps. For example, sequences like multi-echo GRE or ME-MP2RAGE (Metere et al., 2017; Sun et al., 2020), or multi-echo EPI sequences with a longer TR and more echoes, can all yield a more accurate T2* estimation. Further changes to the acquisition strategy of the real-time runs may also benefit future applications. We mentioned voxel sizes above, but other aspects like increases in the number of receive coils, improvements in the implementation of acceleration techniques such as GRAPPA or SENSE, and field strength increases can all lead to lower levels of volume-to-volume noise and subsequent parameter estimations.

Regarding the exploration of tSNR improvements in multi-echo-derived data versus single-echo data, we note that these improvements can stem from different sources. For example, tSNR increases due to multi-echo weighting can originate from signal recovery (i.e. the mean signal owing to the first echo) or decrease of noise fluctuations due to the averaging. Additionally, tSNR changes could be different across brain regions and tissue types (for instance from grey versus white

[10] https://rt-me-fmri.herokuapp.com/

[11] https://github.com/jsheunis/rt-me-fMRI

matter or CSF). Further work to delineate the exact origin of spatial variations of such tSNR improvements will allow future applications to gain use-case-specific benefits. Such investigations should also look closely at changes accompanying different acquisition strategies highlighted above.

In the described preprocessing pipeline, probabilistic cytoarchitectonic maps in MNI152 space (from Eickhoff et al., 2005) were co-registered to the subject functional space to create subject-specific regions of interest. It should be mentioned that these are less subject-specific than alternatives derived from individual anatomical features (such as those generated by the *freesurfer* software package), which points to an option for future improvement. Furthermore we note as did Clare et al. (2001), that the selection of the region of interest within which to investigate activation effects, functional contrast, tSNR and more, can increase the variability of results and subsequent inferences. This issue was evaluated here considering three different ways of delineating the region of interest: FWE, FWE-OR, and atlas-based, and we observed attenuation of effect sizes, T-values and functional contrast as regions become less spatially matched to participants' functional activation localisation. This is particularly important for the real-time neurofeedback context, where a predefined subject-specific region of interest is often required to enable real-time region-based signal extraction. This concern about variability in the performance due to ROI definition extends to the implementation of real-time denoising steps as well, as noted in our previous work on denoising steps in neurofeedback studies (see Chapter 3; Heunis et al. (2020c)). In the current study, we intentionally implemented a minimal real-time processing pipeline to avoid confounding the results.

As summarised in the results discussion above, standardised effect sizes resulting from task analysis of all multi-echo combined time series were very similar in size and distribution, and on average much lower than that of the T2*FIT time series. This phenomenon could benefit from follow-up confirmatory analyses in a future study. Another claim that could be usefully extended into a follow-up investigation is the decision to include all participants in the study irrespective of the amount of motion in their data. As an example, some multi-echo combination schemes may be more or less robust to head motion, and the inclusion of all subjects would allow investigating such variations in higher versus lower motion subjects. Lastly, a key next step for extending the investigation of multi-echo use in offline task analysis is to examine activation clusters in more detail. This work looked at PSC and T-values in specific regions, but an important question to test would be whether multi-echo combined or derived times series yield activation clusters in new or unexpected brain regions, or how they affect existing activation clusters in terms of effect size and extent. The supplementary web-application can also be seen as an evolving resource where other useful metrics, results and visualisations can be added in future. Examples of such additions include pairwise percentage differences in comparison metrics between the different multi-echo combined and derived time series and Echo 2; investigations into new or varying activation clusters resulting from multi-echo time series; or any other aspects

covered here as future work.

While the presented benefits of multi-echo fMRI for real-time experiments are promising, further work is necessary to quantify the effects of a full multi-echo and real-time denoising pipeline on BOLD sensitivity and data quality. Taking into consideration the caveats discussed here, we advise researchers planning real-time fMRI studies to design and conduct effective pilot studies and to evaluate the effects robustly before deciding on the optimal multi-echo implementation settings.

Chapter 9 Discussion and conclusions

What started in the introduction as an abstract exploration of mind reading and the promises that it might hold, ended up as a multitude of pages of information constituting the topics of this thesis: real-time functional magnetic resonance imaging, neurofeedback, scanner hardware setup, quality control metrics, open source software developments, newly acquired datasets, novel acquisition and processing methods, and ultimately increased sensitivity in real-time brain imaging. So did we achieve what we set out to do? What did we learn in the process? What has this contributed to our field? And where do we go from here? In this final chapter, these questions will guide our discussion.

To provide fresh context for this discussion, let us first revisit the background and problem statement of this thesis. Breaking down the complexities of the human mind in order to understand and develop treatments for neurological or psychiatric conditions is an ongoing challenge in neuroscience research and global healthcare. If we are going to make a practical difference in our understanding of these complexities, and ideally in the lives of those who suffer from mental health conditions, we have to rigorously and critically question and ensure the quality of our own scientific measures, methods, and inferences. Real-time functional magnetic resonance imaging is an advanced method that shows promise in allowing us to probe and explore the human mind in a virtual, real-time and non-invasive manner. But how well do we understand this technology and its practical implications? Can we trust its measures and the inferences we draw from them? What can and should we do to improve the quality of real-time fMRI?

Data quality has received little attention in the field of real-time fMRI, while the drawbacks of fMRI and the effects of not accounting for them, on the other hand, are well known. This discrepancy is substantiated by a notable absence of methods for improving real-time fMRI data quality and an absence of practices for methods reporting in the literature. This absence prevents a thorough, community-wide, understanding of real-time fMRI data quality and aspects that might influence, or better yet, improve it. Consequently, adoption of improved methods lags behind in practice, since a lack of understanding and validation hinders implementation at the level of hardware and software tools. Multi-echo fMRI is a core example: its benefits for conventional fMRI are documented, but it is hardly used in real-time applications. In order to validate its possible benefits for improving the quality of real-time fMRI, it requires a thorough understanding, new methods development

for real-time use cases, toolset implementations, novel datasets, and validation experiments.

With this as background, we now discuss the findings and contributions of this work in line with the three high-level themes and their respective research questions.

9.1 Understanding real-time fMRI data quality

RQI.1: Can we provide a comprehensive review of existing methods for improving the quality of real-time fMRI?

RQI.2: What does an improved understanding reveal about the state of real-time quality control methodology and reporting? Do proven signal processing methods exist for removing noise sources that are not of interest? Are there standardised quality control measures and ways to report them?

RQI.3: If our understanding, denoising methodology and reporting practices are lacking, which measures can be introduced to improve the research community's understanding and implementation of improved data quality?

Chapter 2 provided a comprehensive background for understanding the challenges to real-time fMRI related to BOLD sensitivity. The drawbacks of conventional single-echo functional MRI sequences were explained, including acquisition aspects such as signal dropout and suboptimal brain-wide T2*-weighting, as well as subject related aspects such as movement, respiration and cardiac activity. Real-time fMRI is well-positioned to provide practical interventions for improving BOLD sensitivity, i.e. for mitigating the effects of the aforementioned drawbacks such that neuronal activity is more likely linked to the BOLD signal, and to lead to time savings, cost savings, and a general improvement in the quality of functional MRI data. Real-time multi-echo fMRI, in particular, showed promise due to the ability of multi-echo fMRI to separate BOLD and non-BOLD effects and to provide optimal brain-wide T2*-weighting. However, in order to achieve a level of confidence in real-time fMRI and its ability to improve data quality, its methods needed to be thoroughly understood. Which steps do researchers employ when denoising the fMRI signal in real-time, and how are these reported? Do we have a set of evaluated and established quality control metrics that can serve the fMRI community and improve through iterative contributions? And can such metrics and their reporting help us to improve the computational reproducibility and eventual assessment of replicability of studies employing real-time fMRI methods?

Chapter 3 investigated these questions in a methods review of 128 real-time fMRI neurofeedback studies. Our results showed high variability in the reporting of preprocessing methods that are considered to be standard in real-time fMRI, with less than a third of the studies reporting steps like spatial smoothing and

temporal smoothing, and less than half reporting the use of drift removal. Such variable reporting standards not only hinders computational reproducibility, but also casts doubt on what exactly is contained in the real-time fMRI signal and on our consequent ability to assess interventions such as neurofeedback adequately. Attempting to mitigate the effects of this problem, i.e. to improve our ability to delineate the sources of variance in the real-time BOLD signal, our work resulted in a COBIDAS-style checklist (see Appendix B[1]) for researchers to report the implementation of a set of standard real-time fMRI denoising and quality control steps. As with the original COBIDAS checklist (Nichols et al., 2017), this list not only allows thorough reporting of most current real-time denoising and quality control methods so as to ensure methods reproducibility, it is also a valuable resource for researchers to learn about current state of the art. Additionally, the set of quality control measures can form the basis of a common set of standards for the methods community to implement and contribute to.

Chapter 3 went on to identify a need for methodological studies quantifying and comparing the contribution of denoising steps to the neurofeedback signal quality, and more generally that there is room for developing new and improved real-time fMRI sequences and denoising methods. Suggestions were also made for researchers to strive to adopt transparent practices in the form of methods and data sharing and to support open-source real-time fMRI software projects, as few examples of such practices were found in literature.

A core focus for this thesis was consequently determined both by real-time multi-echo fMRI showing potential as a means of improving real-time BOLD sensitivity, and by the methods review indicating a need for novel sequences and analysis methods to achieve the same. To allow a comprehensive exploration of the usefulness of multi-echo fMRI for improving real-time data quality, however, the hardware and software requirements first had to be fulfilled.

9.2 Hardware and software for real-time fMRI analysis and quality control

RQII.1: Can we implement the infrastructure on the scanner level to allow the transfer and processing of (multi-echo) fMRI in real-time?

RQII.2: Can we implement real-time quality control methods on a software level to provide the research community with a tool for methods standardisation and quality control and improvement?

RQII.3: Can we develop and implement novel algorithms for processing multi-echo fMRI data in real-time, allowing validation experiments to be conducted?

[1]Available online at: `https://osf.io/kjwhf/`

Chapter 4 demonstrated that, as a first step, it is achievable to set up the technical scanner and software infrastructure to acquire, transfer, process and visualise whole-brain fMRI data in real-time. The Neu3CA-RT framework was built using a Philips 3T Achieva scanner and MATLAB and SPM12-based software with the aim of advancing scientific knowledge on real-time cognitive brain activity and to promote its translation into clinical practice. This framework allowed a full processing cycle to be applied for each acquired single-echo volume (every 3 s in the demonstrated cases), which included processing steps such as: file type conversion to NIfTI format, 3D volume realignment, trend removal, spatial GLM analysis, mapping GLM beta parameters to the BrainMap behavioural space, and displaying results in a graphical user interface.

Of course, demonstrating viability does not equate to demonstrating state of the art, which is why Chapter 4 noted several shortcomings of the implemented framework. First and foremost, this included the processor implementation and programming language, which were not optimised for processing speed. While the use of MATLAB on a single (multi-core) processor benefits the developer in terms of prototyping capability and ease of use, converting to a parallelised or GPU framework and using lower level compiled programming languages, or at least optimising the performance of MATLAB code, will benefit the application greatly in terms of processing speed. More processing time would allow for the inclusion of additional per-volume preprocessing steps, addressing further concerns such as low data quality due to insufficient denoising. Faster processing would also allow the framework to be used for applications requiring increased brain coverage, higher spatial resolution, higher temporal resolution (i.e. lower repetition time), and high-demand visualisation options.

While the framework implemented a spatial GLM approach to real-time analysis, any of a multitude existing or future methods are possible. Functional connectivity (through causal modeling or correlative approaches), network analysis, signal decomposition, and multivariate pattern analysis are all popular approaches used in offline computational neuroimaging, and porting such methods into a real-time framework should be considered inevitable. Improving the performance of the Neu3CA-RT framework, while ideally retaining the ease of prototyping, would allow these methods to be implemented for real-time applications.

While the framework described in Chapter 4 was not yet tested with multi-echo data, the proof of concept served as a useful starting point for further developments, especially for prototyping real-time quality control approaches. Chapter 5 described the successful demonstration of *rtQC*, a MATLAB and SPM12-based open-source toolbox for real-time fMRI quality control, with a focus on highlighting quality issues between the offline and real-time variants of fMRI data as well as real-time visualisation of quality control metrics. Implemented metrics included a real-time display of framewise displacement (FD), temporal signal-to-noise ratio (tSNR), voxel-based and spatially averaged Z-score, region-based signals, and a real-time 2D representation of voxel intensity fluctuations over time. Additionally, per-volume motion-outliers were classified and visualised in real-time using the

per-volume framewise displacement value and a predefined threshold. Based on the performance improvement recommendations from Chapter 4 that were mentioned here, *rtQC*'s implementation included updated real-time volume realignment and spatial smoothing algorithms to speed up processing time.

Apart from being useful as a software toolbox that can identify data quality issues as they are acquired, *rtQC* is also intended as a community tool to promote the use and continued development of best practices for real-time fMRI quality control. It provides the functionality for calculating the most widely used quality metrics, while providing the open-source code and prototyping capability for developers to add more community-driven features. Suggestions for additional features include real-time DVARS, global signal, global signal correlation, and more metrics and visualisations from widely used community tools such as fmriprep (Esteban et al., 2019) and MRIQC (Esteban et al., 2017). Additionally, the same suggestions relating to performance drawbacks mentioned for Neu3CA-RT apply to *rtQC*, and improvements to code structure and documentation will make the tool more accessible and will encourage further use. These suggestions were taken into account with the development of *fMRwhy*.

As the third contribution to hardware and software tools for fMRI analysis and quality control, Chapter 6 covered what should be viewed as the culmination of the offline and real-time fMRI analysis experience gained over the course of this project. *fMRwhy* is positioned as a MATLAB- and SPM12-based toolbox with a variety of helper functions and BIDS-compatible workflows to assist researchers with their reproducible fMRI analysis journey. We noted in Chapter 6 that aspects such as standardised data manipulation, interoperability, workflow automation, and reproducible analysis pipelines are lacking in MATLAB-based compared to Python-based neuroimaging projects. *fMRwhy*'s goal was to make such developments available to fMRI researchers using SPM12 and MATLAB. More specific to the applications in this thesis, it contains both modularised functionality for the processing of real-time and offline multi-echo fMRI data as well as full-length automated pipelines for quality control and reporting, both of which contributed substantially to the novel developments described in Chapters 7 and 8 (discussed shortly). Additional strong features of *fMRwhy* that contribute to its accessibility and reuse are its comprehensive and open code base[2] and API documentation[3].

It should be noted that *fMRwhy* is not, nor is it intended to be, a fully-fledged fMRI analysis package. Chapter 6 noted that it would not suffice as a replacement tool for the likes of SPM12, FSL, fmriprep, AFNI, or their constituent functionality. It is better positioned as an auxiliary tool for MATLAB and SPM12 users who work with BIDS-formatted fMRI datasets and who want to: 1) generate automatic, user-friendly quality reports, 2) build reproducible SPM12-based processing pipelines, 3) preprocess multi-echo fMRI data, 4) build/test real-time analysis pipelines, or 5) use auxiliary tools for fMRI visualisation and image manipulation. The project

[2] `https://github.com/jsheunis/fMRwhy`

[3] `https://fmrwhy.readthedocs.io/`

is also an ongoing effort, with community contributions encouraged to improve documentation and function modularity, and to develop and add new quality control and multi-echo analysis steps.

In summary, Chapters 4, 5 and 6 documented the staged development of open and accessible tools for real-time analysis, quality control and multi-echo processing. Each chapter highlighted shortcomings of the relevant tool that were addressed in part by the subsequent chapters, and each tool was developed using the cumulative experience gained over time, resulting in a toolset that provides an open code base for real-time, multi-echo fMRI analysis and quality control.

9.3 Real-time multi-echo fMRI

RQIII.1: As a starting point, can we design and collect a novel, real-time multi-echo dataset that will allow the exploration and development of improved signal processing methods? Can we annotate and structure such datasets so as to ensure interoperability with standard tools and pipelines? And can we share this data publicly while still prioritising research ethics and the personal data privacy of data participants?

RQIII.2: Given that no comparable literature exists, can we explore and report possible BOLD sensitivity improvements with real-time multi-echo fMRI? How do newly developed methods perform against current state of the art or conventional offline multi-echo fMRI methods?

RQIII.3: Can we consequently derive preferred multi-echo methods for improving real-time fMRI data quality and develop these into publicly available pipelines for community use and contribution?

The last part of the thesis focused on the promising research avenue: multi-echo fMRI for improving BOLD sensitivity in real-time and offline scenarios. Chapters 2 and 3 presented ample evidence for the benefits of multi-echo over single-echo T2*-weighted data, and its relatively unexplored nature in real-time use cases prompted its focus for this thesis on the quality of real-time fMRI.

The first step was to design an appropriate experiment to capture multi-echo data for a representative set of task-based and resting state use-cases, so as to allow the development and exploration of real-time, multi-echo processing methods for general real-time applications. Chapter 7 described how this was achieved in the form of rt-me-fMRI[4], a multi-echo fMRI dataset (28 healthy participants) with four task-based and two resting state runs as well as cardiac and respiratory data that were collected, curated using the BIDS standard, and made available to the community. A very strong element of this open dataset is the comprehensive description of methods used to collect and curate it, including details about: experimental

[4] Available online at: `https://dataverse.nl/dataverse/rt-me-fmri`

design, acquisition parameters, raw data preparation and standardisation, data preprocessing, quality control measures, and data validation measures. Further valuable resources accompanying the rt-me-fMRI dataset include a web-based application[5] that allows interactive exploration and visualisation of the data and its derivative measures, and supporting information and code for reproducibility and reuse[6]. These resources provide fMRI researchers with the necessary support not only to reproduce the derivative data, but to help advance the development of methods for real-time multi-echo fMRI analysis. Additionally, the variety of functional activation paradigms (finger tapping, emotional face and shape matching, imagined finger tapping and imagined emotion processing) supports a multitude of use cases covering regions across the whole brain.

Thoughtful consideration was given to the privacy of data participants during the process of curating, processing and sharing the rt-me-fMRI dataset. In the interest of transparency and reproducibility of scientific results, data sharing is a desirable outcome; on the other hand, personal data privacy of individuals should not be compromised by sharing identifiable information. In the European Union in particular, where the strict General Data Protection Regulation (GDPR) is in effect to govern personal data privacy, extreme care should be taken to ensure that data sharing practices remain GDPR compliant. Consequently, an approved workflow was followed to minimise the risk to data participants, including: following best practices to de-identify brain images (e.g. removing personally identifiable information from image filenames and metadata and removing facial features from T1-weighted images), converting the data to BIDS format, employing a Data Use Agreement[7], and keeping participants fully informed about each of these steps and the associated risks and benefits. The procedural knowledge gained throughout this process was contributed in turn to the collaborative and open-source Open Brain Consent project (Bannier et al., 2017), thus making it accessible to and reusable by the fMRI community.

The first use of the rt-me-fMRI dataset was covered in Chapter 8, which represents the culmination of all knowledge and findings presented in this thesis: the first comprehensive evaluation of the effects of multi-echo fMRI combination and rapid T2*-mapping on offline and real-time BOLD sensitivity. Citing a lack of recent systematic comparisons of existing multi-echo combination strategies, Chapter 8 compared six different approaches derived from multi-echo data: a single-echo time series (based on Echo 2), the real-time T2*-mapped time series (T2*FIT) and four combined time series (T2*-weighted, tSNR-weighted, TE-weighted, and a new combination scheme termed T2*FIT-weighted). The results showed that the T2*FIT-weighted combination yielded the largest increase in temporal signal-to-noise ratio across task and resting state runs, and results demon-

[5] https://rt-me-fmri.herokuapp.com/

[6] https://github.com/jsheunis/rt-me-fMRI

[7] Available online at: https://github.com/jsheunis/rt-me-fMRI/blob/master/DUA.md

strated additionally for all tasks that the T2*FIT time series consistently yielded the largest offline effect size measures and real-time functional contrasts. These findings support the theoretical backdrop, in that increases in BOLD sensitivity should be expected when analysing quantified T2* fluctuations versus fluctuations in single echo image intensity. This is because the separation of T2*- and S0 should remove system-level, inflow, and subject-motion effects from the T2*-signal to a considerable extent, and what is left in the form of T2*FIT-values would then be more indicative of local neuronal activity than information derived from single echo data. As a caveat, this assumes that noise from the mono-exponential fitting procedure and other confounding factors do not attenuate this contrast substantially, which is a valid concern given the reported decrease in tSNR of the T2*FIT time series.

Even with the mentioned drawbacks, Chapter 8's encouraging findings demonstrated the promises of multi-echo fMRI for real-time use cases, which led to the recommended use and suggested continued exploration of T2*FIT, i.e. rapid T2* mapping, for offline and real-time fMRI analysis. Along with these findings, further outputs of the real-time multi-echo study were the newly developed open-source processing algorithms for multi-echo fMRI, which to our knowledge were the first to be made available for MATLAB users. These include MATLAB and SPM12-based algorithms for offline and real-time realignment of multi-echo data to a preselected template volume or echo, as well as methods for multi-echo parameter estimation (T2* and S0) and all previously mentioned multi-echo combination strategies. All newly developed processing and software methods form part of the fMRwhy software tool, while all results of the multi-echo methods study were included in the interactive web-based application[8] to allow exploration and visualisation. As with Chapter 7, supporting information and code for reproducibility and reuse were made available[9].

9.4 Conclusions, limitations and future work

The results discussed in this chapter showed that we addressed the core research questions of our three high-level themes. To summarise, we:

Part I

Developed a comprehensive understanding of real-time fMRI signal quality, identified the shortcomings of real-time denoising pipeline implementation and reporting, identified the need to develop novel sequences and methods to improve BOLD sensitivity in real-time, and identified the potential of real-time multi-echo analysis.

[8] https://rt-me-fmri.herokuapp.com/

[9] https://github.com/jsheunis/rt-me-fMRI

Part II

Developed a set of three open-source software tools and one real-time hardware integration to advance the use of real-time fMRI quality control standards and to enable real-time multi-echo analysis and automated quality control reporting.

Part III

Collected, curated and shared a multi-echo fMRI dataset, developed and shared the required real-time multi-echo processing algorithms, demonstrated the superiority of multi-echo combination for real-time BOLD sensitivity increases, and recommended the continued use and exploration of rapid T2* mapping for real-time use cases.

So did we achieve what we set out to do? In short, and as was just described in detail, yes. *How well do we understand this technology and its practical implications?* Before this attempt at consolidating literature and practice and generating new knowledge on the quality of real-time fMRI, little other efforts have been reported. Now, after considering the information provided in Chapters 2 and 3, we have formed a comprehensive understanding of the topic. *Can we trust real-time fMRI measures and the inferences we draw from them?* Not at face value and not without carefully considering the knowledge curated and recommendations made in this thesis. *What can and should we do to improve the quality of real-time fMRI?* Succinctly: (1) carefully consider and report the inclusion or exclusion of each processing step in the real-time analysis pipeline; (2) draw from community-contributed standards and methods for real-time quality control and use a tool to calculate and report these measures together with study results; (3) opt for the use of multi-echo fMRI if a sequence is available and all other experimental parameters are satisfied; (4) contribute to the continued exploration, development and testing of rapid T2*-mapping using real-time multi-echo fMRI; (5) prioritise transparency and reproducibility whenever possible such that the data, methods and software can be shared together with a study's results; and (6) always run pilot studies first.

So then, *where do we go from here?* While various specific limitations and recommendations were already covered in each respective results section in this chapter, here we focus on general limitations and future work. It is evident that this thesis made substantial contributions of practical value, but the jury is still out on the uptake of said contributions. How useful is the COBIDAS-style checklist to report the implementation of a set of standard real-time fMRI denoising and quality control steps? Does rtQC and its quality metrics and visualisations help researchers to save time and money and to improve the quality of their data? Are researchers opting for real-time multi-echo over single-echo fMRI acquisition and processing? Without the use of such methods and participation by the community, and the inevitable feedback that such interactions will generate, the impact of

such contributions are difficult to quantify in the short term. In this regard, open development frameworks (such as GitHub or GitLab) will have to be used to track contributions and downloads as a proxy for uptake, aside from more conventional metrics such as publication citations.

In addition to focusing on uptake, care should be taken to improve the accessibility, ease of use, and potential for community-contributed growth of the developed software tools and methods. These aspects can flourish when supported by established software engineering and project maintenance principles such as comprehensive and automated documentation, automated testing, continuous integration, avenues for issue logging and resolution, open contribution guidelines, and open communication platforms. If such procedures are implemented and maintained, ongoing development of features that reflect the interests of the community would be easy to prioritise. This would inherently accommodate further exploration of methods that were left unexplored in this thesis, such as the use and usefulness of cardiac and respiratory data together with real-time multi-echo processing; or a comparison of the effects of including/excluding a variety of standard preprocessing steps on real-time BOLD sensitivity; or continued exploration of multi-echo combination and rapid T2*-mapping for real-time use cases of functional connectivity, network measures, and multivariate pattern analysis.

Whatever the future use case, the contributions made in this thesis resulted in an open real-time multi-echo fMRI dataset and open software tools with which to process this data in a myriad of ways. The transparent and reproducible groundwork has been laid to allow the use of novel data, sequences, software and signals to further our understanding of the human mind, and what is left is but for the interested researcher to accept the invitation and start exploring. Perhaps in that way, together, we can systematically conquer this ultimate challenge, piece by piece, and build up the theory and evidence we need to improve global mental health.

Appendices

Appendix A

Real-time fMRI processing methods

A.1 Context

Chapter 3 provided a comprehensive review of methods reported in real-time fMRI neurofeedback literature and used in studies to improve the quality of the real-time signal. To aid the reader's understanding and guide future use of these methods, Table A.1 in this Appendix summarises the most often reported real-time processing methods. In addition, Table A.1 provides context for analogous methods in conventional fMRI analysis, how the real-time methods differ from their offline counterparts, and recommendations for deciding on implementation.

A.2 Real-time fMRI processing methods

Table A.1 — *A summary of real-time fMRI processing methods*

Conventional method	Real-time method	Differences / notes	Reporting suggestions
0. Example processing step			
Standard method(s) used in conventional offline fMRI processing	*Methods most often used or reported in real-time fMRI and neurofeedback signal processing*	*Main distinctions between offline and online/real-time methods, with additional notes*	*Recommendations on the use of the reported real-time methods, whether to implement them or not, and additional relevant information*
1. Slice timing correction			
Various interpolation methods	Various interpolation methods	No algorithmic differences, as both are done on a per-volume basis	Generally recommended for TR $\geq 2s$
2. 3D volume realignment			
6 degree of freedom rigid body transformation of whole brain data	6 degree of freedom rigid body transformation of whole brain data	• No algorithmic differences, as both are done on a per-volume basis • Template EPI for real-time = previously collected EPI volume • Template EPI for offline = first volume of time-series or mean EPI	Always recommended
3. Spatial smoothing			
3D Gaussian smoothing kernel with a specified FWHM, applied to whole or masked brain data	3.1) 3D Gaussian smoothing kernel with a specified FWHM, applied to whole or masked brain data	No algorithmic differences, as both are done on a per-volume basis	• Typically recommended to increase SNR for all except MVPA-based neurofeedback methods or when using small ROIs (e.g. amygdala) • Recommended kernel size depends on acquisition parameters amongst multiple other factors
	3.2) Averaging voxel values within a pre-specified ROI	Kernel-based smoothing versus basic averaging	Typically recommended to allow calculation of a 1D neurofeedback signal from 3D data
4. Drift removal and frequency filtering			
• Various algorithms for (mostly) high-pass filtering, e.g. a cosine basis set as GLM regressors (SPM) or a Gaussian-weighted running line smoother (FSL). Typically applied to whole or masked brain data. • Low-pass, band-pass or other types of filtering typically applied as part of GLM.	4.1) Incremental GLM (iGLM) with filtering regressors e.g. a cosine basis set and/or a linear trend regressor	• GLM applied to full offline data versus real-time iGLM • Whole brain offline drift removal (filtering) versus drift removal from 1D neurofeedback signal in real-time	• Drift removal is always recommended • Piloting suggested to determine the method best suited for the data • Kopel et al. (2019) recommend a sliding window iGLM algorithm with standard cosine basis set • PSC calculation is always with reference to a baseline. Thus, inherent drift removal through baseline subtraction is recommended; if not a global mean, then least ROI-based; if not cumulative, then at least based on the preceding baseline (non-regulation) block.
	4.2) Exponential moving average (EMA) filter	• No algorithmic differences if applied as digital filter that takes only history into account • Whole brain offline drift removal (filtering) versus filtering of 1D neurofeedback signal in real-time	

Continued on next page

Table A.1 – continued from previous page

Conventional method	Real-time method	Differences / notes	Reporting suggestions
	4.3) Inherent baseline drift removal through subtraction of cumulative global mean from ROI signal during PSC calculation	Mostly limited to real-time application because of PSC calculation for neurofeedback. See related: global signal regression in 6 below.	
5. Temporal filtering or averaging			
Typically, this is an implicit result of filtering as described above	5.1) Moving window time-point averaging of 1D neurofeedback signal	Standard offline filtering versus online 1D signal time-point averaging (comparable to EMA filter)	• No algorithmic differences if applied as digital filter that takes only history into account • Whole brain offline drift removal (filtering) versus filtering of 1D neurofeedback signal in real-time
An AR(1) filter is typically, and explicitly, applied to address autocorrelation in fMRI time-series data	5.2) AR(1) filtering in real-time has been reported but seldom implemented.	No algorithmic differences if applied as digital filter per time-point that takes only history into account	Piloting suggested to determine if AR(1) filtering is useful in addition to and/or influenced by other standard temporal smoothing and filtering steps
6. Nuisance regression (excluding physiological noise removal)			
Various 1D data traces are often included as nuisance regressors in offline GLM (typically applied to whole or masked brain data) including: • Head movement parameters (HMPs) • Volterra expansion of HMPs • Tissue compartment signal averages (CSF, WM, GM) • Global signal	Incremental GLM (iGLM) with minimal filtering regressors e.g.: • Head movement parameters (HMPs) • Tissue compartment signal averages (CSF, WM, GM, global)	• GLM applied to full offline data versus real-time iGLM • Whole brain offline nuisance regression, versus nuisance regression from 1D neurofeedback signal in real-time	• Piloting suggested to determine which nuisance regressors are best suited for the data • Over specification of design matrix (i.e. too many regressors) is not recommended, as iGLM parameter estimates will be noisy and will take considerable time to stabilise (see Misaki et al., 2015) • Global signal regression is controversial in offline and real-time fMRI analysis and should be piloted and well justified
7. Outlier or spike removal			
"Scrubbing" low quality EPI volumes (removing, replacing, averaging) based on a variety of quality metrics, e.g.: • Framewise displacement • DVARS • Standard deviation • Z-score • Other Could be incorporated as an additional scan-nulling regressor in offline GLM	7.1) Possibility to do real-time scan-nulling as part of iGLM, e,g, through real-time outlier detection based on a predefined framewise displacement threshold	• GLM applied to full offline data versus real-time iGLM • Whole brain offline nuisance regression, versus nuisance regression from 1D neurofeedback signal in real-time • Detection thresholds set based on statistical properties of full dataset or group data, versus requirement for predefined threshold for real-time detection	• Piloting suggested to determine if outlier removal is useful, and whether other existing filtering methods (e.g. iGLM regressors, EMA, temporal smoothing) could suffice • Careful thought should be given to predefined detection threshold if real-time outlier detection and scan-nulling is considered • Kalman filter parameters should be piloted, and defaults should not be accepted as best for the data
	7.2) Kalman filter that detects and rejects outliers based on irregular statistical properties (Koush et al., 2012)	• Standard high/low/band-pass filtering is typically used offline on whole brain data. • Adaptive Kalman filter introduced for real-time and implemented on 1D neurofeedback signal	

Continued on next page

Table A.1 – continued from previous page

Conventional method	Real-time method	Differences / notes	Reporting suggestions
8. Physiological noise removal			
Physiological noise is typically modelled using concurrent recordings of respiration and heart rate, e.g. RETROICOR, RVT, HRV. These are then used as nuisance regressors in the offline GLM applied to whole brain data.	8.1) Incremental GLM (iGLM) with additional filtering regressors e.g.: • RETROICOR set • Tissue compartment signal averages (CSF, WM, GM, global)	• GLM applied to full offline data versus real-time iGLM • Whole brain offline nuisance regression, versus nuisance regression from 1D neurofeedback signal in real-time	• Piloting suggested to determine which nuisance regressors are best suited for the data • Over specification of design matrix (i.e. too many regressors) is not recommended, as iGLM parameter estimates will be noisy and will take considerable time to stabilise (see Misaki et al., 2015) • Given the additional technical challenge of processing physiology traces in real-time, RETROICOR nuisance regression is not recommended unless pilot data or new evidence suggest otherwise
	8.2) Differential ROI to (potentially) correct for global effects caused by respiration	• An analogous step to real-time differential ROI does not exist for standard offline analysis • Differential ROI calculations are based on 1D ROI-averaged signals	• Piloting suggested to determine whether this is suited for the data • Care should be taken to ensure that task-relevant information is not subtracted from the • More evidence is to be gathered before this could be considered a recommended real-time processing step, or not
	8.3) High frequency filtering or adaptive Kalman filtering	• Standard high/low/band-pass filtering is typically used offline on whole brain data. • Adaptive Kalman filter introduced for real-time and implemented on 1D neurofeedback signal	Kalman filter parameters should be piloted, and defaults should not be accepted as best for the data
9. Signal scaling			
Global, proportional, and/or grand mean scaling steps are often applied to whole brain time-series data (e.g. prior to 1st level analysis in SPM and FSL), which typically allows the validity of analyses between runs and subjects	Signal scaling is most often done on the ROI-averaged 1D neurofeedback signal, taking historical time-series values into account. Scaling methods include: • Temporal smoothing, as described above in 5. • Using a dynamically updated range based on prior time-series data	Whole brain intensity scaling to allow comparisons across runs/subjects versus scaling the 1D neurofeedback signal to prevent abrupt changes to the display seen by the subject	• Real-time signal scaling for visual quality of the neurofeedback signal is recommended. • The specific scaling method should be determined through piloting
10. Model free denoising methods			

Continued on next page

Table A.1 – continued from previous page

Conventional method	Real-time method	Differences / notes	Reporting suggestions
Principal and/or independent component analysis is often applied to whole brain time-series data in order to extract statistically independent spatial components. These components can be classified as noise sources and subsequently regressed from the whole brain time-series data. Examples include: • MELODIC ICA • ICA-AROMA • aCompCorr • Using a dynamically updated range based on prior time-series data	Model free methods are generally not reported in real-time fMRI analysis, although examples exist (Esposito et al., 2003).	ICA is generally time-consuming and requires (without some form of regularisation) full datasets in order to generate useful noise components. This is a technical challenge for real-time implementation.	ICA-based methods for real-time denoising are generally not recommended unless new algorithms are developed with accompanying evidence that suggests otherwise
11. Offline quality checking			
This offline step serves to report features of the data that can be (often visually) inspected and compared to thresholds in order to assess the overall quality of spatial and time-series aspects of whole brain datasets. Useful tools and metrics include: • MRIQC • QAP • Framewise displacement • DVARS • Timeseries plots	For real-time fMRI, offline quality checking steps are not standardised and hardly reported. A minority of studies investigate possible correlations between physiology or motion traces and the neurofeedback regulation paradigm.	There would essentially be no difference between standard tools and metrics for offline quality control of full datasets and post-hoc real-time datasets, as long as it is done on data as exported from the scanner in a standard way, since real-time exported data might contain differences.	Offline data quality checking and reporting is always recommended, especially with regards to sources of variance that could not sufficiently be corrected for in real-time but could still skew the neurofeedback learning outcomes. Examples include: • Reporting correlations between head movement parameters and the neurofeedback regulation paradigm • Reporting correlations between physiology traces (and derived RETROICOR regressors) and the neurofeedback regulation paradigm • Implementing physiological noise correction in post-hoc analyses

Appendix A

Appendix B

COBIDAS-inspired reporting template for processing and quality control steps in real-time fMRI

B.1 Background

Evidence presented in this thesis suggests a lack of accurate reporting of methods used to calculate the real-time fMRI neurofeedback (rtfMRI-NF) signal. This hinders methods reproducibility and raises concern about the quality of the rtfMRI-NF signal in general. In the field of MRI research, similar concerns have been approached by proposing best practice guidelines for the reporting and sharing of methods and data, with the COBIDAS initiative being the prime example (Nichols et al., 2017). Initial steps have been taken in rtfMRI-NF research to guide overall study method reporting (Ros et al., 2020), although this has not extended to detailed steps in real-time processing of fMRI data.

B.2 Content

Table B.1 in this appendix contains a list of reporting suggestions to improve methods reproducibility in rtfMRI-NF studies, focusing on the real-time processing steps implemented to calculate the neurofeedback signal. Table D.3 (Preprocessing Reporting) of the COBIDAS guidelines was taken as the initial template for the suggestions presented here , with changes made and additional categories added to reflect the different requirements and algorithms for real-time processing. The additional/updated categories are based on a review of commonly implemented and available real-time processing steps (Heunis et al., 2019) and is not fully exhaustive.

B.3 Goal

These suggestions are provided as guidelines to improve methods reporting and reproducibility. The intention is not to prescribe their use. We acknowledge that the included categories might not exhaustively reflect all possible rtfMRI-NF processing options, and encourage community input to expand and improve the content. Ideally, these suggestions would be used in addition to the guidelines provided in Appendix D of the COBIDAS report, and not as a replacement.

Table B.1 — *Categories and reporting suggestions for real-time fMRI neurofeedback processing steps*

Category	Reporting suggestions
General (items apply to all categories)	• Report the space in which each real-time processing is performed (i.e. native volume, native surface, MNI volume, template surface, native structural, other) • Report whether real-time processing steps are executed on the whole brain, within a region of interest (ROI), or on the calculated neurofeedback signal • Report the order in which real-time preprocessing steps were implemented • Provide reasoning if steps were not implemented. • For custom implementations, specify details.
Software (items apply to all categories where software use is reported)	• Software used for real-time processing (e.g. Turbo BrainVoyager, AFNI, SPM + MATLAB, OpenNFT, BART, FRIEND, BioImage Suite, Other, Custom) • Software used for offline processing (with clear distinction from real-time processing) • Indicate when default settings for the implemented software were used. • For each software used, be sure to include version number, revision number, URL and Research Resource Identifier • For custom software/scripts, provide dependencies and link to code if possible.
Slice time correction	• YES/NO • Name of software/method • Whether performed after or before motion correction • Reference slice • Interpolation type and order (e.g., 3rd order spline or sinc)
Motion correction	• YES/NO • Name of software/method • Use of non-rigid registration, and if so the type of transformation • Use of real-time motion susceptibility correction (fieldmap-based unwarping), as well as the particular software/method • Reference scan (e.g. a template volume from the pre-real-time scans or the first volume of the real-time session) • Image similarity metric (e.g. normalised correlation, mutual information, etc.) • Interpolation type (e.g., spline, sinc), and whether image transformations are combined to allow a single interpolation • Use of any slice-to-volume registration methods, or integrated with slice time correction • Explanation of software and hardware used in the case of prospective motion correction

Continued on next page

Table B.1 – continued from previous page

Category	Reporting suggestions
Function-structure (inter-subjective) coregistration	• YES/NO • Name of software/method • Type of transformation (rigid, nonlinear) if nonlinear, type of transformation • Cost function (e.g., correlation ratio, mutual information, boundary-based registration, etc.) • Interpolation method (e.g., spline, linear) • Distinguish between coregistration applied pre-real-time (e.g. to support real-time operations like tissue masking) and coregistration done in real-time.
(Gradient) distortion correction	• YES/NO • Specify if implemented as part of real-time acquisition sequence on (as opposed to as a real-time processing step)
Spatial smoothing	• YES/NO • Name of software/method • Size and type of smoothing kernel • Filtering approach, e.g., fixed kernel or iterative smoothing until fixed FWHM
Nuisance regression	• YES/NO • Specify software and GLM algorithm type (e.g. cumulative, windowed, incremental) with applicable parameters (e.g. window length) • If head motion parameters are included, report the expansion basis and order (e.g. 1st temporal derivatives Volterra kernel expansion) • If tissue signals are included, report the tissue type (e.g. whole brain, gray matter, white matter, ventricles), the tissue definition (e.g. a priori seed, automatic segmentation, spatial regression), and signal definition (e.g., mean of voxels, first singular vector, etc.) • Report any other included regressors and how they are calculated
Detrending / drift removal	• YES/NO • Name of software/method (e.g. nuisance regression using a real-time GLM with linear and/or cosine basis set regressors; exponential moving average filter; custom filter) • If nuisance regression is used, specify the order of regressors and/or cutoff frequency • If nuisance regression is used, specify GLM type (cumulative, windowed, incremental) with applicable parameters (e.g. window length)

Continued on next page

Table B.1 – continued from previous page

Category	Reporting suggestions
Physiological noise removal	• YES/NO • Name of software/method • If differential regions of interest are used (e.g. to cancel global effects of respiration) specify ROI definition and how the difference is calculated per time step. • If respiratory and heart rate information are included in real-time nuisance regression with a GLM, report the modeling choices (e.g. RETROICOR; cardiac and/or respiratory response functions; partial correlation to compartment signals) and number of computed regressors • If RETROICOR-based nuisance regression is used, specify the software/method for computing the regressors and specify how subject physiology traces are accessed in real-time • Distinguish clearly between real-time physiological noise correction and offline correction and quality checking.
High frequency filtering	• YES/NO • Name of software/method (e.g. modified low-pass Kalman filter as implemented in OpenNFT to remove high frequency spikes related to subject physiology)
Volume censoring (a.k.a "scrubbing" or "despiking")	• YES/NO • Name of software/method • Criteria for censoring (e.g. real-time framewise displacement threshold, DVARS threshold, percentage BOLD change threshold, or standardised voxel intensity threshold) • Use of censoring (e.g. temporal censoring regressor in real-time GLM) or interpolation; if interpolation, method used (e.g., spline, spectral estimation)
Serial correlations	• YES/NO • Name of software/method (e.g. a first-order autoregressive model AR(1) as implemented in OpenNFT)
Temporal averaging	• YES/NO • Name of software/method (e.g. a 5-point moving windowed average applied to the neurofeedback signal)

Continued on next page

Table B.1 – continued from previous page

Category	Reporting suggestions
Intensity normalisation / scaling	• YES/NO • Name of software/method • Scaling factor description (e.g. z-score normalisation per voxel using the past n volumes; whole-brain intensity scaling to a mean image intensity of constant k; voxel efficiency scaling to avoid undesired noise weighting in direct averaging of all voxels within the neurofeedback ROI; scaling of the neurofeedback signal to prevent sudden changes in visual feedback display) • Where applicable, provide equations for the scaling of each time step of the volume/ROI/signal
Real-time data quality control	• YES/NO • Name of method (e.g. head motion parameter or physiology trace feedback to subject; real-time display of quality control measures like tSNR to researcher; adaptive acquisition and processing paradigms) • Name of software (e.g. AFNI, FIRMM, rtQC, BART, other, custom) • Where applicable, provide equations and code for calculating the displayed or monitored parameters
Offline data quality control	• YES/NO • Name of method/software to check similarity between real-time and offline exported versions of the neurofeedback session data • Name of method/software to calculate general image quality metrics on neurofeedback session data • Report if offline physiological noise correction was applied in the assessment of subject-specific neurofeedback training effects • Report if motion parameters or other physiological signals were used post-hoc to test as confounds for differences between neurofeedback training groups, or to test for similarities with the task or other fluctuations

Appendix B

Appendix C

Functional quality metrics for the rt-me-fMRI dataset

C.1 Context

This section contains a table with all functional quality metrics of the full *rt-me-fMRI* dataset described in Chapter 7. These metrics were generated by the *fmrwhy_workflow_qc* workflow of the *fMRwhy* software toolbox (see Chapter 6). Metrics include, per functional run:

- Participant number
- Run name
- Mean framewise displacement
- Total framewise displacement
- Framewise displacement outliers (based on a conservative 0.2 mm threshold)
- Framewise displacement outliers (based on a liberal 0.5 mm threshold)
- Mean statistical Z-score
- Temporal signal-to-noise ratio (grey matter)
- Temporal signal-to-noise ratio (white matter)
- Temporal signal-to-noise ratio (cerebrospinal fluid)
- Temporal signal-to-noise ratio (whole brain)

These metrics, summarised in Table C.1 [1] allow possible data users to inspect the quality of the data and to set personalised thresholds for inclusion or exclusion criteria.

[1] Online version: `https://github.com/jsheunis/rt-me-fMRI/blob/master/data/sub-all_task-all_desc-allQCmetrics.tsv`

Table C.1 — *The functional quality metrics of all participants and all runs of the rt-me-fMRI dataset*

Participant	Task	Mean FD	Total FD	FD outliers 0.2mm	FD outliers 0.5mm	Mean Z-score	tSNR (GM)	tSNR (WM)	tSNR (CSF)	tSNR (brain)
sub-001	rest_run-1	0.16	33.22	43	0	0.79	80.44	100.63	32.44	75.13
sub-001	fingerTapping	0.14	29.71	22	0	0.76	87.75	108.04	36.51	81.85
sub-001	emotionProcessing	0.13	27.44	21	0	0.76	89.16	110.19	37.87	83.45
sub-001	rest_run-2	0.16	34.48	43	0	0.77	84.82	106.57	34.35	79.50
sub-001	fingerTappingImagined	0.13	27.39	11	0	0.76	91.05	111.39	38.54	84.88
sub-001	emotionProcessingImagined	0.15	31.08	27	0	0.76	87.59	107.41	36.92	81.58
sub-002	rest_run-1	0.11	22.87	10	1	0.78	76.38	92.39	33.51	71.81
sub-002	fingerTapping	0.11	23.87	21	2	0.76	82.25	101.00	36.08	77.73
sub-002	emotionProcessing	0.11	22.63	16	2	0.76	85.42	102.62	37.93	80.28
sub-002	rest_run-2	0.14	28.81	25	3	0.76	69.03	89.23	29.09	66.25
sub-002	fingerTappingImagined	0.08	16.72	1	0	0.75	94.48	106.71	44.50	87.50
sub-002	emotionProcessingImagined	0.11	23.60	5	0	0.74	86.57	104.55	39.12	81.75
sub-003	rest_run-1	0.12	24.25	17	1	0.78	72.33	84.46	30.61	66.46
sub-003	fingerTapping	0.10	21.59	5	0	0.76	80.22	92.25	35.40	73.70
sub-003	emotionProcessing	0.10	20.93	5	1	0.76	84.57	94.64	38.21	77.23
sub-003	rest_run-2	0.10	21.87	11	0	0.76	78.09	91.01	34.34	72.01
sub-003	fingerTappingImagined	0.11	22.22	12	0	0.76	82.35	93.56	36.90	75.43
sub-003	emotionProcessingImagined	0.12	24.48	17	0	0.75	78.17	91.77	34.78	72.52
sub-004	rest_run-1	0.12	25.55	14	0	0.79	85.52	95.45	37.87	77.93
sub-004	fingerTapping	0.16	34.36	50	2	0.77	75.93	91.25	31.88	70.68
sub-004	emotionProcessing	0.11	23.21	12	0	0.77	95.86	104.04	44.13	86.99
sub-004	rest_run-2	0.16	34.19	33	9	0.76	76.09	91.37	31.40	70.67
sub-004	fingerTappingImagined	0.20	41.47	63	9	0.74	68.81	84.76	28.63	64.63
sub-004	emotionProcessingImagined	0.17	36.46	61	5	0.75	78.05	95.85	33.24	73.38
sub-005	rest_run-1	0.11	24.07	5	0	0.79	94.52	103.95	47.41	85.02
sub-005	fingerTapping	0.13	26.68	11	0	0.77	93.85	105.03	46.54	84.76
sub-005	emotionProcessing	0.12	24.56	4	0	0.76	96.66	104.13	49.79	86.89
sub-005	rest_run-2	0.12	25.91	2	0	0.76	97.48	107.72	49.40	88.16

Continued on next page

Table C.1 – continued from previous page

Participant	Task	Mean FD	Total FD	FD outliers 0.2mm	FD outliers 0.5mm	Mean Z-score	tSNR (GM)	tSNR (WM)	tSNR (CSF)	tSNR (brain)
sub-005	fingerTappingImagined	0.13	27.07	7	0	0.75	95.41	105.97	48.04	86.35
sub-005	emotionProcessingImagined	0.12	24.94	1	0	0.75	98.20	108.69	50.01	88.92
sub-006	rest_run-1	0.12	25.31	16	0	0.78	93.73	112.36	38.60	85.41
sub-006	fingerTapping	0.11	23.32	9	0	0.76	100.25	119.62	42.44	91.57
sub-006	emotionProcessing	0.12	24.22	11	0	0.76	107.57	124.96	46.44	97.79
sub-006	rest_run-2	0.12	25.22	10	0	0.76	97.07	120.83	40.86	90.05
sub-006	fingerTappingImagined	0.11	22.47	6	0	0.75	107.99	126.49	47.62	98.67
sub-006	emotionProcessingImagined	0.10	21.21	5	0	0.75	105.49	126.43	46.48	97.10
sub-007	rest_run-1	0.21	44.13	103	1	0.78	78.38	96.65	31.69	71.08
sub-007	fingerTapping	0.18	38.35	79	0	0.78	84.86	103.12	34.50	76.59
sub-007	emotionProcessing	0.16	33.22	48	0	0.78	90.42	105.06	37.73	80.55
sub-007	rest_run-2	0.25	52.80	134	8	0.77	75.35	95.11	30.23	68.87
sub-007	fingerTappingImagined	0.16	33.80	48	2	0.77	85.67	102.32	35.11	76.91
sub-007	emotionProcessingImagined	0.22	46.50	98	6	0.76	77.88	97.67	30.83	70.96
sub-010	rest_run-1	0.29	59.87	130	23	0.77	47.88	68.61	16.79	47.73
sub-010	fingerTapping	0.23	49.18	94	12	0.76	50.43	71.74	17.81	50.22
sub-010	emotionProcessing	0.32	66.89	114	30	0.75	42.24	63.07	14.09	42.76
sub-010	rest_run-2	0.27	57.14	125	15	0.76	50.64	72.99	17.39	50.53
sub-010	fingerTappingImagined	0.16	34.37	46	2	0.76	67.20	88.96	24.26	65.14
sub-010	emotionProcessingImagined	0.41	85.75	157	51	0.75	42.73	62.08	14.24	42.81
sub-011	rest_run-1	0.14	29.63	30	0	0.78	93.33	106.14	45.41	84.64
sub-011	fingerTapping	0.11	22.48	22	1	0.78	88.59	102.76	42.00	80.60
sub-011	emotionProcessing	0.11	22.82	14	0	0.74	90.91	105.69	44.24	83.24
sub-011	rest_run-2	0.19	39.50	86	0	0.73	87.09	104.50	39.71	79.96
sub-011	fingerTappingImagined	0.13	27.33	27	4	0.72	76.02	96.44	34.51	71.18
sub-011	emotionProcessingImagined	0.14	29.54	35	2	0.72	73.76	90.59	33.73	68.38
sub-012	rest_run-1	0.18	37.65	61	1	0.78	75.35	98.17	31.39	71.67
sub-012	fingerTapping	0.15	31.77	36	1	0.75	87.19	109.33	37.85	82.20
sub-012	emotionProcessing	0.15	30.57	30	0	0.76	80.84	100.99	34.42	75.79

Continued on next page

Table C.1 – continued from previous page

Participant	Task	Mean FD	Total FD	FD outliers 0.2mm	FD outliers 0.5mm	Mean Z-score	tSNR (GM)	tSNR (WM)	tSNR (CSF)	tSNR (brain)
sub-012	rest_run-2	0.19	40.67	80	3	0.75	75.29	101.28	30.61	72.51
sub-012	fingerTappingImagined	0.14	29.51	27	1	0.74	85.11	108.04	37.02	80.65
sub-012	emotionProcessingImagined	0.15	30.55	31	0	0.75	90.43	113.47	39.44	85.31
sub-013	rest_run-1	0.10	20.34	0	0	0.79	89.42	102.42	41.08	82.22
sub-013	fingerTapping	0.14	28.90	30	0	0.77	82.76	99.79	36.49	77.19
sub-013	emotionProcessing	0.09	19.68	1	0	0.76	92.82	107.64	43.68	86.09
sub-013	rest_run-2	0.20	41.03	95	4	0.76	77.49	96.17	33.51	72.97
sub-013	fingerTappingImagined	0.10	20.64	5	0	0.76	92.02	108.66	42.92	85.82
sub-013	emotionProcessingImagined	0.10	20.90	4	0	0.76	85.26	100.50	38.39	79.10
sub-015	rest_run-1	0.12	25.61	26	2	0.78	92.19	105.30	54.47	86.24
sub-015	fingerTapping	0.11	23.38	13	0	0.77	98.69	110.52	59.78	92.13
sub-015	emotionProcessing	0.12	24.22	20	0	0.75	105.84	117.28	66.27	99.02
sub-015	rest_run-2	0.11	23.81	12	0	0.75	93.94	110.76	55.67	88.97
sub-015	fingerTappingImagined	0.10	21.86	12	0	0.75	103.37	112.57	63.54	95.86
sub-015	emotionProcessingImagined	0.11	22.70	14	0	0.75	104.76	114.48	63.68	97.08
sub-016	rest_run-1	0.10	20.98	4	0	0.78	85.82	102.10	39.66	79.19
sub-016	fingerTapping	0.10	21.34	6	0	0.76	92.80	107.62	42.65	84.87
sub-016	emotionProcessing	0.11	22.09	9	2	0.77	83.36	99.55	37.79	76.85
sub-016	rest_run-2	0.13	26.97	18	2	0.75	81.69	101.65	35.71	76.18
sub-016	fingerTappingImagined	0.15	32.46	38	9	0.75	75.76	95.55	33.16	71.00
sub-016	emotionProcessingImagined	0.12	24.92	23	1	0.76	81.76	100.42	36.85	76.11
sub-017	rest_run-1	0.12	26.01	12	0	0.79	83.66	101.42	35.93	80.78
sub-017	fingerTapping	0.14	29.54	32	0	0.77	82.38	101.38	33.83	79.72
sub-017	emotionProcessing	0.14	29.47	35	1	0.78	85.87	101.94	35.40	82.03
sub-017	rest_run-2	0.15	30.81	19	0	0.76	88.96	107.24	38.41	85.76
sub-017	fingerTappingImagined	0.11	22.94	11	1	0.76	88.30	104.85	36.85	84.41
sub-017	emotionProcessingImagined	0.14	29.70	33	1	0.77	77.79	98.84	31.78	76.16
sub-018	rest_run-1	0.16	32.76	43	1	0.78	89.73	112.21	33.45	82.89
sub-018	fingerTapping	0.14	28.96	34	0	0.76	90.88	116.42	35.54	85.03

Continued on next page

Table C.1 – continued from previous page

Participant	Task	Mean FD	Total FD	FD outliers 0.2mm	FD outliers 0.5mm	Mean Z-score	tSNR (GM)	tSNR (WM)	tSNR (CSF)	tSNR (brain)
sub-018	emotionProcessing	0.14	28.52	33	0	0.76	97.42	120.34	38.90	90.33
sub-018	rest_run-2	0.14	29.91	35	0	0.76	89.93	117.11	33.93	84.46
sub-018	fingerTappingImagined	0.14	29.66	34	1	0.76	88.84	116.80	33.47	83.70
sub-018	emotionProcessingImagined	0.13	26.32	18	0	0.76	96.10	123.47	38.42	90.33
sub-019	rest_run-1	0.16	32.60	49	0	0.78	83.76	100.30	35.27	78.06
sub-019	fingerTapping	0.14	29.43	37	0	0.76	85.72	103.31	36.44	80.20
sub-019	emotionProcessing	0.12	25.98	15	0	0.77	86.71	103.48	37.18	80.84
sub-019	rest_run-2	0.13	28.22	29	0	0.75	90.07	110.72	39.48	85.13
sub-019	fingerTappingImagined	0.12	25.46	14	0	0.75	89.78	110.24	38.91	84.72
sub-019	emotionProcessingImagined	0.13	26.98	14	0	0.75	90.71	110.22	39.57	85.37
sub-020	rest_run-1	0.16	34.40	48	0	0.78	89.09	113.76	40.69	84.30
sub-020	fingerTapping	0.17	35.13	33	3	0.75	86.87	112.56	39.55	82.58
sub-020	emotionProcessing	0.14	29.71	37	0	0.75	97.28	119.35	45.62	91.16
sub-020	rest_run-2	0.20	42.42	74	4	0.75	78.71	107.12	35.58	76.02
sub-020	fingerTappingImagined	0.16	34.10	37	6	0.74	91.78	117.27	43.05	87.29
sub-020	emotionProcessingImagined	0.16	32.76	46	1	0.74	86.58	112.45	40.94	82.88
sub-021	rest_run-1	0.26	54.95	88	21	0.77	62.24	90.37	22.33	61.71
sub-021	fingerTapping	0.31	65.41	95	21	0.75	59.72	89.72	21.56	60.12
sub-021	emotionProcessing	0.21	43.20	70	11	0.75	75.80	105.27	29.27	74.36
sub-021	rest_run-2	0.34	71.86	109	33	0.74	57.64	86.26	20.41	57.91
sub-021	fingerTappingImagined	0.33	70.20	118	29	0.73	67.11	97.52	24.20	66.73
sub-021	emotionProcessingImagined	0.53	112.02	163	59	0.74	48.30	75.13	16.67	49.25
sub-022	rest_run-1	0.12	25.73	7	0	0.79	93.13	106.96	37.22	85.35
sub-022	fingerTapping	0.16	32.82	37	0	0.75	90.15	108.32	36.02	84.09
sub-022	emotionProcessing	0.16	32.96	46	1	0.75	89.98	108.16	35.25	83.71
sub-022	rest_run-2	0.12	26.13	14	0	0.75	94.70	113.06	38.33	88.15
sub-022	fingerTappingImagined	0.14	29.06	15	0	0.74	97.16	113.93	39.22	89.86
sub-022	emotionProcessingImagined	0.13	27.48	24	3	0.74	91.83	110.84	36.04	85.56
sub-023	rest_run-1	0.12	24.98	6	0	0.79	92.33	109.22	44.55	85.78

Continued on next page

Table C.1 – continued from previous page

Participant	Task	Mean FD	Total FD	FD outliers 0.2mm	FD outliers 0.5mm	Mean Z-score	tSNR (GM)	tSNR (WM)	tSNR (CSF)	tSNR (brain)
sub-023	fingerTapping	0.12	24.70	11	0	0.76	91.37	109.24	43.27	85.02
sub-023	emotionProcessing	0.10	20.64	4	0	0.77	97.34	113.45	47.32	90.08
sub-023	rest_run-2	0.16	33.59	47	4	0.76	82.11	101.72	37.96	77.28
sub-023	fingerTappingImagined	0.10	21.64	3	0	0.76	91.93	110.46	44.26	85.88
sub-023	emotionProcessingImagined	0.12	24.48	10	0	0.75	93.30	110.09	45.39	86.82
sub-024	rest_run-1	0.12	25.34	7	0	0.78	78.13	98.94	37.07	73.74
sub-024	fingerTapping	0.14	29.07	24	0	0.76	81.63	106.54	38.15	77.77
sub-024	emotionProcessing	0.13	27.59	19	0	0.76	83.22	106.07	39.63	78.83
sub-024	rest_run-2	0.15	30.59	37	0	0.76	81.40	107.04	37.76	77.77
sub-024	fingerTappingImagined	0.13	28.10	19	0	0.76	83.85	107.91	39.65	79.65
sub-024	emotionProcessingImagined	0.17	35.27	55	2	0.76	75.41	102.32	34.85	72.86
sub-025	rest_run-1	0.09	19.74	3	0	0.79	90.56	108.54	38.12	83.40
sub-025	fingerTapping	0.11	24.10	12	0	0.76	85.02	107.82	34.71	79.86
sub-025	emotionProcessing	0.09	18.63	6	0	0.76	96.09	111.92	41.52	87.92
sub-025	rest_run-2	0.12	24.43	11	0	0.76	82.12	104.68	33.59	77.26
sub-025	fingerTappingImagined	0.11	23.12	11	0	0.76	87.24	108.15	36.46	81.43
sub-025	emotionProcessingImagined	0.10	21.80	4	0	0.76	83.22	105.71	34.60	78.36
sub-026	rest_run-1	0.14	30.09	28	0	0.78	94.62	104.59	47.91	84.66
sub-026	fingerTapping	0.17	35.42	50	1	0.77	85.15	100.39	40.49	77.19
sub-026	emotionProcessing	0.16	34.22	35	3	0.76	94.40	108.29	46.18	85.17
sub-026	rest_run-2	0.21	43.14	79	7	0.75	91.40	108.31	44.58	83.41
sub-026	fingerTappingImagined	0.15	31.35	30	1	0.76	98.43	111.74	49.41	88.88
sub-026	emotionProcessingImagined	0.17	34.76	51	2	0.75	98.81	111.99	49.29	89.07
sub-027	rest_run-1	0.22	46.36	108	3	0.78	74.42	93.82	31.40	70.39
sub-027	fingerTapping	0.20	41.02	80	3	0.76	76.77	99.19	32.99	73.68
sub-027	emotionProcessing	0.14	30.10	38	1	0.76	87.27	109.28	39.78	83.24
sub-027	rest_run-2	0.14	29.73	26	4	0.76	76.54	100.37	33.26	74.01
sub-027	fingerTappingImagined	0.11	22.81	11	1	0.75	88.02	110.49	40.56	84.14
sub-027	emotionProcessingImagined	0.11	22.28	14	0	0.74	86.20	109.22	39.47	82.69

Continued on next page

Table C.1 – continued from previous page

Participant	Task	Mean FD	Total FD	FD outliers 0.2mm	FD outliers 0.5mm	Mean Z-score	tSNR (GM)	tSNR (WM)	tSNR (CSF)	tSNR (brain)
sub-029	rest_run-1	0.10	21.12	5	0	0.78	86.45	96.73	43.01	79.05
sub-029	fingerTapping	0.12	25.29	19	1	0.76	80.51	94.45	38.72	74.55
sub-029	emotionProcessing	0.19	39.14	84	2	0.75	76.97	91.56	35.33	71.25
sub-029	rest_run-2	0.14	29.65	42	0	0.75	79.48	94.54	36.74	73.62
sub-029	fingerTappingImagined	0.12	24.57	17	1	0.75	79.92	91.89	36.87	73.10
sub-029	emotionProcessingImagined	0.12	25.40	18	1	0.75	85.17	98.06	41.06	78.39
sub-030	rest_run-1	0.13	26.91	14	0	0.77	96.53	112.29	44.63	85.74
sub-030	fingerTapping	0.13	27.33	23	0	0.77	94.84	110.70	44.63	84.55
sub-030	emotionProcessing	0.11	22.61	4	0	0.76	100.91	115.16	49.60	90.15
sub-030	rest_run-2	0.13	26.89	27	0	0.76	91.91	110.12	43.89	82.79
sub-030	fingerTappingImagined	0.11	23.48	9	0	0.76	97.18	113.41	46.31	86.82
sub-030	emotionProcessingImagined	0.11	22.36	9	0	0.76	95.78	111.85	46.37	85.78
sub-031	rest_run-1	0.13	26.66	8	0	0.78	81.66	97.36	34.63	76.59
sub-031	fingerTapping	0.17	35.50	41	4	0.78	71.22	91.19	29.47	68.33
sub-031	emotionProcessing	0.12	24.50	10	1	0.77	79.66	95.78	33.89	74.95
sub-031	rest_run-2	0.13	27.10	24	0	0.77	79.46	96.99	34.09	75.20
sub-031	fingerTappingImagined	0.12	24.61	11	2	0.76	83.37	99.12	36.47	78.37
sub-031	emotionProcessingImagined	0.16	33.89	41	6	0.76	69.40	89.08	28.20	66.56
sub-032	rest_run-1	0.10	20.19	10	0	0.78	90.83	111.03	43.26	84.50
sub-032	fingerTapping	0.09	17.93	3	0	0.77	93.72	112.87	45.61	87.20
sub-032	emotionProcessing	0.10	20.03	13	1	0.76	95.59	113.67	46.82	88.65
sub-032	rest_run-2	0.10	20.56	2	0	0.76	88.71	112.12	42.16	83.60
sub-032	fingerTappingImagined	0.11	22.53	13	6	0.76	90.07	112.71	41.23	84.23
sub-032	emotionProcessingImagined	0.13	27.30	23	8	0.75	86.88	110.35	39.13	81.51

Appendix C

Appendix D

Mathematical background on weighting, summation and averaging

D.1 Context

Multi-echo fMRI combination via weighted summation is a critical step in multi-echo post-processing that has been reported to increase temporal signal-to-noise ratio, decrease signal drop-out, and improve activation extent for task-analysis. The mathematics of all widely used multi-echo combination schemes are based on the underlying concepts of data weighting, summation and averaging. In this section we provide the basic mathematical equations to describe the underlying assumptions for echo combination schemes.

D.2 Weighting, summation and averaging

Say we have a dataset $\{x_1, x_2, \ldots, x_n\}$ with elements x_i, and the dataset has corresponding weights $\{w_1, w_2, \ldots, w_n\}$ with elements w_i.
The notation for the dataset *summation* is given by:

$$\sum_{i=i}^{n} x_i = x_1 + x_2 + \cdots + x_{n-1} + x_n \tag{D.1}$$

The *weighted summation* is calculated as the summation of the dataset after multiplying each element with its corresponding weight, thus:

$$\sum_{i=i}^{n} x_i w_i = x_1 w_1 + x_2 w_2 + \cdots + x_{n-1} w_{n-1} + x_n w_n \tag{D.2}$$

The *weighted average* or *mean* of the dataset is calculated by dividing the weighted summation by the sum of weights:

$$\bar{x}_w = \frac{\sum_{i=1}^{n} w_i x_i}{\sum_{i=1}^{n} w_i} = \frac{w_1 x_1 + w_2 x_2 + \cdots + w_n x_n}{w_1 + w_2 + \cdots + w_n} \tag{D.3}$$

A special case occurs when the weights are normalised (indicated by w_i') such that the sum of weights is equal to 1. Weights are normalised by dividing each weight element by the sum of weights, i.e.:

$$w'_i = \frac{w_i}{\sum_{j=1}^{n} w_j} \tag{D.4}$$

And hence:

$$\sum_{i=1}^{n} w'_i = 1 \tag{D.5}$$

Calculating the *weighted average of the dataset using normalised weights*, we then get:

$$\bar{x}_{w'} = \frac{\sum_{i=1}^{n} w'_i x_i}{\sum_{i=1}^{n} w'_i} = \sum_{i=1}^{n} w'_i x_i \tag{D.6}$$

since the denominator, the sum of weights, is equal to 1.
It therefore follows that the *weighted average* of a dataset using ordinary non-normalised weights is equal to the *weighted summation* of the dataset when using *normalised weights*.

Bibliography

Alegria, A. A., M. Wulff, H. Brinson, G. J. Barker, L. J. Norman, D. Brandeis, D. Stahl, A. S. David, E. Taylor, V. Giampietro, and K. Rubia (June 2017). "Real-time fMRI neurofeedback in adolescents with attention deficit hyperactivity disorder". en. In: *Human Brain Mapping* 38.6, pp. 3190–3209. ISSN: 1097-0193.

Alkoby, O., A. Abu-Rmileh, O. Shriki, and D. Todder (May 2018). "Can We Predict Who Will Respond to Neurofeedback? A Review of the Inefficacy Problem and Existing Predictors for Successful EEG Neurofeedback Learning". en. In: *Neuroscience*. Neurofeedback and Functional Enhancement: Mechanisms, Methodology, Behavioral and Clinical Applications 378, pp. 155–164. ISSN: 0306-4522.

Allen, M., D. Poggiali, K. Whitaker, T. R. Marshall, and R. A. Kievit (Apr. 2019). "Raincloud plots: a multi-platform tool for robust data visualization". en. In: *Wellcome Open Research* 4, p. 63. ISSN: 2398-502X.

Andersson, P., J. P. W. Pluim, J. C. W. Siero, S. Klein, M. A. Viergever, and N. F. Ramsey (Nov. 2011). "Real-Time Decoding of Brain Responses to Visuospatial Attention Using 7T fMRI". en. In: *PLOS ONE* 6.11, e27638. ISSN: 1932-6203.

Ashburner, J. and K. J. Friston (July 2005). "Unified segmentation". en. In: *NeuroImage* 26.3, pp. 839–851. ISSN: 1053-8119.

Bagarinao, E, K Matsuo, T Nakai, and S Sato (June 2003). "Estimation of general linear model coefficients for real-time application". In: *NeuroImage* 19.2, pp. 422–429. ISSN: 1053-8119.

Bagarinao, E., T. Nakai, and Y. Tanaka (Oct. 2006). "Real-time functional MRI: development and emerging applications". eng. In: *Magnetic resonance in medical sciences: MRMS: an official journal of Japan Society of Magnetic Resonance in Medicine* 5.3, pp. 157–165. ISSN: 1347-3182.

Balteau, E., C. Hutton, and N. Weiskopf (Jan. 2010). "Improved shimming for fMRI specifically optimizing the local BOLD sensitivity". In: *Neuroimage* 49.1, pp. 327–336. ISSN: 1053-8119.

Bandettini, P. A., E. C. Wong, R. S. Hinks, R. S. Tikofsky, and J. S. Hyde (June 1992). "Time course EPI of human brain function during task activation". en. In: *Magnetic Resonance in Medicine* 25.2, pp. 390–397. ISSN: 07403194, 15222594.

Bannier, E., G. Barker, V. Borghesani, N. Broeckx, P. Clement, K. E. Emblem, S. Ghosh, E. Glerean, K. J. Gorgolewski, M. Havu, Y. O. Halchenko, P. Herholz, A. Hespel, S. Heunis, Y. Hu, C.-P. Hu, D. Huijser, M. d. l. I. Vayá, R. Jancalek, V. K. Katsaros, M.-L. Kieseler, C. Maumet, C. A. Moreau, H.-J. Mutsaerts, R. Oostenveld, E. Ozturk-Isik, N. P. L. Espinosa, J. Pellman, C. R. Pernet, F. B. Pizzini, A. Trbalić, P.-J. Toussaint, M. V. d. O. Castello, F. Wang, C. Wang, and H. Zhu (2017). "The Open Brain Consent: Informing research participants and obtaining consent to share brain imaging data". en. In: *Human Brain Mapping* Editorial. ISSN: 1097-0193.

Basilio, R., G. J. Garrido, J. R. Sato, S. Hoefle, B. R. P. Melo, F. A. Pamplona, R. Zahn, and J. Moll (Jan. 2015). "FRIEND Engine Framework: a real time neurofeedback client-server system for neuroimaging studies". In: *Frontiers in Behavioral Neuroscience* 9. ISSN: 1662-5153.

Beckmann, C. F., M. DeLuca, J. T. Devlin, and S. M. Smith (May 2005). "Investigations into resting-state connectivity using independent component analysis". en. In: *Philosophical Transactions of the Royal Society B: Biological Sciences* 360.1457, pp. 1001–1013. ISSN: 0962-8436, 1471-2970.

Behzadi, Y., K. Restom, J. Liau, and T. T. Liu (Aug. 2007). "A Component Based Noise Correction Method (CompCor) for BOLD and Perfusion Based fMRI". In: *NeuroImage* 37.1, pp. 90–101. ISSN: 1053-8119.

Beissner, F., S. Baudrexel, S. Volz, and R. Deichmann (Aug. 2010). "Dual-echo EPI for non-equilibrium fMRI — Implications of different echo combinations and masking procedures". In: *NeuroImage* 52.2, pp. 524–531. ISSN: 1053-8119.

Bellgowan, P. S. F., P. A. Bandettini, P. van Gelderen, A. Martin, and J. Bodurka (Feb. 2006). "Improved BOLD detection in the medial temporal region using parallel imaging and voxel volume reduction". In: *NeuroImage* 29.4, pp. 1244–1251. ISSN: 1053-8119.

Besseling, R. M., J. F. Jansen, G. M. Overvliet, S. J. van der Kruijs, J. S. Vles, S. C. Ebus, P. A. Hofman, A. d. Louw, A. P. Aldenkamp, and W. H. Backes (2013). "Reduced functional integration of the sensorimotor and language network in rolandic epilepsy". en. In: *NeuroImage: Clinical* 2, pp. 239–246. ISSN: 22131582.

Binder, J. R. (Feb. 2011). "Functional MRI is a valid noninvasive alternative to Wada testing". en. In: *Epilepsy & Behavior* 20.2, pp. 214–222. ISSN: 15255050.

Birn, R. M., J. B. Diamond, M. A. Smith, and P. A. Bandettini (July 2006). "Separating respiratory-variation-related fluctuations from neuronal-activity-related fluctuations in fMRI". In: *NeuroImage* 31.4, pp. 1536–1548. ISSN: 1053-8119.

Birn, R. M., M. A. Smith, T. B. Jones, and P. A. Bandettini (Apr. 2008). "The respiration response function: The temporal dynamics of fMRI signal fluctuations related to changes in respiration". en. In: *NeuroImage* 40.2, pp. 644–654. ISSN: 1053-8119.

Bodurka, J., J. Gonzales-Castillo, and P. Bandettini (July 2009). "The Use of Neurofeedback with Real-Time Functional MRI to Suppress Physiological Noise." en. In: *NeuroImage* 47, S194. ISSN: 10538119.

Bodurka, J., F. Ye, N. Petridou, K. Murphy, and P. Bandettini (Jan. 2007). "Mapping the MRI Voxel Volume in Which Thermal Noise Matches Physiological Noise-Implications for fMRI." In: *NeuroImage* 34.2, pp. 542–549. ISSN: 1053-8119.

Bollmann, S., L. Kasper, S. J. Vannesjo, A. O. Diaconescu, B. E. Dietrich, S. Gross, K. E. Stephan, and K. P. Pruessmann (July 2017). "Analysis and correction of field fluctuations in fMRI data using field monitoring". In: *NeuroImage*. Cleaning up the fMRI time series: Mitigating noise with advanced acquisition and correction strategies 154, pp. 92–105. ISSN: 1053-8119.

Boubela, R. N., K. Kalcher, W. Huf, E.-M. Seidel, B. Derntl, L. Pezawas, C. Našel, and E. Moser (May 2015). "fMRI measurements of amygdala activation are confounded by stimulus correlated signal fluctuation in nearby veins draining distant brain regions". en. In: *Scientific Reports* 5.1. Number: 1 Publisher: Nature Publishing Group, p. 10499. ISSN: 2045-2322.

Bright, M. G. and K. Murphy (Jan. 2013). "Removing motion and physiological artifacts from intrinsic BOLD fluctuations using short echo data". In: *Neuroimage* 64.6, pp. 526–537. ISSN: 1053-8119.

Caballero-Gaudes, C., S. Moia, P. Panwar, P. A. Bandettini, and J. Gonzalez-Castillo (Nov. 2019). "A deconvolution algorithm for multi-echo functional MRI: Multi-echo Sparse Paradigm Free Mapping". en. In: *NeuroImage* 202, p. 116081. ISSN: 1053-8119.

Caballero-Gaudes, C. and R. C. Reynolds (July 2017). "Methods for cleaning the BOLD fMRI signal". In: *NeuroImage*. Cleaning up the fMRI time series: Mitigating noise with advanced acquisition and correction strategies 154, pp. 128–149. ISSN: 1053-8119.

Canterberry, M., C. A. Hanlon, K. J. Hartwell, X. Li, M. Owens, T. LeMatty, J. J. Prisciandaro, J. Borckardt, M. E. Saladin, K. T. Brady, and M. S. George (Dec. 2013). "Sustained Reduction of Nicotine Craving With Real-Time Neurofeedback: Exploring the Role of Severity of Dependence". en. In: *Nicotine & Tobacco Research* 15.12, pp. 2120–2124. ISSN: 1462-2203.

Caria, A., R. Sitaram, and N. Birbaumer (Oct. 2012). "Real-Time fMRI: A Tool for Local Brain Regulation". en. In: *The Neuroscientist* 18.5, pp. 487–501. ISSN: 1073-8584.

Chang, C., J. P. Cunningham, and G. H. Glover (Feb. 2009). "Influence of heart rate on the BOLD signal: The cardiac response function". In: *NeuroImage* 44.3, pp. 857–869. ISSN: 1053-8119.

Christopher deCharms, R. (Sept. 2008). "Applications of real-time fMRI". en. In: *Nature Reviews Neuroscience* 9.9, pp. 720–729. ISSN: 1471-003X, 1471-0048.

Clare, S., S. Francis, P. G. Morris, and R. Bowtell (2001). "Single-shot T measurement to establish optimum echo time for fMRI: Studies of the visual, motor, and auditory cortices at 3.0 T". en. In: *Magnetic Resonance in Medicine* 45.5, pp. 930–933. ISSN: 1522-2594.

Cohen, J. D., N. Daw, B. Engelhardt, U. Hasson, K. Li, Y. Niv, K. A. Norman, J. Pillow, P. J. Ramadge, N. B. Turk-Browne, and T. L. Willke (Feb. 2017). "Computational approaches to fMRI analysis". In: *Nature neuroscience* 20.3, pp. 304–313. ISSN: 1097-6256.

Cohen, M. S. (Oct. 2001). "Real-Time Functional Magnetic Resonance Imaging". en. In: *Methods* 25.2, pp. 201–220. ISSN: 10462023.

Collins, D. L., P. Neelin, T. M. Peters, and A. C. Evans (Mar. 1994). "Automatic 3D Intersubject Registration of MR Volumetric Data in Standardized Talairach Space:" en. In: *Journal of Computer Assisted Tomography* 18.2, pp. 192–205. ISSN: 0363-8715.

Cox, R. W. (June 1996). "AFNI: software for analysis and visualization of functional magnetic resonance neuroimages". eng. In: *Computers and Biomedical Research, an International Journal* 29.3, pp. 162–173. ISSN: 0010-4809.

Cox, R. W. and A. Jesmanowicz (1999). "Real-time 3D image registration for functional MRI". en. In: *Magnetic Resonance in Medicine* 42.6, pp. 1014–1018. ISSN: 1522-2594.

Cox, R. W., A. Jesmanowicz, and J. S. Hyde (Feb. 1995). "Real-Time Functional Magnetic Resonance Imaging". en. In: *Magnetic Resonance in Medicine* 33.2, pp. 230–236. ISSN: 07403194, 15222594.

Decharms, R. C. (2012). In: *Proceedings of the Real-time Functional Imaging and Neurofeedback Conference. Switzerland*.

deCharms, R. C. (Nov. 2007). "Reading and controlling human brain activation using real-time functional magnetic resonance imaging". en. In: *Trends in Cognitive Sciences* 11.11, pp. 473–481. ISSN: 13646613.

deCharms, R. C., K. Christoff, G. H. Glover, J. M. Pauly, S. Whitfield, and J. D. E. Gabrieli (Jan. 2004). "Learned regulation of spatially localized brain activation using real-time fMRI". In: *NeuroImage* 21.1, pp. 436–443. ISSN: 1053-8119.

deCharms, R. C., F. Maeda, G. H. Glover, D. Ludlow, J. M. Pauly, D. Soneji, J. D. E. Gabrieli, and S. C. Mackey (Dec. 2005). "Control over brain activation and pain learned by using real-time functional MRI". en. In: *Proceedings of the National Academy of Sciences* 102.51, pp. 18626–18631. ISSN: 0027-8424, 1091-6490.

Deichmann, R., O. Josephs, C. Hutton, D. R. Corfield, and R. Turner (Jan. 2002). "Compensation of Susceptibility-Induced BOLD Sensitivity Losses in Echo-Planar fMRI Imaging". In: *NeuroImage* 15.1, pp. 120–135. ISSN: 1053-8119.

Devlin, J. T., R. P. Russell, M. H. Davis, C. J. Price, J. Wilson, H. E. Moss, P. M. Matthews, and L. K. Tyler (June 2000). "Susceptibility-Induced Loss of Signal: Comparing PET and fMRI on a Semantic Task". en. In: *NeuroImage* 11.6, pp. 589–600. ISSN: 1053-8119.

Di Martino, A., C.-G. Yan, Q. Li, E. Denio, F. X. Castellanos, K. Alaerts, J. S. Anderson, M. Assaf, S. Y. Bookheimer, M. Dapretto, B. Deen, S. Delmonte, I. Dinstein, B. Ertl-Wagner, D. A. Fair, L. Gallagher, D. P. Kennedy, C. L. Keown, C. Keysers, J. E. Lainhart, C. Lord, B. Luna, V. Menon, N. J. Minshew, C. S. Monk, S. Mueller, R.-A. Müller, M. B. Nebel, J. T. Nigg, K. O'Hearn, K. A. Pelphrey, S. J. Peltier, J. D. Rudie, S. Sunaert, M. Thioux, J. M. Tyszka, L. Q. Uddin, J. S. Verhoeven, N. Wenderoth, J. L. Wiggins, S. H. Mostofsky, and M. P. Milham (June 2014). "The autism brain imaging data exchange: towards a large-scale evaluation of the intrinsic brain architecture in autism". eng. In: *Molecular Psychiatry* 19.6, pp. 659–667. ISSN: 1476-5578.

Diedrichsen, J. and R. Shadmehr (Sept. 2005). "Detecting and adjusting for artifacts in fMRI time series data". In: *NeuroImage* 27.3, pp. 624–634. ISSN: 1053-8119.

Dietrich, B. E., D. O. Brunner, B. J. Wilm, C. Barmet, S. Gross, L. Kasper, M. Haeberlin, T. Schmid, S. J. Vannesjo, and K. P. Pruessmann (2016). "A field camera for MR sequence monitoring and system analysis". en. In: *Magnetic Resonance in Medicine* 75.4, pp. 1831–1840. ISSN: 1522-2594.

Dipasquale, O., A. Sethi, M. M. Laganà, F. Baglio, G. Baselli, P. Kundu, N. A. Harrison, and M. Cercignani (2017). "Comparing resting state fMRI de-noising approaches using multi- and single-echo acquisitions". eng. In: *PloS One* 12.3, e0173289. ISSN: 1932-6203.

Dosenbach, N. U. F., J. M. Koller, E. A. Earl, O. Miranda-Dominguez, R. L. Klein, A. N. Van, A. Z. Snyder, B. J. Nagel, J. T. Nigg, A. L. Nguyen, V. Wesevich, D. J. Greene, and D. A. Fair (Nov. 2017). "Real-time motion analytics during brain MRI improve data quality and reduce costs". In: *NeuroImage* 161, pp. 80–93. ISSN: 1053-8119.

DuPre, E., T. Salo, R. Markello, P. Kundu, K. Whitaker, and D. Handwerker (May 2020). *ME-ICA/tedana: 0.0.9a*.

Eickhoff, S. B., K. E. Stephan, H. Mohlberg, C. Grefkes, G. R. Fink, K. Amunts, and K. Zilles (May 2005). "A new SPM toolbox for combining probabilistic cytoarchitectonic maps and functional imaging data". eng. In: *NeuroImage* 25.4, pp. 1325–1335. ISSN: 1053-8119.

Eklund, A., M. Andersson, and H. Knutsson (Feb. 2012). "fMRI analysis on the GPU—Possibilities and challenges". In: *Computer Methods and Programs in Biomedicine* 105.2, pp. 145–161. ISSN: 0169-2607.

Emmert, K., R. Kopel, Y. Koush, R. Maire, P. Senn, D. Van De Ville, and S. Haller (Jan. 2017). "Continuous vs. intermittent neurofeedback to regulate auditory cortex activity of tinnitus patients using real-time fMRI - A pilot study". In: *NeuroImage: Clinical* 14, pp. 97–104. ISSN: 2213-1582.

Emmert, K., R. Kopel, J. Sulzer, A. B. Brühl, B. D. Berman, D. E. J. Linden, S. G. Horovitz, M. Breimhorst, A. Caria, S. Frank, S. Johnston, Z. Long, C. Paret, F. Robineau, R. Veit, A. Bartsch, C. F. Beckmann, D. Van De Ville, and S. Haller (Jan. 2016). "Meta-analysis of real-time fMRI neurofeedback studies using individual participant data: How is brain regulation mediated?" In: *NeuroImage* 124, pp. 806–812. ISSN: 1053-8119.

Esposito, F., E. Seifritz, E. Formisano, R. Morrone, T. Scarabino, G. Tedeschi, S. Cirillo, R. Goebel, and F. Di Salle (Dec. 2003). "Real-time independent component analysis of fMRI time-series". In: *NeuroImage* 20.4, pp. 2209–2224. ISSN: 1053-8119.

Esteban, O., D. Birman, M. Schaer, O. O. Koyejo, R. A. Poldrack, and K. J. Gorgolewski (Sept. 2017). "MRIQC: Advancing the automatic prediction of image quality in MRI from unseen sites". en. In: *PLOS ONE* 12.9, e0184661. ISSN: 1932-6203.

Esteban, O., C. J. Markiewicz, R. W. Blair, C. A. Moodie, A. I. Isik, A. Erramuzpe, J. D. Kent, M. Goncalves, E. DuPre, M. Snyder, H. Oya, S. S. Ghosh, J. Wright, J. Durnez, R. A. Poldrack, and K. J. Gorgolewski (Jan. 2019). "fMRIPrep: a robust preprocessing pipeline for functional MRI". en. In: *Nature Methods* 16.1. Number: 1 Publisher: Nature Publishing Group, pp. 111–116. ISSN: 1548-7105.

Friston, K., J. Ashburner, S. KIEBEL, T. NICHOLS, and W. PENNY (2007). *Statistical Parametric Mapping*. en. Elsevier. ISBN: 978-0-12-372560-8.

Friston, K. J., S. Williams, R. Howard, R. S. J. Frackowiak, and R. Turner (Mar. 1996). "Movement-Related effects in fMRI time-series". en. In: *Magnetic Resonance in Medicine* 35.3, pp. 346–355. ISSN: 07403194.

Gao, K and S Posse (2003). *TurboFIRE: Real-time fMRI with automated spatial normalization and Talairach Daemon database.* Abstract at 9th Annual Meeting of the OHBM, New York, USA. 2003.

Garrison, K. A., D. Scheinost, P. D. Worhunsky, H. M. Elwafi, T. A. Thornhill, E. Thompson, C. Saron, G. Desbordes, H. Kober, M. Hampson, J. R. Gray, R. T. Constable, X. Papademetris, and J. A. Brewer (Nov. 2013). "Real-time fMRI links subjective experience with brain activity during focused attention". In: *NeuroImage* 81, pp. 110–118. ISSN: 1053-8119.

Geissler, A., A. Gartus, T. Foki, A. R. Tahamtan, R. Beisteiner, and M. Barth (2007). "Contrast-to-noise ratio (CNR) as a quality parameter in fMRI". en. In: *Journal of Magnetic Resonance Imaging* 25.6, pp. 1263–1270. ISSN: 1522-2586.

Gelderen, P. v., J. A. d. Zwart, P. Starewicz, R. S. Hinks, and J. H. Duyn (Feb. 2007). "Real-time shimming to compensate for respiration-induced B0 fluctuations". en. In: *Magnetic Resonance in Medicine* 57.2, pp. 362–368. ISSN: 1522-2594.

Gembris, D., J. G. Taylor, S. Schor, W. Frings, D. Suter, and S. Posse (Feb. 2000). "Functional magnetic resonance imaging in real time (FIRE): Sliding-window correlation analysis and reference-vector optimization". en. In: *Magnetic Resonance in Medicine* 43.2, pp. 259–268. ISSN: 1522-2594.

Gitelman, D. R., W. D. Penny, J. Ashburner, and K. J. Friston (May 2003). "Modeling regional and psychophysiologic interactions in fMRI: the importance of hemodynamic deconvolution". In: *NeuroImage* 19.1, pp. 200–207. ISSN: 1053-8119.

Glover, G. H. and C. S. Law (Sept. 2001). "Spiral-in/out BOLD fMRI for increased SNR and reduced susceptibility artifacts". en. In: *Magnetic Resonance in Medicine* 46.3, pp. 515–522. ISSN: 1522-2594.

Glover, G. H., T.-Q. Li, and D. Ress (July 2000). "Image-based method for retrospective correction of physiological motion effects in fMRI: RETROICOR". en. In: *Magnetic Resonance in Medicine* 44.1, pp. 162–167. ISSN: 1522-2594.

Goebel, R. (Aug. 2012). "BrainVoyager — Past, present, future". en. In: *NeuroImage* 62.2, pp. 748–756. ISSN: 10538119.

Gonzalez-Castillo, J., P. Panwar, L. C. Buchanan, C. Caballero-Gaudes, D. A. Handwerker, D. C. Jangraw, V. Zachariou, S. Inati, V. Roopchansingh, J. A. Derbyshire, and P. A. Bandettini (Nov. 2016). "Evaluation of multi-echo ICA denoising for task based fMRI studies: Block designs, rapid event-related designs, and cardiac-gated fMRI". In: *NeuroImage* 141, pp. 452–468. ISSN: 1053-8119.

Goodman, S. N., D. Fanelli, and J. P. A. Ioannidis (June 2016). "What does research reproducibility mean?" en. In: *Science Translational Medicine* 8.341, 341ps12–341ps12. ISSN: 1946-6234, 1946-6242.

Gorgolewski, K., C. D. Burns, C. Madison, D. Clark, Y. O. Halchenko, M. L. Waskom, and S. S. Ghosh (2011). "Nipype: A Flexible, Lightweight and Extensible Neuroimaging Data Processing Framework in Python". English. In: *Frontiers in Neuroinformatics* 5. Publisher: Frontiers. ISSN: 1662-5196.

Gorgolewski, K. J., T. Auer, V. D. Calhoun, R. C. Craddock, S. Das, E. P. Duff, G. Flandin, S. S. Ghosh, T. Glatard, Y. O. Halchenko, D. A. Handwerker, M. Hanke, D. Keator, X. Li, Z. Michael, C. Maumet, B. N. Nichols, T. E. Nichols, J. Pellman, J.-B. Poline, A. Rokem, G. Schaefer, V. Sochat, W. Triplett, J. A. Turner, G. Varoquaux, and R. A. Poldrack (June 2016). "The brain imaging data structure, a format for organizing and describing outputs of neuroimaging experiments". en. In: *Scientific Data* 3.1. Number: 1 Publisher: Nature Publishing Group, p. 160044. ISSN: 2052-4463.

Gowland, P. A. and R. Bowtell (Apr. 2007). "Theoretical optimization of multi-echo fMRI data acquisition". eng. In: *Physics in Medicine and Biology* 52.7, pp. 1801–1813. ISSN: 0031-9155.

Green, M. V., J. Seidel, S. D. Stein, T. E. Tedder, K. M. Kempner, C. Kertzman, and T. A. Zeffiro (Sept. 1994). "Head movement in normal subjects during simulated PET brain imaging with and without head restraint". eng. In: *Journal of Nuclear Medicine: Official Publication, Society of Nuclear Medicine* 35.9, pp. 1538–1546. ISSN: 0161-5505.

Greene, D. J., J. M. Koller, J. M. Hampton, V. Wesevich, A. N. Van, A. L. Nguyen, C. R. Hoyt, L. McIntyre, E. A. Earl, R. L. Klein, J. S. Shimony, S. E. Petersen, B. L. Schlaggar, D. A. Fair, and N. U. F. Dosenbach (May 2018). "Behavioral interventions for reducing head motion during MRI scans in children". In: *NeuroImage* 171, pp. 234–245. ISSN: 1053-8119.

Greer, S. M., A. J. Trujillo, G. H. Glover, and B. Knutson (Aug. 2014). "Control of nucleus accumbens activity with neurofeedback". In: *NeuroImage* 96, pp. 237–244. ISSN: 1053-8119.

Griffanti, L., G. Salimi-Khorshidi, C. F. Beckmann, E. J. Auerbach, G. Douaud, C. E. Sexton, E. Zsoldos, K. P. Ebmeier, N. Filippini, C. E. Mackay, S. Moeller, J. Xu, E. Yacoub, G. Baselli, K. Ugurbil, K. L. Miller, and S. M. Smith (July 2014). "ICA-based artefact removal and accelerated fMRI acquisition for improved resting state network imaging". In: *NeuroImage* 95, pp. 232–247. ISSN: 1053-8119.

Gröne, M., M. Dyck, Y. Koush, S. Bergert, K. A. Mathiak, E. M. Alawi, M. Elliott, and K. Mathiak (Mar. 2015). "Upregulation of the Rostral Anterior Cingulate Cortex can Alter the Perception of Emotions: fMRI-Based Neurofeedback at 3 and 7 T". en. In: *Brain Topography* 28.2, pp. 197–207. ISSN: 0896-0267, 1573-6792.

Hagberg, G. E., I. Indovina, J. N. Sanes, and S. Posse (2002). "Real-time quantification of T changes using multiecho planar imaging and numerical methods". en. In: *Magnetic Resonance in Medicine* 48.5, pp. 877–882. ISSN: 1522-2594.

Hahn, A., G. S. Kranz, E.-M. Seidel, R. Sladky, C. Kraus, M. Küblböck, D. M. Pfabigan, A. Hummer, A. Grahl, S. Ganger, C. Windischberger, C. Lamm, and R. Lanzenberger (Nov. 2013). "Comparing neural response to painful electrical stimulation with functional MRI at 3 and 7T". In: *NeuroImage* 82, pp. 336–343. ISSN: 1053-8119.

Hajnal, J. V., R. Myers, A. Oatridge, J. E. Schwieso, I. R. Young, and G. M. Bydder (Mar. 1994). "Artifacts due to stimulus correlated motion in functional imaging of the brain". en. In: *Magnetic Resonance in Medicine* 31.3, pp. 283–291. ISSN: 1522-2594.

Hamilton, J. P., G. H. Glover, E. Bagarinao, C. Chang, S. Mackey, M. D. Sacchet, and I. H. Gotlib (Mar. 2016). "Effects of salience-network-node neurofeedback training on affective biases in major depressive disorder". In: *Psychiatry Research: Neuroimaging* 249, pp. 91–96. ISSN: 0925-4927.

Hamilton, J. P., G. H. Glover, J.-J. Hsu, R. F. Johnson, and I. H. Gotlib (2010). "Modulation of subgenual anterior cingulate cortex activity with real-time neurofeedback". en. In: *Human Brain Mapping* 32.1, pp. 22–31. ISSN: 1097-0193.

Handwerker, D. A., J. Gonzalez-Castillo, M. D'Esposito, and P. A. Bandettini (Aug. 2012). "The continuing challenge of understanding and modeling hemodynamic variation in fMRI". In: *NeuroImage* 62.2, pp. 1017–1023. ISSN: 1053-8119.

Hariri, A. R., A. Tessitore, V. S. Mattay, F. Fera, and D. R. Weinberger (Sept. 2002). "The amygdala response to emotional stimuli: a comparison of faces and scenes". eng. In: *NeuroImage* 17.1, pp. 317–323. ISSN: 1053-8119.

Harmelech, T., D. Friedman, and R. Malach (Feb. 2015). "Differential Magnetic Resonance Neurofeedback Modulations across Extrinsic (Visual) and Intrinsic (Default-Mode) Nodes of the Human Cortex". en. In: *Journal of Neuroscience* 35.6, pp. 2588–2595. ISSN: 0270-6474, 1529-2401.

Harmelech, T., S. Preminger, E. Wertman, and R. Malach (May 2013). "The day-after effect: long term, Hebbian-like restructuring of resting-state fMRI patterns induced by a single epoch of cortical

activation". eng. In: *The Journal of Neuroscience: The Official Journal of the Society for Neuroscience* 33.22, pp. 9488–9497. ISSN: 1529-2401.

Haugg, A., R. Sladky, S. Skouras, A. McDonald, C. Craddock, M. Kirschner, M. Herdener, Y. Koush, M. Papoutsi, J. N. Keynan, T. Hendler, K. C. Kadosh, C. Zich, J. MacInnes, A. Adcock, K. Dickerson, N.-K. Chen, K. Young, J. Bodurka, S. Yao, B. Becker, T. Auer, R. Schweizer, G. Pamplona, K. Emmert, S. Haller, D. V. D. Ville, M.-L. Blefari, D.-Y. Kim, J.-H. Lee, T. Marins, M. Fukuda, B. Sorger, T. Kamp, S.-L. Liew, R. Veit, M. Spetter, N. Weiskopf, and F. Scharnowski (Jan. 2020). "Can we predict real-time fMRI neurofeedback learning success from pre-training brain activity?" en. In: *bioRxiv*. Publisher: Cold Spring Harbor Laboratory Section: New Results, p. 2020.01.15.906388.

Hawkinson, J. E., A. J. Ross, S. Parthasarathy, D. J. Scott, E. A. Laramee, L. J. Posecion, W. R. Rekshan, K. E. Sheau, N. D. Njaka, P. J. Bayley, and R. C. deCharms (Sept. 2012). "Quantification of Adverse Events Associated with Functional MRI Scanning and with Real-Time fMRI-Based Training". en. In: *International Journal of Behavioral Medicine* 19.3, pp. 372–381. ISSN: 1532-7558.

Hellrung, L., V. Borchardt, F. N. Gotting, J. Stadler, C. Tempelmann, P. Tobler, M. Walter, and J. v. d. Meer (July 2018a). "Motion and physiological noise effects on amygdala real-time fMRI neurofeedback learning". en. In: *bioRxiv*, p. 366138.

Hellrung, L., A. Dietrich, M. Hollmann, B. Pleger, C. Kalberlah, E. Roggenhofer, A. Villringer, and A. Horstmann (Feb. 2018b). "Intermittent compared to continuous real-time fMRI neurofeedback boosts control over amygdala activation". eng. In: *NeuroImage* 166, pp. 198–208. ISSN: 1095-9572.

Hellrung, L., M. Hollmann, O. Zscheyge, T. Schlumm, C. Kalberlah, E. Roggenhofer, H. Okon-Singer, A. Villringer, and A. Horstmann (Apr. 2015). "Flexible Adaptive Paradigms for fMRI Using a Novel Software Package 'Brain Analysis in Real-Time' (BART)". en. In: *PLOS ONE* 10.4. Ed. by N. M. Maurits, e0118890. ISSN: 1932-6203.

Hellrung, L., J. Van der Meer, S. Bergert, R. Sladky, G. S. P. Pamplona, F. Scharnowski, Y. Koush, D. M. A. Mehler, D. E. J. Linden, C. Falcon, J. D. Gispert, J. L. Molinuevo, and S. Skouras (2017). "rtQC: An open-source collaborative framework for quality control methods in real-time fMRI". In: *Proceedings of the Real-time Functional Imaging and Neurofeedback Conference. Nara (Japan)*.

Heunis, J., R. Lamerichs, G. Song, S. Zinger, and B. Aldenkamp (Jan. 2019a). "Improving BOLD sensitivity with real-time multi-echo echo-planar imaging - Towards a cleaner neurofeedback signal". en. In: *Proceedings of the Benelux Chapter of the International Society for Magnetic Resonance in Medicine*.

Heunis, S., M. Breeuwer, C. Caballero-Gaudes, L. Hellrung, W. Huijbers, J. F. Jansen, R. Lamerichs, S. Zinger, and A. P. Aldenkamp (Dec. 2020a). "The effects of multi-echo fMRI combination and rapid T2*-mapping on offline and real-time BOLD sensitivity". en. In: *bioRxiv*. Publisher: Cold Spring Harbor Laboratory Section: New Results, p. 2020.12.08.416768.

Heunis, S., M. Breeuwer, C. C. Gaudes, L. Hellrung, W. Huijbers, J. F. Jansen, R. Lamerichs, S. Zinger, and A. P. Aldenkamp (Dec. 2020b). "rt-me-fMRI: A task and resting state dataset for real-time, multi-echo fMRI methods development and validation". en. In: *bioRxiv*. Publisher: Cold Spring Harbor Laboratory Section: New Results, p. 2020.12.07.414490.

Heunis, S., L. Hellrung, J. Van der Meer, S. Bergert, R. Sladky, G. Pamplona, F. Scharnowski, Y. Koush, D. Mehler, C. Falcon, J. Gispert, J. Molinuevo, and S. Skouras (June 2019b). *rtQC: An open-source toolbox for real-time fMRI quality control*. [IN PREP]. a. Rome, Italy.

Heunis, S., R. Lamerichs, S. Zinger, C. Caballero-Gaudes, J. F. A. Jansen, B. Aldenkamp, and M. Breeuwer (Apr. 2020c). "Quality and denoising in real-time functional magnetic resonance imaging neurofeedback: A methods review". en. In: *Human Brain Mapping*, hbm.25010. ISSN: 1065-9471, 1097-0193.

Hinds, O., S. Ghosh, T. W. Thompson, J. J. Yoo, S. Whitfield-Gabrieli, C. Triantafyllou, and J. D. E. Gabrieli (Jan. 2011). "Computing moment-to-moment BOLD activation for real-time neurofeedback". In: *NeuroImage* 54.1, pp. 361–368. ISSN: 1053-8119.

Hirsch, J., M. I. Ruge, K. H. S. Kim, D. D. Correa, J. D. Victor, N. R. Relkin, D. R. Labar, G. Krol, M. H. Bilsky, M. M. Souweidane, L. M. DeAngelis, and P. H. Gutin (Sept. 2000). "An Integrated Functional Magnetic Resonance Imaging Procedure for Preoperative Mapping of Cortical Areas Associated with Tactile, Motor, Language, and Visual Functions:" en. In: *Neurosurgery* 47.3, pp. 711–722. ISSN: 0148-396X.

Hollmann, M., T. Mönch, S. Mulla-Osman, C. Tempelmann, J. Stadler, and J. Bernarding (Oct. 2008). "A new concept of a unified parameter management, experiment control, and data analysis in fMRI:

Application to real-time fMRI at 3T and 7T". In: *Journal of Neuroscience Methods* 175.1, pp. 154–162. ISSN: 0165-0270.

Huettel, S. A. and G. McCarthy (Nov. 2001). "Regional Differences in the Refractory Period of the Hemodynamic Response: An Event-Related fMRI Study". In: *NeuroImage* 14.5, pp. 967–976. ISSN: 1053-8119.

Jenkinson, M., P. Bannister, M. Brady, and S. Smith (Oct. 2002). "Improved Optimization for the Robust and Accurate Linear Registration and Motion Correction of Brain Images". In: *NeuroImage* 17.2, pp. 825–841. ISSN: 1053-8119.

Johnson, K. A., K. Hartwell, T. LeMatty, J. Borckardt, P. S. Morgan, K. Govindarajan, K. Brady, and M. S. George (Jan. 2012). "Intermittent "Real-time" fMRI Feedback Is Superior to Continuous Presentation for a Motor Imagery Task: A Pilot Study". en. In: *Journal of Neuroimaging* 22.1, pp. 58–66. ISSN: 10512284.

Kadosh, K. C. and G. Staunton (Jan. 2019). "A systematic review of the psychological factors that influence neurofeedback learning outcomes". In: *NeuroImage* 185, pp. 545–555. ISSN: 1053-8119.

Karahanoğlu, F. I. and D. Van De Ville (Nov. 2015). "Transient brain activity disentangles fMRI resting-state dynamics in terms of spatially and temporally overlapping networks". en. In: *Nature Communications* 6.1, p. 7751. ISSN: 2041-1723.

Karakuzu, A., M. Boudreau, T. Duval, T. Boshkovski, I. R. Leppert, J.-F. Cabana, I. Gagnon, P. Beliveau, G. B. Pike, J. Cohen-Adad, and N. Stikov (Sept. 2020). "qMRLab: Quantitative MRI analysis, under one umbrella". en. In: *Journal of Open Source Software* 5.53, p. 2343. ISSN: 2475-9066.

Kasper, L., S. Bollmann, A. O. Diaconescu, C. Hutton, J. Heinzle, S. Iglesias, T. U. Hauser, M. Sebold, Z.-M. Manjaly, K. P. Pruessmann, and K. E. Stephan (Jan. 2017). "The PhysIO Toolbox for Modeling Physiological Noise in fMRI Data". en. In: *Journal of Neuroscience Methods* 276, pp. 56–72. ISSN: 0165-0270.

Kiebel, S. J., S. Klöppel, N. Weiskopf, and K. J. Friston (Feb. 2007). "Dynamic causal modeling: A generative model of slice timing in fMRI". In: *NeuroImage* 34.4, pp. 1487–1496. ISSN: 1053-8119.

Kim, D.-Y., S.-S. Yoo, M. Tegethoff, G. Meinlschmidt, and J.-H. Lee (Aug. 2015). "The inclusion of functional connectivity information into fMRI-based neurofeedback improves its efficacy in the reduction of cigarette cravings". eng. In: *Journal of Cognitive Neuroscience* 27.8, pp. 1552–1572. ISSN: 1530-8898.

Kopel, R., R. Sladky, P. Laub, Y. Koush, F. Robineau, C. Hutton, N. Weiskopf, P. Vuilleumier, D. Van De Ville, and F. Scharnowski (May 2019). "No time for drifting: Comparing performance and applicability of signal detrending algorithms for real-time fMRI". In: *NeuroImage* 191, pp. 421–429. ISSN: 1053-8119.

Koush, Y., J. Ashburner, E. Prilepin, R. Sladky, P. Zeidman, S. Bibikov, F. Scharnowski, A. Nikonorov, and D. V. De Ville (Aug. 2017a). "OpenNFT: An open-source Python/Matlab framework for real-time fMRI neurofeedback training based on activity, connectivity and multivariate pattern analysis". In: *NeuroImage* 156. b, pp. 489–503. ISSN: 1053-8119.

Koush, Y., J. Ashburner, E. Prilepin, R. Sladky, P. Zeidman, S. Bibikov, F. Scharnowski, A. Nikonorov, and D. Van De Ville (Oct. 2017b). "Real-time fMRI data for testing OpenNFT functionality". In: *Data in Brief* 14, pp. 344–347. ISSN: 2352-3409.

Koush, Y., M. J. Rosa, F. Robineau, K. Heinen, S. W. Rieger, N. Weiskopf, P. Vuilleumier, D. Van De Ville, and F. Scharnowski (Nov. 2013). "Connectivity-based neurofeedback: Dynamic causal modeling for real-time fMRI". In: *NeuroImage* 81, pp. 422–430. ISSN: 1053-8119.

Koush, Y., M. Zvyagintsev, M. Dyck, K. A. Mathiak, and K. Mathiak (Jan. 2012). "Signal quality and Bayesian signal processing in neurofeedback based on real-time fMRI". In: *NeuroImage*. Neuroergonomics: The human brain in action and at work 59.1, pp. 478–489. ISSN: 1053-8119.

Krause, F., C. Benjamins, J. Eck, M. Lührs, R. v. Hoof, and R. Goebel (2019). "Active head motion reduction in magnetic resonance imaging using tactile feedback". en. In: *Human Brain Mapping* 40.14, pp. 4026–4037. ISSN: 1097-0193.

Krüger, G. and G. H. Glover (2001). "Physiological noise in oxygenation-sensitive magnetic resonance imaging". en. In: *Magnetic Resonance in Medicine* 46.4, pp. 631–637. ISSN: 1522-2594.

Kundu, P., S. J. Inati, J. W. Evans, W.-M. Luh, and P. A. Bandettini (Apr. 2012). "Differentiating BOLD and non-BOLD signals in fMRI time series using multi-echo EPI". In: *NeuroImage* 60.3, pp. 1759–1770. ISSN: 1053-8119.

Kundu, P., V. Voon, P. Balchandani, M. V. Lombardo, B. A. Poser, and P. A. Bandettini (July 2017). "Multi-echo fMRI: A review of applications in fMRI denoising and analysis of BOLD signals". In:

NeuroImage. Cleaning up the fMRI time series: Mitigating noise with advanced acquisition and correction strategies 154, pp. 59–80. ISSN: 1053-8119.

LaConte, S. M. (May 2011). "Decoding fMRI brain states in real-time". en. In: *NeuroImage* 56.2, pp. 440–454. ISSN: 10538119.

LaConte, S. M., S. J. Peltier, and X. P. Hu (Oct. 2007). "Real-time fMRI using brain-state classification". en. In: *Human Brain Mapping* 28.10, pp. 1033–1044. ISSN: 1097-0193.

Laird, A. R., J. L. Lancaster, and P. T. Fox (2005). "BrainMap: The Social Evolution of a Human Brain Mapping Database". en. In: *Neuroinformatics* 3.1, pp. 065–078. ISSN: 1539-2791.

Linden, D. E. J., I. Habes, S. J. Johnston, S. Linden, R. Tatineni, L. Subramanian, B. Sorger, D. Healy, and R. Goebel (June 2012). "Real-Time Self-Regulation of Emotion Networks in Patients with Depression". en. In: *PLOS ONE* 7.6, e38115. ISSN: 1932-6203.

Liu, T. T. (Dec. 2016). "Noise contributions to the fMRI signal: An overview". In: *NeuroImage* 143, pp. 141–151. ISSN: 1053-8119.

Logothetis, N. K. (May 2003). "The Underpinnings of the BOLD Functional Magnetic Resonance Imaging Signal". en. In: *Journal of Neuroscience* 23.10, pp. 3963–3971. ISSN: 0270-6474, 1529-2401.

Lombardo, M. V., B. Auyeung, R. J. Holt, J. Waldman, A. N. V. Ruigrok, N. Mooney, E. T. Bullmore, S. Baron-Cohen, and P. Kundu (Nov. 2016). "Improving effect size estimation and statistical power with multi-echo fMRI and its impact on understanding the neural systems supporting mentalizing". en. In: *NeuroImage* 142, pp. 55–66. ISSN: 1053-8119.

Lui, S., X. J. Zhou, J. A. Sweeney, and Q. Gong (Nov. 2016). "Psychoradiology: The Frontier of Neuroimaging in Psychiatry". en. In: *Radiology* 281.2, pp. 357–372. ISSN: 0033-8419, 1527-1315.

Lührs, M. and R. Goebel (2019). "Increase the quality and consistency of real-time fMRI Neurofeedback experiments using Turbo-BrainVoyager". In: *Proceedings of the Real-time Functional Imaging and Neurofeedback Conference. Maastricht, The Netherlands.* Maastricht, The Netherlands.

Maclaren, J., M. Herbst, O. Speck, and M. Zaitsev (2012). "Prospective motion correction in brain imaging: A review". en. In: *Magnetic Resonance in Medicine* 69.3, pp. 621–636. ISSN: 1522-2594.

Magland, J. F., C. W. Tjoa, and A. R. Childress (Apr. 2011). "Spatio-temporal activity in real time (STAR): Optimization of regional fMRI feedback". en. In: *NeuroImage* 55.3, pp. 1044–1053. ISSN: 10538119.

Manuck, S. B., S. M. Brown, E. E. Forbes, and A. R. Hariri (Oct. 2007). "Temporal stability of individual differences in amygdala reactivity". eng. In: *The American Journal of Psychiatry* 164.10, pp. 1613–1614. ISSN: 0002-953X.

Marins, T. F., E. C. Rodrigues, A. Engel, S. Hoefle, R. Basílio, R. Lent, J. Moll, and F. Tovar-Moll (2015). "Enhancing Motor Network Activity Using Real-Time Functional MRI Neurofeedback of Left Premotor Cortex". English. In: *Frontiers in Behavioral Neuroscience* 9. ISSN: 1662-5153.

Marxen, M., M. J. Jacob, D. K. Müller, S. Posse, E. Ackley, L. Hellrung, P. Riedel, S. Bender, R. Epple, and M. N. Smolka (2016). "Amygdala Regulation Following fMRI-Neurofeedback without Instructed Strategies". English. In: *Frontiers in Human Neuroscience* 10. ISSN: 1662-5161.

Mathiak, K. and S. Posse (2001). "Evaluation of motion and realignment for functional magnetic resonance imaging in real time". en. In: *Magnetic Resonance in Medicine* 45.1, pp. 167–171. ISSN: 1522-2594.

Mathiak, K., A. Rapp, T. T. J. Kircher, W. Grodd, I. Hertrich, N. Weiskopf, W. Lutzenberger, and H. Ackermann (July 2002). "Mismatch responses to randomized gradient switching noise as reflected by fMRI and whole-head magnetoencephalography". en. In: *Human Brain Mapping* 16.3, pp. 190–195. ISSN: 1097-0193.

McCaig, R. G., M. Dixon, K. Keramatian, I. Liu, and K. Christoff (Apr. 2011). "Improved modulation of rostrolateral prefrontal cortex using real-time fMRI training and meta-cognitive awareness". In: *NeuroImage* 55.3, pp. 1298–1305. ISSN: 1053-8119.

McDonald, A. R., J. Muraskin, N. T. Van Dam, C. Froehlich, B. Puccio, J. Pellman, C. C. Bauer, A. Akeyson, M. M. Breland, V. D. Calhoun, S. Carter, T. P. Chang, C. Gessner, A. Gianonne, S. Giavasis, J. Glass, S. Homan, M. King, M. Kramer, D. Landis, A. Lieval, J. Lisinski, A. Mackay-Brandt, B. Miller, L. Panek, H. Reed, C. Santiago, E. Schoell, R. Sinnig, M. Sital, E. Taverna, R. Tobe, K. Trautman, B. Varghese, L. Walden, R. Wang, A. B. Waters, D. Wood, F. X. Castellanos, B. Leventhal, S. J. Colcombe, S. LaConte, M. P. Milham, and R. C. Craddock (Feb. 2017). "The Real-time fMRI Neurofeedback Based Stratification of Default Network Regulation Neuroimaging Data Repository". In: *NeuroImage* 146, pp. 157–170. ISSN: 1053-8119.

Megumi, F., A. Yamashita, M. Kawato, and H. Imamizu (Mar. 2015). "Functional MRI neurofeedback training on connectivity between two regions induces long-lasting changes in intrinsic functional network". In: *Frontiers in Human Neuroscience* 9. ISSN: 1662-5161.

Menon, R. S., S. Ogawa, D. W. Tank, and K. Uğurbil (1993). "4 Tesla gradient recalled echo characteristics of photic stimulation-induced signal changes in the human primary visual cortex". en. In: *Magnetic Resonance in Medicine* 30.3, pp. 380–386. ISSN: 1522-2594.

Metere, R., T. Kober, H. E. Möller, and A. Schäfer (Jan. 2017). "Simultaneous Quantitative MRI Mapping of T1, T2* and Magnetic Susceptibility with Multi-Echo MP2RAGE". en. In: *PLOS ONE* 12.1. Publisher: Public Library of Science, e0169265. ISSN: 1932-6203.

Misaki, M., N. Barzigar, V. Zotev, R. Phillips, S. Cheng, and J. Bodurka (Dec. 2015). "Real-time fMRI processing with physiological noise correction – Comparison with off-line analysis". In: *Journal of Neuroscience Methods* 256, pp. 117–121. ISSN: 0165-0270.

Misaki, M., R. Phillips, V. Zotev, C.-K. Wong, B. E. Wurfel, F. Krueger, M. Feldner, and J. Bodurka (Jan. 2018). "Real-time fMRI amygdala neurofeedback positive emotional training normalized resting-state functional connectivity in combat veterans with and without PTSD: a connectome-wide investigation". en. In: *NeuroImage: Clinical* 20, pp. 543–555. ISSN: 2213-1582.

Mišić, B. and O. Sporns (Oct. 2016). "From regions to connections and networks: new bridges between brain and behavior". en. In: *Current Opinion in Neurobiology* 40, pp. 1–7. ISSN: 09594388.

Moia, S., M. Termenon, E. Uruñuela, R. C. Stickland, M. G. Bright, and C. Caballero-Gaudes (Sept. 2020). "ICA-based Denoising Strategies in Breath-Hold Induced Cerebrovascular Reactivity Mapping with Multi Echo BOLD fMRI". en. In: *bioRxiv*. Publisher: Cold Spring Harbor Laboratory Section: New Results, p. 2020.08.18.256479.

Morawetz, C., P. Holz, C. Lange, J. Baudewig, G. Weniger, E. Irle, and P. Dechent (Jan. 2008). "Improved functional mapping of the human amygdala using a standard functional magnetic resonance imaging sequence with simple modifications". English. In: *Magnetic Resonance Imaging* 26.1, pp. 45–53. ISSN: 0730-725X, 1873-5894.

Munafò, M. R., B. A. Nosek, D. V. M. Bishop, K. S. Button, C. D. Chambers, N. P. d. Sert, U. Simonsohn, E.-J. Wagenmakers, J. J. Ware, and J. P. A. Ioannidis (Jan. 2017). "A manifesto for reproducible science". en. In: *Nature Human Behaviour* 1.1, p. 0021. ISSN: 2397-3374.

Murphy, K., R. M. Birn, and P. A. Bandettini (Oct. 2013). "Resting-state FMRI confounds and cleanup". In: *NeuroImage* 80, pp. 349–359. ISSN: 1053-8119.

Murphy, K., J. Bodurka, and P. A. Bandettini (Jan. 2007). "How long to scan? The relationship between fMRI temporal signal to noise and necessary scan duration". In: *NeuroImage* 34.2, pp. 565–574. ISSN: 1053-8119.

Murphy, K. and M. D. Fox (July 2017). "Towards a consensus regarding global signal regression for resting state functional connectivity MRI". In: *Neuroimage* 154, pp. 169–173. ISSN: 1053-8119.

Nichols, T. E., S. Das, S. B. Eickhoff, A. C. Evans, T. Glatard, M. Hanke, N. Kriegeskorte, M. P. Milham, R. A. Poldrack, J.-B. Poline, E. Proal, B. Thirion, D. C. Van Essen, T. White, and B. T. T. Yeo (Mar. 2017). "Best practices in data analysis and sharing in neuroimaging using MRI". en. In: *Nature Neuroscience* 20.3. Number: 3 Publisher: Nature Publishing Group, pp. 299–303. ISSN: 1546-1726.

Nicholson, A. A., D. Rabellino, M. Densmore, P. A. Frewen, C. Paret, R. Kluetsch, C. Schmahl, J. Théberge, R. W. Neufeld, M. C. McKinnon, J. P. Reiss, R. Jetly, and R. A. Lanius (Jan. 2017). "The neurobiology of emotion regulation in posttraumatic stress disorder: Amygdala downregulation via real-time fMRI neurofeedback". en. In: *Human Brain Mapping* 38.1, pp. 541–560. ISSN: 1065-9471, 1097-0193.

Noll, D. C. and W. Schneider (Nov. 1994). "Theory, simulation, and compensation of physiological motion artifacts in functional MRI". In: *Proceedings of 1st International Conference on Image Processing*. Vol. 3, 40–44 vol.3.

Oblak, E. F., J. A. Lewis-Peacock, and J. S. Sulzer (July 2017). "Self-regulation strategy, feedback timing and hemodynamic properties modulate learning in a simulated fMRI neurofeedback environment". en. In: *PLOS Computational Biology* 13.7, e1005681. ISSN: 1553-7358.

Ogawa, S., R. S. Menon, S.-G. Kim, and a. K. Ugurbil (1998). "On the Characteristics of Functional Magnetic Resonance Imaging of the Brain". In: *Annual Review of Biophysics and Biomolecular Structure* 27.1, pp. 447–474.

Olafsson, V., P. Kundu, E. C. Wong, P. A. Bandettini, and T. T. Liu (May 2015). "Enhanced identification of BOLD-like components with multi-echo simultaneous multi-slice (MESMS) fMRI and multi-echo ICA". eng. In: *NeuroImage* 112, pp. 43–51. ISSN: 1095-9572.

Omer Faruk Gulban, Dylan Nielson, Russ Poldrack, john lee, Chris Gorgolewski, Vanessasaurus, and Satrajit Ghosh (Oct. 2019). *poldracklab/pydeface: v2.0.0*.

Oostenveld, R., P. Fries, E. Maris, and J.-M. Schoffelen (2011). "FieldTrip: Open source software for advanced analysis of MEG, EEG, and invasive electrophysiological data". eng. In: *Computational Intelligence and Neuroscience* 2011, p. 156869. ISSN: 1687-5273.

Parrish, T. B., D. R. Gitelman, K. S. LaBar, and M.-M. Mesulam (Dec. 2000). "Impact of signal-to-noise on functional MRI". en. In: *Magnetic Resonance in Medicine* 44.6, pp. 925–932. ISSN: 1522-2594.

Pears, J. A., S. T. Francis, S. E. Butterworth, R. W. Bowtell, and P. A. Gowland (2003). "Investigating the BOLD effect during infusion of Gd-DTPA using rapid T mapping". en. In: *Magnetic Resonance in Medicine* 49.1, pp. 61–70. ISSN: 1522-2594.

Perlbarg, V., P. Bellec, J.-L. Anton, M. Pélégrini-Issac, J. Doyon, and H. Benali (Jan. 2007). "CORSICA: correction of structured noise in fMRI by automatic identification of ICA components". In: *Magnetic Resonance Imaging* 25.1, pp. 35–46. ISSN: 0730-725X.

Pernet, C. R. (2014). "Misconceptions in the use of the General Linear Model applied to functional MRI: a tutorial for junior neuro-imagers". English. In: *Frontiers in Neuroscience* 8. Publisher: Frontiers. ISSN: 1662-453X.

Peters, A. M., M. J. Brookes, F. G. Hoogenraad, P. A. Gowland, S. T. Francis, P. G. Morris, and R. Bowtell (July 2007). "T2* measurements in human brain at 1.5, 3 and 7 T". en. In: *Magnetic Resonance Imaging*. Proceedings of the International School on Magnetic Resonance and Brain Function 25.6, pp. 748–753. ISSN: 0730-725X.

Poldrack, R. A. (Mar. 2007). "Region of interest analysis for fMRI". In: *Social cognitive and affective neuroscience* 2.1, pp. 67–70. ISSN: 1749-5016.

Poldrack, R. A., K. J. Gorgolewski, and G. Varoquaux (2019). "Computational and Informatic Advances for Reproducible Data Analysis in Neuroimaging". In: *Annual Review of Biomedical Data Science* 2.1, pp. 119–138.

Poldrack, R. A., J. A. Mumford, and T. E. Nichols (June 2011). *Handbook of Functional MRI Data Analysis*. en.

Poser, B. A., M. J. Versluis, J. M. Hoogduin, and D. G. Norris (June 2006). "BOLD contrast sensitivity enhancement and artifact reduction with multiecho EPI: Parallel-acquired inhomogeneity-desensitized fMRI". en. In: *Magnetic Resonance in Medicine* 55.6, pp. 1227–1235. ISSN: 1522-2594.

Posse, S, S Wiese, C Kessler, D Gembris, U Weiss, M Peyerl, M. Grosse-Ruyken, B Elghawaghi, T Richards, and S Dager (1998). "Single Shot T2*-Sensitive Spectroscopic Imaging Increases fMRI Sensitivity: Preliminary Evidence from Visual and Olfactory Activation." In: *International Society for Magnetic Resonance in Medicine.* Vol. 299.

Posse, S., E. Ackley, R. Mutihac, J. Rick, M. Shane, C. Murray-Krezan, M. Zaitsev, and O. Speck (May 2012). "Enhancement of temporal resolution and BOLD sensitivity in real-time fMRI using multi-slab echo-volumar imaging". In: *NeuroImage* 61.1, pp. 115–130. ISSN: 1053-8119.

Posse, S., F. Binkofski, F. Schneider, D. Gembris, W. Frings, U. Habel, J. B. Salloum, K. Mathiak, S. Wiese, V. Kiselev, T. Graf, B. Elghahwagi, M.-L. Grosse-Ruyken, and T. Eickermann (2000). "A new approach to measure single-event related brain activity using real-time fMRI: Feasibility of sensory, motor, and higher cognitive tasks". en. In: *Human Brain Mapping* 12.1, pp. 25–41. ISSN: 1097-0193.

Posse, S., D. Fitzgerald, K. Gao, U. Habel, D. Rosenberg, G. J. Moore, and F. Schneider (Mar. 2003a). "Real-time fMRI of temporolimbic regions detects amygdala activation during single-trial self-induced sadness". en. In: *NeuroImage* 18.3, pp. 760–768. ISSN: 1053-8119.

Posse, S., Z. Shen, V. Kiselev, and L. J. Kemna (Feb. 2003b). "Single-shot T2* mapping with 3D compensation of local susceptibility gradients in multiple regions". In: *NeuroImage* 18.2, pp. 390–400. ISSN: 1053-8119.

Posse, S., S. Wiese, D. Gembris, K. Mathiak, C. Kessler, M.-L. Grosse-Ruyken, B. Elghahwagi, T. Richards, S. R. Dager, and V. G. Kiselev (July 1999). "Enhancement of BOLD-contrast sensitivity by single-shot multi-echo functional MR imaging". en. In: *Magnetic Resonance in Medicine* 42.1, pp. 87–97. ISSN: 1522-2594.

Power, J. D. (July 2017). "A simple but useful way to assess fMRI scan qualities". In: *NeuroImage*. Cleaning up the fMRI time series: Mitigating noise with advanced acquisition and correction strategies 154, pp. 150–158. ISSN: 1053-8119.

Power, J. D., K. A. Barnes, A. Z. Snyder, B. L. Schlaggar, and S. E. Petersen (Feb. 2012). "Spurious but systematic correlations in functional connectivity MRI networks arise from subject motion". In: *Neuroimage* 59.3, pp. 2142–2154. ISSN: 1053-8119.

Power, J. D., A. Mitra, T. O. Laumann, A. Z. Snyder, B. L. Schlaggar, and S. E. Petersen (Jan. 2014). "Methods to detect, characterize, and remove motion artifact in resting state fMRI". In: *NeuroImage* 84. ISSN: 1053-8119.

Power, J. D., M. Plitt, S. J. Gotts, P. Kundu, V. Voon, P. A. Bandettini, and A. Martin (Feb. 2018). "Ridding fMRI data of motion-related influences: Removal of signals with distinct spatial and physical bases in multiecho data". en. In: *Proceedings of the National Academy of Sciences*, p. 201720985. ISSN: 0027-8424, 1091-6490.

Power, J. D., M. Plitt, T. O. Laumann, and A. Martin (Feb. 2017). "Sources and implications of whole-brain fMRI signals in humans". In: *NeuroImage* 146, pp. 609–625. ISSN: 1053-8119.

Project, P. C. (2014). "PCP Quality Assessment Protocol. [ONLINE] Available at: http://preprocessed-connectomes-project.org/quality-assessment-protocol/. [Accessed 28 May 2018]." In:

Ramot, M. and J. Gonzalez-Castillo (Mar. 2019). "A framework for offline evaluation and optimization of real-time algorithms for use in neurofeedback, demonstrated on an instantaneous proxy for correlations". In: *NeuroImage* 188, pp. 322–334. ISSN: 1053-8119.

Randell, E., R. McNamara, L. Subramanian, K. Hood, and D. Linden (Apr. 2018). "Current practices in clinical neurofeedback with functional MRI—Analysis of a survey using the TIDieR checklist". English. In: *European Psychiatry* 50, pp. 28–33. ISSN: 0924-9338.

Rangaprakash, D., G.-R. Wu, D. Marinazzo, X. Hu, and G. Deshpande (2018). "Hemodynamic response function (HRF) variability confounds resting-state fMRI functional connectivity". en. In: *Magnetic Resonance in Medicine* 0.0. ISSN: 1522-2594.

Ros, T., S. Enriquez-Geppert, V. Zotev, K. D. Young, G. Wood, S. Whitfield-Gabrieli, F. Wan, P. Vuilleumier, F. Vialatte, D. Van De Ville, D. Todder, T. Surmeli, J. S. Sulzer, U. Strehl, M. B. Sterman, N. J. Steiner, B. Sorger, S. R. Soekadar, R. Sitaram, L. H. Sherlin, M. Schönenberg, F. Scharnowski, M. Schabus, K. Rubia, A. Rosa, M. Reiner, J. A. Pineda, C. Paret, A. Ossadtchi, A. A. Nicholson, W. Nan, J. Minguez, J.-A. Micoulaud-Franchi, D. M. Mehler, M. Lührs, J. Lubar, F. Lotte, D. E. Linden, J. A. Lewis-Peacock, M. A. Lebedev, R. A. Lanius, A. Kübler, C. Kranczioch, Y. Koush, L. Konicar, S. H. Kohl, S. E. Kober, M. A. Klados, C. Jeunet, T. Janssen, R. J. Huster, K. Hoedlmoser, L. M. Hirshberg, S. Heunis, T. Hendler, M. Hampson, A. G. Guggisberg, R. Guggenberger, J. H. Gruzelier, R. W. Göbel, N. Gninenko, A. Gharabaghi, P. Frewen, T. Fovet, T. Fernández, C. Escolano, A.-C. Ehlis, R. Drechsler, R Christopher deCharms, S. Debener, D. De Ridder, E. J. Davelaar, M. Congedo, M. Cavazza, M. H. Breteler, D. Brandeis, J. Bodurka, N. Birbaumer, O. M. Bazanova, B. Barth, P. D. Bamidis, T. Auer, M. Arns, and R. T. Thibault (Mar. 2020). "Consensus on the reporting and experimental design of clinical and cognitive-behavioural neurofeedback studies (CRED-nf checklist)". en. In: *Brain*, awaa009. ISSN: 0006-8950, 1460-2156.

Ruiz, S., N. Birbaumer, and R. Sitaram (2013). "Abnormal Neural Connectivity in Schizophrenia and fMRI-Brain-Computer Interface as a Potential Therapeutic Approach". In: *Frontiers in Psychiatry* 4. ISSN: 1664-0640.

Salo, T. (May 2020). *tsalo/convert-eprime: 0.0.1*.

Sato, J. R., R. Basilio, F. F. Paiva, G. J. Garrido, I. E. Bramati, P. Bado, F. Tovar-Moll, R. Zahn, and J. Moll (Dec. 2013). "Real-Time fMRI Pattern Decoding and Neurofeedback Using FRIEND: An FSL-Integrated BCI Toolbox". en. In: *PLoS ONE* 8.12. Ed. by E. Yacoub, e81658. ISSN: 1932-6203.

Scheffler, K., E. Seifritz, R. Haselhorst, and D. Bilecen (1999). "Titration of the BOLD effect: Separation and quantitation of blood volume and oxygenation changes in the human cerebral cortex during neuronal activation and ferumoxide infusion". en. In: *Magnetic Resonance in Medicine* 42.5, pp. 829–836. ISSN: 1522-2594.

Scheinost, D., M. Hampson, M. Qiu, J. Bhawnani, R. T. Constable, and X. Papademetris (July 2013). "A Graphics Processing Unit Accelerated Motion Correction Algorithm and Modular System for Real-time fMRI". en. In: *Neuroinformatics* 11.3, pp. 291–300. ISSN: 1539-2791, 1559-0089.

Schulte, A.-C., O. Speck, C. Oesterle, and J. Hennig (2001). "Separation and quantification of perfusion and BOLD effects by simultaneous acquisition of functional I0- and T-parameter maps". en. In: *Magnetic Resonance in Medicine* 45.5, pp. 811–816. ISSN: 1522-2594.

Shibata, K., T. Watanabe, M. Kawato, and Y. Sasaki (Sept. 2016). "Differential Activation Patterns in the Same Brain Region Led to Opposite Emotional States". en. In: *PLOS Biology* 14.9, e1002546. ISSN: 1545-7885.

Shibata, K., T. Watanabe, Y. Sasaki, and M. Kawato (Dec. 2011). "Perceptual Learning Incepted by Decoded fMRI Neurofeedback Without Stimulus Presentation". en. In: *Science* 334.6061, pp. 1413–1415. ISSN: 0036-8075, 1095-9203.

Siegel, J. S., J. D. Power, J. W. Dubis, A. C. Vogel, J. A. Church, B. L. Schlaggar, and S. E. Petersen (May 2014). "Statistical improvements in functional magnetic resonance imaging analyses produced by censoring high-motion data points". en. In: *Human Brain Mapping* 35.5, pp. 1981–1996. ISSN: 1097-0193.

Sitaram, R., T. Ros, L. Stoeckel, S. Haller, F. Scharnowski, J. Lewis-Peacock, N. Weiskopf, M. L. Blefari, M. Rana, E. Oblak, N. Birbaumer, and J. Sulzer (Feb. 2017). "Closed-loop brain training: the science of neurofeedback". en. In: *Nature Reviews Neuroscience* 18.2, pp. 86–100. ISSN: 1471-003X, 1471-0048.

Sladky, R., P. Baldinger, G. S. Kranz, J. Tröstl, A. Höflich, R. Lanzenberger, E. Moser, and C. Windischberger (May 2013). "High-resolution functional MRI of the human amygdala at 7T". In: *European Journal of Radiology* 82.5, pp. 728–733. ISSN: 0720-048X.

Sladky, R., K. J. Friston, J. Tröstl, R. Cunnington, E. Moser, and C. Windischberger (Sept. 2011). "Slice-timing effects and their correction in functional MRI". In: *NeuroImage* 58.2, pp. 588–594. ISSN: 1053-8119.

Sladky, R., N. Geissberger, D. M. Pfabigan, C. Kraus, M. Tik, M. Woletz, K. Paul, T. Vanicek, B. Auer, G. S. Kranz, C. Lamm, R. Lanzenberger, and C. Windischberger (Mar. 2018). "Unsmoothed functional MRI of the human amygdala and bed nucleus of the stria terminalis during processing of emotional faces". In: *NeuroImage*. Neuroimaging with Ultra-high Field MRI: Present and Future 168, pp. 383–391. ISSN: 1053-8119.

Smink J, Häkkinen M, Holthuizen R, Krueger S, Ries M, Berber Y, Moonen C, Köhler M, and Vahala E (2011). "eXTernal Control (XTC): a flexible, real-time, low-latency, bi-directional scanner interface." In: vol. 19.

Smyser, C., T. J. Grabowski, R. J. Frank, J. W. Haller, and L. Bolinger (Feb. 2001). "Real-time multiple linear regression for fMRI supported by time-aware acquisition and processing". en. In: *Magnetic Resonance in Medicine* 45.2, pp. 289–298. ISSN: 1522-2594.

Sorger, B., T. Kamp, N. Weiskopf, J. C. Peters, and R. Goebel (May 2018). "When the Brain Takes 'BOLD' Steps: Real-Time fMRI Neurofeedback Can Further Enhance the Ability to Gradually Self-regulate Regional Brain Activation". In: *Neuroscience*. Neurofeedback and Functional Enhancement: Mechanisms, Methodology, Behavioral and Clinical Applications 378, pp. 71–88. ISSN: 0306-4522.

Sorger, B., J. C. Peters, C van Den Boomen, A Zilverstrand, J Reithler, and R Goebel (2010). "Real-time decoding of the locus of visuospatial attention using multi-voxel pattern classification." In:

Sorger, B., J. Reithler, B. Dahmen, and R. Goebel (July 2012). "A Real-Time fMRI-Based Spelling Device Immediately Enabling Robust Motor-Independent Communication". en. In: *Current Biology* 22.14, pp. 1333–1338. ISSN: 09609822.

Spetter, M. S., R. Malekshahi, N. Birbaumer, M. Lührs, A. H. van der Veer, K. Scheffler, S. Spuckti, H. Preissl, R. Veit, and M. Hallschmid (May 2017). "Volitional regulation of brain responses to food stimuli in overweight and obese subjects: A real-time fMRI feedback study". In: *Appetite* 112, pp. 188–195. ISSN: 0195-6663.

Spunt, B. (Nov. 2016). *spunt/bspmview: BSPMVIEW v.20161108*.

Stoeckel, L. E., K. A. Garrison, S. S. Ghosh, P. Wighton, C. A. Hanlon, J. M. Gilman, S. Greer, N. B. Turk-Browne, M. T. deBettencourt, D. Scheinost, C. Craddock, T. Thompson, V. Calderon, C. C. Bauer, M. George, H. C. Breiter, S. Whitfield-Gabrieli, J. D. Gabrieli, S. M. LaConte, L. Hirshberg, J. A. Brewer, M. Hampson, A. Van Der Kouwe, S. Mackey, and A. E. Evins (Jan. 2014). "Optimizing real time fMRI neurofeedback for therapeutic discovery and development". In: *NeuroImage: Clinical* 5, pp. 245–255. ISSN: 2213-1582.

Subramanian, L., J. V. Hindle, S. Johnston, M. V. Roberts, M. Husain, R. Goebel, and D. Linden (Nov. 2011). "Real-Time Functional Magnetic Resonance Imaging Neurofeedback for Treatment of Parkinson's Disease". en. In: *Journal of Neuroscience* 31.45, pp. 16309–16317. ISSN: 0270-6474, 1529-2401.

Sulzer, J., S. Haller, F. Scharnowski, N. Weiskopf, N. Birbaumer, M. Blefari, A. Bruehl, L. Cohen, R. deCharms, R. Gassert, R. Goebel, U. Herwig, S. LaConte, D. Linden, A. Luft, E. Seifritz, and R. Sitaram (Aug. 2013a). "Real-time fMRI neurofeedback: Progress and challenges". en. In: *NeuroImage* 76. a, pp. 386–399. ISSN: 10538119.

Sulzer, J., R. Sitaram, M. L. Blefari, S. Kollias, N. Birbaumer, K. E. Stephan, A. Luft, and R. Gassert (Dec. 2013b). "Neurofeedback-mediated self-regulation of the dopaminergic midbrain". In: *NeuroImage* 83. b, pp. 817–825. ISSN: 1053-8119.

Sun, H., J. O. Cleary, R. Glarin, S. C. Kolbe, R. J. Ordidge, B. A. Moffat, and G. B. Pike (2020). "Extracting more for less: multi-echo MP2RAGE for simultaneous T1-weighted imaging, T1 mapping, mapping, SWI, and QSM from a single acquisition". en. In: *Magnetic Resonance in Medicine* 83.4. _eprint: https://onlinelibrary.wiley.com/doi/pdf/10.1002/mrm.27975, pp. 1178–1191. ISSN: 1522-2594.

Thesen, S., O. Heid, E. Mueller, and L. R. Schad (Sept. 2000). "Prospective acquisition correction for head motion with image-based tracking for real-time fMRI". eng. In: *Magnetic Resonance in Medicine* 44.3, pp. 457–465. ISSN: 0740-3194.

Thibault, R. T., A. MacPherson, M. Lifshitz, R. R. Roth, and A. Raz (May 2018). "Neurofeedback with fMRI: A critical systematic review". In: *NeuroImage* 172, pp. 786–807. ISSN: 1053-8119.

Triantafyllou, C., R. D. Hoge, G. Krueger, C. J. Wiggins, A. Potthast, G. C. Wiggins, and L. L. Wald (May 2005). "Comparison of physiological noise at 1.5 T, 3 T and 7 T and optimization of fMRI acquisition parameters". In: *NeuroImage* 26.1, pp. 243–250. ISSN: 1053-8119.

Van Dijk, K. R. A., M. R. Sabuncu, and R. L. Buckner (Jan. 2012). "The influence of head motion on intrinsic functional connectivity MRI". In: *NeuroImage*. Neuroergonomics: The human brain in action and at work 59.1, pp. 431–438. ISSN: 1053-8119.

Van Essen, D. C., K. Ugurbil, E. Auerbach, D. Barch, T. E. J. Behrens, R. Bucholz, A. Chang, L. Chen, M. Corbetta, S. W. Curtiss, S. Della Penna, D. Feinberg, M. F. Glasser, N. Harel, A. C. Heath, L. Larson-Prior, D. Marcus, G. Michalareas, S. Moeller, R. Oostenveld, S. E. Petersen, F. Prior, B. L. Schlaggar, S. M. Smith, A. Z. Snyder, J. Xu, E. Yacoub, and WU-Minn HCP Consortium (Oct. 2012). "The Human Connectome Project: a data acquisition perspective". eng. In: *NeuroImage* 62.4, pp. 2222–2231. ISSN: 1095-9572.

Vidaurre, C. and B. Blankertz (June 2010). "Towards a Cure for BCI Illiteracy". en. In: *Brain Topography* 23.2, pp. 194–198. ISSN: 1573-6792.

Voyvodic (2011). "Automated real-time behavioral and physiological data acquisition and display integrated with stimulus presentation for fMRI". In: *Frontiers in Neuroinformatics*. ISSN: 16625196.

Voyvodic, J. T. (Aug. 1999). "Real-Time fMRI Paradigm Control, Physiology, and Behavior Combined with Near Real-Time Statistical Analysis". In: *NeuroImage* 10.2, pp. 91–106. ISSN: 1053-8119.

Wang, Y., B. Keller, M. Capota, M. J. Anderson, N. Sundaram, J. D. Cohen, K. Li, N. B. Turk-Browne, and T. L. Willke (Dec. 2016). "Real-time full correlation matrix analysis of fMRI data". In: *2016 IEEE International Conference on Big Data (Big Data)*. Washington DC,USA: IEEE, pp. 1242–1251. ISBN: 978-1-4673-9005-7.

Ward, H. A., S. J. Riederer, and C. R. Jack (2002). "Real-time autoshimming for echo planar timecourse imaging". en. In: *Magnetic Resonance in Medicine* 48.5, pp. 771–780. ISSN: 1522-2594.

Watanabe, T., Y. Sasaki, K. Shibata, and M. Kawato (Dec. 2017). "Advances in fMRI Real-Time Neurofeedback". In: *Trends in Cognitive Sciences* 21.12, pp. 997–1010. ISSN: 1364-6613.

Weiskopf, N., K. Mathiak, S. W. Bock, F. Scharnowski, R. Veit, W. Grodd, R. Goebel, and N. Birbaumer (June 2004a). "Principles of a brain-computer interface (BCI) based on real-time functional magnetic resonance imaging (fMRI)". In: *IEEE Transactions on Biomedical Engineering* 51.6. a, pp. 966–970. ISSN: 0018-9294.

Weiskopf, N. (Aug. 2012). "Real-time fMRI and its application to neurofeedback". en. In: *NeuroImage* 62.2, pp. 682–692. ISSN: 10538119.

Weiskopf, N., C. Hutton, O. Josephs, and R. Deichmann (Nov. 2006). "Optimal EPI parameters for reduction of susceptibility-induced BOLD sensitivity losses: A whole-brain analysis at 3 T and 1.5 T". In: *NeuroImage* 33.2, pp. 493–504. ISSN: 1053-8119.

Weiskopf, N., C. Hutton, O. Josephs, R. Turner, and R. Deichmann (Feb. 2007a). "Optimized EPI for fMRI studies of the orbitofrontal cortex: compensation of susceptibility-induced gradients in the readout direction". en. In: *Magnetic Resonance Materials in Physics, Biology and Medicine* 20.1. a, pp. 39–49. ISSN: 0968-5243, 1352-8661.

Weiskopf, N., U. Klose, N. Birbaumer, and K. Mathiak (Feb. 2005). "Single-shot compensation of image distortions and BOLD contrast optimization using multi-echo EPI for real-time fMRI". In: *NeuroImage* 24.4, pp. 1068–1079. ISSN: 1053-8119.

Weiskopf, N., F. Scharnowski, R. Veit, R. Goebel, N. Birbaumer, and K. Mathiak (July 2004b). "Self-regulation of local brain activity using real-time functional magnetic resonance imaging (fMRI)".

In: *Journal of Physiology-Paris*. Decoding and interfacing the brain: from neuronal assemblies to cyborgs 98.4. b, pp. 357–373. ISSN: 0928-4257.

Weiskopf, N., R. Sitaram, O. Josephs, R. Veit, F. Scharnowski, R. Goebel, N. Birbaumer, R. Deichmann, and K. Mathiak (July 2007b). "Real-time functional magnetic resonance imaging: methods and applications". en. In: *Magnetic Resonance Imaging* 25.6. b, pp. 989–1003. ISSN: 0730725X.

Weiskopf, N., J. Suckling, G. Williams, M. M. Correia, B. Inkster, R. Tait, C. Ooi, E. T. Bullmore, and A. Lutti (June 2013). "Quantitative multi-parameter mapping of R1, PD*, MT, and R2* at 3T: a multi-center validation". In: *Frontiers in Neuroscience* 7. ISSN: 1662-4548.

Welvaert, M. and Y. Rosseel (Nov. 2013). "On the Definition of Signal-To-Noise Ratio and Contrast-To-Noise Ratio for fMRI Data". en. In: *PLOS ONE* 8.11, e77089. ISSN: 1932-6203.

Whitfield-Gabrieli, S. and A. Nieto-Castanon (May 2012). "Conn: A Functional Connectivity Toolbox for Correlated and Anticorrelated Brain Networks". In: *Brain Connectivity* 2.3, pp. 125–141. ISSN: 2158-0014.

Whittall, K. P., A. L. MacKay, and D. K. B. Li (1999). "Are mono-exponential fits to a few echoes sufficient to determine T2 relaxation for in vivo human brain?" en. In: *Magnetic Resonance in Medicine* 41.6, pp. 1255–1257. ISSN: 1522-2594.

Wilkinson, M. D., M. Dumontier, I. J. Aalbersberg, G. Appleton, M. Axton, A. Baak, N. Blomberg, J.-W. Boiten, L. B. da Silva Santos, P. E. Bourne, J. Bouwman, A. J. Brookes, T. Clark, M. Crosas, I. Dillo, O. Dumon, S. Edmunds, C. T. Evelo, R. Finkers, A. Gonzalez-Beltran, A. J. G. Gray, P. Groth, C. Goble, J. S. Grethe, J. Heringa, P. A. C. 't Hoen, R. Hooft, T. Kuhn, R. Kok, J. Kok, S. J. Lusher, M. E. Martone, A. Mons, A. L. Packer, B. Persson, P. Rocca-Serra, M. Roos, R. van Schaik, S.-A. Sansone, E. Schultes, T. Sengstag, T. Slater, G. Strawn, M. A. Swertz, M. Thompson, J. van der Lei, E. van Mulligen, J. Velterop, A. Waagmeester, P. Wittenburg, K. Wolstencroft, J. Zhao, and B. Mons (Mar. 2016). "The FAIR Guiding Principles for scientific data management and stewardship". en. In: *Scientific Data* 3.1. Number: 1 Publisher: Nature Publishing Group, p. 160018. ISSN: 2052-4463.

Wilms, M., L. Schilbach, U. Pfeiffer, G. Bente, G. R. Fink, and K. Vogeley (Mar. 2010). "It's in your eyes—using gaze-contingent stimuli to create truly interactive paradigms for social cognitive and affective neuroscience". en. In: *Social Cognitive and Affective Neuroscience* 5.1, pp. 98–107. ISSN: 1749-5016.

Wise, R. G., K. Ide, M. J. Poulin, and I. Tracey (Apr. 2004). "Resting fluctuations in arterial carbon dioxide induce significant low frequency variations in BOLD signal". In: *NeuroImage* 21.4, pp. 1652–1664. ISSN: 1053-8119.

Yamashita, A., S. Hayasaka, M. Kawato, and H. Imamizu (Oct. 2017). "Connectivity Neurofeedback Training Can Differentially Change Functional Connectivity and Cognitive Performance". eng. In: *Cerebral Cortex (New York, N.Y.: 1991)* 27.10, pp. 4960–4970. ISSN: 1460-2199.

Yang, S., T. J. Ross, Y. Zhang, E. A. Stein, and Y. Yang (Aug. 2005). "Head motion suppression using real-time feedback of motion information and its effects on task performance in fMRI". In: *NeuroImage* 27.1, pp. 153–162. ISSN: 1053-8119.

Yarkoni, T., C. J. Markiewicz, A. d. l. Vega, K. J. Gorgolewski, T. Salo, Y. O. Halchenko, Q. McNamara, K. DeStasio, J.-B. Poline, D. Petrov, V. Hayot-Sasson, D. M. Nielson, J. Carlin, G. Kiar, K. Whitaker, E. DuPre, A. Wagner, L. S. Tirrell, M. Jas, M. Hanke, R. A. Poldrack, O. Esteban, S. Appelhoff, C. Holdgraf, I. Staden, B. Thirion, D. F. Kleinschmidt, J. A. Lee, M. V. O. d. Castello, M. P. Notter, and R. Blair (Aug. 2019). "PyBIDS: Python tools for BIDS datasets". en. In: *Journal of Open Source Software* 4.40, p. 1294. ISSN: 2475-9066.

Yarkoni, T., R. A. Poldrack, T. E. Nichols, D. C. Van Essen, and T. D. Wager (Aug. 2011). "Large-scale automated synthesis of human functional neuroimaging data". en. In: *Nature Methods* 8.8. Number: 8 Publisher: Nature Publishing Group, pp. 665–670. ISSN: 1548-7105.

Yoo, S.-S. and F. A. Jolesz (Aug. 2002). "Functional MRI for neurofeedback: feasibility study on a hand motor task". eng. In: *Neuroreport* 13.11, pp. 1377–1381. ISSN: 0959-4965.

Young, K. D., G. J. Siegle, V. Zotev, R. Phillips, M. Misaki, H. Yuan, W. C. Drevets, and J. Bodurka (Aug. 2017). "Randomized Clinical Trial of Real-Time fMRI Amygdala Neurofeedback for Major Depressive Disorder: Effects on Symptoms and Autobiographical Memory Recall". en. In: *American Journal of Psychiatry* 174.8, pp. 748–755. ISSN: 0002-953X, 1535-7228.

Young, K. D., V. Zotev, R. Phillips, M. Misaki, H. Yuan, W. C. Drevets, and J. Bodurka (Feb. 2014). "Real-Time fMRI Neurofeedback Training of Amygdala Activity in Patients with Major Depressive Disorder". en. In: *PLOS ONE* 9.2, e88785. ISSN: 1932-6203.

Zaitsev, M., C. Dold, G. Sakas, J. Hennig, and O. Speck (July 2006). "Magnetic resonance imaging of freely moving objects: prospective real-time motion correction using an external optical motion tracking system". eng. In: *NeuroImage* 31.3, pp. 1038–1050. ISSN: 1053-8119.

Zaitsev, M., J. Hennig, and O. Speck (2004). "Point spread function mapping with parallel imaging techniques and high acceleration factors: Fast, robust, and flexible method for echo-planar imaging distortion correction". en. In: *Magnetic Resonance in Medicine* 52.5, pp. 1156–1166. ISSN: 1522-2594.

Zilverstand, A., B. Sorger, D. Slaats-Willemse, C. C. Kan, R. Goebel, and J. K. Buitelaar (Jan. 2017). "fMRI Neurofeedback Training for Increasing Anterior Cingulate Cortex Activation in Adult Attention Deficit Hyperactivity Disorder. An Exploratory Randomized, Single-Blinded Study". en. In: *PLOS ONE* 12.1, e0170795. ISSN: 1932-6203.

Zilverstand, A., B. Sorger, J. Zimmermann, A. Kaas, and R. Goebel (Jan. 2014). "Windowed Correlation: A Suitable Tool for Providing Dynamic fMRI-Based Functional Connectivity Neurofeedback on Task Difficulty". en. In: *PLOS ONE* 9.1, e85929. ISSN: 1932-6203.

Research outputs

The following research outputs have been published as a result of the work done over the course of this thesis.

Journal articles

Armeni, K., L. Brinkman, R. Carlsson, A. Eerland, R. Fijten, R. Fondberg, V. E. Heininga, S. Heunis, W. Q. Koh, M. Masselink, N. Moran, A. Baoill, A. Sarafoglou, A. Schettino, H. Schwamm, Z. Sjoerds, M. Teperek, O. v. d. Akker, A. v. t. Veer, and R. Zurita-Milla (Oct. 2020). "Towards wide-scale adoption of open science practices: The role of open science communities". In: *MetaArXiv*.

Bannier, E., G. Barker, V. Borghesani, N. Broeckx, P. Clement, K. E. Emblem, S. Ghosh, E. Glerean, K. J. Gorgolewski, M. Havu, Y. O. Halchenko, P. Herholz, A. Hespel, S. Heunis, Y. Hu, C.-P. Hu, D. Huijser, M. d. l. I. Vayá, R. Jancalek, V. K. Katsaros, M.-L. Kieseler, C. Maumet, C. A. Moreau, H.-J. Mutsaerts, R. Oostenveld, E. Ozturk-Isik, N. P. L. Espinosa, J. Pellman, C. R. Pernet, F. B. Pizzini, A. Trbalić, P.-J. Toussaint, M. V. d. O. Castello, F. Wang, C. Wang, and H. Zhu (2021). "The Open Brain Consent: Informing research participants and obtaining consent to share brain imaging data". In: *Human Brain Mapping* Editorial. ISSN: 1097-0193.

Besseling, R., R. Lamerichs, B. Michels, S. Heunis, A. de Louw, A. Tijhuis, J. Bergmans, and B. Aldenkamp (May 2018). "Functional network abnormalities consistent with behavioral profile in Autism Spectrum Disorder". In: *Psychiatry Research: Neuroimaging* 275, pp. 43–48. ISSN: 0925-4927.

Botvinik-Nezer, R. et al. (June 2020). "Variability in the analysis of a single neuroimaging dataset by many teams". In: *Nature* 582.7810. Number: 7810 Publisher: Nature Publishing Group, pp. 84–88. ISSN: 1476-4687.

Gau, R. et al. (Feb. 2021). "Brainhack: developing a culture of open, inclusive, community-driven neuroscience". In: *PsyArXiv*.

Heunis, S., R. Besseling, R. Lamerichs, A. de Louw, M. Breeuwer, B. Aldenkamp, and J. Bergmans (Dec. 2018b). "Neu3CA-RT: A framework for real-time fMRI analysis". In: *Psychiatry Research: Neuroimaging* 282, pp. 90–102. ISSN: 09254927.

Heunis, S., M. Breeuwer, C. Caballero-Gaudes, L. Hellrung, W. Huijbers, J. F. Jansen, R. Lamerichs, S. Zinger, and A. P. Aldenkamp (Dec. 2020a). "The effects of multi-echo fMRI combination and rapid T2*-mapping on offline and real-time BOLD sensitivity". In: *bioRxiv*. Publisher: Cold Spring Harbor Laboratory Section: New Results, p. 2020.12.08.416768.

Heunis, S., M. Breeuwer, C. C. Gaudes, L. Hellrung, W. Huijbers, J. F. Jansen, R. Lamerichs, S. Zinger, and A. P. Aldenkamp (Dec. 2020b). "rt-me-fMRI: A task and resting state dataset for real-time, multi-echo fMRI methods development and validation". In: *bioRxiv*. Publisher: Cold Spring Harbor Laboratory Section: New Results, p. 2020.12.07.414490.

Heunis, S., R. Lamerichs, S. Zinger, C. Caballero-Gaudes, J. F. A. Jansen, B. Aldenkamp, and M. Breeuwer (Aug. 2020c). "Quality and denoising in real-time functional magnetic resonance imaging neurofeedback: A methods review". In: *Human Brain Mapping* 41.12, pp. 3439–3467. ISSN: 1097-0193.

Levitis, E., C. G. v. Praag, R. Gau, S. Heunis, E. DuPre, G. Kiar, K. Bottenhorn, T. Glatard, A. Nikolaidis, K. Whitaker, M. Mancini, G. Niso, S. Afyouni, E. A. Ortiz, S. Appelhoff, A. Arnatkeviciute, M. S. Atay, T. Auer, G. Baracchini, J. M. M. Bayer, M. J. S. Beauvais, J. Bijsterbosch, I. P. Bilgin, S. Bollmann, S. Bollmann, R. Botvinik-Nezer, M. Bright, V. D. Calhoun, X. Chen, S. Chopra, H. Chuan-Peng, T. Close, S. Cookson, C. Craddock, A. D. L. Vega, B. D. Leener, D. Demeter, P. D. Maio, E. W. Dickie, S. B. Eickhoff, O. Esteban, K. Finc, M. Frigo, S. Ganesan, M. Ganz, K. Garner, E. A. Garza-Villarreal, G. Gonzalez-Escamilla, R. Goswami, J. Griffiths, T. Grootswagers, S. Guay, O. Guest, D. A. Handwerker, P. Herholz, K. Heuer, D. Huijser, V. Iacovella, M. Joseph, A. Karakuzu, D. Keator, X. Kobeleva, M. Kumar, A. Laird, L. J. Larson-Prior, A. Lautarescu, A. Lazari, J. H. L. Gorroño, X.-Y. Li, J. Lv, S. L. Mansour, D. Meunier, D. Moraczewski, T. Nandi, S. A. Nastase, M. Nau, S. Noble, M. Norgaard, J. Obungoloch, R. Oostenveld, E. R. Orchard, A. L. Pinho, R. Poldrack, A. Qiu, P. R. Raamana, A. Rokem, S. Rutherford, M. Sharan, T. Shaw, W. T. Syeda, M. Testerman, R. Toro, S. L. Valk, S. V. D. Bossche, G. Varoquaux, F. Vasa, M. Veldsman, J. Vohryzek, A. S. Wagner, R. Walsh, T. White, zuxfoucault, X. Xie, C.-G. Yan, Y.-F. Yang, Y. Yee, G. E. Zanitti, A. V. Gulick, E. Duff, and C. Maumet (Mar. 2021). "Centering inclusivity in the design of online conferences". In: *PsyArXiv*.

Ros, T., S. Enriquez-Geppert, V. Zotev, K. D. Young, G. Wood, S. Whitfield-Gabrieli, F. Wan, P. Vuilleumier, F. Vialatte, D. Van De Ville, D. Todder, T. Surmeli, J. S. Sulzer, U. Strehl, M. B. Sterman, N. J. Steiner, B. Sorger, S. R. Soekadar, R. Sitaram, L. H. Sherlin, M. Schönenberg, F. Scharnowski, M. Schabus, K. Rubia, A. Rosa, M. Reiner, J. A. Pineda, C. Paret, A. Ossadtchi, A. A. Nicholson, W. Nan, J. Minguez, J.-A. Micoulaud-Franchi, D. M. A. Mehler, M. Lührs, J. Lubar, F. Lotte, D. E. J. Linden, J. A. Lewis-Peacock, M. A. Lebedev, R. A. Lanius, A. Kübler, C. Kranczioch, Y. Koush, L. Konicar, S. H. Kohl, S. E. Kober, M. A. Klados, C. Jeunet, T. W. P. Janssen, R. J. Huster, K. Hoedlmoser, L. M. Hirshberg, S. Heunis, T. Hendler, M. Hampson, A. G. Guggisberg, R. Guggenberger, J. H. Gruzelier, R. W. Göbel, N. Gninenko, A. Gharabaghi, P. Frewen, T. Fovet, T. Fernández, C. Escolano, A.-C. Ehlis, R. Drechsler, R. Christopher deCharms, S. Debener, D. De Ridder, E. J. Davelaar, M. Congedo, M. Cavazza, M. H. M. Breteler, D. Brandeis, J. Bodurka, N. Birbaumer, O. M. Bazanova, B. Barth, P. D. Bamidis, T. Auer, M. Arns, and R. T. Thibault (June 2020). "Consensus on the reporting and experimental design of clinical and cognitive-behavioural neurofeedback studies (CRED-nf checklist)". In: *Brain* 143.6. Publisher: Oxford Academic, pp. 1674–1685. ISSN: 0006-8950.

International conference contributions

Algermissen, J., D. M. Mehler, S. Heunis, and R. Gau (June 2019). "Creating a pre-registration tool for human neuroimaging studies (M/EEG, fMRI)". In: *SIPS2019 - Society for the Improvement of Psychological Science*.

Heunis, S., R. Besseling, R. Lamerichs, A. De Louw, B. Aldenkamp, and J. Bergmans (Jan. 2018a). "Dynamic T2* and S0 mapping towards real-time multi-echo fMRI denoising." In: *Proceedings of the Benelux Chapter of the International Society for Magnetic Resonance in Medicine*.

Heunis, S., L. Hellrung, V. D. Meer, S. Bergert, R. Sladky, G. S. P. Pamplona, F. Scharnowski, Y. Koush, D. Mehler, C. Falcon, J. D. Gispert, J. L. Molinuevo, and S. Skouras (June 2019a). "rtQC: an open-source toolbox for real-time fMRI quality control". In: *Proceeding of the international meeting of the Organization for Human Brain Mapping 2019*.

Heunis, S., R. Lamerichs, G. Song, S. Zinger, and B. Aldenkamp (Jan. 2019b). "Improving BOLD sensitivity with real-time multi-echo echo-planar imaging - Towards a cleaner neurofeedback signal". In: *Proceedings of the Benelux Chapter of the International Society for Magnetic Resonance in Medicine*.

Invited talks and lectures

Heunis, S. (Oct. 2018). "Real-time fMRI neurofeedback - from technology to applications". In: *Donders Discussions 2019*. Nijmegen, The Netherlands.

Heunis, S. (Jan. 2019a). "Introduction to open science and OpenMR Benelux". In: *OpenMR Benelux 2019*. Leiden, The Netherlands.

Heunis, S. (July 2019b). "Open Brain Consent - GDPR edition". In: *Society for the Improvement of Psychological Science 2019*. Rotterdam, The Netherlands.

Heunis, S. (June 2019c). "Real-time fMRI neurofeedback methodology: current challenges, possible solutions and future perspectives." In: *Dutch Neuroscience Meeting 2019*. Lunteren, The Netherlands.

Heunis, S. (Dec. 2019d). "Real-time (fMRI) quality control". In: *rtFIN2019 International Real-time Functional Imaging and Neurfeedback meeting*. Aachen, Germany.

Heunis, S. (July 2020a). "Brain research data and personal data privacy: practical tips to share and protect". In: *Think Open Rovereto Workshop*. Trento, Italy.

Heunis, S. (Sept. 2020b). "Hands-on fMRI code and data sharing". In: *Food for Psychologists*. The Hague, The Netherlands.

Heunis, S. (June 2020c). "Open neuroimaging data and personal data privacy: anonymization". In: *OHBM Open Science Room 2020*. Virtual online.

Heunis, S. (June 2020d). "Open neuroimaging data and personal data privacy: convergence or divergence?" In: *OHBM Open Science Room 2020*. Virtual online.

Patent filings

Lamerichs, R. and Heunis, S. (2018). Real-time fMRI: analysis based on T2* imaging. European patent application No. 18209210.6. World Intellectual Property Organization filing No. PCT/EP2019/081863.

Acronyms

ADHD Attention Deficit and Hyperactivity Disorder

API Application Programming Interface

AR Autoregressive

BCI Brain-Computer Interface

BIDS Brain Imaging Data Structure

BOLD Blood Oxygen Level-Dependent

CBF Cerebral Blood Flow

CBV Cerebral Blood Volume

cGLM Cumulative General Linear Model

CNR Contrast-to-Noise Ratio

COBIDAS Committee on Best Practice in Data Analysis and Sharing

CPU Central Processing Unit

CR Cardiac Rate

CSF Cerebrospinal Fluid

DCM Dynamic Causal Modeling

DecNef Decoded Neurofeedback

DNR Did/do Not Report

DOI Digital Object Identifier

DUA Data Use Agreement

DVARS Differential Variance Root-Mean-Squared

EEG Electroencephalography

EMA Exponential Moving Average

EPI Echo Planar Imaging

EU European Union

FAIR Findable, Accessible, Interoperable, Reusable

FCNef Functional Connectivity Neurofeedback

FD Framewise Displacement

fMRI Functional Magnetic Resonance Imaging

FOV Field Of View

FT Finger Tapping

FWE Familywise Error

FWHM Full Width at Half Maximum

GDPR General Data Protection Regulation

GLM General Linear Model

GM Grey Matter

GPU Graphical Processing Unit

GUI Graphical User Interface

HMP Head Motion/Movement Parameter

HRF Haemodynamic Response Function

HRV Heart Rate Variability

HTML Hypertext Markup Language

ICA Independent Component Analysis

iCAPS Innovation-driven Coactivation Pattern

iGLM Incremental General Linear Model

JSON JavaScript Object Notation

LDA Linear Discriminant Analysis

ME Multi-echo

ME-fMRI Multi-Echo Functional Magnetic Resonance Imaging

MNI Montreal Neurological Institute

MoAE Mother of All Experiments

MRI Magnetic Resonance Imaging

MVPA Multivariate Pattern Analysis

NF Neurofeedback

PAID Parallel-acquired Inhomogeneity-desensitized

PC Personal Computer

PCA Principal Component Analysis

PNG Portable Network Graphics

PSC Percentage Signal Change

PSCNef Percentage Signal Change Neurofeedback

PSF Point Spread Function

PTSD Post-traumatic Stress Disorder

QA Quality Assurance

QC Quality Control

RAM Random Access Memory

RETROICOR Retrospective Image Correction

ROI Region Of Interest

RT Real-time

rt-me-fMRI Real-time Multi-Echo Functional Magnetic Resonance Imaging

rtfMRI Real-time Functional Magnetic Resonance Imaging

rtfMRI-NF Real-time Functional Magnetic Resonance Imaging Neurofeedback

rtQC Real-time Quality Control

RVM Relevance Vector Machine

RVT Respiratory Volumer per Time

SE-fMRI Multi-Echo Functional Magnetic Resonance Imaging

SNR Signal-to-Noise Ratio

SPM Statistical Parametric Mapping

SSE Sum of Squared Errors

SSS Sum of Squared Signal

SVM Support Vector Machine

SW Scalar Weight

TBV Turbo-BrainVoyager

tCNR Temporal Contrast-to-Noise Ratio

TE Echo Time

tPSC Temporal Percentage Signal Change

TR Repetition Time

tSNR Temporal Signal-to-Noise Ratio

TSV Tab-separated Value

WM White Matter

Acknowledgements

I have the opportunity, now, to acknowledge and give thanks to those who have provided me with support, insight, knowledge, friendship and (frankly and thankfully!) money over the course of this academic journey. I can state without a doubt that these have been the most challenging yet rewarding years of my life and I would have fared far worse without the help I received. Moving to a new continent, navigating personal and professional life in an entirely different culture, becoming a parent (twice), enduring a global pandemic, exploring the fascinating research fields of neuroimaging and open science, and successfully defending a doctoral thesis: only fools would live through such experiences and claim victory purely for themselves. I am indebted to many.

Firstly, most importantly, I would like to thank my partner and best friend, Tosca. You are the one person that I can truly share life on this planet with, no matter what. You are strong, smart, funny, supportive, a brilliant parent, and (unfathomably) interested in being there for me without fail. I am so grateful, happy and excited to be able to share this journey, and the many to follow, with you. And with our two wonderful (and currently highly energetic) children, of course. Matthias and Lisa, you have made my life richer and have given me a new sense of wonder, an uplifting experience that cannot be quelled even through difficult times. Thank you for being my family, I look forward to experiencing life with you.

I have a whole team of supervisors to thank for years of support and guidance. Firstly, Jan, thank you so much for giving me the opportunity to join the team at the SPS group and to start my journey into neuroimaging research. Your office door was always open, you listened when I asked (too many?) questions, and you always supported me and my family when we needed it. I am sincerely grateful for your help. Bert, I have always appreciated your guidance and insights into successfully managing a research project. Thank you for giving me free rein to follow my (often diverging) research ideas, and for giving constructive feedback that kept the project on track. Without your support to kick off and guide the project, and without support from our funders (thank you, Health Holland!), my doctoral journey would not have been possible. To Marcel, René, and Anton: even though I spent less time with you over the course of the project, these times have been both impactful and fun. Thank you so much for your guidance and for your input into the research project and my professional development. Rolf, thank you for bringing this neuroimaging rookie up to speed on our many trips to the scanner, and thanks for all the lifts too! It has been great to collaborate with you on this project and to have insightful discussions about real-time fMRI, multi-

echo sequences, and what really is signal versus noise. Lastly, Sveta, thank you for taking on the job of supervisor while you already had a lot on your plate. It has been great to have you as part of the team, not only as a guiding force in the project but also as a person who understands the challenges of academia and who listens and supports when it is needed most. I am deeply thankful.

To the members of the doctoral committee who gave their time and expertise to assess my work and provide constructive feedback, thank you so much for your help. Apart from my supervisors, I also thank Prof.dr.ir. Massimo Mischi, Prof.dr. David Linden, Prof.dr. Frank Scharnowski and Prof.dr. Raymond Van Ee. In particular, I would like to thank David and Frank for their detailed, insightful and thoughtful comments. It is an honour to be able to receive such feedback from you who have done so much for the field of real-time fMRI neurofeedback.

I am also immensely grateful to the many collaborators who have been integral to the success of my journey. To Hans, Raf, Remco, Roy, Ronnie and the rest of the staff at the MRI scanner at Kempenhaeghe, thank you so much for your support throughout this project. Without your help, I would not have been able to spend as much time with the scanner or conduct my main research studies. You have played a very important role in this work and I thank you for that. I have also been lucky enough to have built up several research collaborations from which I have benefited both professionally and personally. Jaap, your knowledge and support through the latter half of my project came at a time when I needed it most. Your pragmatic suggestions were often a necessary counterbalance to my idealistic tendencies and helped move my project forward. Thank you so much. Lydia, I am lucky to be able to call you a friend and colleague. I have learnt so much from your experience and your intuitive understanding of the field of real-time fMRI (and the amygdala), and I hope to continue doing so. Thank you also for always having understanding and encouraging words to share. Willem, even though we collaborated for only a short time, I learnt so much from you during our many fruitful discussions about study design, multi-echo protocols, data quality, and conducting research in both academia and industry. I hope we get the chance to work together in future. César, I often recount the story of how our journey started: out of 30 widely published researchers that I emailed to ask for advice about fMRI denoising practices, you were one of only a handful who replied, and the only one who responded both with kindness and insightful advice. Thank you for being the best collaborator, a good friend, and just generally a great person to know. I look forward to working with you in future, and hopefully having some fun times in Spain or The Netherlands.

Then, there are of course my SPS friends and colleagues who have supported me in and outside of the office, both with administrative and research tasks, and personally through both the challenging and easier times of this journey. Anja, Marieke, and Carla, thanks for always being there to support and to understand. You bring a much needed positive energy to an environment that could often feel a bit lonely, and this has always brought a spark to my day. Debby, thanks for the friendship and many discussions on life as a parent and early career re-

searcher. You were always available to talk and to listen, even if it was mostly just me complaining about broken systems. Antoine, I will always remember our long discussions on selecting the right preprocessing steps, on our mostly futile attempts at having enough statistical power, and on snowboarding and religion, all while we were actually supposed to be writing papers. Thanks for being a great office mate. Jesper, I was fortunate to have met you and to spend some time together in the office during the last part of my project. Thanks for making this experience both fun and interesting. I would also like to thank Marco and Patrick for our many coffee-fuelled conversations on life, academia and the interesting differences between South African, Italian and Dutch cultures.

I have been extremely lucky to have made true friends on this international research journey that can otherwise so easily be fraught with loneliness, and I mostly have open science communities to thank for that. If not for communities like Brainhack, OpenMR Benelux and the wonderful OHBM crowd, I would not have had the great fortune of getting to know friends like Remi, Dorien, Camille, and so many other kind people who are putting immense effort into creating a better environment for all in academia. Cass, I would like to thank you, especially, for being a constant source of support, comfort, understanding, and much fun from the moment that we met. I consider you to be a true and close friend and I hope that we will have an increasing number of opportunities in future to grow our friendship, to collaborate professionally, and to work together on social justice initiatives in science.

Lastly, I would not be where I am now without the support of my loving family. Apart from their obvious contributions to my experiences of a healthy and privileged childhood and young adulthood, they have never stopped supporting me and my partner and children during this most recent journey. Gert, Odile, Ingrid, Daniel, Marizanne, Christoff, Henrike, Marius, Annet, Hanje, Johann and Lukas: thank you so much for being constant sources of love and support through the good times as well as the challenging times. Thank you for opening your homes and arms when we visited South Africa. Thank you for dutifully listening to me complain about the Dutch weather. Thank you for being the ray of sun that we often needed during cloudy times. Thank you for visiting us, for spending time with Matthias and Lisa, for sending stories for them to listen to, and for endless video calls. Aan elkeen van julle: baie, baie dankie!

Curriculum vitae

Stephan heunis has an M.Sc. in Biomedical Engineering and Robotics from Stellenbosch University in South Africa. He worked as a commercial and software engineer for four years in two industries (Industrial Automation and Enterprise Mobility) before moving to the Netherlands with the goal of conducting research in neuroscience. His doctoral research at the Eindhoven University of Technology and in collaboration with Philips Research focused on developing new acquisition and signal processing methods for functional magnetic resonance imaging (MRI) that allow improved tracking and visualisation of brain activity in real-time. These developments resulted in higher sensitivity of the neural measures used in clinical practice to study and develop treatments for mental health conditions.

Stephan is passionate about brains, accessible education, and making scientific practice more transparent and inclusive. Throughout his doctoral research, he has been active in the Dutch network of Open Science Communities and he founded OpenMR Benelux[1], a community working on wider adoption of open science practices in MRI research through talks, discussions, workshops and hackathons. Stephan has since continued this passion as a Research Data and Software Engineer at the Forschungszentrum Jülich in Germany[2], where he works on software solutions for neuroinformatics and decentralised research data management. He also holds post-doctoral positions in the SYNC developmental neuroscience lab[3] at Erasmus University Rotterdam and Leiden University in the Netherlands.

Find out more on Stephan's personal website[4].

[1] https://openmrbenelux.github.io/
[2] https://www.psychoinformatics.de/
[3] https://erasmus-synclab.nl/
[4] https://jsheunis.github.io/